AERODYNAMICS OF CABLE STAYED BRIDGES

A THESIS

*submitted in fulfilment of the
requirements for the award of the degree
of*
DOCTOR OF PHILOSOPHY
in
CIVIL ENGINEERING

By

B. G. NARESH KUMAR

DEPARTMENT OF CIVIL ENGINEERING
UNIVERSITY OF ROORKEE
ROORKEE - 247 667 (INDIA)
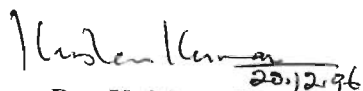
AUGUST, 1994

CANDIDATE'S DECLARATION

I hereby certify that the work which is being presented in the thesis entitled "**Aerodynamics of Cable Stayed Bridges**" in fulfilment of the requirement for the award of the *Degree of Doctor of Philosophy* and submitted in the Department of Civil Engineering of the University is an authentic record of my own work carried out during a period from Jan., 1991 to July, 1994 under the supervision of **Dr. Prem Krishna** and **Dr. Krishen Kumar**.

The matter presented in this thesis has not been submitted by me for the award of any other degree of this or any other University.

(B.G.Naresh Kumar)

This is to certify that the above statement made by the candidate is correct to the best of our knowledge.

Date: 6.8.1994

Dr. Krishen Kumar
Professor
Dept. of Civil Engg.
UOR, Roorkee

Dr. Prem Krishna
Professor
Dept. of Civil Engg.
UOR, Roorkee

The Ph. D. Viva-Voce examination of B.G.Naresh Kumar, Research Scholar, has been held on 04 Oct. 1997

Signature of Supervisor(s)   Signature of H.O.D.

(S. A. Reddi)
Signature of External Examiner

ACKNOWLEDGEMENT

B.G.Naresh Kumar

ABSTRACT

The present day long span cable supported bridges are amongst the more flexible of the civil engineering structures, and, are prone to aerodynamic oscillations. Vibrations of some existing bridges like Golden Gate, Deer Isle and some others have influenced the need for continued research into the phenomena of aerodynamic effects on long span bridges. Cable stayed bridges with composite I-Girder decks have come into greater use recently, because of advantages that they offer in terms of speedy construction and economy besides meeting the stiffness criteria. However, there has not been any comprehensive study on their aerodynamic behaviour. It was therefore decided to study the behaviour of composite I-Girder cable stayed bridges in this thesis.

Under the influence of wind, a long span bridge may undergo any of the following types of motions: (i) Flutter : in which the bridge deck displays exponentially growing motions that are limited only by structural non-linearities or failure, (ii) Buffeting : in which the bridge moves in random manner that reflects the random characteristic of wind, but is stable, and (iii) Vortex induced vibrations: characterised by the wake of the bridge deck forming a street of alternating vortices where the frequency of shedding approximately coincides with the natural frequency of vibration of the bridge in one of its natural mode of vibration, causing the bridge to oscillate with amplitudes which may far exceed the permissible values.

Scanlan et al.(1969,1986,1988) have developed a system identification technique in which 'section model' of the deck is used for evaluating the flutter derivatives in an attempt to establish the flutter criterion for the bridge decks. They however applied the concept to truss and box girder deck bridges. Okauchi et al.(1979) carried out experiments in the field, and tested a large section model of the bridge deck (1:10 scale) to confirm the reliability of wind tunnel studies. Davenport(1972) developed a simplified approach and proposed a 'taut-strip' model to study the behaviour of cable bridges. Miyata et al.(1992) carried out studies in Japan on full size models of suspended bridges using especially designed and built large boundary layer wind tunnel.

The present study was undertaken with a view to find the influence of the following parameters on the aerodynamic behaviour of the cable stayed bridges with this type of deck:

1. Relative span of the bridge
2. Type of flow : smooth and turbulent
3. Simulated eddy sizes as given by appropriate integral scales

4. Fairings : over part and full length of the deck

5. Wind incidence angle

The method of 'section model test' to obtain flutter derivative coefficients has been used. It is partly experimental and partly theoretical and offers the advantage of the use of a much larger geometrical scale for the model (enhancing the accuracy of scaling effects). The theory involves the modal analysis of the system for which inverse iteration with Sturm sequence technique (Bathe and Wilson, 1987) has been used.

Necessary softwares and graphics packages have also been developed for analysis and presentation.

Following the success of pilot test runs on a rectangular section, the section model of a composite I-girder deck (Bridge #1) was made to a scale of 1:60 and tested under two flow conditions- smooth flow and three grid generated turbulent flows. The spectral densities of the turbulence were measured and non-dimensionlized spectrum was found to corroborate with that of the atmospheric spectra (Simiu and Scanlan,1986). Computer programmes were developed to acquire data through Keithely DAC system. The raw data was smoothened by filtering the noise for which Asystant+ software was used. Finally, FORTRAN programmes were developed to determine the various flutter derivatives.

Vertical flutter of the section model was not observed during the tests. This is also confirmed from the trend for the coefficient $H_1^*(K)$ for all wind incidence angles under smooth flow conditions, where it is found to increase with the reduced velocity and follows a monotonic trend.

In case of grid generated flows the trend of $H_1^*(K)$ is not regular but it shows substantial increase in magnitude.

Torsional flutter is observed in all cases, the critical onset velocity varying with the test condition. This is confirmed from the trend for $A_2^*(K)$, the derivative representing the effect of aerodynamic damping. At the point of critical velocity the total damping becomes zero indicated by derivative $A_2^*(K)$ changing sign from -ve to +ve. Also steady-state torsional amplitudes are observed only under smooth flow.

Further, based on the derivative $A_2^*(K)$, results for the critical velocity are found to be as follows:

(i) For the unmodified bridge section critical velocity varies from 36 m/sec to 54 m/sec as the wind incidence angle change from -5 to +5 degrees.

(ii) In case of the fully faired bridge section, critical velocity varies from 49 m/sec to 70 m/sec as the wind incidence angle changes from -5 to +5 degrees.

(iii) The threshold velocity varies, increasing with increase in the structural damping.

Making use of the flutter derivatives, the aerodynamic stability criterion for the prototype bridge could be analysed. In case of Bridge #1 it was found that the first unsymmetrical torsional mode is having a tendency to get into the critical flutter zone at a wind speed of 81.2 m/sec. This tendency was significantly delayed (92.4 m/sec) in case of the faired deck section. In case of Bridge #2, the tendency to get into the critical flutter zone was at a velocity of 46.5 m/sec. Interestingly, for this bridge, with a main span of 457.2 m, which is much larger than that of Bridge #1, no significant change was observed with the fairing attached to the deck section. This could be due to its modal characteristics being significantly different from those of Bridge #1.

The buffeting response of the two bridges was analysed using the Simiu spectra (1986) for wind loading, which yields results as following:

(i) Bridge #1 has a maximum excursing edge deflection at the quarter span points of the order of 0.8 m and 0.3 m in the vertical and torsional modes respectively at a wind speed of 50 m/s.

(ii) Bridge #2 shows a maximum excursing edge deflection at the mid span point of the order of 3.4 m and 3.6 m in the vertical and torsional modes respectively at a wind speed of 50 m/sec.

The main findings of this work are as follows:

(i) From the flutter derivatives determined from section model tests it is observed that the upstream turbulence has considerable effect on the values of the flutter derivatives, the turbulence improving the bridge deck stability.

(ii) The wind angle of attack also influences the derivatives considerably. With an increase in the wind incidence angle beyond +3 degrees, the stability of section model was found to increase in the torsional modes of vibration.

(iii) The fairings improve the stability of the section model.

(iv) Buffeting response of the cable stayed bridges of the form studied is maximum near the quarter-span point for short spans (around 200 m main span) and near the mid-span point for longer spans (around 450 m main span).

CONTENTS

(xi)

LIST OF FIGURES

(xvii)

LIST OF TABLES

CHAPTER 1
INTRODUCTION

1.1 GENERAL

The effect of wind loading is a critical factor in the design of many large-scale civil engineering structures. One of the more notable types of structures which are susceptible to wind loading problems are the long-span suspended-span bridges.

Among the various bridge systems the cable supported bridges (suspension and cable stayed bridges) are distinguished by their ability to cover large spans in the range 150 m to 1500 m. These long span bridges are relatively lighter, more flexible and possess lower levels of structural damping than other types. These are susceptible to wind induced vibrations that can lead to problems in serviceability and maintenance. Some bridges have even been reported to develop vibrations of catastrophic magnitudes. It is mainly on account of their much larger flexibility that the cable supported systems may get excited to potentially large dynamic oscillations under wind forces. Earlier to 1940 a number of cable supported bridges had either been damaged or destroyed due to wind induced oscillations. In the past century wind induced oscillations are known to have severely damaged eleven suspension bridges, as shown in Table 1.1[6], including Tacoma Narrows Bridge. The span of these bridges ranges from 75 m to 850 m. This indicates that wind effects are significant not only in the middle and large span ranges of the cable bridges but may also influence the smaller span bridges. The common feature of these bridge failures has been that the wind induced large oscillations in the bridge deck which eventually caused the key structural

members to get over stressed and give way. The Tacoma Narrows bridge failure can be considered as a classical example of the wind induced collapse of flexible long span bridges.

Table 1.1
Bridges Severely Damaged or Destroyed by Wind[6]

Bridge	Location	Designer	Span(m)	Year of Failure
Deyburh Abbey	Scotland	John & William Smith	79.25	1818
Union	England	Sir Samuel Brown	199.50	1821
Nassau	Germany	Lossen and Wolf	74.68	1834
Brighton Chain Pier	England	Sir Samuel Brown	77.72	1836
Montrose	Scotland	Sir Samuel Brown	131.76	1838
Menai Straits	Wales	Thomas Telford	176.78	1839
Roche-Bernard	France	Le Blanc	195.38	1852
Wheeling	U.S.A.	Charles Ellet	307.85	1854
Niagara-Lewiston	U.S.A.	Edward Serrell	317.30	1864
Niagara-Clifton	U.S.A.	Samuel Keefer	384.00	1889
Tacoma Narrows	U.S.A.	Leon Moisseiff	853.40	1940

The Tacoma Narrows bridge, a 3-span suspension bridge with central span length of 851.2 m and two side spans, each 334.4 m long, collapsed in a storm wind estimated to be only 67.5 Kmph (18.7 m/sec) on 7th November 1940 after being in service for only four months, since it was opened to traffic on 1st July 1940[13]. The deck shape of the ill fated bridge is illustrated in Fig.1.1.

In the recent past there have been a number of innovations in structural analysis, materials and fabrication and erection procedures. Also with the advance in technology, bridge structures with continually increasing spans and deck widths have been coming up. These have greater flexibility, reduced dead weight and generally reduced damping. The natural frequencies reduce and the energy absorption capacity decreases on account of the reduced damping, making them more vulnerable to wind induced oscillations.

The fairly recent advent of Cable Stayed bridge and the continued poor aeroelastic performance of certain existing suspension bridges - like the Golden Gate, the Deer Isle Sedgwick and the Bronx-Whitestone as illustrated in Table 1.2[6,13] - has reinforced the need for continued research into the aerodynamic phenomena.

Table 1.2
Bridges having Large Oscillations in Wind|6,13|

Bridge	Year	Span(m)	Type of stiffening
Fydsesund (Germany)	1937	228.6	Rolled I-beam
Golden Gate (U.S.A.)	1937	1280.2	Truss
Thousand Island (U.S.A.)	1938	243.8	Plate Girder
Deer Isle (U.S.A.)	1939	329.2	Plate Girder
Bronx Whitestone (U.S.A.)	1939	710.0	Plate Girder
Long's Creek (Canada)	1967	217.3	Plate Girder

Prior to the Tacoma Narrows incident the wind design of all suspension bridges was based on static principles[6]. From then onwards research work on the subject of bridge aerodynamics has grown steadily. The wind induced dynamic response of long span bridges can be classified into three major categories depending on the mechanism involved [12]. These are:

(i) Flutter, in which the bridge deck displays exponentially growing motions that are limited only by structural non-linearities or failure.

(ii) Buffeting response, in which the bridge moves in random manner that reflects the random character of wind, but is stable.

(iii) Vortex induced response, in which vortex shedding lock-in effects occur (characterised by the wake of the bridge deck forming a street of alternating vortices). When the frequency of eddy shedding approximately coincides with the natural frequency of the bridge, large oscillations would be induced. Unlike flutter instability, the motion associated with vortex-shedding is self limiting.

An experimental study to determine the relevant aerodynamic coefficients from section model tests of the deck of a cable bridge is one possible approach, which has been adopted in the present study. It is possible to predict the aerodynamic response as well as the stability of typical cable stayed bridges using these experimentally obtained aerodynamic coefficients. Other techniques include the full scale model testing and the so called taut-strip model representing the full deck of the bridge.

1.2 BRIEF REVIEW OF LITERATURE

A considerable amount of research and investigation have gone into the study of the

behaviour of these bridges under wind loads after the collapse of Tacoma Narrows bridge. To study the behaviour of a bridge under wind, it is essential to carry out wind tunnel tests. Such tests are carried out either on a model of the full bridge, or a taut-strip model or on a section model. Most of the early wind tunnel studies had been carried out under smooth or gusty wind conditions. There are only very few instances[3,10] wherein the wind tunnel tests have been carried out under grid generated turbulent flows, which offer the advantage of simulating the eddy sizes present in the turbulent wind and expressed by the integral length scale.

Scanlan et al.[9,10] have done much useful work in the direction of bridge aerodynamics and they developed the system identification technique to extract the flutter derivative coefficients from section model tests, which are a most useful set of parameters for analytical evaluation of the bridge response including instability criterion. Scanlan & Lin [10] made an attempt to study the effect of turbulence on flutter derivative coefficients using a standard aluminium channel section to represent the bridge deck. Okauchi et al.[5] observed the response by testing a large scale section model(1:10) in field. Houston[2] tested some H-type and rectangular sections to update the data bank of flutter derivatives under smooth and turbulent flows. In an attempt to increase the stability of an unstable bridge deck, Houston et al.[3] tested an unstable bridge deck with the addition of fairings to the sides under suitably scaled actively generated gusty wind flow conditions. Shengpei et al.[11] have tabulated flutter derivative coefficients for various b/d ratios of rectangular sections with and without fairings. Bosch[1] examined the aeroelastic behaviour of an unstable cable stayed bridge section under smooth flow and with various wind incidence angles. Recently Sarkar et al.[7] have developed a system identification technique to estimate flutter derivative coefficients from a single two degree of freedom section model test along with the use of numerical simulation. Jones et al.[4] studied the effect of section model details on aeroelastic parameters in particular to the details of railings of a particular cable stayed bridge.

1.3 PROBLEM IDENTIFICATION AND SCOPE OF THE WORK

From a brief review of the earlier works, it has been observed that various investigators have considered the common bridge deck shapes like box girder and truss stiffened decks (Fig.1.2). Recently one of the cable stayed bridge adopted the composite construction with I-section as the main (and cross) girders[8] and a roadway slab on top of the girders, as shown in Fig.1.3. Some of the other bridges in which the composite construction has been employed are Quincy bridge, U.S.A., Annacis Island bridge, Canada and Sunshine Skyway Alternate, U.S.A.[6]. Therefore, there is a need to examine the girder type composite deck section for its aerodynamic performance.

As seen in the literature, in most of the wind tunnel studies smooth flow or gusty wind flow conditions have been considered. The effect of grid generated flow on the flutter derivative coefficients has not been much investigated. There is a reason, therefore, to conduct wind tunnel studies on section models under grid generated flows.

Further, the effect of integral length scale (L_x) on flutter derivative coefficients of the girder deck section has been a neglected area, calling for more studies.

The research programme undertaken in this study has been aimed at a better and greater understanding of the aerodynamic behaviour of cable stayed bridges with composite concrete slab plus steel girder type decks with a view to establish their aerodynamic stability limits under different flow types (smooth and turbulent) and different wind incidence angles, and finally, to study the improvement possible with different extents of fairings. In order to carry out the stability analysis, as also to evaluate the bridge responses in the stable region of wind velocities, an experimental study was planned on a section model and its variation of a composite deck for cable stayed bridges. From these experiments the aerodynamic coefficients, called flutter derivatives, could be extracted for the deck shapes studied.

The scope of the experimental study is as follows:

(i) To study the behaviour of the section model under smooth flow (turbulence intensity 0.5% - 1.0%) with various wind incidence angles.

(ii) To study the effect of fairings on the behaviour of the same deck under smooth flow for various wind incidence angles.

(iii) To study the change in the values of the flutter derivatives due to change in length scale of turbulence of wind for both partially and fully faired section model.

In order to carry out the above tests the following steps had to be taken:

(i) As the conditions in the tunnel were not suitable for fixing the side supported section model, several modifications had to be made to install the section model in the tunnel.

(ii) Pilot test runs were carried on a standard rectangular deck section to confirm proper working of the modified tunnel and the Data Acquisition System (DAS) and indeed to check the expected performance of the standard deck section.

(iv) The girder bridge deck section models were designed and fabricated. Suitable fairings to be attached subsequently were also prepared.

(v) The unfaired section as well as the model with fairings were tested under smooth flow and with the wind incidence angles ranging from -5 to +5 degrees. Two independent set of tests, one in vertical and other in the torsional degree of freedom were conducted to extract the various flutter derivative coefficients.

(vi) Suitable grids were designed & fabricated to vary the simulated length scale of turbulence (L_x)

(vii) Wind tunnel tests have been carried out on unfaired as well as faired sections of the girder bridge deck under smooth and grid generated turbulent flow conditions in order to study the sensitivity of flutter derivatives to length scale.

Using the results of experimental studies to compute the aerodynamic response of typical cable stayed bridges, two prototype examples were chosen. A three dimensional dynamic analysis was first carried out for these bridges to determine relevant modal parameters and their response determined.

To carry out this investigation, several softwares were written and developed. The first one is to extract the flutter derivative coefficient from the raw data obtained from

the results of the section model tests. Another software was developed for three dimensional dynamic analysis of the cable stayed bridges along with graphic capabilities to plot the three dimensional view of the bridge and its mode shapes.

1.4 ORGANIZATION OF THE THESIS

This thesis consists of 7 chapters which are organized as follows:

A review of the earlier work done in the area of experimental and theoretical aspects of the aerodynamics of bridge is illustrated in Chapter 2.

Chapter 3 explains about the three dimensional dynamic analysis procedure to determine the modal parameters after idealization of the bridge including development of software and the graphic packages. The details of the bridges selected for the present study are also given in this chapter.

Chapter 4 deals with the aerodynamic formulation of the flutter criterion and buffeting response of the prototype bridge.

The facilities used and developed to conduct the extensive experimental work along with the fabrication of the section model and transducers and also the characterisation of the flow are presented in Chapter 5

The experimental results obtained and the analytical responses computed for the prototype bridges are discussed in Chapter 6.

Finally, this piece of work has been concluded in chapter 7. The possible scope for future research work in the area is also suggested.

Appendix-A describes the data acquisition system and steps involved in acquiring strain gauge data.

REFERENCES

1. Bosch,H.R., (1990), "Section Model Studies of the Deer Isle Sedgwick Suspension Bridge", Jnl. of Wind Engg. and Ind. Aero., Vol 36, pp 601-610.

2. Houston,D.R., (1987), "Flutter Derivatives from 14 Generic Deck Sections", Proc. ASCE Speciality Conference on Bridges and Transmission Line Structures, Lambert Tall, Orlando, pp 281-291.

3. Houston,D.R., H.R.Bosch, and R.H.Scanlan, (1988), "The Effects of Fairings and of Turbulence on the Flutter Derivatives of a Notable Unstable Bridge Deck", Jnl. of Wind Engg. and Ind. Aero., Vol 29, pp 339-349.

4. Jones,N.P., R.H.Scanlan, P.P.Sarkar, and L.Singh, (1993), "The Effect of Section Model Details on Aeroelastic Phenomena", Proc. of III APSOWE, Hongkong, pp 71-76.

5. Okauchi,I., J.Tajima, and H.Akiyama, (1979), "Response of the Large Scale Bridge Model to Natural Wind", Proc. of V ICWE, Colorado, U.S.A., pp 841-852.

6. Podolny,W.Jr. and J.B.Scalzi, (1989), "Construction and Design of Cable Stayed Bridges", IInd Ed., John Wiley & Sons.

7. Sarkar,P.P., N.P.Jones, and R.H.Scanlan, (1992), "System Identification for estimation of flutter derivatives", Jnl. of Wind Engg. and Ind. Aero., Vol 41-44, pp 1243-1254.

8. Sastry,M.V., (1985), "The Second Hoogly Bridge at Calcutta", Indian Concrete Journal, June 1985, pp. 7-9.

9. Scanlan,R.H., and J.Tomko, (1971), "Airfoil and Bridge Deck Flutter Derivatives", Jnl. Engg Mech Div., ASCE, Vol.97, No. EM6, Dec., pp 1717-1737.

10. Scanlan,R.H., and W.H.Lin, (1978), "Effects of Turbulence on Bridge Flutter Derivatives", Jnl. Engg Mech Div., ASCE, Vol. 104, No. EM4, Aug., pp 719-733.

11. Shangpei,L., and Chen Xin, (1989), "Experimental Identification of Flutter Derivatives from Several Typical Deck Sections", Proc. II APSOWE, China, pp 610-617.

12. Simiu,E., and R.H.Scanlan, (1986), "Wind Effects on Structures", IInd Edition, John Wiley ltd.

13. "The Failure of the Tacoma Narrows Bridge", (1944), Bulletin of the Agri. and Mech. College of Texas, Vol. 15, no. 1, Jan.
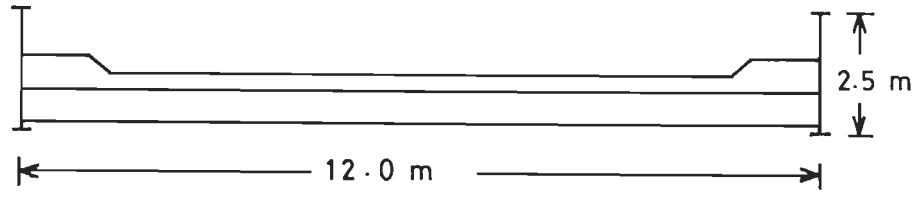
Fig.1.1 Line diagram of the old Tacoma Narrows bridge deck
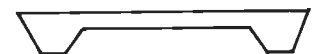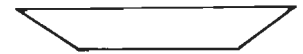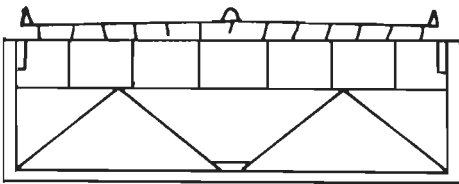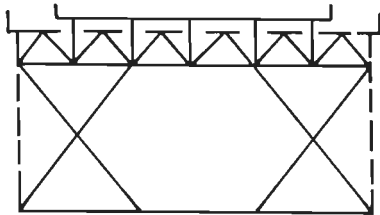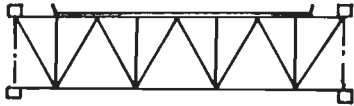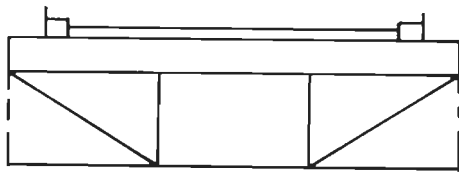
(a) TRUSS STIFFENED DECKS

(b) BOX GIRDER DECKS
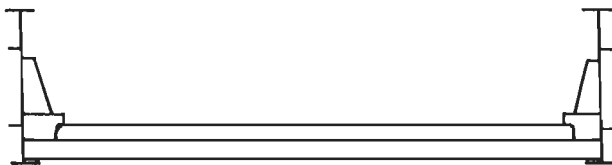
(c) COMPOSITE DECK

Fig.1.2 Some of the deck shapes studied in earlier investigations
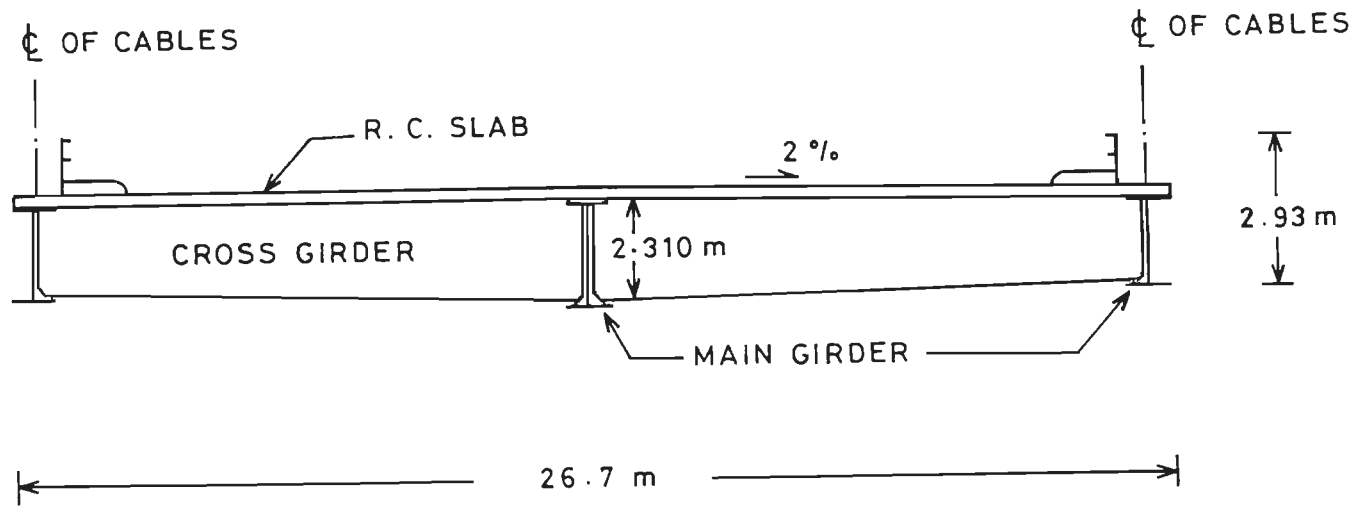
Fig.1.3 Composite I-girder deck investigated

CHAPTER 2
LITERATURE REVIEW

2.1 INTRODUCTION

With the failure of Tay Bridge in 1879, the need for a better understanding of wind load on civil engineering structures was felt. Further, till the failure of Tacoma Narrows bridge in 1940 the wind loads were used to be represented by equivalent static loads. It was only from then onwards that a deep general realization of the potential aeroelastic nature (air-structure interaction) of the phenomena was firmly emphasized. In case of wind induced oscillations the most affected component of the bridge structure is the deck. The types of aerodynamic instabilities are flutter, buffeting and vortex shedding responses.

The original focus of aeroelastic studies on bridge models was the flutter problem, since flutter had destroyed the original Tacoma Narrows Bridge. Flutter is self-excited oscillation that sets in at some critical cross-wind velocity and does not diminish, but instead increases in severity and finally ends up in the collapse of the structure. This is because the associated aerodynamic forces induce negative damping in the system which works as an energy feeder for the system. The phenomenon can best be studied through controlled wind tunnel experiments on bridge models with adequate simulation of the essential parameters, if not all the parameters involved in the physical system. In wind tunnel investigations it is possible to use three different types of models[33], described below.

2.1.1 Full Bridge Models

These models must be geometrically similar to the prototype bridge, in addition they

must satisfy the similarity requirements pertaining to mass distribution, reduced frequency, mechanical damping and shapes of vibration modes. A detailed treatment of the similarity requirements is given in reference[12]. The construction of full-scale bridge models is thus elaborate and their cost is therefore relatively high. Generally the order of the scale used has been around 1/300, although a scale of 1/100 has been used in a few cases.

2.1.2 Taut-Strip Models

The taut-strip model was first introduced by Davenport in 1972[5]. In these models two wires stretched across the wind tunnel serve as the basic inner structure, which is then externally clad to geometrically resemble a given bridge. The tensioned wire selected must represent to scale the fundamental bending and torsional frequencies and mode shapes of the bridge. Such models represent the central portion of suspended bridges.

2.1.3 Section Models

Section models consist of representative spanwise sections of the deck constructed to scale, spring supported at the ends to allow both vertical and torsional motion, and, usually enclosed between end plates to reduce aerodynamic end effects. Section models are relatively inexpensive. They can be constructed to scales of the order 1/60 to 1/25.

2.2 OVERVIEW OF LITERATURE

One of the earliest theoretical approach on bridge aeroelasticity was based on flat plate theory by Bleich in 1948[2] which served as the basis for the subsequent development. In the absence of adequate aerodynamic data he defended and used Theodorsen thin airfoil aerodynamics[8] for truss stiffened decks. Despite of this improvement the analysis resulted in incorrect predictions of bridge flutter because the Theodorsen theory could not be correctly applied to bluff bodies such as bridge decks.

Later after the collapse of Tacoma Narrows bridge, Farquharson during 1949-1954[6] carried out work to diagnose the fault in original Tacoma Narrows bridge and further developed a stable configuration for its replacement. Farquharson was also the first to make

static and dynamic wind tunnel tests on a model of the Old Tacoma Narrows Bridge in 1941 at the University of Washington. From 1942 to 1943 another aerodynamic research program on the Old Tacoma Narrows bridge was carried out by Dunn[37] under the direction of Von Karman at the California Institute of Technology. Both groups obtained similar experimental results.

Parallel to the above works, an experimental investigation of the aerodynamic stability of suspension bridges with special reference to proposed Severn bridge was carried out by Frazer et al.[7] and Scruton[31] in England, using full-scale as well as section models. The deck of Severn bridge was a Truss Stiffened one. The general conclusion drawn was that Truss stiffened decks are stable in vertical motion but they will have tendency for instability in torsional oscillations. Further, they concluded that the test on section model was adequate enough to predict the aerodynamic stability.

In mid 1960's a method was developed in Japan by Ukeguchi et al.[34] to extract flutter derivatives (aerodynamic coefficients accompanying bridge deck oscillations) of bridge decks for use in the analytical study of bridge flutter stability. The method used a machine to drive a rigid bridge deck section model through a certain prescribed oscillation amplitude, at a range of frequencies, in the wind tunnel. A key item was the simultaneous oscillation of a dummy model outside the air stream, in order to develop equal and opposite inertial forces which were subtracted from the measured total force to obtain the net forces of aerodynamic origin.

In U.S.A. during 1967 a comparatively simpler technique, the so called 'free-vibration' method was initiated at the George Vincent Wind Tunnel by Scanlan and Sabzevari[24]. Essentially the method allows the free oscillation of the bridge deck model of a part of the span in a cross wind and infers the appropriate flutter derivatives from system identification techniques applied to the study of the model oscillatory response to various values of the reduced velocities U/nB. This method gained its advantage because of its simplicity as well as accuracy. Use of the method has been illustrated by testing the section model of the original Tacoma Narrows Bridge.

Sabzevari and Scanlan[21] tested various box girder deck shapes using section models of the same. From the experimentally obtained coefficients, along with the analytical flutter criteria, three parameters were stated for the general aerodynamic stability of suspension bridges, they are (i) the shape, (ii) torsional stiffness and (iii) the damping.

The free oscillation technique developed earlier by Scanlan and Sabzevari[20,21,24] was fully exploited later by Scanlan and Tomko[25]. They presented the test results carried out on various deck shapes, like truss-stiffened, box girders and H-shaped sections in the form of aerodynamic flutter coefficients in non-dimensional form. The study carried out was confined to low Reynolds numbers ($< 10^5$), and simulation under laminar flow conditions. This amounted to be the shortcomings of the study, since it fell short of duplicating true full scale flow conditions.

The free vibration technique under laminar flow has further been used by Gade[9] in U.S.A and by a group under Wardlaw[35] in Canada to obtain flutter derivative coefficients.

Whereas the earlier works were carried out in smooth flow conditions, it was well recognised that the fluctuations in wind velocity could alter the aerodynamics of the deck sections. In 1977 attempt was made by Scanlan et al.[27] and Lin[14] to study the effect of turbulence on bridge flutter derivatives. They utilized power spectral density method to obtain the flutter derivative coefficients for a channel section taken for the bridge deck. The obtained flutter derivative coefficients were compared with those determined for laminar flow, and it was found that the two did not differ much for the model selected. But it was suggested that it may not be the same for the actual bridge decks, since decks are more bluff in shape.

A comprehensive report on the action of flexible bridges under wind with respect to flutter theory was made by Scanlan[28] in 1978. Here, some of the modal parameters of the bridge deck, like the generalized mass, inertia and various modal constants, were utilized to study the aerodynamic performance of the full bridge under flutter conditions using the experimentally obtained flutter derivative coefficients. Further, Scanlan et al.[26]

illustrated the use of flutter derivatives to predict the response of bridge under gusty wind by taking two typical bridges with principal attention to vertical and torsional responses.

Okauchi et al.[17] have studied the response of a large scale bridge deck section model (1/10 scale) under natural wind by collecting response data for three years. Their study and comparison of results of the data indicated the reliability of results obtained from wind tunnel section model tests. Thus establishing the section model approach, which is only partly experimental, on a firm footing.

During 1970's an abridged version of the full model was introduced by Davenport[5]. This is the so-called "Taut-Strip" model technique for testing quite small, three dimensional scaled models under scaled turbulence. In this technique, careful observation and interpretation of the model action are necessary for correct prediction of the prototype behaviour. However, the taut strip model gives a direct impression of the prototype performance.

In continuation of the research on the taut-strip model Wardlaw et al.[36] have studied the effect of turbulence on the aerodynamic behaviour of taut-strip model and compared the results with that of the section model. Comparison has been made for different flow conditions. From the experiments it was observed that the plate girder and box sections are prone to vortex shedding excitation in smooth flow. The same still appears in turbulent flow but with smaller amplitudes.

Bienkiewicz et al.[1] studied the effects of turbulence on H-type bridge section model. The results of their tests show that turbulence significantly affects the response and the flutter derivatives. Further, from the values of the flutter derivatives it was clear that the tested bridge deck should be aerodynamically more stable in turbulent flows than in a smooth flow.

Scanlan and Houston[29], used active turbulence generators by means of flapping airfoils to simulate the prototype wind gustiness. The flapping airfoils were made to flap

in such a way as to get required wind gusts with pre-selected frequency. From the study carried out it was justified that the motion dependant aerodynamic forces depend on the presence of upstream wind gustiness.

Houston[10] reported useful data with respect to flutter derivative coefficients for some generic sections like H-type and rectangle sections, with different depth to width aspect ratio. It was an attempt to standardize the bridge deck section model technique.

Scanlan[30] illustrated the analysis for flutter criterion based on the experimentally obtained flutter derivatives and the modal data obtained from free vibration analysis. Based on the interpretation of various aeroelastic models, the section model testing technique proves to be sufficient as well as accurate in predicting the responses.

It was thought that the stability of an unstable bridge section can be improved by adding suitably designed fairings by Houston et al.[11]. They studied the effect of fairings along with turbulence on the flutter derivatives using an unstable bridge deck section similar to the shape of the Old Tacoma Narrows bridge deck. Results indicate that the addition of various extent of fairing coverage to the deck will enhance the stability of the section.

In China, Shangpei et al.[32] have presented test results of flutter derivative coefficients for several typical bridge deck models including rectangular and H-section, both with and without fairings. The influence of deck section geometry and upstream flow turbulence has been considered for discussion. The tests were mainly aimed at obtaining results which can be compared with the results obtained at different wind tunnel laboratories by other investigators in order to find the cause of tunnel discrepancies.

Bosch[3] conducted a section model study on 1:25 scale model of the Deer Isle Sedgwick suspension bridge, to evaluate the overall aerodynamic performance of the bridge. Modifications, particularly in sectional shapes were also made and evaluated to improve the aerodynamic performance of the bridge. Bosch[4] has also carried out a more recent wind tunnel investigation on the truss stiffened deck of a cable stayed bridge, using 1:60 scaled

section model. A parametric study has been carried out with respect to wind incidence angles ranging form -4 to +6 degrees. Under these conditions the bridge section model showed almost hardly any tendency for vertical motion. But the sections have shown sensitivity towards the vortex induced torsional vibrations over the full range of wind angles. The critical velocities reported will still contain a degree of conservatism since the tests ʳwere conducted solely in smooth flow.

Wind tunnel tests of the proposed suspension bridge for Great Belt link have been conducted at the Denmark Maritime Institute by Reinhold et al.[19]. They have compared the buffeting response of the bridge obtained from the section model and the taut-strip model approach. The predicted response levels are quite similar although the turbulence levels were different in the two cases.

In Japan, full-scale model studies have been carried out using especially designed large wind tunnels. Miyata et al.[15,16] conducted preliminary tests to choose the most appropriate deck shape for the proposed largest suspension bridge (main span of 1990 m). The big boundary layer wind tunnel of cross section 41m x 19.5 m was built and the proposed Akashi Kaikyo bridge 1:100 full model was tested to predict the response of the bridge.

Recently in U.S.A. Sarkar et al.[23] have modified the system identification method to estimate the cross flutter derivative coefficients. This will be of help in case of coupled flutter analysis. They described the system identification procedure to extract the flutter derivative data simultaneously from a single experiment using a flexibly mounted two degree of freedom model by identifying the effective damping and stiffness matrices. The method described works better than the conventional logarithmic decrement method under a very noisy signal condition.

Jones et al.[13] studied the effect of railing details on the aeroelastic parameters using a section model. It was shown that some of the flutter derivative coefficients seem to be very sensitive to the small details of the deck.

Scanlan et al.[38] present an analytical method based on a flutter derivative

formulation for wind induced response of cable stayed bridge structures. In this investigation the flutter criterion for a twin-deck cable-stayed bridge - with side-by-side roadways was evolved in two stages- for configurations during erection and for the completed bridge. Attention has been given to the effects of turbulence present in the incoming flow. The flutter derivative approach was effectively used to explain the phenomena that could occur in practice.

Sato and Toriumi[39] have briefly presented the bridge aerodynamic stability criteria in the 'Wind Resistant Design Manual for Highway Bridges in Japan'. The Manual draws mainly upon the experience gained from the wind resistant design of Honshu-Shikoku bridges in Japan, and is useful for understanding the behaviour of long span bridges. In the Manual an attempt has been made to put forward generalised guidelines applicable to the most adverse conditions that have been met over a wide range of bridges for the wind resistant design. Criteria for wind induced vibrations like Flutter, Galloping, Vortex induced vibrations and Gust response have been expressed through simplified formulae.

2.3 OBJECTIVES OF THE PRESENT STUDY

From the review of the literature carried out it has been observed that most of the investigators have studied either truss stiffened or box girder bridge deck of suspended bridges. Recently some of the cable stayed bridge decks are coming up with composite construction [18,22]. Therefore it was decided to analyse the composite I-Girder type deck cable stayed bridge in the present study under wind loads for flutter and buffeting. Flutter being of greatest importance due to its destructive nature and buffeting, yielding the deformations in the stable range of wind speed, were chosen for the study.

Further, since only a few investigators have studied the effect of turbulence on the flutter derivative coefficients, it was considered to investigate the effect of turbulence, along with the change in length scale of turbulence, on the flutter derivative coefficients of the composite deck types.

As observed from the literature, a modification in the geometric shape of the bridge

deck with fairings yields some improvement in the stability of bridge. It is therefore considered worthwhile to examine the variations in flutter derivative coefficients with the addition of fairings to the deck.

The flutter derivative coefficients have been used to predict the flutter criterion and the buffeting response of the full bridge. Therefore, with the use of modal data of the bridge deck and the flutter derivatives to be obtained from the section model tests it was decided to analyse the bridge chosen in the experimental study to determine the flutter criterion, and also to predict the buffeting response.

Further, flutter derivatives obtained for a bridge deck have been employed to analyse another bridge with the same shape of the deck but having a different span and other characteristics. Information in the literature on this aspect is lacking, but it is reasonable to assume similarity in the forces exerted on bluff bodies of similar shape provided the flow parameters do not change. In the case of aeroelastic systems, two more parameters enter the scene and these are amplitude and frequency of vibration. The former would cause a variation in the wind incidence angle over a full range oscillation cycle, which inturn may alter the corresponding flow pattern. A change in the frequency would alter the time scale visa-a-vis the major eddy/turbulent frequency. Besides the cross-sectional problems discussed hitherto, there is the additional effect of the mode shape describing the distribution of the vibration amplitude over the entire length of the structure. This however, would be taken care of by the various modal integrals in the response equation.

Thus it is assumed that the various parameters discussed above would meet the similarity conditions for the non-dimensional analysis to be applicable, at least within a certain range of parameters for the particular structure on which experimental study was conducted. With these assumptions another bridge was chosen to analyse for flutter criterion and to predict the buffeting response.

References

1. Bienkiewicz,B., J.E.Cermak, and J.A.Peterka, (1987), "Wind Tunnel Study of Aerodynamic Stability and Response of Cable Stayed Bridge Deck", Jnl. of Wind Engg. and Ind. Aero., Vol. 26, pp 341-352.

2. Bleich,F., (1948), "Dynamic Instability of Truss Stiffened Suspension Bridges under Wind Loads", Proc. ASCE, Vol.74, Oct., pp 1269-1314.

3. Bosch,H.R., (1990), "Section Model Studies of the Deer Isle Sedgewick Suspension Bridge", Jnl. of Wind Engg. and Ind. Aero., Vol. 34, pp 601-610.

4. Bosch,H.R., (1990), "Aerodynamic Stability of A Truss Stiffened Cable Stayed Bridge", Jnl. of Wind Engg. and Ind. Aero., Vol. 34, pp 1331-1340.

5. Davenport,A.G., (1972) "The use of Taut-Strip Model in the Prediction of the Response of Long Span Bridges to Turbulent Winds", Proc. of Flow Induced Structural Vibration, Karlshrushe, pp 373-382.

6. Farquharson,F.B., F.C.Smith, and G.C. Vincent, (1949-1954), "Aerodynamic Stability of Suspension Bridges", Parts 1 to 5, Bulletin 116 , Structural Research Lab., University of Washington.

7. Frazer,A.C., and C.Scruton, (1952), "Aerodynamic Investigations of Proposed Severn Suspension Bridge", N.P.L., Aero, 222.

8. Fung,Y., (1955), "An Introduction to the Theory of Aeroelasticity", John Wiley & Sons, Inc., N.Y.

9. Gade,R.H., (1974), "Status of the Investigation of the Aerodynamic behaviour of the Sitka Harbor Bridge", Symp. on Full Scale Measurements of Wind Effects on Tall Buildings and other Structures, London, Ontoria, Canada, June.

10. Houston,D.R., (1987), "Flutter Derivatives from 14 Generic Deck Sections", Proc. of ASCE Structural Congress on Bridges and Transmission Line Structures, Orlando, pp 281-191.

11. Houston,D.R., H.R.Bosch, and R.H.Scanlan, (1988), "The Effect of Fairings and Turbulence on Flutter Derivatives of a Notably Unstable Bridge Deck", Jnl. of Wind Engg. and Ind. Aero., Vol. 29, pp 339-349.

12. Irwin,P.A., (1992), "Full Aeroelastic Model Tests", Proc. of Aerodynamics of Large Bridges, Balkema, Rotterdam, pp 125-135.

13. Jones,N.P., R.H.Scanlan, P.P.Sarkar, and L.Singh, (1993), "The Effect of Section Model Details on Aeroelastic Parameters", Proc. III APSOWE, Hongkong, Dec. 1993, pp 71-76.

14. Lin,W.H., (1977), "Forced and Self Excited Response of Bluff Structure in a Turbulent Wind", Ph.D., Dissertation, Princeton University, U.S.A.

15. Miyata,T., K.Yokoyama, M.Yasuda, and Y.Hikami, (1992), "Akashi Kaikyo Bridge: Wind Effects and Full Model Tests", Proc. Aerodynamics of Large Bridges, Copenhagen, Denmark, pp 217-236.

16. Miyata,T., H.Yamada, M.Yasuda, and H.Morikawa, (1992), "Aerodynamics of Wind Effects on Long Span Cable Supported Bridges", Proc. of IASS-CSCE, Int. Congress 1992, Innovative Large Span Structures, Vol. 1, pp 243-254.

17. Okauchi,I., J.Tajima, and H.Akiyama, (1979), "Response of the Large Scale Bridge Model to Natural Wind", Proc. of V ICWE, pp 841-852.

18. Podolny,W.Jr. and J.B.Scalzi, (1989), "Construction and Design of Cable Stayed Bridges", IInd Ed., John Wiley & Sons, N.Y.

19. Reinhold,T.A., M.Brinch and A.Damsgaard, (1992), "Wind Tunnel Tests for the Great Belt Link", Proc. Aerodynamics of Large Bridges, Copenhagen, Denmark, pp 255-267.

20. Sabzevari,A., and R.H.Scanlan, (1968), "Aerodynamic Instability of Suspension Bridges", Jnl. of Engg. Mech. Div., Proc. ASCE, Vol. 94, April, pp 489-519.

21. Sabzevari,A., and R.H.Scanlan, (1969), "Aerodynamic Investigations of Box Girder Bridges", Jnl. of Struct. Div., Proc. ASCE, Vol. 95, No. ST7, July, pp 1517-1532.

22. Sastry,M.V, (1985), "The Second Hoogly Bridge at Calcutta", Indian Concrete Journal, Jan., pp 7-9.

23. Sarkar,P.P., N.P.Jones, and R.H.Scanlan, (1992), "System Identification for Estimation of Flutter Derivatives", Progress in Wind Engineering, Jnl. Wind Engg. and Ind. Aero., Vol, 41-44, pp 1243-1254.

24. Scanlan,R.H., and A.Sabzevari, (1969), "Experimental Aerodynamic Coefficients in the Analytical Study of Suspension Bridge Flutter", Jnl. of Mechanical Engg. Science, Vol. 11, No. 3, pp 234-242.

25. Scanlan,R.H., and J.Tomko, (1971), "Airfoil and Bridge Deck Flutter Derivatives", Jnl. of Engg. Mech. Div., Proc. ASCE, Vol. 97, Dec., pp 1717-1737.

26. Scanlan,R.H., and R.H.Gade, (1977), "Motion of Suspended Bridge Spans under Gusty Wind", Jnl. of Structural Div., ASCE, Vol.103,ST9, September, pp 1867-1883.

24

27. Scanlan,R.H., and W.H.Lin, (1978), "Effects of Turbulence on Bridge Flutter Derivatives", Jnl. Engg. Mech. Div., Proc. ASCE, Vol. 104, Aug. 1978, pp 719-733.

28. Scanlan,R.H., (1978), "The Action of Flexible Bridges under Wind-I Flutter Theory", Jnl. Sound and Vibration, Vol. 60-2, pp 187-199.

29. Scanlan,R.H., and D.Houston, (1985), "Sensitivity of Bridge Decks to Turbulent Wind", Proc. I APSOWE, Roorkee, India, pp 167-172.

30. Scanlan,R.H., (1987), "Interpreting Aeroelastic Models of Cable Stayed Bridges", Jnl. of Engg. Mechanics Div., ASCE, Vol.113,EM4, April, pp 555-575.

31. Scruton,C., (1960), "An Experimental Investigation of the Aerodynamic Stability of Suspension Bridges with Special Reference to the Proposed Severn Bridge", I.C.E. London, pp 189-222.

32. Shangpei,L and Chen Xin, (1989), "Experimental Identification of Flutter Derivatives from Several Typical Deck Sections", Proc. II APSOWE, China, pp 610-617.

33. Simiu, E., and R.H.Scanlan, (1986), "Wind Effects on Structures" II Ed., John Wiley and Sons, N.Y.

34. Ukeguchi,N., H.Sakata, and H.Nishitani, (1966), "An Investigation of Aeroelastic Instability of Suspension Bridges", Proc. Int. Symposium on Suspension Bridges, Lisbon, pp 79-100.

35. Wardlaw,R.L., (1971), "Some Appraoches for Improving the Aerodynamic Stability of Bridge Road Decks", Proc. III Int. Conf. on Wind Effects on Buildings and Structures, Tokyo, Japan, Sept.

36. Wardlaw,R.L., H.Tanaka, and H.Utsunomiya, (1983), "Wind Tunnel Experiments on the Effects of Turbulence on the Aerodynamic Behaviour of Bridge Road Decks", Proc. VI ICWE, Australia/Newzealand, pp 1-11.

37. "Experimental Investigations on the Aerodynamic Characteristics of the Suspended Structure of the Tacoma Narrows Bridge", (1944), Bulletin of Agri. and Mech. College of Texas, Vol. 15, Appendix - VIII.

38. Scanlan,R.H., and N.P.Jones, (1990), "Aeroelastic Analysis of Cable Stayed Bridges", Jnl. Strul. Engg. Div., Proc. ASCE, Vol. 116, No.2, Feb. 1990, pp 279-297.

39. Sato,H., and R.Toriumi, (1994), "On the Wind Resistant Design Manual for Highway Bridges in Japan", National Seminar on Wind Loads- Codal Provisions, April 1994, Structural Engg. Research Centre, Ghaziabad, India, pp 13-1 to 13-15.

CHAPTER 3
FREE VIBRATION ANALYSIS OF THE BRIDGE

3.1 INTRODUCTION

The natural frequencies, mode shapes and associated modal parameters form a part of the basic data, which along with the flutter coefficients help to evaluate the response of the bridge under the action of wind loads. The present chapter is devoted to the description and the use of three-dimensional free vibration analysis for the estimation of the dynamic characteristics of a cable stayed bridge. Further the results of free vibration analysis for the bridges considered in the study are illustrated.

3.2 THE CABLE STAYED BRIDGE DEFINED

The main components of a composite deck cable stayed bridge are:

(i)the deck consisting of a reinforced concrete slab resting on cross girders and the longitudinal main girders,

(ii)the towers providing support to the deck,

(iii)the cables tied to the top of the towers and at points of the deck thus supporting the deck, and

(iv)the piers and foundations

The bridge structure can be idealized as a skeleton structure with high kinematic indeterminacy.

3.2.1 Idealization as Space System

The bridge is represented by a rigid jointed three dimensional skeletal structure for the free vibration analysis. The deck girders along with the slab are replaced by transverse and longitudinal elements of appropriate mass and stiffnesses. Assumptions made for simplification of the analysis are:

(i)The cables possess only axial stiffness and are completely flexible otherwise.

(ii)The nodes are taken at the points of intersections, points of supports and at intermediate points along the height of the tower.

(iii)The deck is supported on the substructure through a hinge at one end and rollers at the other end support.

(iv)The mass of the central girder and its mass moment of inertia have been distributed to the end main girders and cross girders.

3.2.2 The Stiffness Approach

Dynamic analysis of the bridge has been carried out using a computer programme for analysis of three dimensional frames. Stiffness approach is chosen for the analysis since it has the advantage of utilizing the banded formulation.

3.2.2.1 Element Stiffness Matrix

Fig.3.1 shows a beam segment of three dimensional frame with its 12 nodal coordinates. The general convention is adopted to label the three translatory displacements and three rotational displacements of a joint.

The stiffness matrix for a 3-D uniform beam segment is readily written by the superposition of the flexural stiffness matrix of a plane frame beam element, the axial stiffness matrix of a plane prismatic beam and the torsional stiffness matrix of a grid beam[6].

(i)The flexural stiffness matrix of the plane frame beam element shown in Fig.3.2 can be written as,

$$
\begin{Bmatrix} P_1 \\ P_2 \\ P_3 \\ P_4 \end{Bmatrix} = \frac{2EI}{L^3} \begin{bmatrix} 6 & 3L & -6 & 3L \\ 3L & 2L^2 & -3L & L^2 \\ -6 & -3L & 6 & -3L \\ 3L & L^2 & -3L & 2L^2 \end{bmatrix} \begin{Bmatrix} \delta_1 \\ \delta_2 \\ \delta_3 \\ \delta_4 \end{Bmatrix}
\tag{3.1}
$$

(ii)the axial stiffness matrix of plane frame prismatic beam segment shown in Fig.3.3 will be,

$$
\begin{Bmatrix} p^1 \\ p^2 \end{Bmatrix} = \frac{AE}{L} \begin{bmatrix} 1 & -1 \\ -1 & 1 \end{bmatrix} \begin{Bmatrix} \delta^1 \\ \delta^2 \end{Bmatrix}
\tag{3.2}
$$

and (iii) the torsional stiffness matrix of a grid beam element shown in Fig.3.4 can be written as,

$$\left\{ \begin{array}{c} P_1 \\ P_2 \end{array} \right\} = \frac{JG}{L} \left[\begin{array}{cc} 1 & -1 \\ -1 & 1 \end{array} \right] \left\{ \begin{array}{c} \delta_1 \\ \delta_2 \end{array} \right\} \tag{3.3}$$

The flexural stiffness matrix of plane frame beam (eqn.3.1) is used twice in forming the stiffness matrix of a three dimensional beam segment to account for the flexural effects in the two principal planes of the cross section. Proceeding to combine these matrices (eqns.3.1, 3.2 and 3.3), we get eqn.3.4, the stiffness equation for a uniform beam segment of a 3-D frame, as follows

$$\left[\begin{array}{c} P_1 \\ P_2 \\ P_3 \\ P_4 \\ P_5 \\ P_6 \\ P_7 \\ P_8 \\ P_9 \\ P_{10} \\ P_{11} \\ P_{12} \end{array} \right] = \left[\begin{array}{cccccccccccc} \frac{EA}{L} & & & & & & & & & & & \\ 0 & \frac{12EI_z}{L^3} & & & & & & & & & & \\ 0 & 0 & \frac{12EI_y}{L^3} & & & & & & & & & \\ 0 & 0 & 0 & \frac{GJ}{L} & & & & \text{SYMMETRICAL} & & & & \\ 0 & 0 & \frac{-6EI_y}{L^2} & 0 & \frac{4EI_y}{L} & & & & & & & \\ 0 & \frac{6EI_z}{L^2} & 0 & 0 & 0 & \frac{4EI_z}{L} & & & & & & \\ \frac{-EA}{L} & 0 & 0 & 0 & 0 & 0 & \frac{EA}{L} & & & & & \\ 0 & \frac{-12EI_z}{L^3} & 0 & 0 & 0 & \frac{-6EI_z}{L^2} & 0 & \frac{12EI_z}{L^3} & & & & \\ 0 & 0 & \frac{-12EI_y}{L^3} & 0 & \frac{6EI_y}{L^2} & 0 & 0 & 0 & \frac{12EI_y}{L^3} & & & \\ 0 & 0 & 0 & \frac{-GJ}{L} & 0 & 0 & 0 & 0 & 0 & \frac{GJ}{L} & & \\ 0 & 0 & \frac{-6EI_y}{L^2} & 0 & \frac{2EI_z}{L} & 0 & 0 & 0 & \frac{6EI_y}{L^2} & 0 & \frac{4EI_y}{L} & \\ 0 & \frac{6EI_z}{L^2} & 0 & 0 & 0 & \frac{2EI_z}{L} & 0 & \frac{-6EI_z}{L^2} & 0 & 0 & 0 & \frac{4EI_z}{L} \end{array} \right] \left[\begin{array}{c} \delta_1 \\ \delta_2 \\ \delta_3 \\ \delta_4 \\ \delta_5 \\ \delta_6 \\ \delta_7 \\ \delta_8 \\ \delta_9 \\ \delta_{10} \\ \delta_{11} \\ \delta_{12} \end{array} \right]$$

(3.4)

or in condensed notation

$$\{P\} = [K]\{\delta\} \tag{3.5}$$

in which I_y and I_z are respectively the cross section moments of inertia with respect to the principal axes labeled as Y and Z in Fig.3.1 and L, A and J are respectively length, cross sectional area and torsional constant of the beam element.

The general stiffness matrix given in eqn.3.4 can be simplified for cases of members where the end conditions are specified, like the simple truss members with no rotational restraint, the cables having no flexural rigidity or the partially restrained members.

3.2.3 Rotation Transformation Matrix

Rotation matrix R_T is required to transform the member stiffness matrix from member axes to global axes. R_T can be obtained from a rotation matrix (R) expressed in terms of direction cosines of the members.

For space frame member it is given as

$$R_T = \begin{bmatrix} R & 0 & 0 & 0 \\ 0 & R & 0 & 0 \\ 0 & 0 & R & 0 \\ 0 & 0 & 0 & R \end{bmatrix} \tag{3.6}$$

The form of rotation matrix R depends upon the orientation of the member axes. For a member having principal axes of its cross-section lying in horizontal and vertical planes, the member axes are defined as follows:

x is the axis of the member,

y is the axis located in a vertical plane passing through X and Y axes,

z is the axis located in a horizontal plane lying in X-Z plane,

where X, Y and Z refer to the axes of the structure.

For the member axes specified in the manner described above and for inclined members the rotation matrix (R) is

$$R = R_S = \begin{bmatrix} C_X & C_Y & C_Z \\ \dfrac{C_X C_Y}{\sqrt{C_X^2 + C_Z^2}} & \sqrt{C_X^2 + C_Z^2} & \dfrac{-C_X C_Y}{\sqrt{C_X^2 + C_Z^2}} \\ \dfrac{-C_Z}{\sqrt{C_X^2 + C_Z^2}} & 0 & \dfrac{C_Z}{\sqrt{C_X^2 + C_Z^2}} \end{bmatrix}$$

where, $C_X = \dfrac{X_j - X_i}{L}$, $C_Y = \dfrac{Y_j - Y_i}{L}$, $C_Z = \dfrac{Z_j - Z_i}{L}$

and $L = \sqrt{(X_j - X_i)^2 + (Y_j - Y_i)^2 + (Z_j - Z_i)^2}$ (3.8)

X_i, Y_i, Z_i, X_j, Y_j and Z_j refer to the coordinates of the two ends of a member in space.

3.2.4 Element Mass Matrix

The lumped mass matrix of a uniform beam segment in a 3-D frame is simply a diagonal matrix in which coefficients corresponding to translatory and torsional displacements are equal to one half of the total inertia of the beam segment while the coefficients corresponding to flexural rotations are assumed to be zero. The diagonal lumped mass matrix for the uniform beam of distributed mass $\bar{m}$ and polar mass moment of inertia $I_{\bar{m}}$ per unit length may be written conveniently as

$$M = \frac{\bar{m} L}{2} [1 \quad 1 \quad 1 \quad I_{\bar{m}}/\bar{m} \quad 0 \quad 0 \quad 1 \quad 1 \quad 1 \quad I_{\bar{m}}/\bar{m} \quad 0 \quad 0] \tag{3.9}$$

or in condensed form

$$\{P\} = [M] \{\ddot{\delta}\} \tag{3.10}$$

The lumped mass matrix has been preferred over the consistent mass matrix since the difference in results reported earlier is small, being around 1%, for the structure of the kind analysed[10,11].

3.3 FREE VIBRATION ANALYSIS

When a multidegree of freedom system is set into a mode of vibration such that all masses of the system attain maximum amplitudes of that mode simultaneously and, also, all masses pass through the equilibrium position simultaneously, the system is said to vibrate in a natural (or principal or normal) mode of harmonic vibration. When all the masses of the

system vibrate in phase, the mode is the fundamental or the lowest mode of vibration and the frequency associated with this mode is lowest in magnitude. When all the adjacent masses vibrate out of phase with each other, the mode is the highest and the frequency associated with this mode is the highest. The fundamental and a few higher frequencies and modes of a multidegree of freedom system are of primary significance and can be determined, with reasonable accuracy, by the method described in the following articles.

3.3.1 Frequency and Mode Shape Determination

The equation of motion of a multidegree of freedom system can be written as [2,3],

$$[M]_n \{\ddot{X}\}_n + [C]_n \{\dot{X}\}_n + [K]_n \{X\}_n = \{F(t)\}_n \tag{3.11}$$

where,

$[M]$ = mass matrix,

$[C]$ = damping matrix,

$[K]$ = stiffness matrix,

$\{X\}$ = displacement vector,

$\{\dot{X}\}$ = velocity vector,

$\{\ddot{X}\}$ = acceleration vector,

$\{F(t)\}$ = force vector and,

n = order of matrices and vectors.

Considering undamped free vibration, eqn.3.11 reduces to,

$$[M]_n \{\ddot{X}\}_n + [K]_n \{X\}_n = 0 \tag{3.12}$$

If we assume $X = x \sin pt$, eqn.3.12 is converted to

$$K_n x_n = f^2 M_n x_n \tag{3.13}$$

Eqn.3.13 in the form of a standard eigenvalue problem, $A'X = \lambda \cdot B \cdot X$. Inverse iteration techniques coupled with Sturm Sequence procedure (Bathe & Wilson[1]), applied to eqn.3.13 will yield the highest and the subsequent eigenvalues in the descending order. However, to obtain the lowest and a few more eigenvalues in the ascending order, eqn.3.13 can be expressed in the form

$$K_n^{-1} M_n x_n = \frac{1}{f^2} x_n \tag{3.14}$$

Eqn.3.14 retains the analogy of the standard eigenvalue problem, $A'X = \lambda B X$, and yields lowest and higher eigenvalues in required number by repeated application of inverse iteration with sturm sequence techniques. A considerable reduction in computational effort can be achieved by adopting algorithms which take advantage of symmetry of the matrix for eigenvalue determination. The product $K^{-1}M$ of eqn.3.14 is able to maintain symmetry conditionally if $m_1 = m_2 = \ldots = m_n$, where m_1, m_2, ... m_n are the diagonal elements of [M] of order n. In general, this condition may never be achieved and the symmetry can be enforced by resorting to the following transformation:

$$[M^{1/2}]_n [K^{-1}]_n [M^{1/2}]_n [M^{1/2}]_n \{X\}_n = 1/f^2 [M^{1/2}]_n \{X\}_n \qquad (3.15)$$

Substituting,

A'_n (the modified dynamic stiffness matrix) $= [M^{1/2}]_n [K^{-1}]_n [M^{1/2}]_n$,

$Y = [M^{1/2}] \{X\}$

= mode shape vector of the modified dynamic matrix, and,

$\lambda = 1/f^2$ = eigenvalue of the system (which remains unaltered),

we get,

$$[A']_n \{Y\}_n = \lambda \{Y\}_n \qquad (3.16)$$

The eigenvector of the original system (eqn.3.14) may be calculated by,

$$\{X\} = [M^{-1/2}] \{Y\} \qquad (3.17)$$

Eqn.3.16 can be solved by a number of available techniques among which Rayleigh quotient and iteration type of techniques are more popular. The approximation to the Rayleigh Quotient is achieved in the following manner to get the lowest eigenvalue and its associated eigenvector.

Pre multiply both sides of eqn.3.16 by $\{Y^T\}$.

$$\{Y^T\}_n [A']_n \{Y\}_n = \lambda \{Y^T\}_n \{Y\}_n \qquad (3.18)$$

$$\text{of } \lambda = \frac{\{Y^T\}_n [A'] \{Y\}_n}{\{Y^T\}_n \{Y\}_n} \qquad (3.19)$$

The termination criterion of the iterative solution of eqn.3.16

is $\dfrac{\lambda_r^i - \lambda_r^{i-1}}{\lambda_r^i} \leq \varepsilon$ (3.20)

where, λ_r^i = ith iteration for rth eigenvalue

λ_r^{i-1} = (i-1)th iteration for the eigenvalues,

ε = a small quantity, say 0.00001

Another limitation on the iterative procedure can be imposed by specifying the maximum number of iterations.

At the end of the iterative procedure for one particular eigenvalue (λ_r), which is the lowest every time, it is deemed that

$\{X_r\} = \{X_r^i\}$

where $\{X_r\}$ = final mode shape of ith iteration for the rth mode.

3.3.2 Modal Parameters

The modal quantities like generalized mass, inertia and modal integrals required for use in the analytical formulation of aerodynamics of bridges can be obtained from the mode shape of the corresponding bridge. These quantities have been determined considering the deck portion only, since deck is the main component of the bridge considered for subsequent formulations.

The generalized mass is given by

$$m_i = \int\limits_{span} m(x)\, h_i^2(x)\, dx$$ (3.21)

where $m(x)$ is mass per unit span of the deck portion,

and $h_i(x)$ is the dimensionless mode deflection form in the bending mode.

Similarly, the generalized mass moment of inertia will be given by

$$I_i = \int\limits_{span} I(x)\, \alpha_i^2(x)\, dx$$ (3.22)

where $\alpha_i(x)$ is dimensionless mode deflection in torsion mode,

and I is mass moment of inertia per unit span of the deck.

The geometric modal integrals can be defined by the expression as below

$$G_{r_i s_j} = \int_{span} r_i(x) \, s_j(x) \, dx \qquad\qquad (3.23)$$

where r,s = the dimensionless modal deflection h, sway p and torsional rotation α of particular mode i or j.

3.4 DEVELOPMENT OF COMPUTER PROGRAMME

A Software package in Fortran 77 for the 3-D free vibration analysis of bridge, using the stiffness formulation and the solution technique approach described earlier, has been developed and run on IBM compatible PC/AT-486 computer. It is a general purpose package and can be used for the free vibration analysis of other civil engineering structures with slight modification in input data.

In the first step, the stiffness and mass matrices are generated and the iterative technique described earlier is employed for the eigensolution of the equation of the form

$$M \, \ddot{x} + K \, x = 0$$

In the next step the modal parameters like the generalized inertia, mass and geometric integrals, which are to be used for the aerodynamic analysis were computed using various subroutines. The details of the package have been presented through a flow chart given in Fig.3.5.

3.4.1 Graphics Package

A software package in Plot 88[9], to have the visualisation of mode shapes, has been developed and implemented on IBM compatible computers.

The package uses the normalized modal eigenvectors and presents a 3-D view of the various vibration modes.

3.5 TEST EXAMPLE

To illustrate the applicability and validity of the package developed a test example of a simple portal frame was selected and tested using the programme. The values of frequencies and modes obtained from the package are in good agreement with the classical values.

3.6 ANALYSIS OF BRIDGES

Two Cable stayed bridges of span 383 m and 82ℑ m were selected for a detailed the study of their aerodynamic behaviour. These bridge configurations have been numbered in the thesis as #1 [4,5] and #2 [7,8] respectively. The former has the configuration of the Chung Yang Highway Bridge in Taiwan and later that of the second Hoogly bridge at Calcutta. The details of the bridges are shown in Fig.3.6(a) and (b). The deck shape for both the bridges has been assumed to be the same. A composite I-girder as shown in Fig.3.6 was adopted for these bridges. As mentioned earlier both the bridges have been idealized as skeletal frameworks using the stiffness approach. These are shown in Figs.3.7(a) and 3.7(b). Table 3.1 shows the dimensions, number of nodes, members and other details used for the free vibration analysis of the two example bridges considered.

Table 3.1
Details of the bridges considered

Particulars	Bridge #1	Bridge #2
Main Span	199.9 m	457.2 m
Side Spans	92.0 m	182.88 m
No. of Cables	76	136+16bs
Deck Width	26.7 m	35.0 m
Type of Deck	Composite I-Girder	Composite I-Girder
No. of Nodes	144	196
No. of Members	256	404

bs - back stay cables

Figs.3.8 to 3.15 illustrate some of the natural modes obtained for the bridge #1 and bridge #2 using the approach described above. Since, the deck plays a vital role in the aerodynamic behaviour of the total bridge structure, the tower modes and other sway modes are not significant, hence not shown. The Table 3.2 summarizes the natural frequencies of vibration of the various modes obtained from the analysis with the corresponding mode shapes shown in Figs.3.8 to 3.15 .

The modal frequencies and modal integrals corresponding to the bending, sway and torsional mode deflections (for the first 30 modes) for the deck portion of the example bridges studied are listed in Table 3.3(a) and 3.3(b). The results of this section will be utilized to predict the response of the bridges in subsequent chapters.

Table 3.2(a)

Details of Vertical Modes of Bridge #1

Mode No.	Symmetric		Unsymmetric	
	Mode Shape	Freq(Hz)	Mode Shape	Freq(Hz)
1	Fig.3.8(a)	0.491	Fig.3.9(a)	0.656
2	(b)	0.988	(b)	1.283
3	(c)	1.142	(c)	1.768
4	(d)	1.499	(d)	2.120
5	(e)	1.939	(e)	2.123

Table 3.2(b)

Details of Torsional Modes of Bridge #1

Mode No.	Symmetric		Unsymmetric	
	Mode Shape	Freq(Hz)	Mode Shape	Freq(Hz)
1	Fig.3.10(a)	0.606	Fig.3.11(a)	0.769
2	(b)	1.138	(b)	1.262
3	(c)	1.505	(c)	1.359
4	(d)	2.004	(d)	1.801
5	(e)	2.270	(e)	2.401

Table 3.2(c)

Details of Vertical Modes of Bridge #2

Mode No.	Symmetric		Unsymmetric	
	Mode Shape	Freq(Hz)	Mode Shape	Freq(Hz)
1	Fig.3.12(a)	0.352	Fig.3.13(a)	0.429
2	(b)	0.668	(b)	0.810
3	(c)	0.723	(c)	0.833
4	(d)	0.953	(d)	0.854
5	(e)	1.182	(e)	1.030

Table 3.2(d)

Details of Torsional Modes of Bridge #2

Mode No.	Symmetric		Unsymmetric	
	Mode Shape	Freq(Hz)	Mode Shape	Freq(Hz)
1	Fig.3.14(a)	0.395	Fig.3.15(a)	0.874
2	(b)	0.743	(b)	1.047
3	(c)	0.938	(c)	1.080
4	(d)	1.071	(d)	1.314
5	(e)	1.341	(e)	1.398

Table 3.3(a)

Modal Integrals for Bridge #1

Mode	Freq. (Hz)	Ghh	Gpp	$G\alpha\alpha$
1	0.472	0.38597E-08	0.73063E-05	0.92722E-09
2	0.491	0.14148E-04	0.64634E-10	0.48166E-13
3	0.579	0.49878E-19	0.20568E-06	0.61758E-07
4	0.585	0.67357E-12	0.18833E-08	0.21171E-08
5	0.606	0.12539E-09	0.34555E-06	0.14272E-06
6	0.656	0.54298E-01	0.59302E-09	0.20901E-09
7	0.769	0.39119E-09	0.57820E-06	0.51616E-05
8	0.988	0.71466E-05	0.30752E-13	0.78230E-15
9	1.138	0.77316E-11	0.44764E-09	0.17718E-08
10	1.142	0.21712E-00	0.71835E-08	0.21085E-07
11	1.262	0.15844E-10	0.20471E-05	0.16537E-07
12	1.283	0.19322E-00	0.23221E-08	0.35222E-10
13	1.359	0.125743-06	0.69612E-04	0.40794E-04
14	1.499	0.24820E-04	0.14407E-09	0.71433E-10
15	1.505	0.58873E-08	0.80376E-07	0.45406E-07
16	1.768	0.64374E-00	0.17722E-07	0.40393E-10
17	1.801	0.78019E-10	0.38213E-07	0.12584E-06
18	1.939	0.29168E-02	0.90611E-10	0.33430E-12
19	1.983	0.60058E-07	0.15102E-13	0.45809E-17
20	1.985	0.55695E-10	0.17577E-13	0.64006E-15
21	2.004	0.37959E-10	0.87323E-08	0.41691E-07
22	2.120	0.92690E-01	0.54932E-05	0.17436E-04
23	2.123	0.18916E-00	0.36914E-06	0.12436E-05
24	2.235	0.60516E-00	0.15018E-05	0.14088E-07
25	2.270	0.27114E-09	0.19340E-04	0.15146E-06
26	2.354	0.45080E-08	0.43944E-03	0.24147E-05
27	2.400	0.12995E-03	0.47094E-08	0.37306E-09
28	2.401	0.54815E-05	0.66524E-06	0.53228E-07
29	2.499	0.64640E-11	0.10642E-06	0.24062E-08
30	2.500	0.43413E-09	0.73292E-05	0.16594E-06

Table 3.3(b)
Modal Integrals for Bridge #2

Mode	Freq. (Hz)	Ghh	Gpp	Gαα
1	0.196	0.14572E-06	0.18879E-04	0.35755E-08
2	0.352	0.17324E-01	0.29123E-08	0.36054E-11
3	0.395	0.12071E-04	0.47991E-03	0.50620E-04
4	0.429	0.46848E-03	0.25360E-11	0.37704E-12
5	0.453	0.79626E-04	0.63745E-04	0.53693E-04
6	0.460	0.11837E-03	0.17387E-03	0.18371E-04
7	0.482	0.13754E-03	0.48435E-03	0.17976E-03
8	0.638	0.20404E-05	0.48120E-04	0.49284E-07
9	0.668	0.11571E-00	0.10107E-06	0.30418E-09
10	0.723	0.72579E-00	0.14844E-06	0.18477E-07
11	0.743	0.15115E-07	0.44739E-06	0.57703E-07
12	0.810	0.40236E-01	0.23221E-11	0.47577E-12
13	0.833	0.400463-03	0.13425E-13	0.48834E-14
14	0.854	0.10505E-03	0.30168E-13	0.46169E-14
15	0.874	0.16697E-07	0.56655E-07	0.72068E-08
16	0.938	0.53263E-02	0.13486E-02	0.26513E-02
17	0.953	0.49325E-00	0.37028E-07	0.10724E-06
18	1.030	0.40263E-00	0.21142E-10	0.21011E-10
19	1.047	0.58552E-08	0.41068E-08	0.54298E-08
20	1.071	0.16455E-08	0.87678E-08	0.90418E-09
21	1.080	0.24934E-08	0.96964E-08	0.30512E-07
22	1.174	0.45791E-02	0.57903E-01	0.57476E-03
23	1.182	0.46719E+01	0.48533E-03	0.28348E-05
24	1.281	0.27581E-05	0.20977E-04	0.12807E-06
25	1.290	0.39631E-02	0.48931E-09	0.30157E-11
26	1.312	0.12021E-02	0.60170E-09	0.36611E-09
27	1.314	0.80258E-03	0.48982E-03	0.31250E-03
28	1.341	0.63703E-03	0.96693E-02	0.26825E-03
29	1.376	0.57625E-04	0.29174E-13	0.10626E-14
30	1.398	0.16717E-07	0.99945E-08	0.43546E-07

38

References

1. Bathe,K.J. and E.L.Wilson, (1987), "Numerical Methods in Finite Element Analysis", Prentice-Hall India Pvt. Ltd., India.

2. Biggs,J.M., (1964), "Introduction to Structural Dynamics", McGraw Hill Company.

3. Krishna,J. and A.R.Chandrasekaran, (1976), "Elements of Earthquake Engineering", Saritha Prakashan, Meerut, India.

4. Lin, S.J. and C.C.Tseng, (1987), "Design of Chung Yang Bridge", Proc. Int. Conf. on Cable Stayed Bridges, Bangkok, Nov., pp 1286-1297.

5. Lin,S.J., Y.Yamada, H.Iemura and C.C.Tseng, (1987), "Earthquake Resistant Analysis of Chung Yang Highway Bridge", Proc. Int. Conf. on Cable Stayed Bridges, Bangkok, Nov., pp 490-501.

6. Paz,M., (1987), "Structural Dynamics: Theory and Computation", II Ed., CBS Publishers, India.

7. Sastry,M.V., (1985), "The Second Hoogly Bridge at Calcutta", Indian Concrete Journal, January, pp 7-9.

8. Schlaich,J. and R.Bergarmann, (1988), "Variety of Cable Bridge Design", Indian Concrete Journal, September, pp 454-461.

9. Young.T.L. and M.L.Venwoert, (1984), "Plot 88 Software Library Reference Manual", Plotworks Inc., Ramona, U.S.A.

10. Fleming,J.F and E.A.Egeseli,(1980), "Dynamic Behaviour of Cable Stayed Bridge", Earthquake Engineering and Structural Dynamics, Vol.8,pp 1-16.

11. Namini,A.H.,(1990), "Investigation of Analytical Modeling for Long Span Bridge Flutter", Proc. of VIII Int. Conf. of Wind Engg., Canada. pg1277.

Notations

|	
A	cross sectional area
A'	modified dynamic mass matrix
C_x, C_y, C_z	direction cosines of members
E	Young's modulus of elasticity
G	shear modulus of elasticity
G_{ij}	modal integrals of a particular mode i or j.
$I_{\bar{m}}$	mass moment of inertia per unit span
I_x, I_y, I_z	moment of inertia in X,Y and Z axes respectively
J	torsional constant
K	stiffness matrix
L	length of the member
P	nodal force component
R	rotation matrix of each member
f	natural frequency of structure
h_i	modal non-dimensional deflection deformations in bending mode
$\bar{m}$	mass per unit span of the member
α_i	modal non-dimensional angular deformations in torsion mode
δ	nodal displacement component
λ	eigenvalue of the system
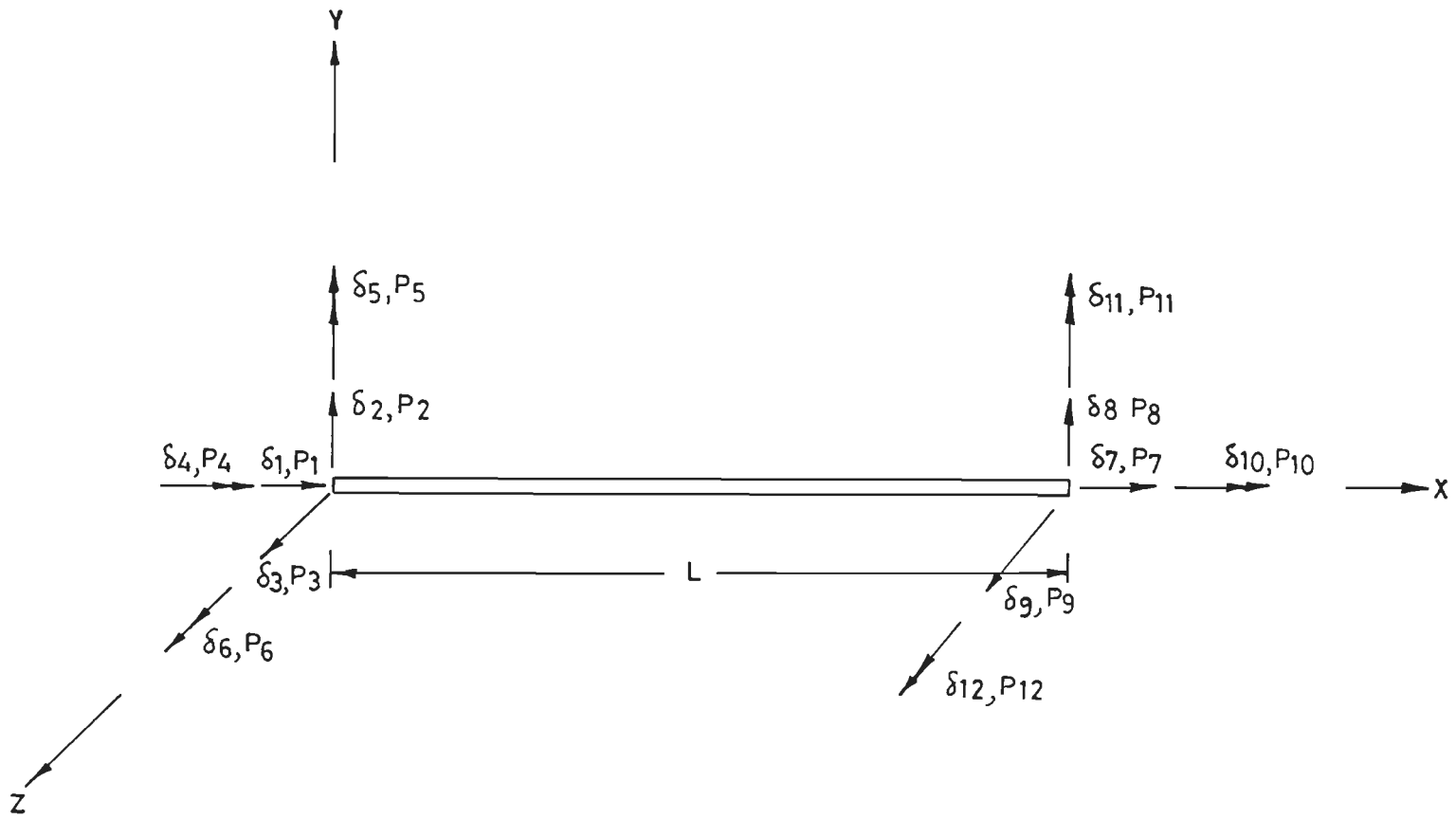
Fig. 3·1   Beam segment of a three dimensional frame showing forces
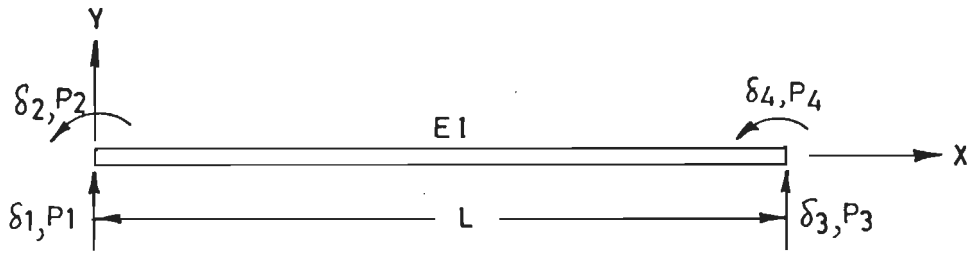   and displacements at the nodal co-ordinates

Fig. 3·2 Beam segment of two dimensional frame showing forces and displacements at the nodal co-ordinates
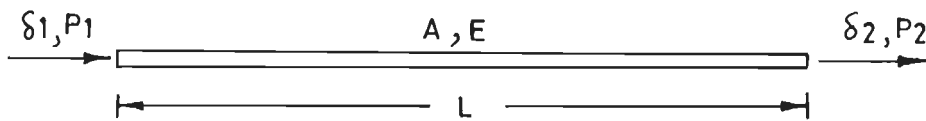

Fig. 3·3 Beam element with nodal axial loads and corresponding nodal displacements
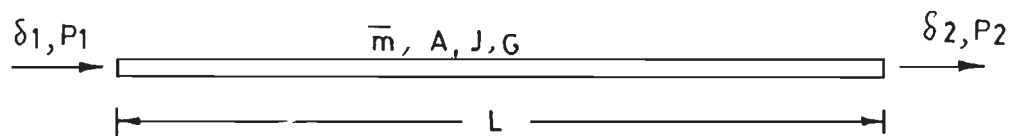
Fig. 3·4 Grid beam element showing model torsional co-ordinates

START

Read Input Data: Nodes, Members,Connectivity
Coordinates and Properties

DO i=1,members

Next members

Assembly of member
Stiffness and Mass matrix

Transform into global stiff-
ness matrix using rotation matrix

End do

Solution for eigenvalue

Iteration Begins

Compute eigen value and
corresponding eigenvectors
using Inverse Iteration Tech.

Next iteration

$$\frac{\lambda_r^i - \lambda_r^{i-1}}{\lambda^i} \leq \epsilon$$

NO

YES

Print eigenvalue & vectors

Compute Gen. inertia, mass
and geometric integrals

Print Gen. inertia, mass and
geometric integrals

Next eigenvalue

Modes ≥ Limit

NO

YES

STOP

Fig.3.5 Flow chart showing the various steps in free
vibration analysis

(i) Elevation

R.C. Pylontower

Steel cables

₵ Pier

R.C. Side pier

5 m

8@3m

24 m

68 m

72·17 m

30 m

13·17

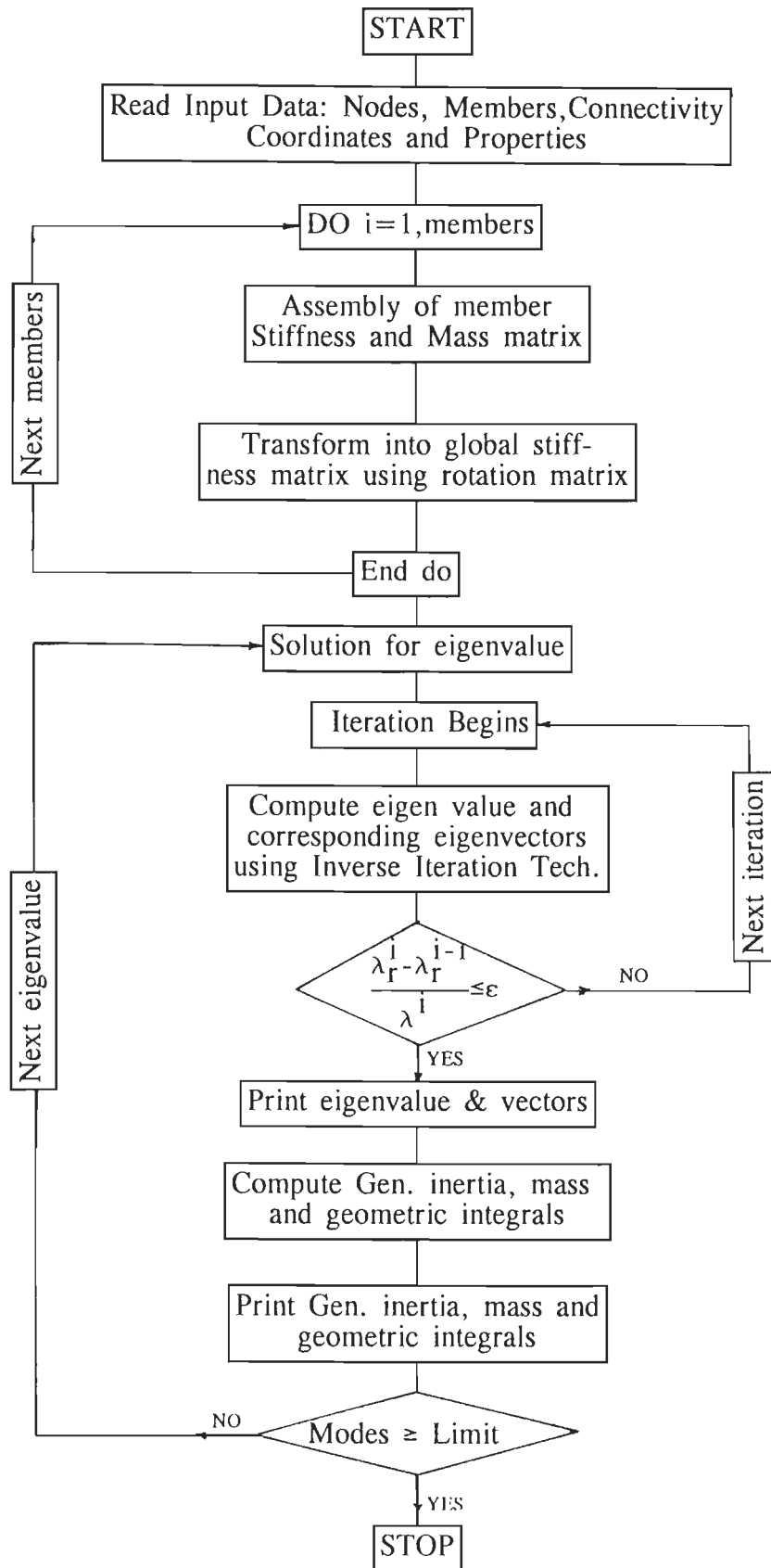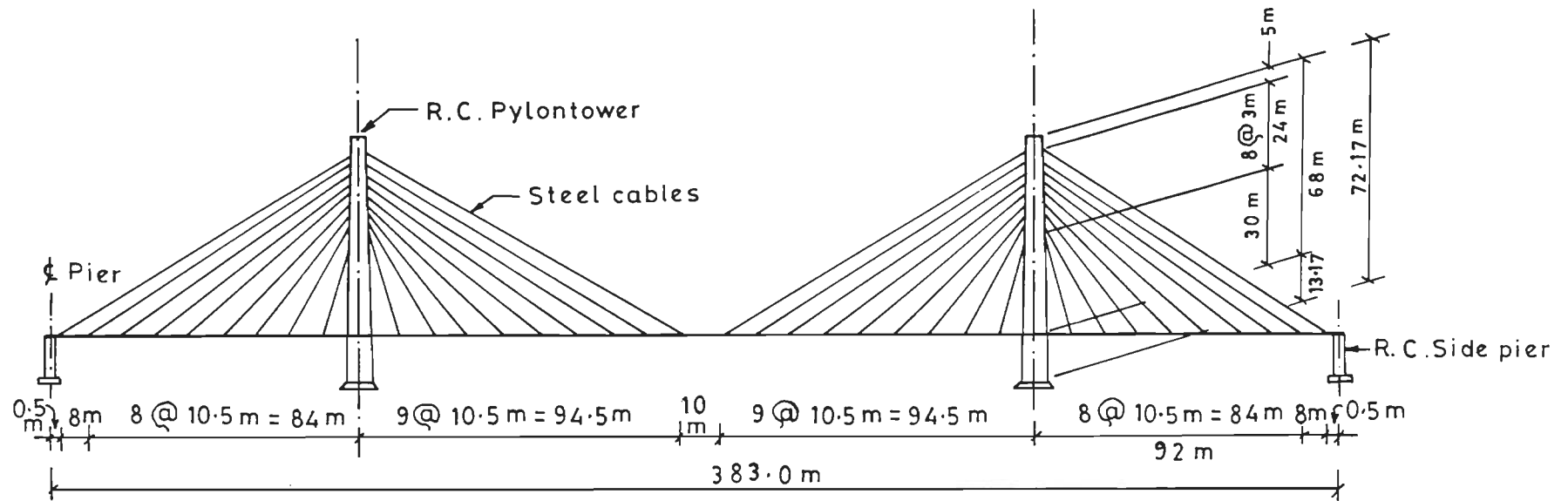0.5 m | 8m | 8 @ 10·5 m = 84 m | 9@ 10·5 m = 94·5 m | 10 m | 9 @ 10·5 m = 94·5 m | 8 @ 10·5 m = 84 m | 8m | 0.5 m

92 m

383·0 m

(ii) Pylon Tower

3m

31 m

23 m

3 | 5

72·17 m

36 m

5 | 3

13·17 m

5 m
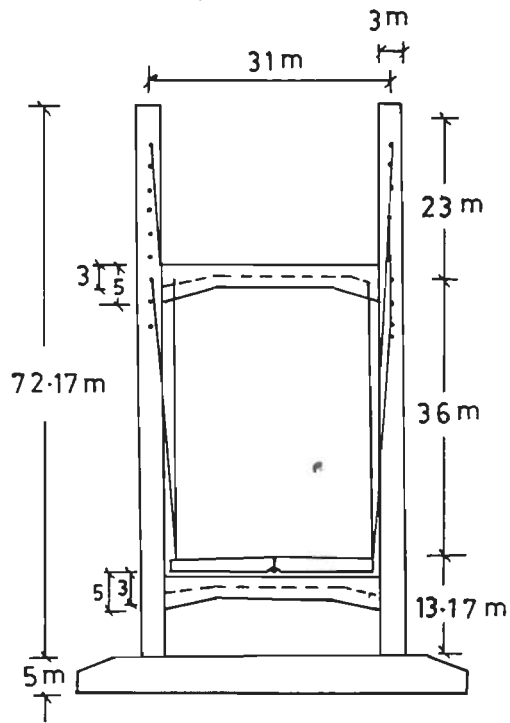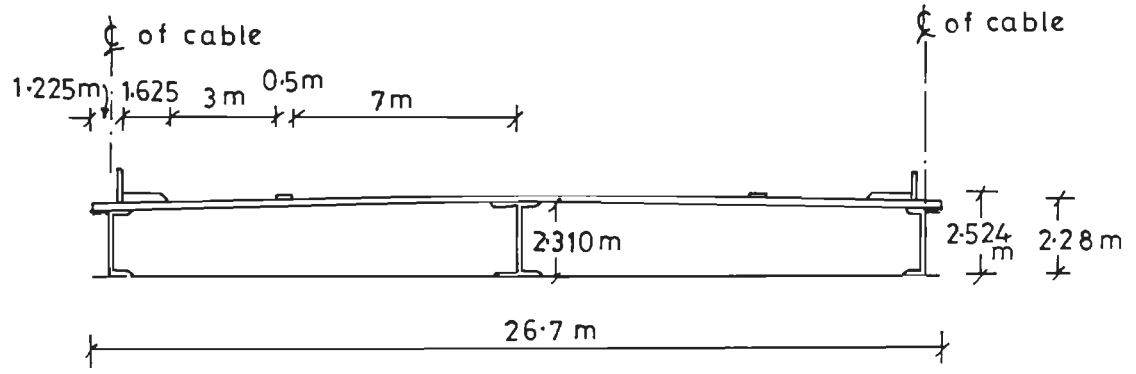
(iii) Cross section of deck

₵ of cable

₵ of cable

1·225m | 1·625 | 3 m | 0·5m | 7m

2·310 m

2·524 m

2·28 m

26·7 m

44

Fig. 3·6(a) Details of cable stayed Bridge # 1

R.L.+135.30 m

R.L.+117.10 m

Road crown
+45.34 m

Cable No.1

Cable No.34

Road crown
+32.30 m

+32.38m

+0.61m

+30.32m

Datum ± 0.00 m

34.73m minimum

+13.00m

+6.10m

−22.86m

−21.34m

2

−32.20m

3

4

−22.66m

Ø 12.00m

Ø 20.60m

Ø 23.00m

Ø 8.00m

Foundation No.1

₵ of bridge

182.88 m

457.20 m

182.88 m

(a)

14.55   14.55

99.40

22.60

(c) Pylon elevation

Cable

35.00

Cable

2.00

14.55

14.55

2.95

2.95
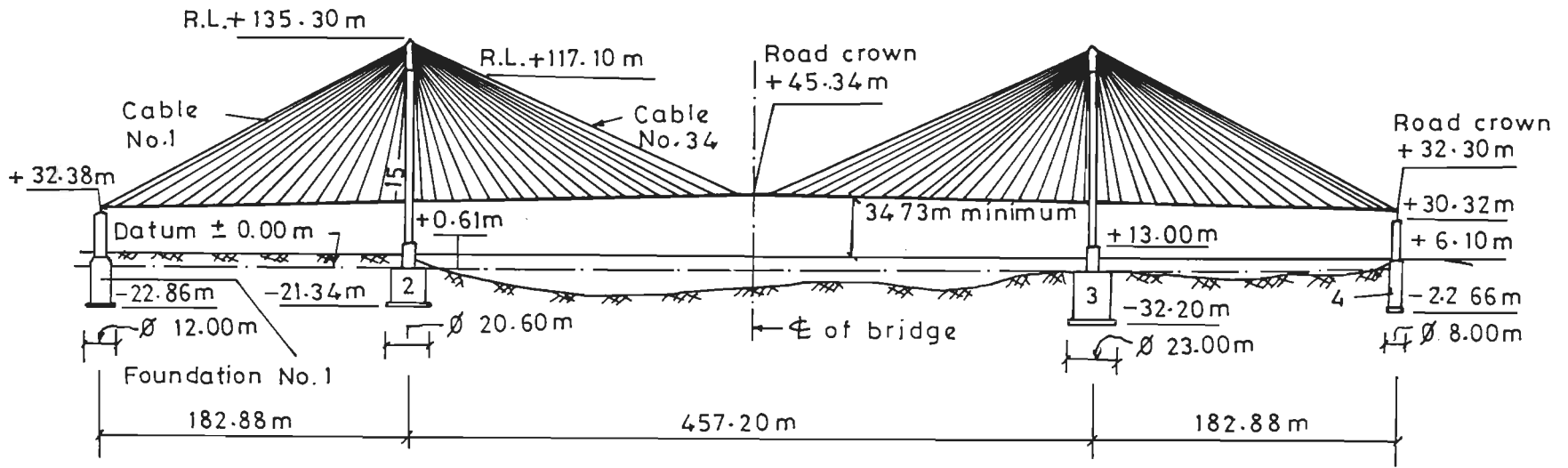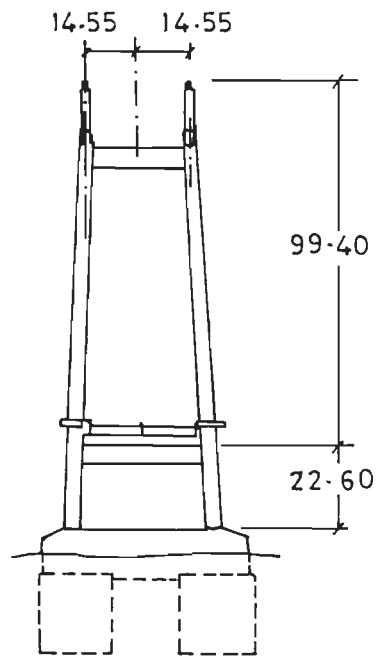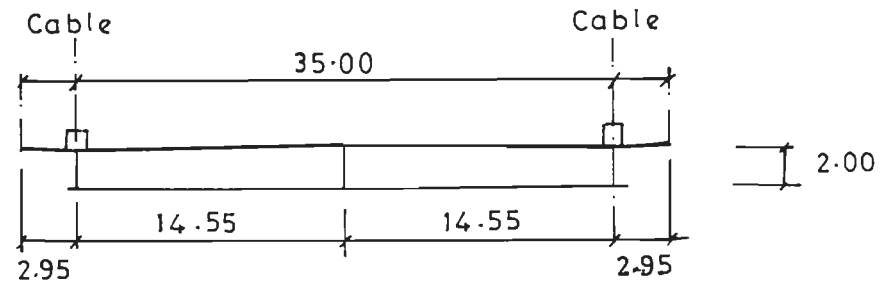
(b) Cross-section

Fig. 3.5(b) — Details of cable stayed bridge # 2

Fig. 3.7(a) Idealized bridge # 1 configuration
Nodes = 140, Members = 252

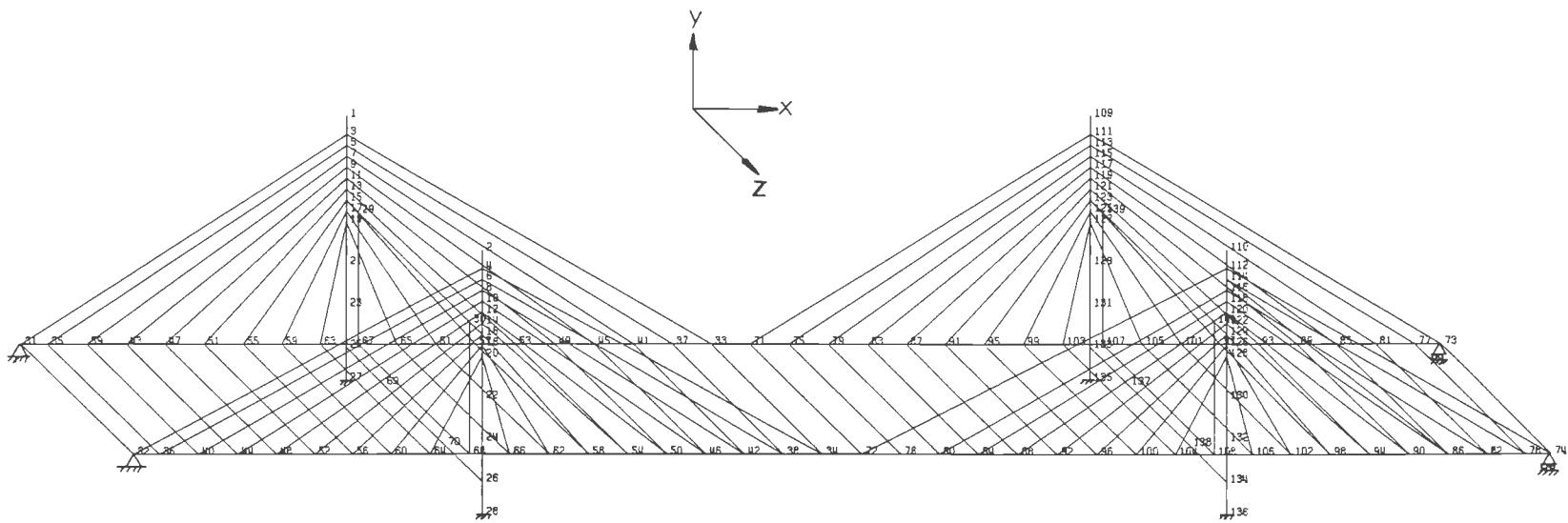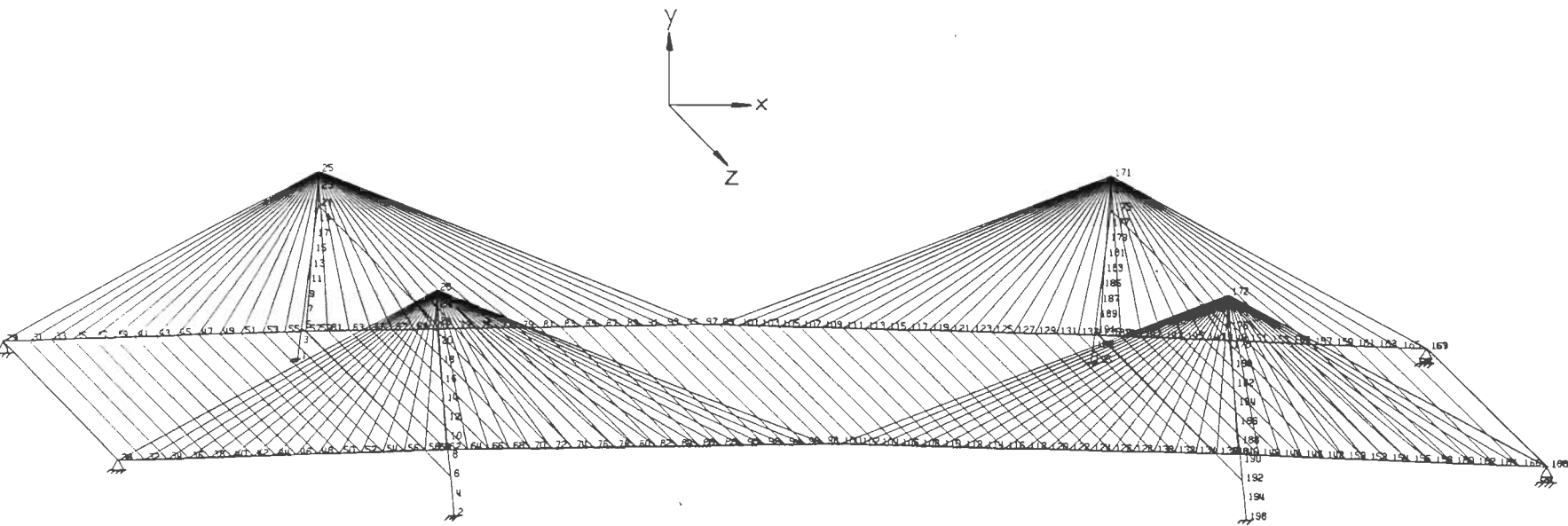Fig. 3.7(b) Idealized bridge # 2 configuration
Nodes = 196, Members = 404
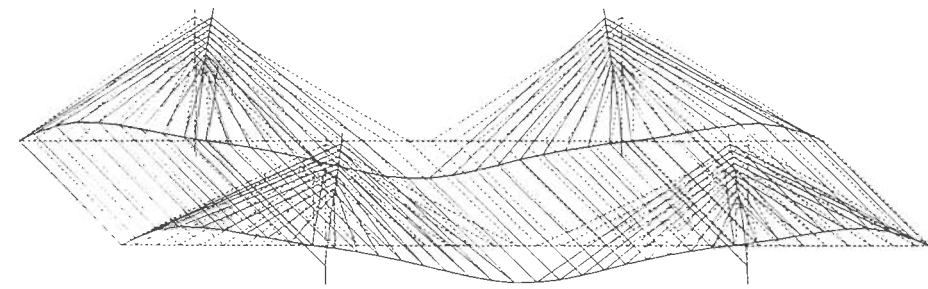
(a) 0.491 Hz
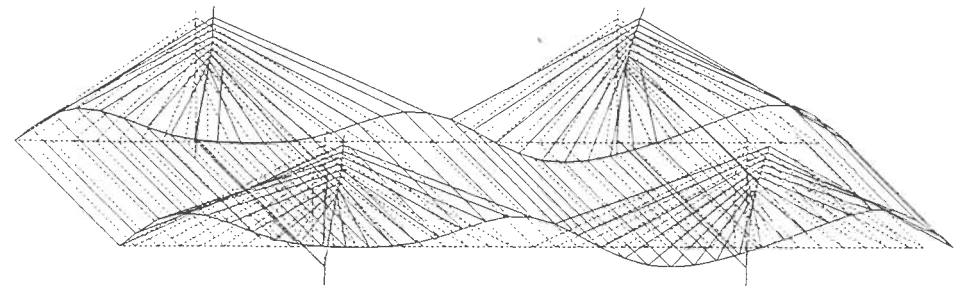
(b) 0.988 Hz
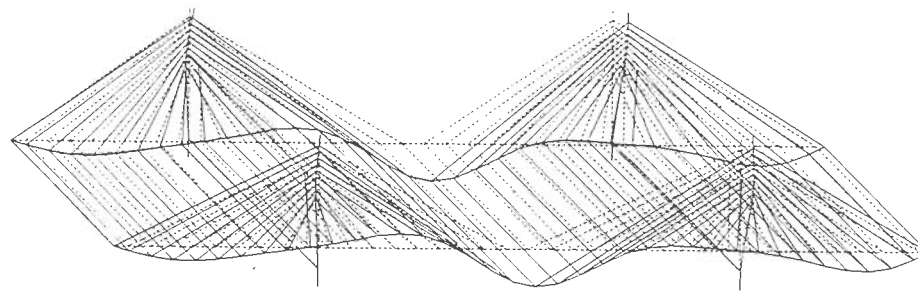
(c) 1.142 Hz
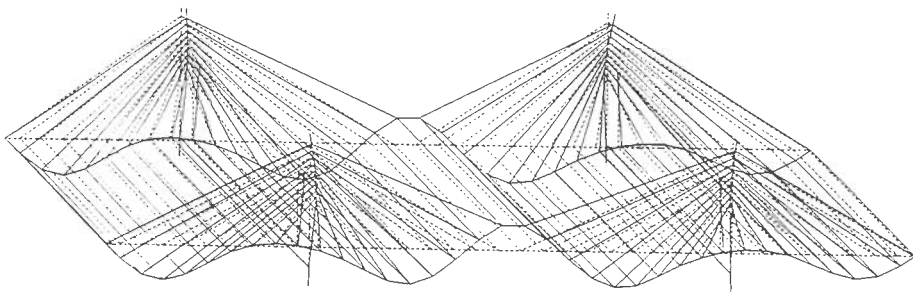
(d) 1.499 Hz
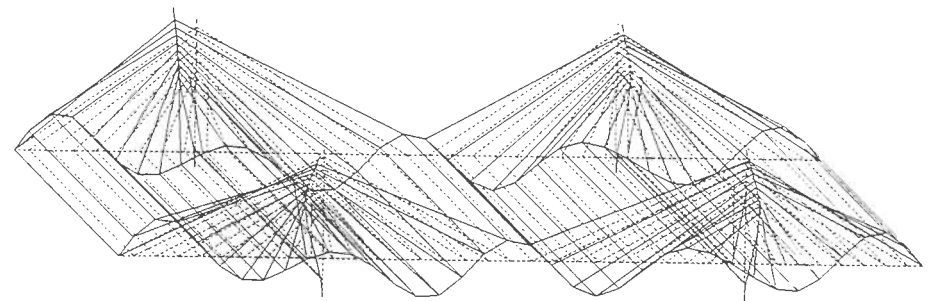
(e) 1.939 Hz

Fig. 3.8 Symmetrical vertical modes of bridge # 1
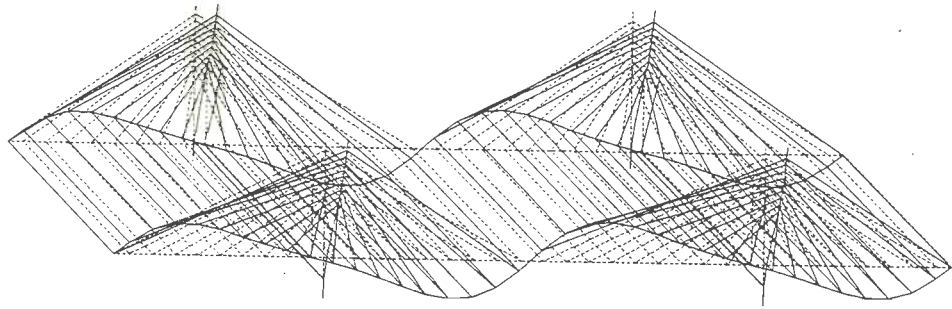
(a) 0.656 Hz
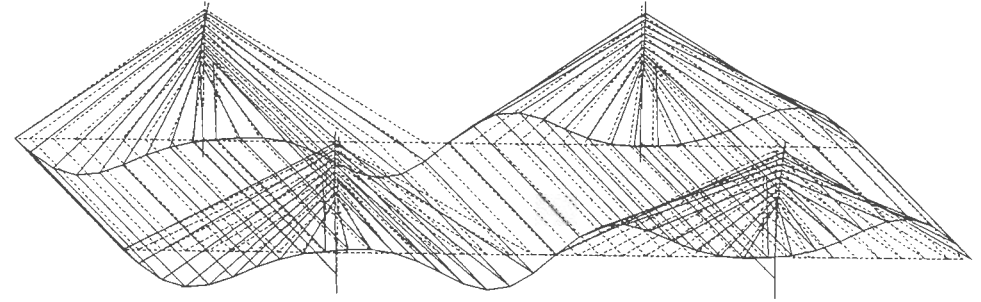
(b) 1.283 Hz
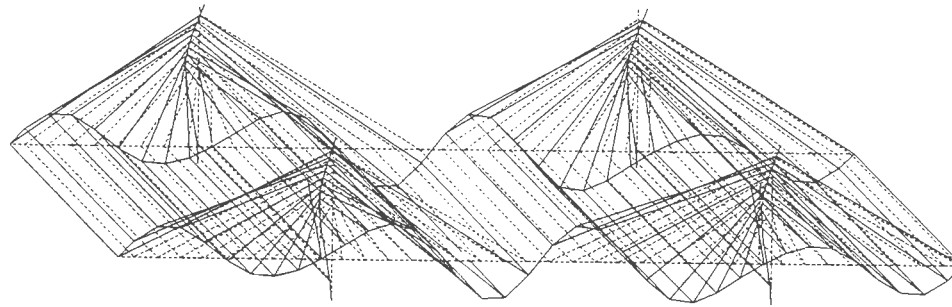
(c) 1.768 Hz
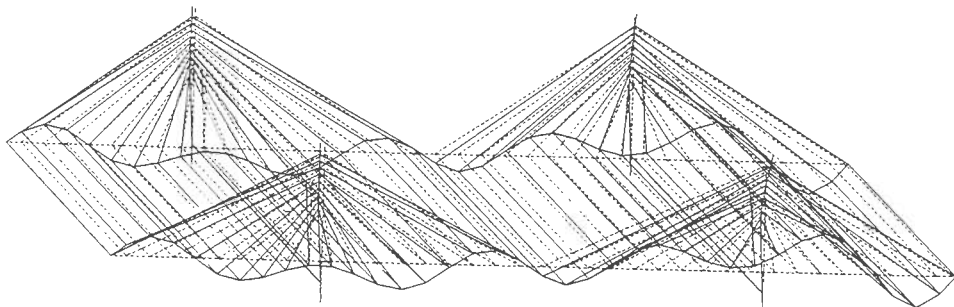
(d) 2.120 Hz
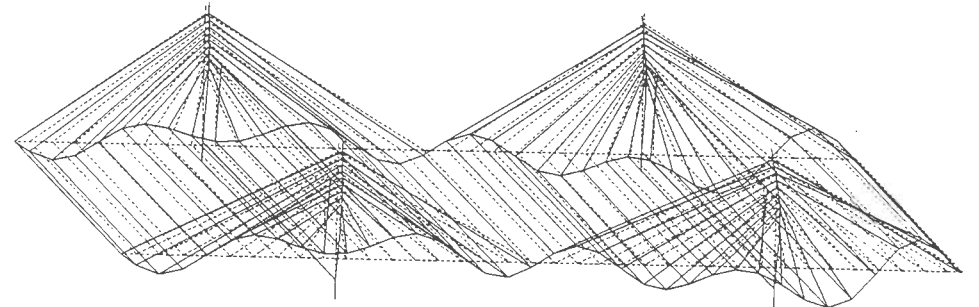
(e) 2.123 Hz

Fig. 3.9 Unsymmetrical vertical modes of bridge # 1
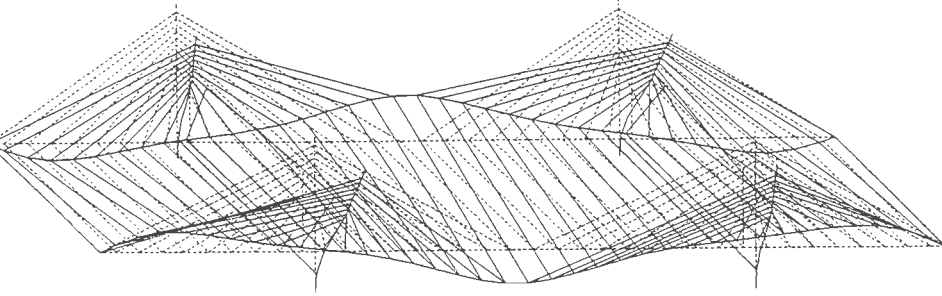
(a) 0.606 Hz
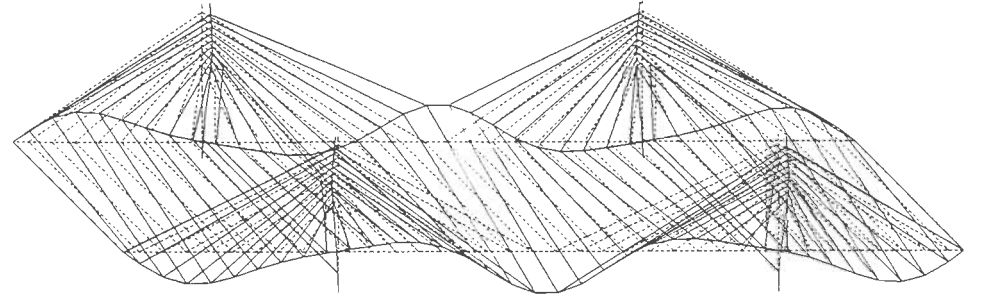
(b) 1.138 Hz
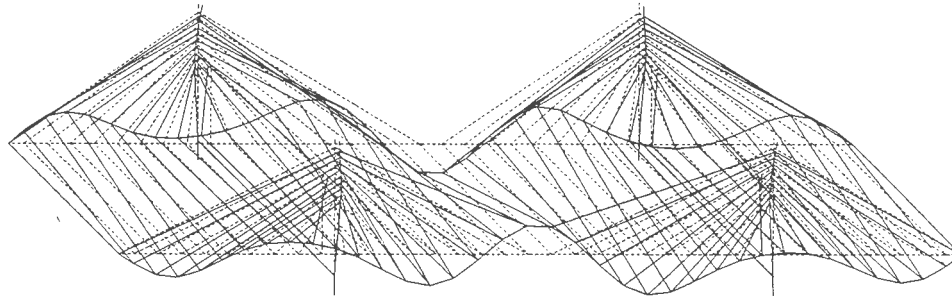
(c) 1.505 Hz
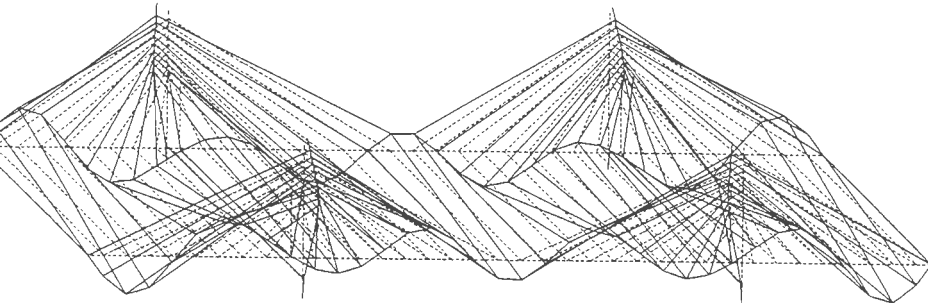
(d) 2.004 Hz
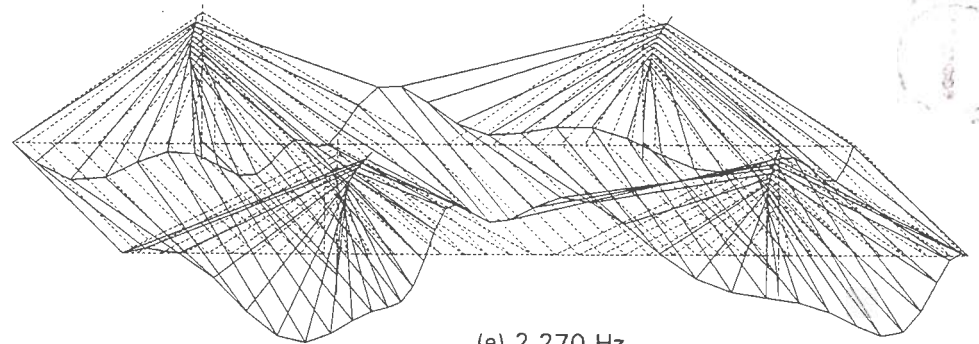
(e) 2.270 Hz

Fig. 3.10 Symmetrical torsional modes of bridge # 1
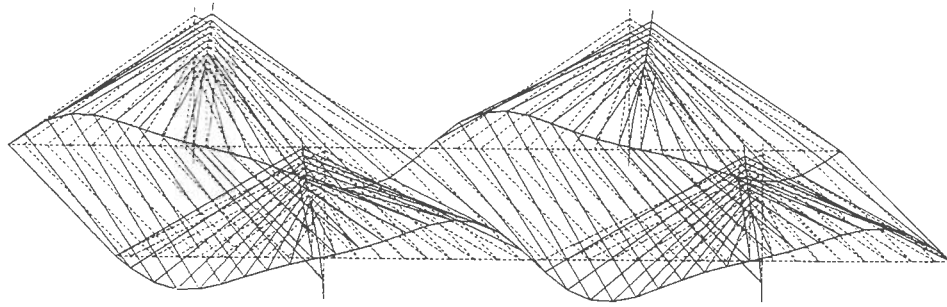
(a) 0.769 Hz
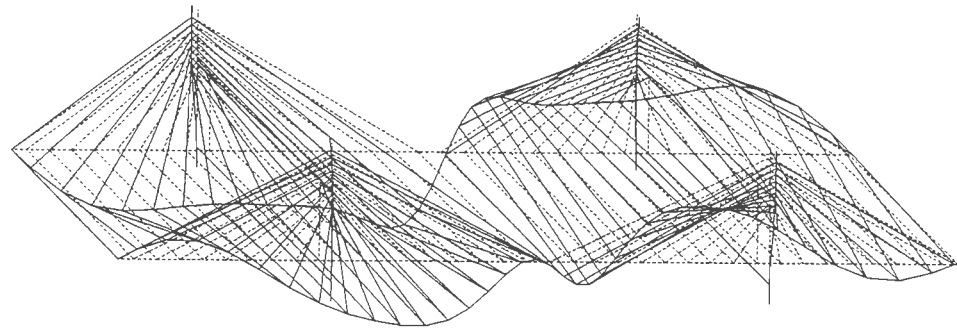
(b) 1.262 Hz
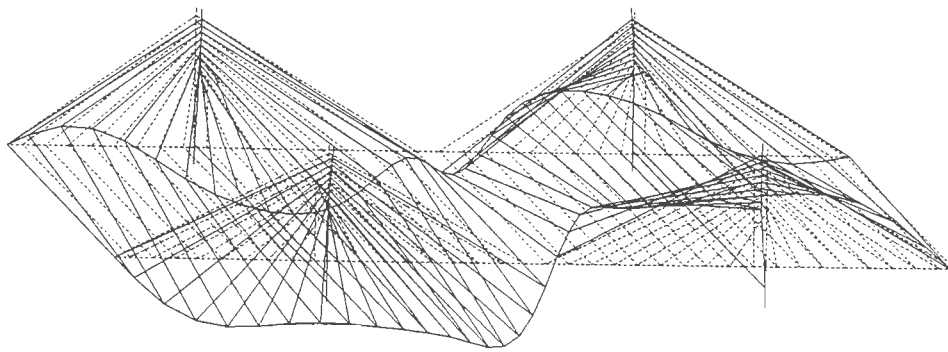
(c) 1.359 Hz
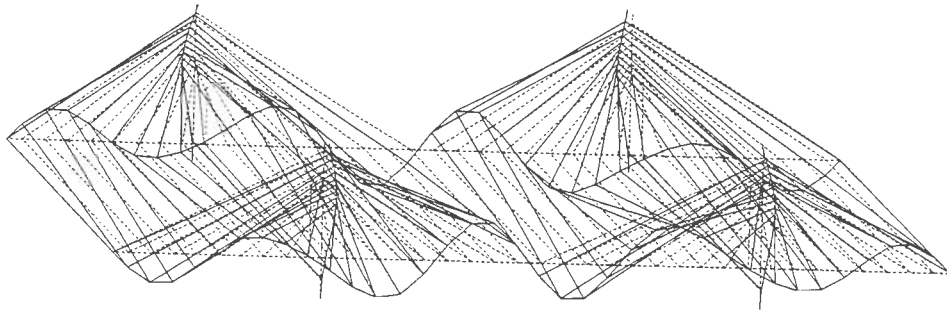
(d) 1.801 Hz
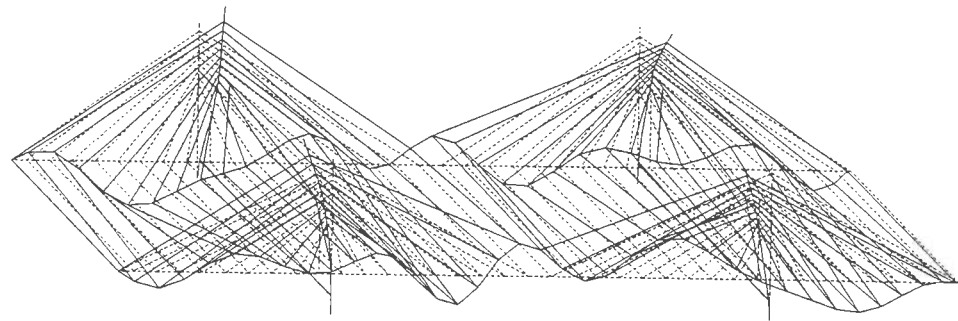
(e) 2.401 Hz

Fig. 3.11 Unsymmetrical torsional modes of bridge # 1
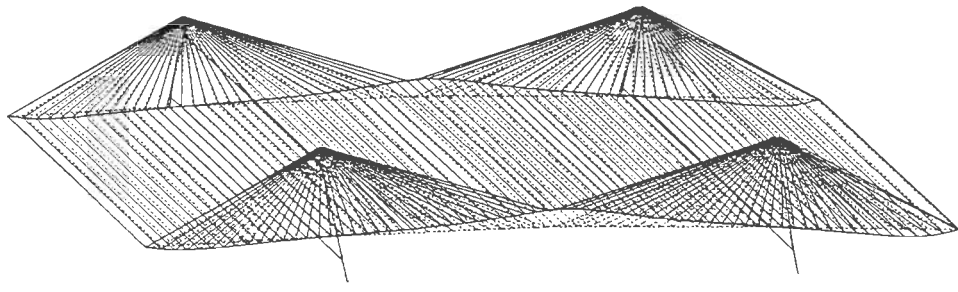
(a) 0.353 Hz
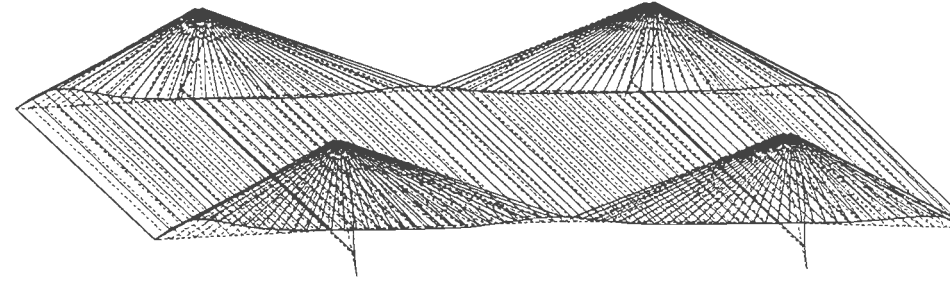
(b) 0.668 Hz
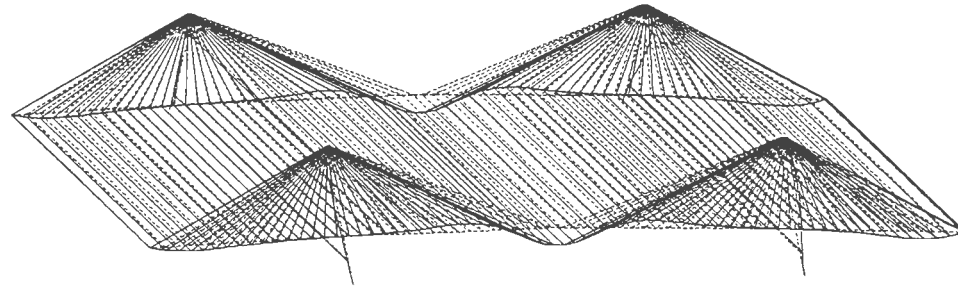
(c) 0.723 Hz
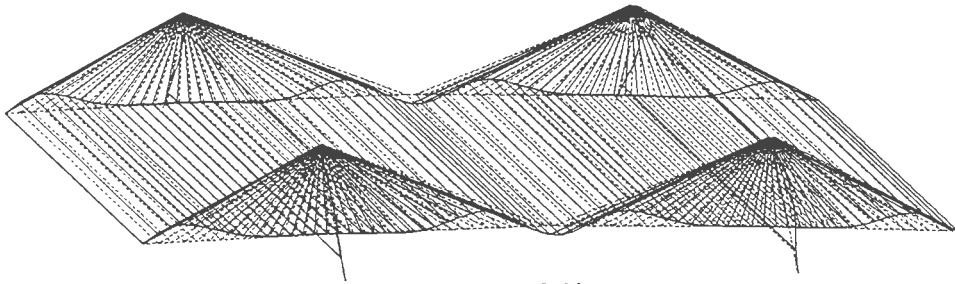
(d) 0.953 Hz
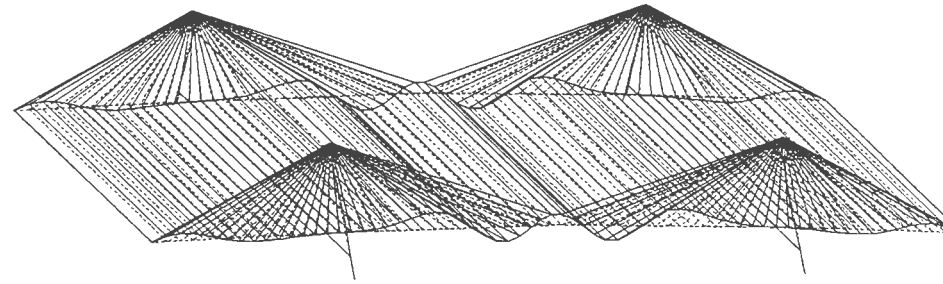
(e) 1.182 Hz

Fig. 3.12 Symmetrical vertical modes of bridge # 2
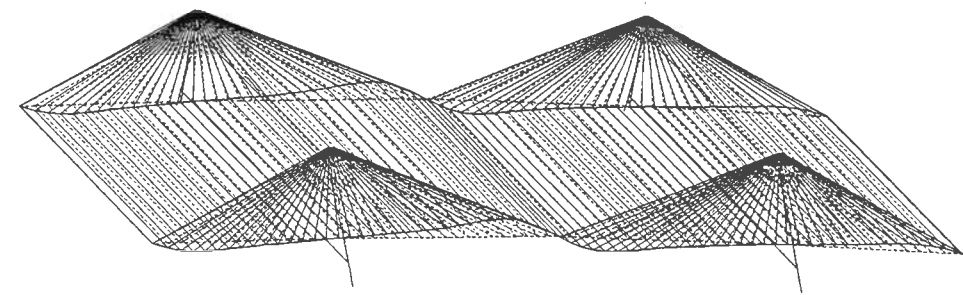
(a) 0.429 Hz
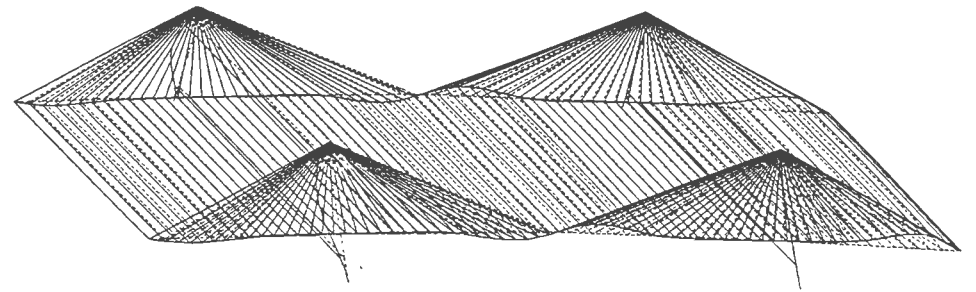
(b) 0.810 Hz
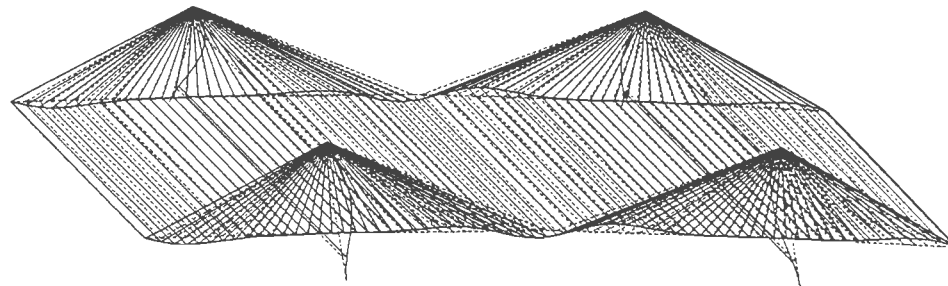
(c) 0.833 Hz
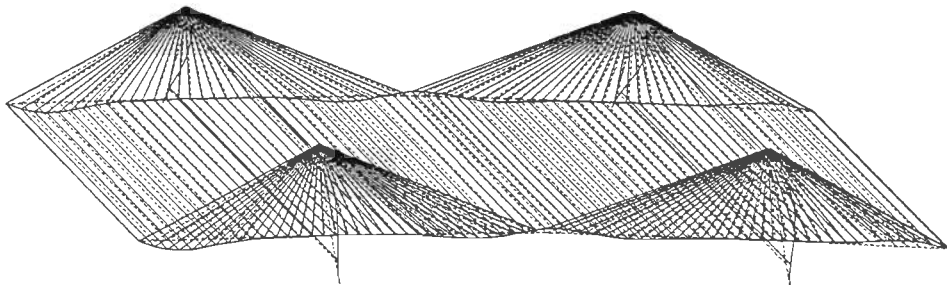
(d) 0.854 Hz
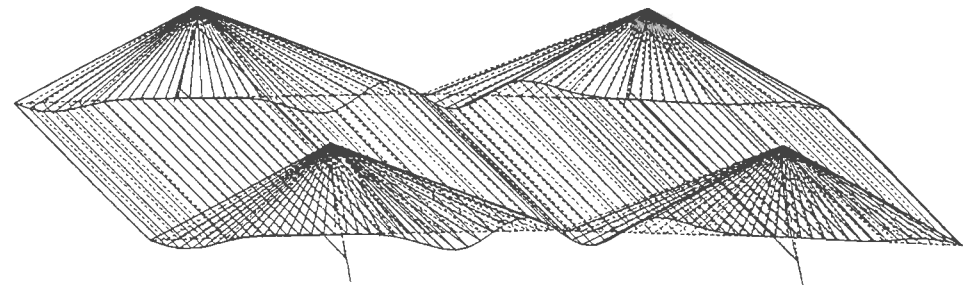
(e) 1.030 Hz

Fig. 3.13 Unsymmetrical vertical modes of bridge # 2
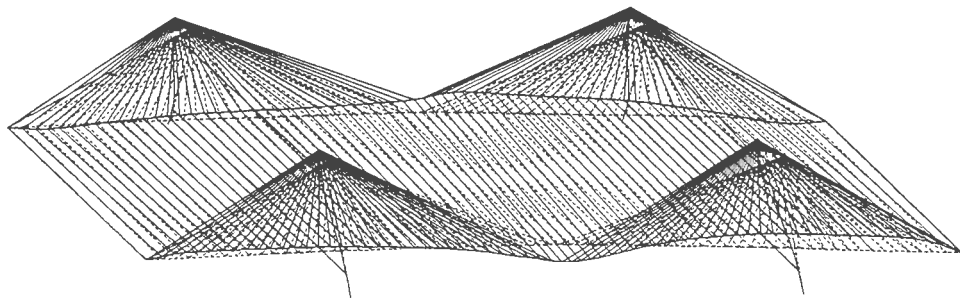
(a) 0.395 Hz
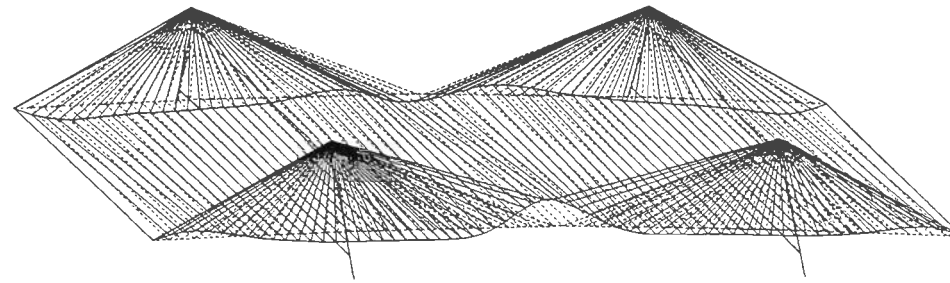
(b) 0.743 Hz
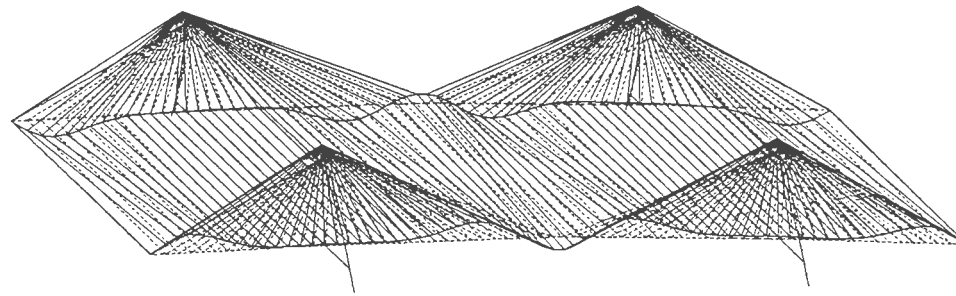
(c) 0.938 Hz
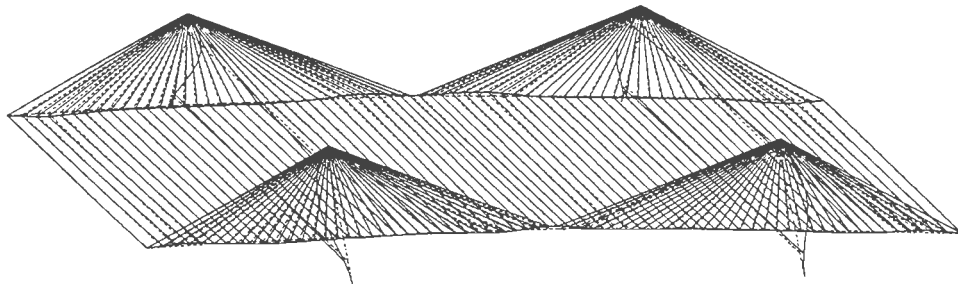
(d) 1.071 Hz
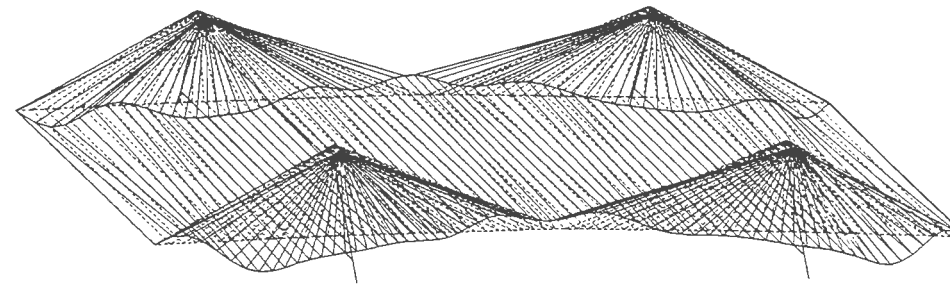
(e) 1.341 Hz

Fig. 3.14 Symmetrical torsional modes of bridge # 2
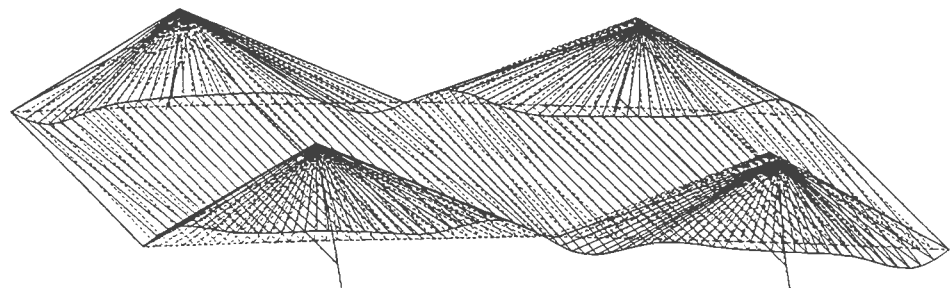
(a) 0.874 Hz
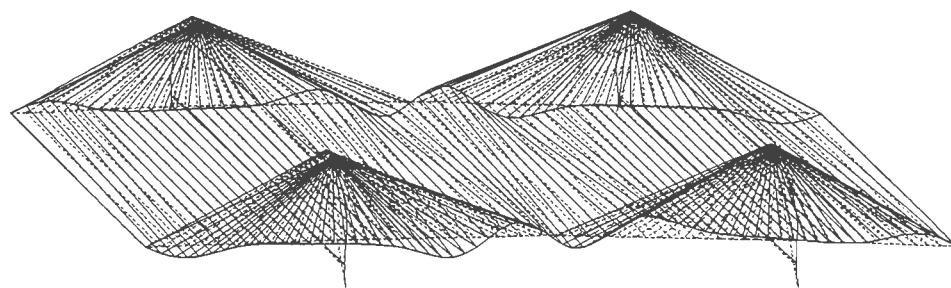
(b) 1.047 Hz
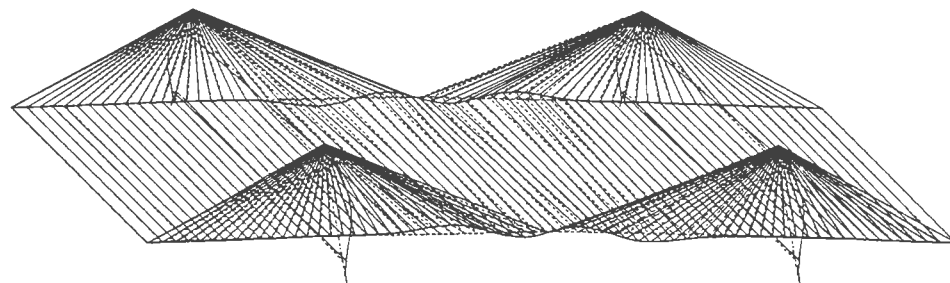
(c) 1.080 Hz
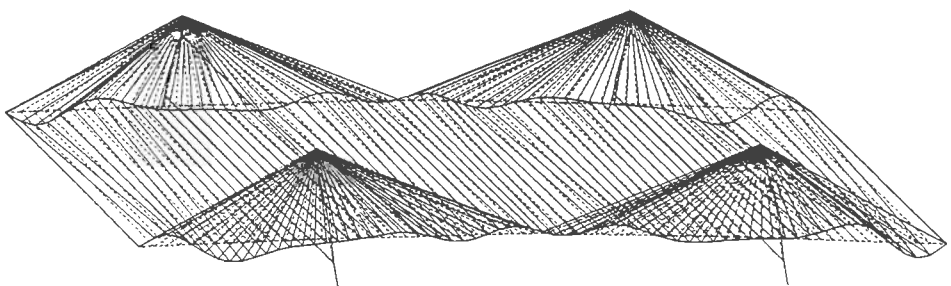
(d) 1.314 Hz
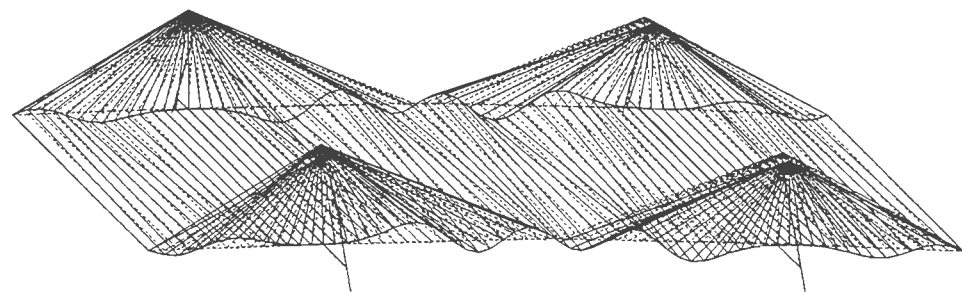
(e) 1.398 Hz

Fig. 3.15 Unsymmetrical torsional modes of bridge # 2

CHAPTER 4
FORMULATION FOR AERODYNAMIC ANALYSIS

4.1 INTRODUCTION

This chapter is devoted to a discussion of analytical formulations involving the aerodynamics of bluff sectional shapes of cable supported bridges along with the formulations for full bridge response in flutter and buffeting. Bluff sections are the primary concern in the wind engineering of civil engineering structures such as long span bridges, chimneys, tall buildings and other wind sensitive structures.

Bluff body aerodynamics differs significantly from the aerodynamics of thin airfoils. However, it has been observed by some investigators in the past that the thin airfoil theory serves as a valuable guide in problems involving bluff sections. For this reason, a brief review of some of the classical theories of thin airfoils has been made herein.

4.2 CLASSICAL THEORIES OF THIN AIRFOIL

As shown in Fig.4.1 the airfoil section is assumed to have vertical(h), torsional(α) and the sway(p) degrees of freedom of motion. The lift(L), moment(M) and drag(D) respectively are the forces associated with these degrees of freedom. Sign conventions used are shown in Fig.4.1.

In general, for the bluff section oscillating in h and α degrees of freedom, the governing equations of motion are

$$m[\ddot{h} + 2\zeta_h\omega_h\dot{h} + \omega_h^2 h] = L \tag{4.1}$$

$$I[\ddot{\alpha} + 2\zeta_\alpha\omega_\alpha\dot{\alpha} + \omega_\alpha^2\alpha] = M \tag{4.2}$$

where m is mass per unit span length,

I is mass moment of inertia per unit span length,

ζ is critical damping ratio and

ω_h and ω_α are natural frequency of vibration in bending and torsion, respectively.

The aerodynamic lift(L) and moment(M) are given by functions as given below.

4.2.1 Theodorsen Function

It is noted (Von Karman & Sears[14]) that the theory of oscillating airfoils was first developed for flapping wings of flying machines. The circulatory lift and moment developed can be written as

$$L = \frac{1}{2} \rho U B C_L^{'} C(K) w \tag{4.3}$$

$$M = \frac{1}{4} \rho U B^2 C_M^{'} C(K) w \tag{4.4}$$

where L is the lift force acting at 1/4-th chord point and M is the moment about the mid chord point; C(k) is the so called Theodorsen Function, U is the flight speed (horizontal wind velocity), and w is the vertical velocity of air, $C_L^{'}$ and $C_M^{'}$ denote respectively the slopes of lift and moment coefficients with respect to α. For thin airfoils these are given as $C_L^{'} = 2\pi$ and $C_M^{'} = \pi$. These are represented as $\dfrac{dC_L}{d\alpha}$ and $\dfrac{dC_M}{d\alpha}$ respectively in the present study.

The dimensionless frequency K is given by

$$K = \frac{\pi n B}{U} \tag{4.5}$$

where n is the circulatory frequency of oscillation of the airfoil. The Theodorsen Function can be expressed as a complex function in the form (Fung[4])

$$C(K) = F(K) + iG(K) \tag{4.6}$$

the real part F(K) and imaginary part G(K) are expressed in terms of Bessel's Functions of the first and second kinds respectively.

4.2.2 Wagner Function

If an airfoil is given an impulsive forward velocity U at time s=0 keeping α constant, as in Fig.4.2, s being the non- dimensionalised time given as

$$s = \frac{U t}{B} \tag{4.7}$$

then, using Wagner Function $\phi(s)$ the circulatory parts of lift and moment at any time s are given as

$$L(s) = \frac{1}{2} \rho UBC_L' \phi(s)w_0 \tag{4.8}$$

$$M(s) = \frac{1}{4} \rho UB^2 C_M' \phi(s)w_0 \tag{4.9}$$

where w_0 is the uniform downward movement due to the forward motion expressed as,

$$w_0 = U\alpha \tag{4.10}$$

For small values of α, Wagner Function can be approximated as [4],

$$\phi(s) = 1.0 - 0.165 \, e^{-0.0415} - 0.335 \, e^{-0.325} \tag{4.11}$$

In Fourier transform domain the Wagner Function is related to the Theodorsen Function as [4]

$$\bar{\phi}(K) = \frac{C(K)}{iK} \tag{4.12}$$

where $\bar{\phi}(K)$ is the Fourier transform of the Wagner function $\phi(K)$.

4.2.3 Sears Function

For an airfoil flying through a sinusoidal gust field, Fig.4.3, the total aerodynamic lift and the moment on the airfoil is given by Sears Function[5] as follows:

$$L = \frac{1}{2} \rho UBC_L \, \phi(K)we^{iks} \tag{4.13}$$

$$M = \frac{1}{4} \rho UB^2 C_M \, \phi(K)we^{iks} \tag{4.14}$$

where $w(s) = we^{iks}$ gives the vertical velocity distribution of the gust field relative to the airfoil and the Sears function $\phi(K)$ is given by

$$\phi(K) = [J_0(K) - iJ_1(K)]C(K) + iJ_1(K) \tag{4.15}$$

The Sears Function expresses the effectiveness of sinusoidal gust field of frequency K in creating aerodynamic forces. These relationships are commonly termed as aerodynamic admittance functions. It is also seen that although for the thin airfoil this admittance function for the lift and the moment force is the same, in general, this would not be true.

4.3 THEORETICAL MODELLING OF BRIDGE DECK

A nearly horizontal wind flow past a cable supported bridge deck would exert vertical forces (lift) besides the drag force. In the case of bluff bridge decks, major part of the deck would fall in the wake zone of the flow (unlike airfoils), giving rise to large dynamic forces. As one could expect that the elastically supported bridge deck, with its natural frequencies of vibrations in the various vertical and torsional modes might get into

'flutter' oscillations, generally with a single mode of vibration dominating the total response. It is the shape of the deck section and its natural frequency of vibration in one of its vibrational mode, which are, therefore, of prime importance in determining the aerodynamic performance of the deck and hence the bridge.

The problem can thus be tackled by first isolating the deck section and studying its aerodynamic performance in a wind tunnel. In this approach, the deck system can be made rigid and the elasticity imparted by supporting it on springs. Further simplification can be achieved by constraining the system to have either only a vertical motion or only a rotational motion representing only the vertical or the torsional mode of vibration respectively. Thus the various aerodynamic parameters governing the response of the complex cable bridge can be isolated and evaluated separately for subsequent use in the analysis of total system for its aerodynamic response involving several modes of vibrations with the distributed elasticity of the real system. Hence the relevance of the simplified experimental approach, popularly known as the section model technique.

4.3.1 Flutter Derivative Formulation

This section will discuss the detailed mathematical formulation for the aeroelastic behaviour of a rigid section model of a bridge deck, of unit length, elastically mounted so that it can vibrate in two degrees of freedom, the vertical and rotational (Fig.4.4). The deck section is symmetric about vertical plane passing through its longitudinal axis. The bridge deck model is itself two dimensional with symmetry about the central vertical plane. The elastic supports are thus considered to be acting at the centre of mass of the model.

Under the action of aerodynamic loading with viscous structural forces the equation of motion will be as given by eqns.4.1 and 4.2, where L and M are the self excited aerodynamic lift and moment of the section model respectively.

System identification and flutter stability calculations are often aided by recasting the motion dependent aerodynamic forces into a hybrid time and frequency formulation. This hybrid formulation, known as the flutter derivative formulation, was originally proposed for vertical and torsional degrees of freedom section model by Scanlan

et al[8]. Scanlan et al[9] augmented the flutter derivative model with two additional terms. The modified flutter derivative formulation for the motion dependent aerodynamic forces in terms of reduced frequency is given as

$$L = \frac{1}{2} \rho U^2 2B[KH_1^*(K)\frac{\dot{h}}{U} + KH_2^*(K)\frac{B\dot{\alpha}}{U} + K^2 H_3^*(K)\alpha + K^2 H_4^*(K)\frac{h}{U}] \qquad (4.16)$$

$$M = \frac{1}{2} \rho U^2 2B^2[KA_1^*(K)\frac{\dot{h}}{U} + KA_2^*(K)\frac{B\dot{\alpha}}{U} + K^2 A_3^*(K)\alpha + K^2 A_4^*(K)\frac{h}{U}] \qquad (4.17)$$

where $H_i^*(K)$, $A_i^*(K)$ are the so called flutter derivatives and dots(.) indicate differentiations with respect to time t and B is the deck width. The measurement of flutter derivative coefficients of the section model(s) constitutes the major component of the aerodynamic stability necessary to be performed for the cable suspended bridges before the bridge deck section is finalised and built. Eqns.4.16 and 4.17 hold, strictly speaking, only for sinusoidal oscillations. However, it has been shown by Scanlan and Tomko[8] that they, nevertheless, hold very well for exponentially modified oscillations like

$$h = h_0 e^{\lambda t} \sin \omega t \qquad (4.18)$$

$$\alpha = \alpha_0 e^{\lambda t} \sin(\omega t - \theta) \qquad (4.19)$$

where h_0, α_0 define the amplitudes; θ the relative phase; and λ the rate of decay or build-up of oscillations (which have been classically assumed to be of small amplitude and in a linear range of deformations).

In the above formulation the inertial terms such as $\ddot{h}$ and $\ddot{\alpha}$ are neglected. It is customary to neglect these terms in wind engineering practice of civil engineering structures since the wind velocities concerned are moderate, the accelerations involved are small, the structures are relatively heavy, and the forces associated with the acceleration of the air masses are usually negligible when compared to the other forces involved.

A study of the flutter derivative equations of motion indicates that H_4^* and A_4^* flutter derivatives describe the amount of motion dependent aerodynamic lift force and moment caused by a vertical displacement of the bridge deck. These derivatives are often dropped, having relatively insignificant. However, in the present study A_4^* and H_4^* flutter derivative coefficients were retained in the aeroelastic analysis, because their inclusion

provides certain amount of symmetry in the representation of the domain. Further, H_4^* is included in the analysis of the full bridge in order to study the response in pure vertical motion.

For the airfoil case coefficients H_i^* and A_i^* may be obtained theoretically but for the bridge deck they must be obtained from wind tunnel tests on section models because of its bluff shape.

The coefficients for the thin airfoil are given theoretically in terms of Theodorsen Function as (Fig. 4.5)

$$
\begin{array}{ll}
K H_1^* = -2\pi F \ ; & K H_2^* = -\pi[1 + F + 2G/K] \\
K^2 H_3^* = -2\pi[F - KG/2] \ ; & K^2 H_4^* = \pi[K + 2G] \\
K A_1^* = \pi F \ ; & K A_2^* = \pi/2 \ [2G/K + F - 1] \\
K^2 A_3^* = \pi[F - KG/2 + K^2/8] \ ; & K A_4^* = -\pi G
\end{array}
\tag{4.20}
$$

where F and G are the real and imaginary parts respectively of the well known Theodorsen Function , i.e., $C(K) = F(K) + iG(K)$.

In the absence of experimental aerodynamic data (and also in some instances for the comparison of the derivatives), earlier researchers have even tried to utilize the above derivatives of airfoils for the analysis of bridge decks, which, however, may entail large departures, greatly affecting the accuracy.

For a bluff section the flutter derivatives are to be extracted from wind tunnel experiments on a section model using the free oscillation technique (Chapter 5).

4.4 FULL BRIDGE AERODYNAMICS

In a true sense, section models, even fully three dimensional ones, cannot duplicate prototype behaviour completely. However, the short and long span section models, are repeatedly used for economic and other reasons. The results of the section models have been used in the subsequent analytical modeling to obtain the full bridge response for the prototype. Prominent among the wind induced problems of cable supported bridges are flutter and buffeting which have been, therefore, considered in the present study.

4.4.1 Full Bridge Flutter Dynamics

Eqns.4.16 and 4.17 are further generalized to the case of a bridge which is curved either in elevation or in plan [11].

In the above general case the torsion involves some lateral sway in case of decks curved in elevation while bending couples with the torsion in the second case. For the latter case the vertical modes of the bridge are in fact three dimensional with components of vertical deflection, lateral deflection and torsion identifiable at any point along the line of centre of gravity of the bridge deck section from the structural vibration analysis. For example they may be defined as

$$h(x,t) = \sum_i \xi_i(t)h_i(x)B \tag{4.21}$$

$$p(x,t) = \sum_i \xi_i(t)p_i(x)B \tag{4.22}$$

$$\alpha(x,t) = \sum_i \xi_i(t)\alpha_i(x) \tag{4.23}$$

where h, p and α are the vertical, sway and torsional motions respectively, $\xi_i(t)$ the generalized coordinate of mode i and $h_i(x)$, $p_i(x)$ and $\alpha_i(x)$ the non-dimensional i^{th} mode components of vertical, sway and torsional motions respectively.

The generalized equation of motion of the ith mode is then

$$I_i[\ddot{\xi}_i + 2\zeta_i\omega_i\dot{\xi}_i + \omega_i^2\xi_i] = (Q_i)_{se} \tag{4.24}$$

where $(Q_i)_{se}$ is the generalized self excited force appropriate to mode i, I_i is the generalized inertia of mode i, and ζ_i and ω_i are its damping and the natural frequency of vibration in rad/sec. If m(x) and I(x) are respectively the mass and mass moment of inertia per unit span about the sections c.g., then,

$$I_i = M_{vi}B^2 + M_{li}B^2 + I_{oi} \tag{4.25}$$

where

$$M_{vi} = \int_{span} m(x)h_i^2(x)dx$$

$$M_{li} = \int_{span} m(x)p_i^2(x)dx$$

64

$$I_{oi} = \int_{span} I(x)\alpha_i^2(x)dx \tag{4.26}$$

The generalized self excited force is

$$(Q_i)_{se} = \int_{span} [L_{se}h_i(x)B + D_{se}p_i(x)B + M_{se}\alpha_i(x)]dx \tag{4.27}$$

where L_{se}, D_{se} and M_{se} are lift, drag and moment per unit span respectively acting at spanwise section x.

The integrations in eqns. 4.26 and 4.27 could alternatively be carried over the entire structure. The difference would however tend to nullify due to similar integration limits applied to both sides of the equation 4.24. This has been suggested in Ref. 12 and 13.

In terms of flutter derivatives, the linearized self-excited (flutter) forces associated with oscillatory lift, drag and moment per unit span, are of the form,

$$L_{se} = \frac{1}{2}\rho U^2 2B[KH_1^*(K)\frac{\dot{h}}{U} + KH_2^*(K)\frac{B\dot{\alpha}}{U} + K^2H_3^*(K)\alpha + K^2H_4^*(K)\frac{h}{U} + KH_5^*(K)\frac{\dot{p}}{U} + K^2H_6^*(K)p]$$

$$D_{se} = \frac{1}{2}\rho U^2 2B[KP_1^*(K)\frac{\dot{p}}{U} + KP_2^*(K)\frac{B\dot{\alpha}}{U} + K^2P_3^*(K)\alpha + K^2P_4^*(K)\frac{p}{U} + KP_5^*(K)\frac{\dot{h}}{U} + K^2P_6^*(K)h]$$

$$M_{se} = \frac{1}{2}\rho U^2 2B^2[KA_1^*(K)\frac{\dot{h}}{U} + KA_2^*(K)\frac{B\dot{\alpha}}{U} + K^2A_3^*(K)\alpha + K^2A_4^*(K)h + KA_5^*(K)\frac{\dot{p}}{U} + K^2A_6^*(K)p]$$

The equations-of-motion dependent forces contain eighteen flutter derivative coefficients, ten of which are due to lateral degrees of freedom. The experimentally determined dimensionless "flutter" coefficients that characterize the self-excited aerodynamics of the bridge deck form are expressed as functions of K, K being the dimensionless flutter frequency ($K = B\omega/U$). H_i^* and A_i^* are to be extracted from wind tunnel experiments on the section model of the given deck (Chapter 6), but for P_i^*, some quasi-static approximations have been used along with the drag coefficient(C_D) given in Ref. 13.

$$L_{se} = \frac{1}{2}\rho U^2 2B\left[KH_1^*(K)\frac{\sum_j \dot{\xi}_j h_j B}{U} + KH_2^*(K)\frac{\sum_j \alpha_j \dot{\xi}_j B}{U} + K^2H_3^*(K)\sum_j(\xi_j\alpha_j)\right.$$

$$\left. + K^2H_4^*(K)\sum_j\xi_jh_j B + KH_5^*(K)\frac{\sum_j \dot{\xi}_j p_j B}{U} + K^2H_6^*(K)\sum_j\xi_jp_j B\right] \tag{4.31}$$

$$D_{se} = \frac{1}{2}\rho U^2 2B\left[KP_1^*(K)\frac{\sum_j \dot{\xi}_j\, p_j B}{U} + KP_2^*(K)\frac{\sum_j \alpha_j\, \dot{\xi}_j B}{U} + K^2 P_3^*(K)\sum_j (\xi_j \alpha_j)\right.$$

$$\left. + K^2 P_4^*(K)\sum_j \xi_j p_j\, B + KP_5^*(K)\frac{\sum_j \dot{\xi}_j\, h_j B}{U} + K^2 P_6^*(K)\sum_j \xi_j h_j\, B\right] \tag{4.32}$$

$$M_{se} = \frac{1}{2}\rho U^2 2B^2\left[KA_1^*(K)\frac{\sum_j \dot{\xi}_j\, h_j B}{U} + KA_2^*(K)\frac{\sum_j \alpha_j\, \dot{\xi}_j B}{U} + K^2 A_3^*(K)\sum_j (\xi_j a_j)\right.$$

$$\left. + K^2 A_4^*(K)\sum_j \xi_j h_j\, B + KA_5^*(K)\frac{\sum_j \dot{\xi}_j\, p_j B}{U} + K^2 A_6^*(K)\sum_j \xi_j p_j\, B\right] \tag{4.33}$$

Substituting these in eqn.4.27 and expressing explicitly, one gets,

$$(Q_i)_{se} = \frac{1}{2}\rho U^2 2B^2 \int_{span}\left\{\left[KH_1^*(K)\frac{\sum_j \dot{\xi}_j\, h_j B}{U} + KH_2^*(K)\frac{\sum_j \alpha_j\, \dot{\xi}_j B}{U} + K^2 H_3^*(K)\sum_j (\xi_j \alpha_j)\right.\right.$$

$$\left. + K^2 H_4^*(K)\sum_j \xi_j h_j\, B + KH_5^*(K)\frac{\sum_j \dot{\xi}_j\, p_j B}{U} + K^2 H_6^*(K)\sum_j \xi_j p_j\, B\right] h_i(x)$$

$$+ \left[KP_1^*(K)\frac{\sum_j \dot{\xi}_j\, p_j B}{U} + KP_2^*(K)\frac{\sum_j \alpha_j\, \dot{\xi}_j B}{U} + K^2 P_3^*(K)\sum_j (\xi_j \alpha_j)\right.$$

$$\left. + K^2 P_4^*(K)\sum_j \xi_j p_j\, B + KP_5^*(K)\frac{\sum_j \dot{\xi}_j\, h_j B}{U} + K^2 P_6^*(K)\sum_j \xi_j h_j\, B\right] p_i(x)$$

$$+ KA_1^*(K)\frac{\sum_j \dot{\xi}_j\, h_j B}{U} + KA_2^*(K)\frac{\sum_j \alpha_j\, \dot{\xi}_j B}{U} + K^2 A_3^*(K)\sum_j (\xi_j \alpha_j)$$

$$\left. + K^2 A_4^*(K)\sum_j \xi_j h_j\, B + KA_5^*(K)\frac{\sum_j \dot{\xi}_j\, p_j B}{U} + K^2 A_6^*(K)\sum_j \xi_j p_j\, B\right] \alpha_i(x)\right\} dx \tag{4.34}$$

From the eqn.4.34 it is clear that several vibrational modes of the bridge are in principle intercoupled by the aerodynamic forces that contribute to $(Q_i)_{se}$.

Though the coupling derivatives may become important for much larger and complex

bridges, these can be dropped in an attempt to simplify the analysis for bridges of the kind studied in the present work[11]. Bridge flutter is mainly of the separated flow type with single structural mode playing the predominant role (as it was observed in Tacoma Narrows case).

With the flutter occurring in a single mode of the structure, and introducing the definition,

$$G_{r_m s_n} = \int r_m(x) \, s_n(x) \, dx \tag{4.35}$$

where $r,s = h, p$ or α and $m, n = i$ or j.

Substituting eqn.4.35 into eqn.4.34, the generalized force Q_i will be

$$(Q_i)_{se} = \rho U^2 B^2 \left\{ \frac{K}{U} \left[\sum_i \dot{\xi}_i (H_1^* G_{h_i h_i} + H_2^* G_{\alpha_i h_i} + H_5^* G_{p_i h_i} + P_1^* G_{p_i p_i} \right. \right.$$

$$+ P_5^* G_{\alpha_i p_i} + P_5^* G_{h_i p_i} + A_1^* G_{h_i \alpha_i} + A_2^* G_{\alpha_i \alpha_i} + A_5^* G_{p_i \alpha_i})$$

$$+ \frac{KU}{B} \sum_i \xi_i (H_3^* G_{\alpha_i h_i} + H_4^* G_{h_i h_i} + H_6^* G_{p_i h_i} + P_3^* G_{\alpha_i p_i} + P_4^* G_{p_i p_i} + P_6^* G_{h_i p_i}$$

$$\left. \left. + A_3^* G_{\alpha_i \alpha_i} + A_4^* G_{h_i \alpha_i} + A_6^* G_{p_i \alpha_i}) \right] \right\} \tag{4.36}$$

The detailed characteristics of the coupling involved in eqns.4.34 and 4.36 depend upon the numerical values of flutter derivatives and the modal integrals $G_{r_m s_n}$. To have an idea of the resulting response it is required to check for stability and attempt a solution of the complete system. For such an analysis it is necessary to simplify the above system, in some directed way (to a single mode of vibration), so that the solution will become straight-forward for a specified wind velocity.

The coupling derivatives in eqn.4.36 constitute a mechanism of energy dispersion into several bridge modes, with some modes tending to be favourable to the overall bridge stability. Such a situation is likely to protect potentially unstable systems.

On the other hand, it is a matter of observation - mainly of models, though the famous Tacoma Narrows film record also lends some insight - that flutter, when it does occur, usually involves strong action of one mode in particular. Bridge flutter is most commonly a bluff-body separated flow phenomenon in which a single torsion mode becomes

unstable and drives the system to extremely large oscillations. One seeks out such worst cases, however unlikely, as depicting the most critical circumstances of flutter for a given bridge design. Hence a simplification of the complex eqn.4.36 is justified.

4.4.1.1 Simplified Flutter Dynamics

Under such conditions as explained in the preceding section the cross coupling aerodynamic effects can be ignored in the investigations of common types of flutter, or, at least, the tendencies, mode by mode, of negative damping driven flutter to occur may systematically be examined by the simplified version of eqn.4.36 (Scanlan[13]) as

$$(Q_i)_{se} = \rho U^2 B^2 \left\{ \frac{KB}{U} \left[\xi_i (H_1^* G_{h_i h_i} + P_1^* G_{p_i p_i} + A_2^* G_{\alpha_i \alpha_i}) \right.\right.$$

$$\left.\left. + \frac{KU}{B} \xi_j (H_4^* G_{h_i h_i} + P_4^* G_{p_i p_i} + A_3^* G_{\alpha_i \alpha_i}) \right] \right\} \tag{4.37}$$

Here the derivatives H_i^*, A_i^* are obtained from experiments on section models of the bridge deck while the derivative $P_1^* = \frac{-2}{K} C_D$, where C_D is aerodynamic static drag coefficient.

For any specified velocity U, the value of $K \simeq B\omega_i/U$ will be a good approximation, since the relative effect of wind for natural frequencies is small. The system equation may alternatively be expressed as one describing free oscillations,as,

$$I_i | \ddot{\xi}_i + 2\zeta_i \tilde{\omega}_i \dot{\xi}_i + \tilde{\omega}_i^2 \xi_i | = (Q_i)_{s.e.} \tag{4.38}$$

$$\text{in which } \tilde{\omega}_i = \left[\frac{\omega_i^2}{1 + \frac{\rho B^4}{I_i} (H_4^* G_{h_i h_i} + A_3^* G_{\alpha_i \alpha_i})} \right]^{1/2} \tag{4.39}$$

and

$$\tilde{\zeta}_i = \zeta_i \frac{\omega_i}{\tilde{\omega}_i} - \frac{\rho B^4}{2 I_i} (H_1^* G_{h_i h_i} + P_1^* G_{p_i p_i} + A_2^* G_{\alpha_i \alpha_i}) \tag{4.40}$$

Given a specified value of velocity U, eqns.4.38 and 4.39 may be solved for $\tilde{\omega}_i$ and $\tilde{\zeta}_i$. In eqn.4.40, $\tilde{\zeta}_i$ becoming zero defines onset of flutter. This can be obtained approximately by first taking $\tilde{\omega}_i = \omega_i$ and successively using iterative technique until the

value $\widetilde{\zeta}_i$ becomes zero. After few iterations values of K and $\widetilde{\omega}_i$ for flutter may be established, from which, the critical wind velocity U_{cr} causing flutter can be obtained from using eqn.4.5 as follows:

$$U_{cr} = \frac{B\,\widetilde{\omega}_i}{\widetilde{K}} \tag{4.41}$$

In other words, the criterion for flutter at the specific velocity U will then be given by $\widetilde{\zeta}_i \leq 0$,

Rewriting eqn.4.40 we get

$$\widetilde{\zeta}_i = \zeta_i \frac{\omega_i}{\widetilde{\omega}_i}\left[1 - \frac{\widetilde{\omega}_i\,\rho B^4}{2\,\omega_i\zeta_i I_i}\,(H_1^* G_{h_i h_i} + P_1^* G_{p_i p_i} + A_2^* G_{\alpha_i \alpha_i})\right] \tag{4.42}$$

so that the flutter criterion will be

$$\frac{\widetilde{\omega}_i\,\rho B^4}{\omega_i\zeta_i I_i}\,(H_1^* G_{h_i h_i} + P_1^* G_{p_i p_i} + A_2^* G_{\alpha_i \alpha_i}) \geq 1 \tag{4.43}$$

From the eqns.4.39 and 4.43 it can be seen if the specified velocity U will induce flutter or not. The criterion stated in this section has been used in the present work to estimate the critical wind velocity U_{cr} (eqn.4.41) for the girder bridge deck of the cable stayed bridge that produces the flutter condition.

It is also evident that an increase (algebraic) in the values of the derivatives H_1^* and A_2^* would tend to reduce the aerodynamic stability of the bridge deck system, while an increase in the coefficients H_4^* and A_3^* would enhance the stability of the system.

4.4.2 Full Bridge Buffeting Response

Buffeting is defined as the dynamic loading of a structure by velocity fluctuations in the on coming flow. As clarified in the earlier section, it is necessary to obtain the aerodynamic data like flutter derivative coefficients and other structural properties from section model tests in wind tunnel in order to estimate the flutter criterion. The aerodynamic information, derived for the girder deck section, can then be generalized for the full span of the bridge by analytical considerations. In the present study the two dimensional buffeting response (torsional and vertical) has been estimated for the bridges under investigation.

The formulation to estimate the buffeting response[10,12] is explained in the following articles.

Considering the section of the bridge deck shown in Fig.4.4 the governing equations of motion are

$$m[\ddot{h} + 2\zeta_h\omega_h\dot{h} + \omega_h^2 h] = L_{se}+L_b(t) \tag{4.44}$$

$$I[\ddot{\alpha} + 2\zeta_\alpha\omega_\alpha\dot{\alpha} + \omega_\alpha^2\alpha] = M_{se}+M_b(t) \tag{4.45}$$

where $L_b(t)$ is the gust force in lift per unit span, and $M_b(t)$ is the gust moment per unit span, on the model.

The self-excited force components L_{se} and M_{se} are given by eqns.4.16 and 4.17. The forces $L_b(t)$ and $M_b(t)$ are active forces due to impingement of the gusty wind upon the deck section. In the presence of varying components $U(t)$ and $w(t)$ respectively, the non-dimensional aerodynamic lift and moment are obtained as follows[10]

$$L^*(t) = \frac{L_b(t)}{\frac{1}{2}\rho\, U^2 B} = -C_L(\alpha_o)\left[1 + \frac{2u(x,t)}{U}\right]-\left[\left.\frac{dC_L}{d\alpha}\right|_{\alpha=\alpha_o}+\frac{A}{B}\,C_D(\alpha_o)\right]\frac{w(x,t)}{U} \tag{4.46}$$

$$M^*(t) = \frac{M_b(t)}{\frac{1}{2}\rho\, U^2 B^2} = \left[C_M(\alpha_o) + C_D(\alpha_o)\frac{Ar}{B2}\right]\left[1 +2\frac{u(x,t)}{U}\right]+\left.\frac{dC_M}{d\alpha}\right|_{\alpha=\alpha_o}\frac{w(x,t)}{U} \tag{4.47}$$

where

A = deck projected area normal to wind per unit span

r = distance from deck mass centre to effective rotation axis

C_L = lift coefficient of the deck section in steady flow

$\frac{dC_L}{d\alpha} = C_L^{'}$ = slope of lift coefficient curve versus angle of attack α

C_M = moment coefficient of the deck section in steady flow

$\frac{dC_M}{d\alpha} = C_M^{'}$ = slope of lift coefficient curve versus angle of attack α

C_D = drag coefficient of the deck section in steady flow.

The values of the coefficients are selected at $\alpha = \alpha_0$, the equilibrium position of the bridge in steady wind, and generally $\alpha_0 = 0$. Since the response calculation is based on the section model aerodynamic data, the use of aerodynamic admittance is eliminated in the

present formulation.

The approach is somewhat similar to that originally given by Davenport[1] and adopted by Scanlan[12] to calculate the mean response of individual bridge models to wind. The principal difference in the present study is the inclusion of the effects of the additional self-excited term(H_4^*) apart from the principal uncoupling flutter derivative coefficients H_1^*, A_2^*, A_3^* utilized by Scanlan and Gade[10].

4.4.2.1 Pure Torsion of Deck Section

For the formulation of full bridge torsional response, the response formulation of deck section needs to be done. The equations of motion 4.45 along with self-excited terms may be rewritten in simpler form using uncoupled flutter derivative coefficients and through the introduction of the dimensionless time variable s, where

$$s = Ut/B \tag{4.48}$$

then from eqns.4.45 and 4.47

$$I[\alpha'' + 2\zeta_\alpha K_\alpha \alpha' + K_\alpha^2 \alpha] = \rho B^4 \left[K A_2^* \alpha' + K^2 A_3^* \alpha + M^*(s) \right] \tag{4.49}$$

in which $\alpha' = B/U\ \alpha$ and $K_\alpha = B\omega_\alpha/U$

$$M^*(s) = C_M \frac{u(s)}{U} + \frac{1}{2} C_M' \frac{w(s)}{U} \tag{4.50}$$

Now defining K_t and γ_t as,

$$K_t = \left[K_\alpha^2 - \frac{\rho B^4}{I} K^2 A_3^*(K) \right]^{\frac{1}{2}} \tag{4.51}$$

$$\gamma_t = \frac{1}{2K_t} \left[2\zeta K_\alpha - \frac{\rho B^4}{I} K A_2^*(K) \right] \tag{4.52}$$

the eqn.4.49 simplifies to

$$\alpha'' + 2\zeta_t K_t \alpha' + K_t^2 \alpha = \rho B^4 M^*(s) \tag{4.53}$$

where $M^*(s)$ is random in s.

So this problem is similar to that of random vibrations. Therefore, the spectrum of response S_α is then given by

$$S_\alpha(K) = \left| \mathcal{A}(K) \right|^2 (\frac{\rho B^4}{I})^2 \frac{S_M(K)}{U^2} \tag{4.54}$$

in which

$$S_M(K) = C_M^2 S_u(K) + \tfrac{1}{2} C_M C_M' \left[S_{uw}(K) + S_{wu}(K) \right] + \tfrac{1}{4} C_M' S_w(K) \qquad (4.55)$$

and $\mathcal{A}(K) = \left[K_t^2 - K^2 + 2i\gamma_t K_t K \right]^{-1}$ (4.56)

with $S_u(K) \to$ spectrum of $u(t)$

$S_w(K) \to$ spectrum of $w(t)$

$S_{uw}(K) \to$ Cross-spectrum of u,w and

$S_{wu}(K) \to$ Cross-spectrum of w,u.

The variance of the response will be

$$\sigma_\alpha^2 = \int_0^\infty S_\alpha(K) dK \qquad (4.57)$$

which can be further simplified from eqn.4.54 noting that $\left| \mathcal{A}(K) \right|^2$ is highly peaked in the neighbourhood of $K = K_t$, reflecting the fact that the main contribution to $S_\alpha(K)$ comes from this source. Then

$$\int_0^\infty \left| \mathcal{A}(K) \right|^2 dK = \int_0^\infty \frac{dK}{(K_t^2 - K^2)^2 + 4\gamma_t^2 K_t^2 K^2} = \frac{\pi}{4\gamma_t K_t^3} \qquad (4.58)$$

results in $\sigma_\alpha^2 = \dfrac{\pi}{4\gamma_t K_t^3} (\rho \dfrac{B^4}{I})^2 \dfrac{S_M(K)}{U^2}$ (4.59)

which, if the assumption is made that u and w are negligibly correlated then

$$S_M(K) = C_M^2 S_u(K) + \tfrac{1}{4} C_M' S_w(K) \qquad (4.60)$$

$S_u(K)$ and $S_w(K)$ have been discussed later in this chapter.

4.4.2.2 Full Bridge Response in Torsion

Assuming that the bridge response takes place as the superposition of N torsion modes, then

$$\alpha(x,s) = \sum \alpha_r(x) \, \eta_r(s) \qquad (4.61)$$

By reasoning analogous to that for the deck section mentioned earlier, the response in mode r to the applied random moment $\rho B^4 M^*(x,s) dx$ is governed by

$$\eta_r''(s) + 2\gamma_{tr} K_{tr} \eta_r'(s) + K_{tr}^2 \eta_r(s) = \frac{\rho B^4}{I_r} \int_0^L M^*(x,s) \alpha_r(x) dx \qquad (4.62)$$

in which   and K_{tr} and γ_{tr} are analogous to eqns.4.51 and 4.52 for the rth mode, and integration is over the span L,

$$M^*(x,s) = C_M \frac{u(x,s)}{U} + \frac{1}{2} C_M' \frac{w(x,s)}{U} \tag{4.63}$$

and, $I_r = \int_0^L I \, \alpha_r^2(x)dx \tag{4.64}$

equals the generalized torsional inertia for mode 'r'.

The spectrum of the response at point x of the span for all modes N is, under these conditions given to a close approximation by

$$S_\alpha(x,K) \simeq \sum_{r=1}^N \left[\frac{\alpha_r^2(x)}{(K_{tr}^2 - K^2)^2 + 4\gamma_{tr}^2 K_{tr}^2 K^2} (\rho \frac{B^4 L}{I_r})^2 \frac{1}{U^2} \int_0^L \right.$$
$$\left. \int_0^L \alpha_r(x_A)\alpha_r(x_B)S_M(x_A,x_B;K)\frac{dx_A}{L} \frac{dx_B}{L} \right] \tag{4.65}$$

in which $S_M(x_A,x_B;K)$ is the cross spectrum of $M = U\, M^*$ relative to points x_A,x_B. This response takes place about the steady deflection due to the mean wind velocity, which is not considered in the present study.

To use eqn.4.65 the cross spectrum $S_M(x_A,x_B;K)$ must be given in explicit form. Making the following assumptions similar to that of Davenport[2],

   :only co-spectra are retained

   :quadrature-spectra produces negligible contribution

   :lateral force co-herence values follow lateral wind co-herence patterns

So the co-spectrum in its explicit form is

$$S_M(x_A,x_B;K) = S_M(K) \, e^{-C|x_A-x_B|/L} \tag{4.66}$$

   in which the value of 'C' was estimated as [3]

$$C = \frac{7nL}{U} \tag{4.67}$$

   n - frequency in Hz.

With the above approximation introduced, we can write for $C \geq 3$

$$\int_0^L \int_0^L \alpha_r(x_A)\alpha_r(x_B)S_M(x_A,x_B;K)\frac{dx_A}{L} \frac{dx_B}{L} \right] \simeq G_t\left[\frac{2C(C-1)}{C^2}\right] S_M(K) \tag{4.68}$$

in which

$$G_t = \int_0^L \alpha_r^2(x)dx/L$$

$$2(C-1)/C^2 \simeq \int_0^L \int_0^L e^{-C|x_A-x_B|} \frac{dx_A}{L} \frac{dx_B}{L} \tag{4.69}$$

Since these approximations will yield results within 3% [10] of the exact ones estimated from eqn.4.65, this formulation is adopted for the present study to evaluate the response of the cable stayed bridges.

Introducing these approximations the eqn.4.65 becomes

$$S_\alpha(x,K) = \sum_{r=1}^N \left\{ \frac{\alpha_r^2(x)}{(K_{tr}^2 - K^2)^2 + 4\gamma_{tr}^2 K_{tr}^2 K^2} (\frac{\rho B^4 L}{I_r})^2 \frac{1}{U^2} G_t \left[\frac{2(C-1)}{C^2} \right] S_M(K) \right\} \tag{4.70}$$

From this and using eqn.4.57, the mean square torsional response will be

$$\sigma_\alpha^2 = \sum_{r=1}^N \frac{\pi \alpha_r^2(x)}{4\gamma_{tr} K_{tr}^3} (\frac{\rho B^4 L}{I_r})^2 G_t \left[\frac{2(C-1)}{C^2} \right] \frac{S_M(K_{tr})}{U^2} \tag{4.71}$$

4.4.2.3 Full Bridge Response in Bending

Analogous to the preceding section 4.4.2.2, assuming that the response takes place as the superposition of N vertical modes, we may write for the full bridge response in bending,

$$\frac{h}{B}(x,s) = \sum_{r=1}^N \frac{h_r(x)}{B} \xi_r(s) \tag{4.72}$$

in which $h_r(x)$ is the dimensionless r^{th} bending mode; and ξ_r is the corresponding generalized coordinate. By following the steps of the preceding derivations the spectrum of response at point x along the span will be

$$S_{h/B}(x,K) = \sum_{r=1}^N \left\{ \frac{h_r^2(x)}{(K_{hr}^2 - K^2)^2 + 4\gamma_{hr}^2 K_{hr}^2 K^2} (\frac{\rho B^2 L}{M_r})^2 G_B \left[\frac{2(C-1)}{C^2} \right] \frac{S_L(K_{hr})}{U^2} \right\} \tag{4.73}$$

and the variance will be

$$\sigma_{h/B}^2 = \sum_{r=1}^N \frac{\pi h_r^2(x)}{4\gamma_{hr} K_{hr}^3} (\frac{\rho B^2 L}{M_r})^2 G_B \left[\frac{2(C-1)}{C^2} \right] \frac{S_L(K_{hr})}{U^2} \tag{4.74}$$

74

in which

$$G_B = \int_0^L h_r^2(x)dx/L \tag{4.75}$$

$$M_r = \int_0^L m \ h_r^2(x)/B^2 dx \tag{4.76}$$

$$C = 7n_{hr}L/U \tag{4.77}$$

$$S_L(K) = C_{Lu}^2 \ S_u + C_{Lw}^2 \ S_w \tag{4.78}$$

with $C_{Lu} = -C_L$ (4.79)

and $\quad C_{Lw} = \frac{1}{2} [\ C_L' + \frac{A}{B} \ C_D]$ (4.80)

The procedure is analogous to that for calculating 4.71 with reference to the formulae given. In particular, slight modification occurs in the terms like

$$K_{hr} = \frac{2\pi B n_{hr}}{U} \tag{4.81}$$

$$K_{vr} = \left[K_{hr}^2 - \frac{\rho B^2}{m} K_{hr}^2 H_4^*(K_{hr}) \right]^{\frac{1}{2}} \tag{4.82}$$

$$\gamma_{hr} = \frac{1}{2K_{vr}} \left[2\zeta_{hr}K_{hr} - \frac{\rho B^2}{m} K_{hr}H_1^*(K_{hr}) \right] \tag{4.83}$$

From eqns.4.70, 4.71, 4.73 and 4.74 and using the wind characteristics given in the following article, the response of pure torsion and bending for the selected bridges are given in chapter 6.

4.4.2.4 Wind Spectra

In the absence of wind data at the site, one might choose from the various wind spectra available in different forms[7]. The wind spectra given by Simiu[6] has been utilized in the present analysis to estimate the response of the prototype bridges since these have been widely acclaimed to represent the atmospheric wind turbulence.

The expression for Longitudinal wind spectra $S_u(n)$ is given by Simiu [6] in the form

$$\frac{nS_u(n)}{U_*^2} = \frac{2\,00 \ f}{(1+50f)^{5/3}} \tag{4.84}$$

and the expression for vertical wind spectra $S_w(n)$ is given in the form

$$\frac{nS_w(n)}{U_*^2} = \frac{6 \ f}{(1+4f)^{5/3}} \tag{4.85}$$

In eqns.4.84 and 4.85 the term

$$f = \frac{nZ}{U} = \frac{KZ}{2\pi B} \tag{4.86}$$

in which Z is the bridge deck height from the reference level, generally taken as the mean retarding surface, and

$$U_* = \frac{U(Z_r)}{2.5 \; \ln\dfrac{Z_r - Z_d}{Z_0}} \tag{4.87}$$

Z_r is any reference altitude at which U is known, Z_d is the smaller of 20 m or 0.75 H where H is the mean height of buildings in the surrounding area ; $Z_d = 0$ in open regions, and Z_0 is roughness length given in table 4.1.

Table 4.1

Boundary Layer Data with Roughness Length

Type of Surface	Range of Z_0, in meters
Sea surface, sand	0.000003 to 0.004
Snow surface	0.001 to 0.006
Mowed grass	0.001 to 0.04
High grass	0.04 to 0.10
Forest medium dense	0.90 to 1.00
Suburbs, outskirts to centre	0.20 to 0.45
Large city centres	0.60 to 0.80

References

1. Davenport,A.G., (1962), "Buffeting of a Suspension Bridge by Storm Winds", Jnl. Structural Div., ASCE, Vol. 88, ST3, June, pp 234-264.

2. Davenport,A.G., (1962), "The Response of Slender, Line Like Structures to a Gusty Wind ", Proc. of Institution of Civil Engineers, Paper 6610, London, pp 389-407.

3. Davenport,A.G., (1963), "The Relationship of Wind Structure to Wind Loading", Proc. Symposium on Wind Effects on Building and Structures, Vol.1, Teddington, U.K., June, pp 54-102.

4. Fung,Y.C., (1955), "An Introduction of the Theory of Aeroelasticity", John Wiley & Sons, N.Y.

5. Sears,W.R., (1941), "Some Aspects of Non-Stationary Airfoil Theory and Its Practical Applications", Jnl. Aeronautical Science, No.8.

6. Simiu,E., (1974), "Wind Spectra and Dynamic Along Wind Response", Jnl. Structural Div., ASCE, Vol. 100, ST9, September, pp 1897-1910.

7. Simiu,E. and R.H.Scanlan, (1986), "Wind Effects on Structures", II Ed., John Wiley and Sons, N.Y.

8. Scanlan,R.H., and J.Tomko, (1971), "Airfoil and Bridge Deck Flutter Derivatives", Jnl. of Engg. Mech. Div., Proc. ASCE, Vol. 97, Dec., pp 1717-1737.

9. Scanlan,R.H., J.G.Belivean and K.S.Budlong, (1974), "Indicial Aerodynamic Functions for Bridge Decks", Jnl. Engg. Mechanics Div., ASCE, Vol. 100, EM4, August, pp 657-672.

10. Scanlan,R.H., and R.H.Gade, (1977), "Motion of Suspended Bridge Spans under Gusty Wind", Jnl. of Structural Div., ASCE, Vol.103,ST9, September, pp 1867-1883.

11. Scanlan,R.H., (1978), "The Action of Flexible Bridges under Wind-I Flutter Theory", Jnl. Sound and Vibration, Vol. 60-2, pp 187-199.

12. Scanlan,R.H., (1978), "The Action of Flexible Bridges under Wind-II Buffeting Theory", Jnl. Sound and Vibration, Vol. 60-2, pp 201-211.

13. Scanlan,R.H., (1987), "Interpreting Aeroelastic Models of Cable Stayed Bridges", Jnl. of Engg. Mechanics Div., ASCE, Vol.113,EM4, April, pp 555-575.

14. Von Karman and W.R.Sears, (1938), "Airfoil Theory for Non Uniform Motion", Jnl. of Aeronautical Science, No.10.

Notations

A_i^*	flutter derivatives($i = 1, 2, ..$)
B	width of section model/airfoil section
C_D	drag coefficient
$C(K)$	Theodorsen Function
C_L	lift coefficient
C_L'	slope of lift coefficient with respect to wind incidence angle
C_M	moment Coefficient
C_M'	slope of moment coefficient with respect to wind incidence angle
D	aerodynamic drag force
D_{se}	self excited drag force
$G_{r_i s_i}$	Geometric modal integrals
H_i^*	flutter derivatives($i = 1, 2, ..$)
I_r	generalized torsional inertia
$I(x)$	mass moment of inertia at section X
K	reduced frequency
L	aerodynamic lift force
L_b	buffeting lift force
L_{se}	self excited lift force
M	aerodynamic moment force
M_b	buffeting moment force
M_{se}	self excited moment force
P_i^*	flutter derivative($i = 1, 2, ..$)
Q_i	generalized self excited force in i^{th} mode
$S_u(K)$	spectrum of longitudinal velocity component u(t)
$S_w(K)$	spectrum of vertical velocity component w(t)
S_{uw}	cross spectrum of u and w
S_{wu}	cross spectrum of w and u
U	mean wind velocity
U_{cr}	Critical wind velocity
Z_0	surface roughness length
Z	deck height from reference level
Z_r	reference altitude
Z_d	average height of obstructions
f	frequency of turbulence wind
h	vertical displacement
$m(x)$	mass at section X

n	circular frequency of oscillation in Hz
p	translational displacement(sway)
$u*$	shear velocity
$u(t)$	fluctuating component of longitudinal velocity
$w(t)$	fluctuating component of vertical velocity
α	rotational displacement
λ	decay rate
ρ	air density
σ_α	variance of spectral density
θ	relative phase difference
ω_h, ω_α	natural frequency of vibration in bending and torsion
ζ_i	generalized coordinates in mode i
ζ_h	damping ratio in bending
ζ_α	damping ratio in torsion
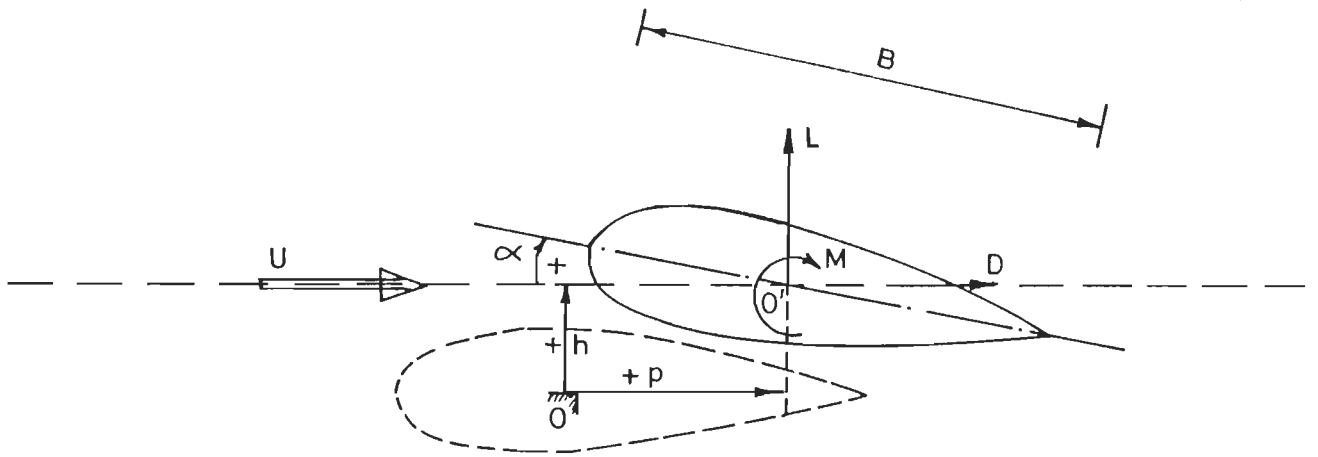
Fig. 4·1   Force components on Airfoil section
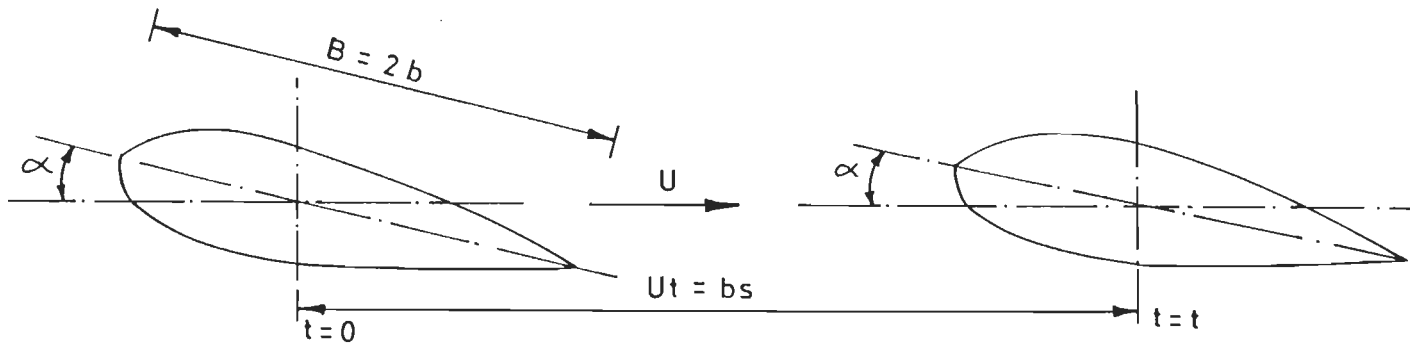
Fig. 4·2   Airfoil under impulsive forward motion (Wagner function)
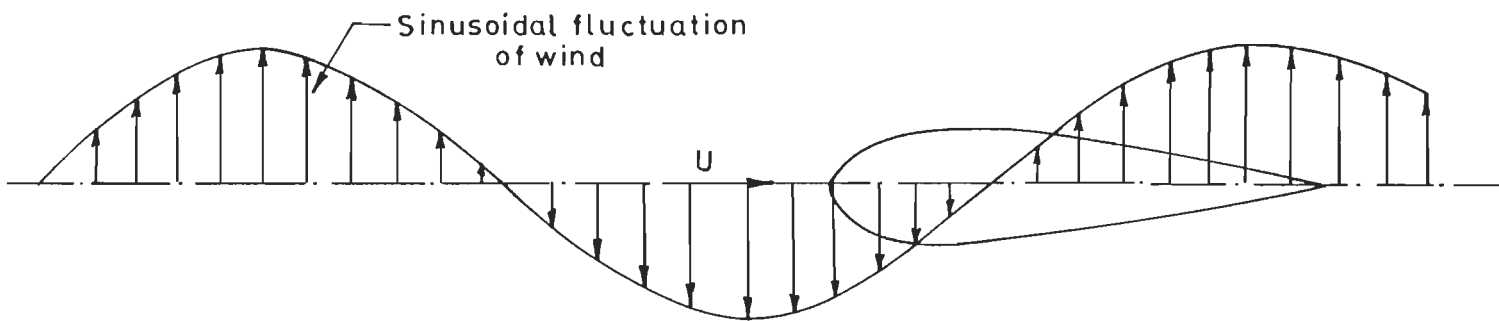
Fig. 4·3   Airfoil flying through a sinusoidal gust field (Sears function)
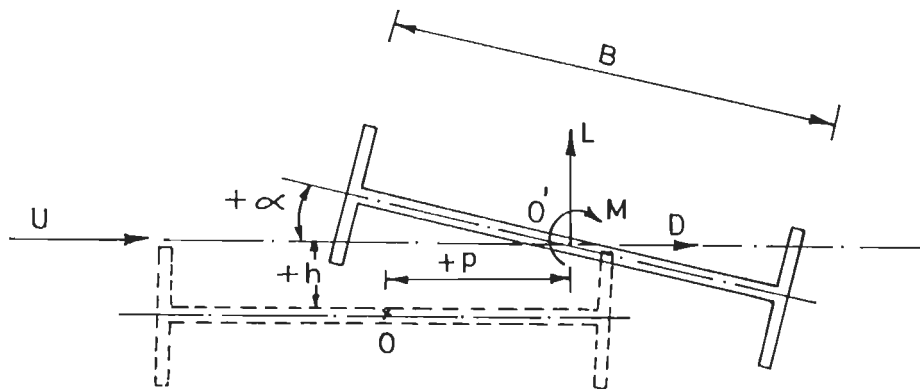
Fig. 4·4 Degrees of freedom and Aerodynamic forces
on Bridge Deck
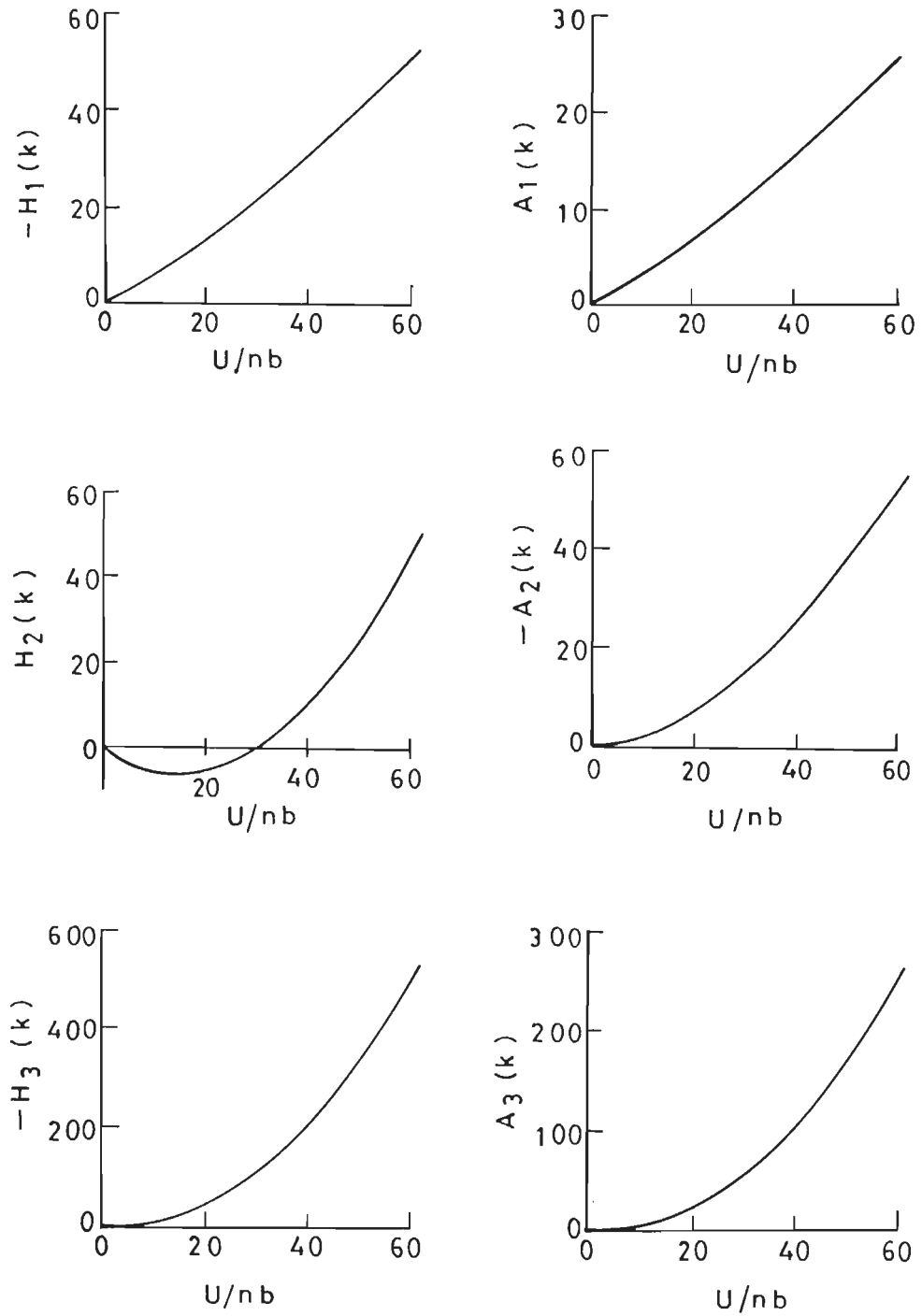
Fig. 4·5   Air foil   flutter Derivatives (Theoretical)

CHAPTER 5
DESCRIPTION OF EXPERIMENTAL INVESTIGATIONS

5.1 GENERAL

As mentioned in preceding chapter the aerodynamic flutter derivative coefficients associated with bluff bodies such as bridge decks could not be obtained from theoretical approach because of the complexity of the flow around the moving bluff structure. Experimental methods provide a feasible way to determine the above said derivatives. In this chapter the experimental set up which consists of flow generating system, test model, instrumentation and flow conditions will be discussed along with detailed description of the particular technique adopted.

5.2 WIND TUNNEL

5.2.1 Description

The flow generating system used in the present study to test the bridge section models is the open circuit type boundary layer wind tunnel at the University of Roorkee. The tunnel has a test cross section of 2.0 m x 1.85 m at the inlet end and varies uniformly to 2.0 m x 2.10 m at the section of testing. A schematic line diagram of the wind tunnel and its salient features are shown in Fig.5.1. With the addition of an eddy current type dynodrive mechanism to the existing 125 HP driving motor it has become possible to set the fan speed at any specified r.p.m. and hence to maintain accurately a constant wind speed throughout the test. A calibration plot with respect to the r.p.m. of the dynodrive and the mean flow velocity in the wind tunnel at the test section is shown in Fig.5.2. Under normal circumstances, without any surface roughening devices, the wind tunnel generates 20 cm thick boundary layer, with fairly smooth flow (turbulence intensity 0.5 % - 1.0 %).

5.2.2 Modifications Necessitated in the Wind Tunnel

As the wind tunnel had provisions for testing of only the floor mounted models like buildings and towers, it required several modifications for fixing and testing the section models. The side - view windows on the two sides of the turn table (Fig.5.1) replaced with specially designed slit windows so that the section model fixtures could be passed through the tunnel walls. The slits are covered with flexible membranes. Any possibility of non-uniformity of flow near the vicinity of the model on this account is ruled out. Suitable bearing fixtures were designed and fabricated to be fitted into the slits in the special window panels so as to allow the section model to vibrate in one of the required mode of vibration, i.e., either torsional or vertical. Two A-frames were especially fabricated to support the model at either ends, outside the tunnel section, through four helical springs at each A-frame. The A-frames described above are illustrated by a line diagram in Fig.5.3.

5.3 SECTION MODEL

As stated earlier, the section model test was undertaken to extract the aerodynamic static and flutter derivative coefficients. This section describes the various scaling parameters to be considered in the design and fabrication of the section model. These considerations establish the scaling targets.

5.3.1 Geometric Scaling

The geometric scale of the model of a bridge deck should be chosen to maintain the equality of the ratios of various deck dimensions. Testing only a part of the structure allows somewhat larger models to be used. Typical geometric length scales range are between 1:10 and 1:100. Considering the blockage effect and the order of length scale of turbulence expected in the present study, a geometric length scale of 1:60 was selected ($\lambda_L = 1/60$).

5.3.2 Mass Modelling

The modelling of the mass of the structure is determined by the requirement that the inertia forces of the structure and those of the flow are scaled consistently. Similarity of inertia forces is achieved by maintaining a constant ratio of bulk density of the structure to the density of air. The equation to express density scaling is

$$\left(\frac{\rho_s}{\rho_a}\right)_m = \left(\frac{\rho_s}{\rho_a}\right)_p \tag{5.1}$$

where ρ_s and ρ_a are structural bulk density and air density respectively. m and p indicate the model and prototype structure respectively.

Since the air density for the model and the prototype are the same, the density scaling becomes,

$$\lambda_\rho = \left(\frac{\rho_m}{\rho_p}\right) \tag{5.2}$$

The scaling of the generalized mass and the mass moment of inertia for a particular mode of vibration can be obtained as follows.

For mass scaling:

$$\frac{M_m}{M_p} = \frac{\rho_m L_m^3}{\rho_p L_p^3} = \lambda_\rho \frac{L_m^3}{L_p^3}$$

$$M_m = \lambda_\rho \lambda_L^3 M_p \tag{5.3}$$

$$\lambda_M = \lambda_\rho \lambda_L^3 \tag{5.4}$$

where M_m mass per unit span of model

M_p mass per unit span of protype

For mass moment of inertia scaling :

$$\frac{{}^I M_m}{{}^I M_p} = \frac{\rho_m L_m^5}{\rho_p L_p^5} = \lambda_\rho \frac{L_m^5}{L_p^5}$$

$${}^I M_m = \lambda_\rho \lambda_L^5 \, {}^I M_p \tag{5.5}$$

$$\lambda_I = \lambda_\rho \lambda_L^5 \tag{5.6}$$

where ${}^I M_m$ - mass moment of inertia per unit span of model

${}^I M_p$ - mass moment of inertia per unit span of protype

5.3.3 Damping

Similarity of damping forces is maintained by taking ζ, the critical damping ratio in particular mode of vibration, the same in model as well as prototype structure.

5.3.4 Stiffness and Frequency Scaling

The forces which resist the deformation of the structure must be scaled consistently

with the scaling of inertia forces. For structures in which the resistance to deformation is influenced by the action of gravity (cable stayed bridges or guyed structures), it becomes necessary to maintain the similarity of the Froude number F_r.

$$\text{i.e.,} \quad (\frac{U^2}{gL}) = \text{constant}$$

where U is the mean wind velocity and L is any pertinent length dimension.

The acceleration due to gravity 'g' is essentially equal for both the model and the prototype, so the wind speed scale becomes the square root of the length scale. This is an important practical constraint for small scale models because the wind tunnel must then be operated at low speeds with disadvantages like i) reduction of forces and hence the responses which affect the accuracy of measurement and ii) increased flexibility of a side-mounted model due to the large length of the model (which has to be compatible with the width of the tunnel as in the present case) which should idealy have infinite rigidity; besides the general impairment in geometrical accuracies that can be practically achieved. Thus

$$\lambda_U = \sqrt{\lambda_L} \tag{5.7}$$

It is also peculiar to cable stayed bridges that both elastic and gravity forces contribute to the stiffness of the structure. The scaling of the elastic forces will be based on Cauchy Number(C_a) equality. Thus we have

$$\frac{(E_{eff})_m}{(E_{eff})_p} = \frac{(\rho U^2)_m}{(\rho U^2)_p} \tag{5.8}$$

Further, in the aeroelastic response of structures, the model deformations and frequencies play a dominant role. Thus in the model studies of elastic structures subjected to wind forces, for any mode of vibration, the relationship between length, time and velocity shall be based on the equality of the reduced frequency in the model and the prototype and can be expressed as

$$K = \frac{nL}{U} = \text{constant} \tag{5.9}$$

where n is natural frequency of a mode of vibration

and the term $1/K = U/nL$ is known as the reduced velocity.

Combining the condition for Froude's number similarity as given by eqn.5.7 with the reduced frequency similarity condition (eqn.5.9), we have

$$\lambda_n = \frac{\lambda_u}{\lambda_L} = \frac{\sqrt{\lambda_L}}{\lambda_L} = \sqrt{1/\lambda_L} \qquad (5.10)$$

In all the above expressions L represents a significant length dimension of the structure. In case of bridges the deck width, B represents the length parameter. So the reduced velocity may be written as U/nB.

The aeroelastic scaling parameters described above have been used in the present section model study of girder decks of typical cable stayed bridges.

5.3.5 Design of Section Model

A typical girder deck of a cable stayed bridge with three main girders and closely spaced cross girders, along with variations introduced by fairings, was selected for detailed study.

The various scaling parameters, along with the values adopted are given in Table 5.1.

Table 5.1

Scaling Parameters of Section Model

Sl.No.	Parameter	Scaling requirement	Design value
1	Length	$\lambda_L = L_m/L_p$	1/60
2	Density	$\lambda_\rho = \rho_m/\rho_p$	1
3	Velocity	$\lambda_u = \sqrt{\lambda_L}$	0.129
4	Frequency	$\lambda_n = \sqrt{1/\lambda_L}$	7.746
5	Mass/m	$\lambda_m = \lambda_\rho \lambda_L^2$	2.778e-3
6	Mass M.I./m	$\lambda_L = \lambda_\rho \lambda_L^4$	7.716e-8

5.3.6 Fabrication of Model and its Suspension System

The section model is a rigid model of a representative length of the girder deck of the cable stayed bridge (Bridge #1, section 3.6), spring supported at the ends to allow the freedom of vibrations in the required mode of vibration.

Three different variations of the section model were used for the present study. The original section model tested is shown in Fig.5.4. Further, to study the effect of fairings on the original girder deck two modified section models were subsequently tested with

different percentage levels of fairings attached at the edges, i.e., (i)Fully faired model with 100 % fairings on both edges (Fig.5.5(a))of the deck and (ii)partially faired model having 60 % fairings on either side of the unmodified section model (Fig.5.5(b)).

The original bridge section model (unmodified section model) was made by making use of plywood, zinc, aluminium and copper.

(i)0.8 mm thick zinc sheet was glued to a 3 mm plywood sheet to represent the deck slab,

(ii)4 mm thick aluminium strips have been used to represent foot paths and 1mm thick aluminium channel with suitable openings to represent hand rails,

(iii)Very thin copper strips have been used to represent girders at the bottom and thin copper sheets to represent the fairings. Fig.5.5(c) shows the details of the fairing dimensions.

Considerable care was exercised to achieve geometric accuracy in the section model. Fig.5.4 shows the geometric details of the section model fabricated (unmodified). In case of the section models, since they represent dynamically mounted rigid parts or sections of bridge deck, the flow will be treated as two dimensional. So, to ensure two dimensional flow over the deck section, two large elliptic perspex end plates with sharp edges were attached to each end of the model. The section model with end plates and the steel pipe truss assembly at the extremes, was fabricated as a rigid structure. Fig.5.6 shows the photograph of the models tested. Care was taken in fixing the pipes(connecting the model to the A-frame at the two ends of the model) so that these do not obstruct the flow pattern around the model.

The main component of the model support system is an A-frame assembly. The details of the A-frame assembly, with the dimensions marked thereon are shown in Fig.5.3. To get the static aerodynamic coefficients the model was mounted on load cells on either end. This enabled the measurement of the lift, drag and moment forces for various wind incidence angles.

Further, to perform flutter and self excited oscillation experiments, the model truss assembly was mounted on the A frames by using four pairs of flexible helical springs, two at each end (Fig.5.7). These springs were especially designed and fabricated to get the

required stiffness. Provision was made in the A-frame assembly to alter the position of the springs to achieve symmetry about the model's centre of gravity. The geometric and the dynamic properties of the prototype, as well as the scaled and finally achieved after the fabrication of the actual model are tabulated in Table 5.2. The stiffness approach using the equivalent mass (or mass moment of inertia) has been used to calculate the model frequency in bending and torsion mode of vibration. The calculated and measured values are shown in Table 5.2.

Table 5.2
Structural Parameters

Property	Units	Prototype	Model (Scale : 1/60)		
			Scaled	Actual	
				Calculated	Measured
Weight/m of Span	Kg/m	21783	6.050	6.250	6.250
Location of C.G.	m	2.325	3.875	3.875	3.875
Mass/unit span	kg cm s²/m	2220	0.617	0.637	0.637
Natural Frequency					
Vertical	Hz	0.491	3.803	3.231	3.226
Torsional	Hz	0.606	4.686	4.796	4.803

5.4 FLOW MODELLING

The modelling of the wind characteristics for wind tunnel studies can be placed under two categories

(i)The simulation of the average characteristics of the approaching turbulent boundary layer wind. These flow characteristics are defined generally by the following major parameters:

(a) Mean wind velocity distribution in horizontal and vertical directions,

(b) Spectral quantities of velocity components

* Intensity of turbulence
* Integral scale of turbulence
* Spectra in the relevant frequency range
* Correlation of turbulence components.

(ii)The simulation of wind structure in the immediate proximity field which of course is largely influenced by the particular topographical conditions.

For the second part the effects of the surrounding topography have to be considered. These are usually generated by installing the geometrically scaled model of 'near field' proximity. To what extent the surrounding topography needs to be simulated is a question still not well answered but should be decided in relation to the development of the boundary layer flow as generated by the proximity model.

5.4.1 Simulation of Wind for Section Model Test

A perfect simulation of the atmospheric wind field is difficult in the wind tunnel.

The flow conditions in the wind tunnel ensures that the mean wind flow direction coincides with the longitudinal axis of the wind tunnel.

So far as the bridge deck section model tests are concerned, the most important factors to be simulated are the followings:

(b) U, $I_U\%$ and L_X at the elevation of the bridge deck,

(b) S(f), the spectrum of longitudinal velocity component,and

(c) to ensure that the general homogeneity of the flow field for the various parameters is maintained over the transverse length of the deck section.

In the present investigation, the various similarity parameters have been considered and simulated by means of the passive approach using grids.

Apart from the above, the smooth flow condition is also considered in the study, since it is critical for the bridge decks.

5.5 INSTRUMENTATION

This section describes the major instruments designed, fabricated and used for the measurement of various parameters.

5.5.1 Measurement of Flow Characteristics:

To measure the mean and fluctuating components of velocity at any specified point, a constant temperature anemometer of Dantec make, Denmark has been used. The output of its 55M01 main unit was directly fed to a P.C. based data acquisition system (AcqWire software). The software is capable of processing the raw velocity data to

get the mean velocity, turbulence intensity, autocorrelation and the wind velocity spectrum. Further, the software has built-in procedure for the calibration of the probes.

The particular probe used for the measurement of the raw velocity data was 55P11 (5 μ thick platinum coated tungsten wire). The arrangement of a special calibration wind tunnel of small size (total length 2 m) used for calibration and of the anemometer system is shown in the photograph in Fig.5.8.

5.5.2 Measurement of Static Force

For the measurement of static force in lift, drag and moment components the 3 and 5 component load cells (Nissho Electric Works Co. Ltd., Japan) with D.C. strain amplifiers were used.

5.5.3 Measurement of Vibrations

5.5.3.1 Design and fabrication of strain gauge transducers

For measuring the vibrations (model displacements) of the section model, especially designed cantilever type strain gauge displacement transducers were fabricated to meet the amplitude requirements. These transducers were fixed at each helical spring support, through connectors, to pick the strains. This type of transducers will have an advantage over the 'strain link transducers' attached to helical springs used in some of the earlier works (Houston[1], Scanlan[3]) since these transducers do not come in contact with the helical springs. The chances of transmission of the axial twisting motion from the helical spring to the transducer link is thus avoided in this case. The photograph in Fig.5.9 shows the total assembly of the transducers. The Micro Measurement Inc. 350 ohm resistance with 2.08 gauge factor strain gauges were used on either sides of the transducer strip.

5.5.3.2 Measurement of strains

Using the algorithms developed to interface data acquisition system-Keithley 500A (Appendix-A) and the personnel computer, the raw data of strains were acquired and stored for further processing. The processing of raw data has been carried out using the Keithley Asyst software.

The photograph in Fig.5.10 gives a view of the data acquisition and other systems in

the control room. Fig.5.11 shows layout of the various instruments used during the experimental study.

5.6 FLOW MEASUREMENT AND CHARACTERISTICS

The section models were first tested under smooth flow and later, to study the effect of grid generated turbulence on the flutter derivatives, under three different grid generated flows. These four flow patterns have been named as "smooth", "Grid #1", "Grid #2" and "Grid #3".

The smooth flow was generated in the wind tunnel without any turbulence generating obstructions or floor roughness, whereas for the grid generated flows, different grid sizes and positions were chosen. The grids were so designed as to produce length scales,

(i)approximately equal to deck width,

(ii)lesser than the deck width, and,

(iii)larger than the deck width.

The selection of size of grid and the upstream distances were based on the empirical formula proposed by Laneville and referred in Saathoff et al.[2] as follows.

$$L_x = 0.358 \ b(x/b)^{4/9} \qquad (5.11)$$

where b is the bar width of grid,

and x is the down-stream distance of test section measured from the grid.

The evaluation of length scale for the grid generated flows is a rather arbitrary procedure. There are several types of length scale statistics that appear in the literature as listed by Simiu and Scanlan[5]. Perhaps the most widely used method of assigning a length scale to a turbulent flow is the so called integral scale method. The integral scale is defined as the area under the autocorrelation curve of the fluctuating velocity component in (x,t). Since autocorrelation measurements are usually temporal measurements at a fixed point, Taylor's hypothesis[1] is used to convert the area under the autocorrelation function into units of length as shown below

$$L_x = U \int_0^\infty R_u(\tau)d\tau \qquad (5.12)$$

where Lx is the integral length scale, U the mean velocity and $R_u(\tau)$ is the autocorrelation function of the fluctuating velocity component in (x,t).

The major problem with the integral scale method is that the autocorrelation function is often highly oscillatory. Typical ones are shown in Figs.5.15(c) through 5.20(c). Hence, in Fig.5.15(c) and 5.20(c) the area under the curve tends to cancel out, which will gives an unrealistically small length scale. A common method of overcoming this problem is to define the integral scale as the area under the autocorrelation curve for the values occurring before the first zero crossing of the autocorrelation plot.

A good corroboration comparison between the length scale obtained from the empirical formula (eqn.5.11) and that obtained using the autocorrelation technique (eqn.5.12) substantiated the usefulness of the empirical formula to estimate the size and position of the grids. With three different grid sizes of bar width 246 mm , 260 mm and 298 mm and positions at an upstream distance from the model edge of 8.2 m, 9.5 m and 10.5 m respectively the length scales estimated were 0.42 m, 0.46 m and 0.52 m respectively, while the width of the section model is 0.46 m. The bar size of the grids obtained and their centre to centre spacing, allowed the use of only a single horizontal wooden strip in the tunnel cross-section. Fig.5.12 shows the details of grid arrangements used in wind tunnel with their positions from the edge of the section model. The turbulence intensities were of the order 10 % to 12 %.

Since the section model used in this study was 1.6 m long and about 40 mm thick, it was decided to measure the homogeneity of mean flow by taking horizontal component of wind velocity at points located in a vertical plane that was positioned 0.8 m upstream of the deck section. These 99 points formed a 1.8 m by 0.4 m grid as shown in Fig.5.13, which ascertains that the flow is essentially two-dimensional in nature.

Fig.5.14 contains the results of the measurements of the mean flow velocity for the "smooth" flow. Wind velocity measurements were taken at 99 points for a midstream wind speed of 13 m/sec. The plots show the homogeneity in the flow all along the length of the deck. The measurements were made using the probe of the hot-wire anemometer placed in different

positions with the help of an automated stepped motor controlled traverse system.

The velocity fluctuations which were present in all the flow conditions were measured with Dantec hot-wire anemometer. The data were filtered, digitized and recorded for further analysis. Figs.5.15(a) through 5.20(a) contain the plots of selected time histories of horizontal components of velocity for the three different flow conditions. Figs.5.15(a) and 5.16(a) contain plots of the horizontal component of velocity time histories for the "Grid #1" flow at mean wind velocities of 3.9 m/sec and 8.2 m/sec respectively. Similarly the time histories for flow controlled by of "Grid #2" and "Grid #3" are shown in Figs.5.17(a) through 5.20(a). The plots also show the corresponding turbulence intensity and the maximum velocity during the time history.

All the time history plots show the presence of certain amount of high frequency peaks. It is believed that these high frequency peaks are the result of imperfect grounding of the earth wire and were eliminated by using appropriate filters before processing the data further. The turbulence intensities computed from measurements in the various flow conditions are shown in Table 5.3. The turbulence intensity measurements shown in the table were taken at nominal wind speeds of 3.9 m/sec or 8.2 m/sec. The intensity for the smooth flow ranged from 0.5 % to 1 % and in the cases with grids it ranged from 10 % to 12 %. As could be expected the turbulence intensities obtained for three different grids were of the same order, the size of the grid bars being close to each other.

The non-dimensionalized power spectral density (f $S(f)/\sigma^2$) for the different grid generated flows at mid-stream are shown in Figs.5.15(b) through 5.20(b) along with Von Karman spectrum shown by dotted lint. The non-dimensional plot has been made between f $S(f)/\sigma^2$ and fB/U. From these plots it is cleat that the spectra corroborate with each other. These spectra show that grid-generated flow contains a good proportion of the total energy in the lower frequency range (upto 20Hz).

Table 5.3

Flow Characteristics for different flow conditions

Flow Conditions	Grid Size / Upstream Distance (m)	Flow Characteristics		
		Velocity	Iu %	Length Scale (Lx)
Smooth	—	4.0 m/sec	0.5 ~ 1.0	-
Grid #1	0.246/8.20	8.20 m/sec	~ 11.4	0.42 m
Grid #2	0.260/9.58	8.20 m/sec	~ 11.4	0.46 m
Grid #3	0.298/10.68	8.20 m/sec	~ 11.3	0.51 m

5.7 TESTS ON SECTION MODEL

Before testing the section models of the bridge decks, a rectangular section model of 30 cm width and 3 cm depth (i.e., B/d = 1:10) was tested to commission the set-up. The rectangular model was tested in its vertical degree of freedom and the corresponding time histories of vibration were recorded in smooth flow condition. These time histories were further processed to extract the flutter derivatives using the softwares developed and they were found to corroborate with the earlier results[4].

This section will describe the series of wind tunnel section model experiments that were designed to measure the motion dependent aerodynamic forces, in terms of flutter derivatives, that act on the section model as it is subjected to various flow conditions. The basic assumption employed in these experiments is that all of the motion dependent structural and aerodynamic forces are linear and therefore superposable. The frequency and damping values are the basic parameters defining the aerodynamic behaviour of the system. These parameters can be obtained from the recorded free vibration motion of the section model (Transient time history records), generated by giving an initial vertical or torsional displacement.

In these experiments, a single degree aeroelastic system was created by restraining either the vertical or torsional degree of freedom with suitable attachments (Fig.5.3,Section 5.2). Further, to give initial displacement to the section model a thin high strength wire of negligible weight was utilized. The wire was fixed at the centre of the section model to give a vertical displacement. For giving a torsional displacement to

the model, it was fixed to an edge of the model.

Each set of experiment was conducted in the·following manner. First, the model was given an initial displacement and released suddenly in still air. This was repeated and each time the dynamic displacement signal was recorded. The wind flow was then induced. The motor speed was adjusted to the minimum possible (25 r.p.m). This motor speed induced a mean flow velocity of about 2.23 m/sec. The section model was given an initial displacement and then released suddenly. The displacement and release procedure was repeated again. This repetition of the test under the same flow conditions provided a check on the accuracy of the experimental data acquired. The wind tunnel fan motor was then incremented by 25 r.p.m. The experiment was carried out twice at each velocity. The wind tunnel velocity was incremented again and the tests were repeated until the wind reached a speed at which the section model became unstable (growing vibrations). After completing one set of observations, the model was to give a tilt incrementally by 1^0 or 2^0 to attain angles of attack from 1^0 to 5^0. The total procedure described above was repeated for the changed angle of incidence of the wind.

The dynamic displacement data were acquired through data aquisition system (DAS) in terms of strains and stored in different files on computer for each set of experiment. The results of the test and the flutter derivatives obtained from these experiments are presented in the next chapter.

References

1. Houston,D.R., H.R.Bosch, and R.H.Scanlan, (1988), "The Effect of Fairings and Turbulence on Flutter Derivatives of a Notably Unstable Bridge Deck", Jnl. of Wind Engg. and Ind. Aero., Vol. 29, pp 339-349.

2. Saathoff,P.J. and W.H.Melbourne, (1987), "Free-stream Turbulence and Wind Tunnel Blockage Effects on Streamwise Surface Pressures", Jnl. of Wind Engg. and Ind. Aero., Vol. 25, pp 353-370.

3. Scanlan,R.H., and J.Tomko, (1971), "Airfoil and Bridge Deck Flutter Derivatives", Jnl. of Engg. Mech. Div., Proc. ASCE, Vol. 97, Dec., pp 1717-1737.

4. Shangpei,L. and Chen Xin, (1989), "Experimental Identification of Flutter Derivatives from Several Typical Deck Sections", Proc. II APSOWE, China, pp 610-617.

5. Simiu,E. and R.H.Scanlan, (1986), "Wind Effects on Structures", IInd Ed., John Wiley and Sons, N.Y.

98

Notations

B	bridge deck width
E	Young's modulus of elasticity
I_{Mm}	mass moment of inertia of the model
I_{Mp}	mass moment of inertia of the prototype
$I_u\%$	turbulence intensity
K	reduced frequency
L_m	representative length of the model
L_p	representative length of the prototype
L_x	integral length scale of turbulence(L_{ux})
M_m	mass per unit span of the model
M_p	mass per unit span of the prototype deck
R_u	autocorrelation of the fluctuating velocity ($C(t)$)
$S(f)$	spectral density of longitudinal velocity component
U	mean wind velocity
b	bar width of the grid
f	frequency of velocity fluctuations
g	gravitational acceleration
n	natural frequency of vibration
x	distance of grid from the section model
λ_L	length scale
λ_M	mass scale
λ_n	frequency scale
λ_U	velocity scale
λ_ρ	density ratio
ρ_a	air density
ρ_m	section model density
ρ_p	prototype structure density
ρ_s	structural bulk density
σ	variance of fluctuating velocity component
τ	time interval

SECTIONAL ELEVATION

PLAN

A – INSTRUMENTATION ROOM
B – DATA ACQUISITION AND CONTROL ROOM
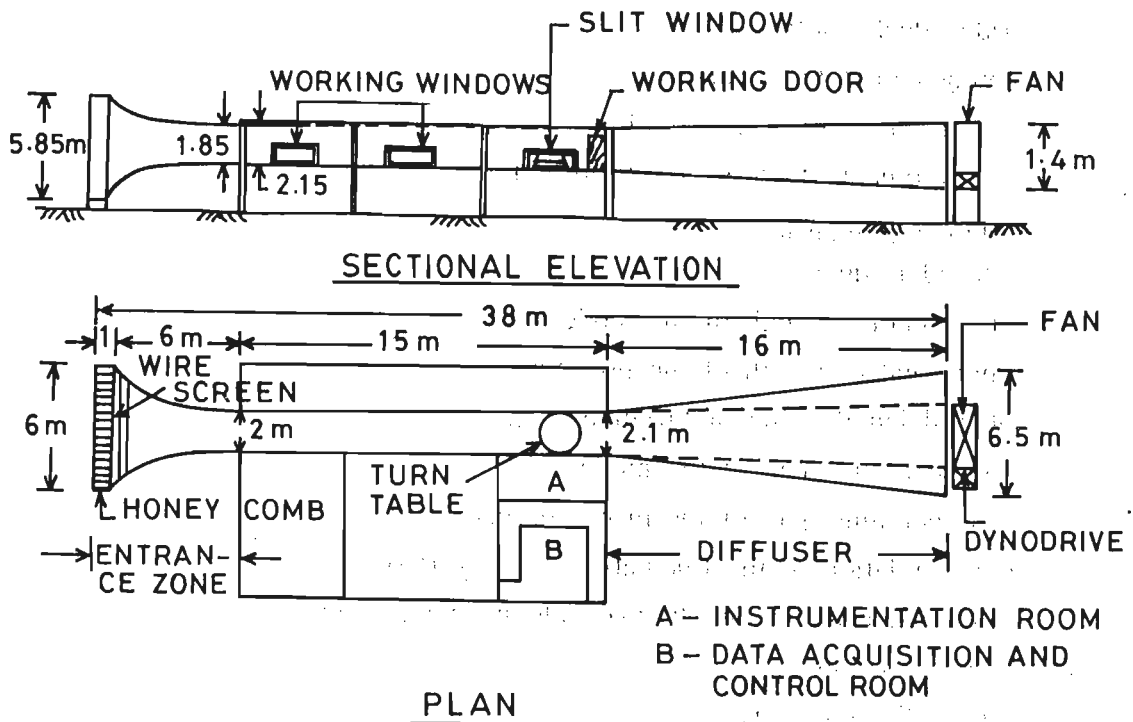
SALIENT FEATURES

Total length of wind tunnel	:	38 m
Length of test section	:	15 m
Length of diffuser	:	16 m
Test section cross section	:	2.00 x 1.85 m upstream end
		2.10 x 2.15 m downstream end
Contraction ratio of effuser	:	9.5 : 1
Effuser profile	:	Elliptical
Wind speed	:	2 m/s to 25 m/s
		(continuously variable through eddy current controls)
Boundary layer thickness	:	0.2 m (smooth flow)
		1.0 m (with roughening devices)
Capacity of blower(fan)	:	75 m³/s
Power of motor	:	125 H.P.
Speed of dynodrive	:	1200 r.p.m.

Fig.5.1 Schematic diagram of boundary layer wind tunnel at University of Roorkee
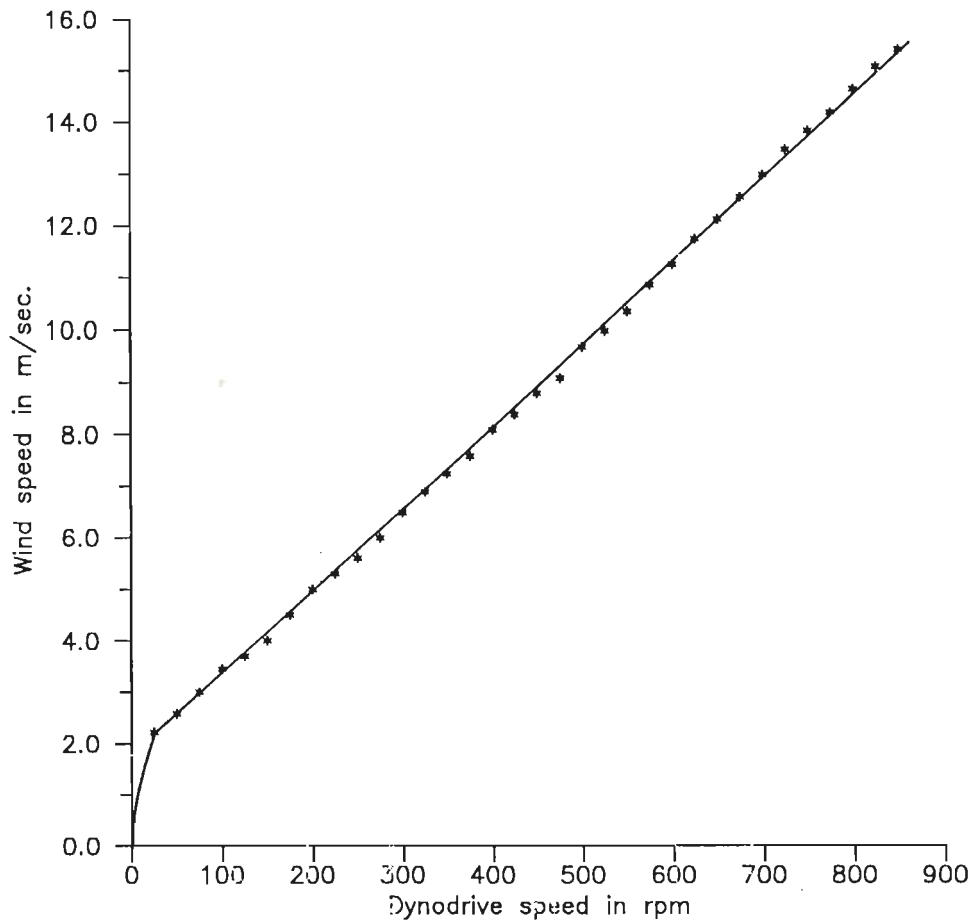
Fig. 5.2 Calibration plot of wind speed with dynodrive speed

Window of wind tunnel wall

M.S. Strip (5mm) length 60 cm

20cm

25 cm

M.S. angle stand to support springs

Bronze strip strain gauge to measure transducer displacements

≤ 65cm

Sill level of window (W.T)

W.T. floor

Clamp with the sill of window

Side elevation

(a) A – Frame stand with details

Bearing fixed to Al. strip sliding vertically

Aluminium strip

Screw arrangement for changing angles

Steel rod connecting to nodel

Sliding surface

Slit made (M.S.Iron)

(b) For vertical degree of freedom

Wedge

Outer bearing surface fixed

Steel rod connected to model

Inner bearing allows rotation

Wedge

(c) For rotational degree of freedom

Fig. 5·3   A-frame stand with details of side bearing
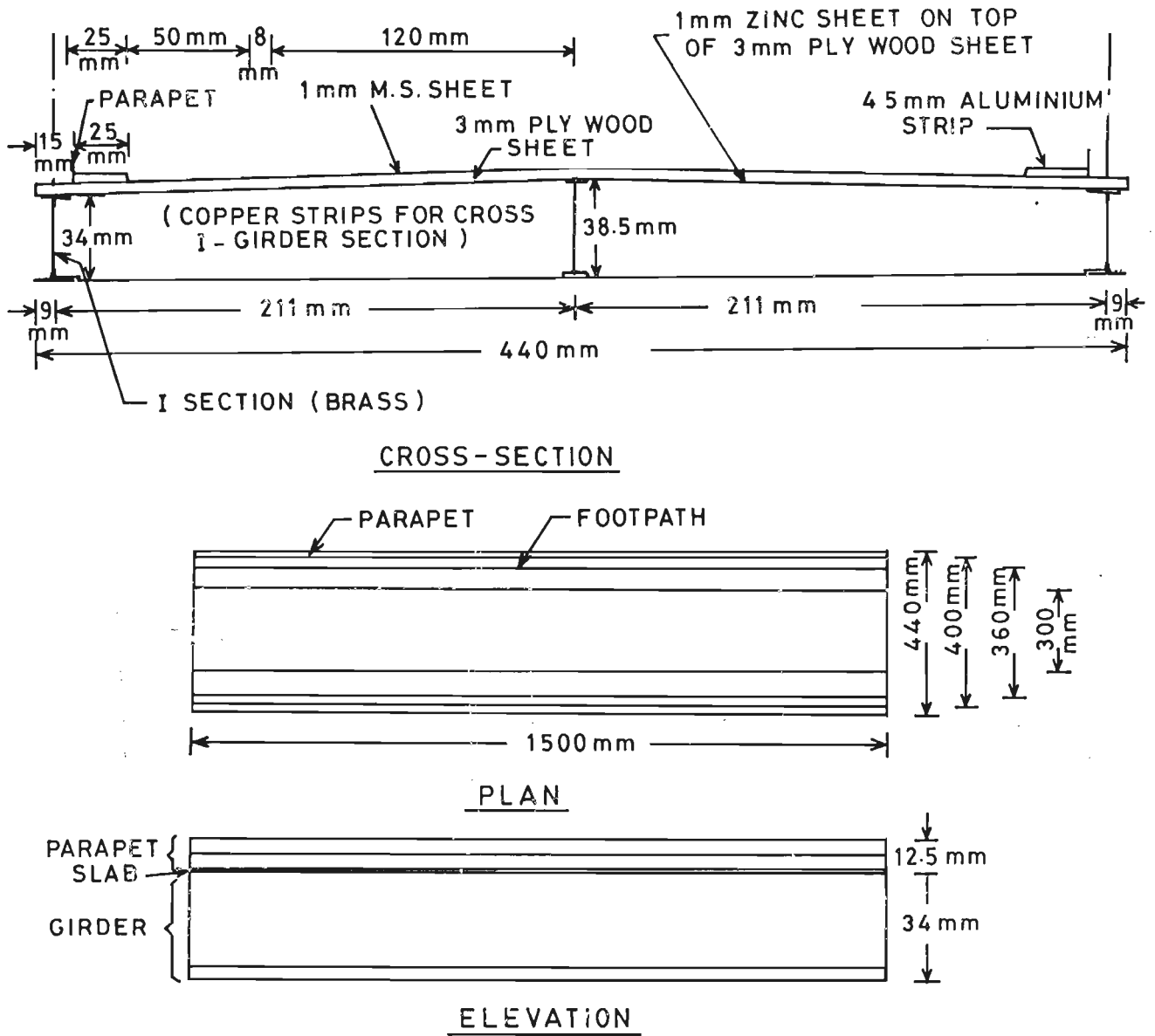
Fig.5.4 Geometric details of section model
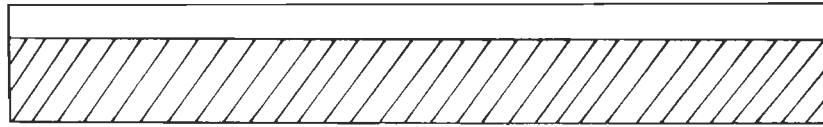
(a) 100 % fairing
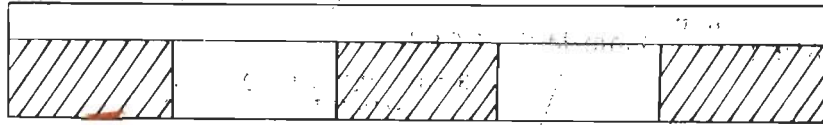
(b) 60 % fairing

Elevation showing different fairing extents used
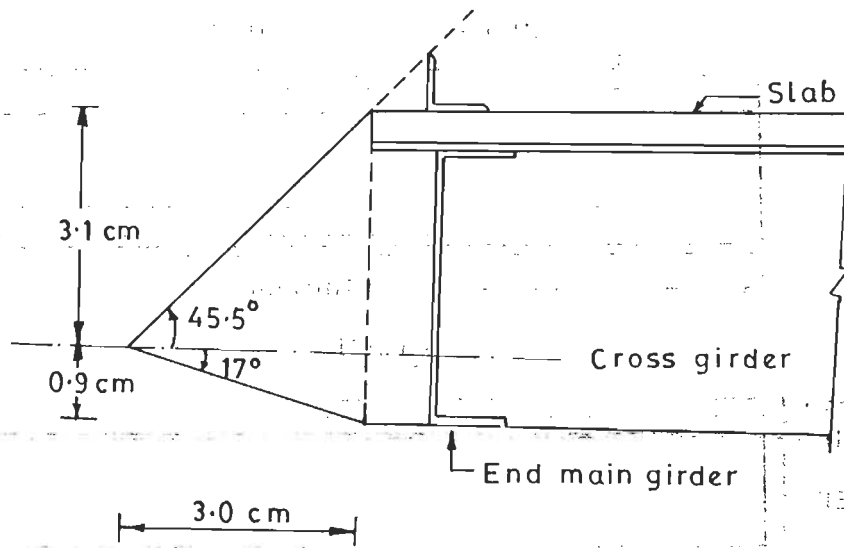
(c) Elevation

Fig. 5·5   Details of fairing used in section model
and its extents.
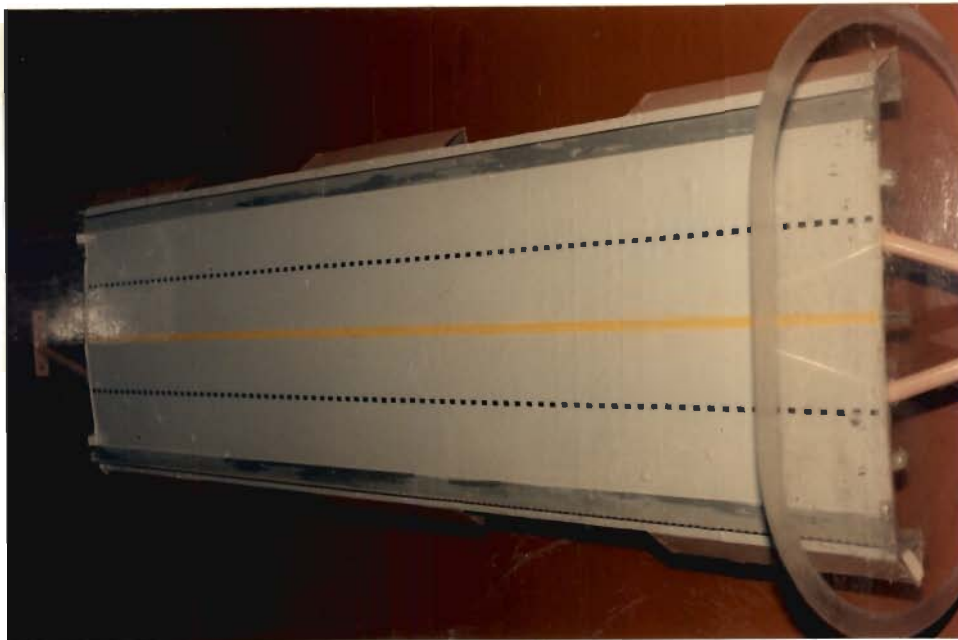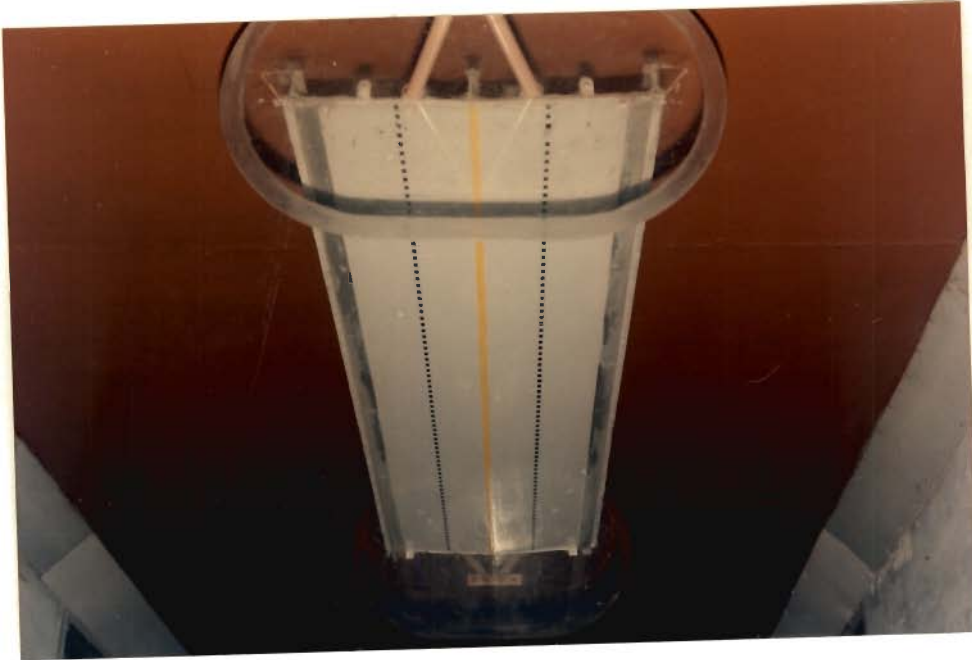
Fig.5.6(a) Photographs showing top view of section model

Fig.5.6(b) Photograph showing partially faired section model
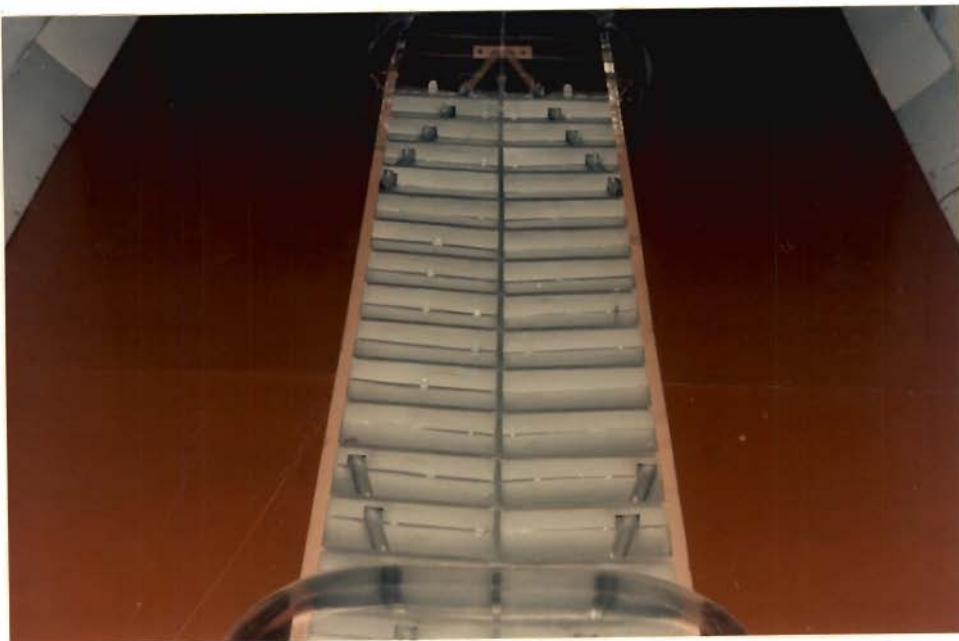
Fig.5.6(c) Photograph showing bottom view with main and cross girders
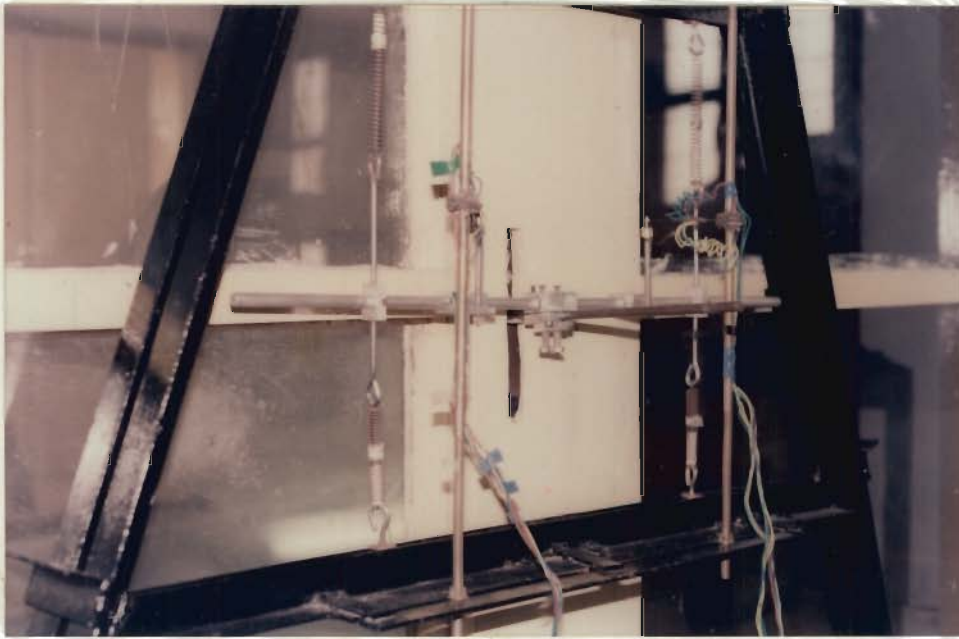
Fig.5.7 Photograph showing the details of spring supports of the model along with the A - frame

Fig.5.8 Calibration tunnel with instrumentation
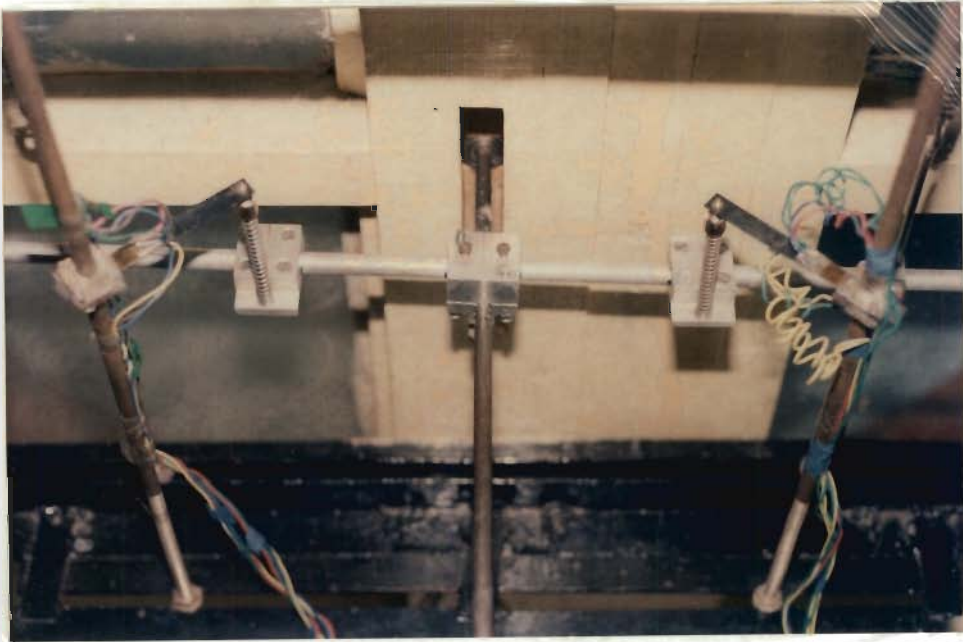
Fig.5.9 View of the spring loaded transducer system

Fig.5.10 View of acquisition and other systems in the control room

Section Model

Hotwire Sensor

Constant temperature bridge unit

Strain Gauge Transducer

Eddy current controller to increase wind speed in tunnel

Keithley 500A Strain Gauge Module

AcqWire Software

Calibration data

Acquisition through Software(P.C.) Raw Data

Processing to get Velocity(RMS,Mean) and storing

processing

processing

Spectral Density

Autocorrelation

Smoothening, Filtering and storing data through Asystant +

Non-dimensionalized Spectrum

Lengh Scale of turbulence

Printing Device

Scanning records of time history

Determination of log decay & frequency

Extraction of flutter derivatives thro' programs

Tabulation of results

Fig.5.11 Schematic diagram of various instrumentation and steps involved in section model experiments
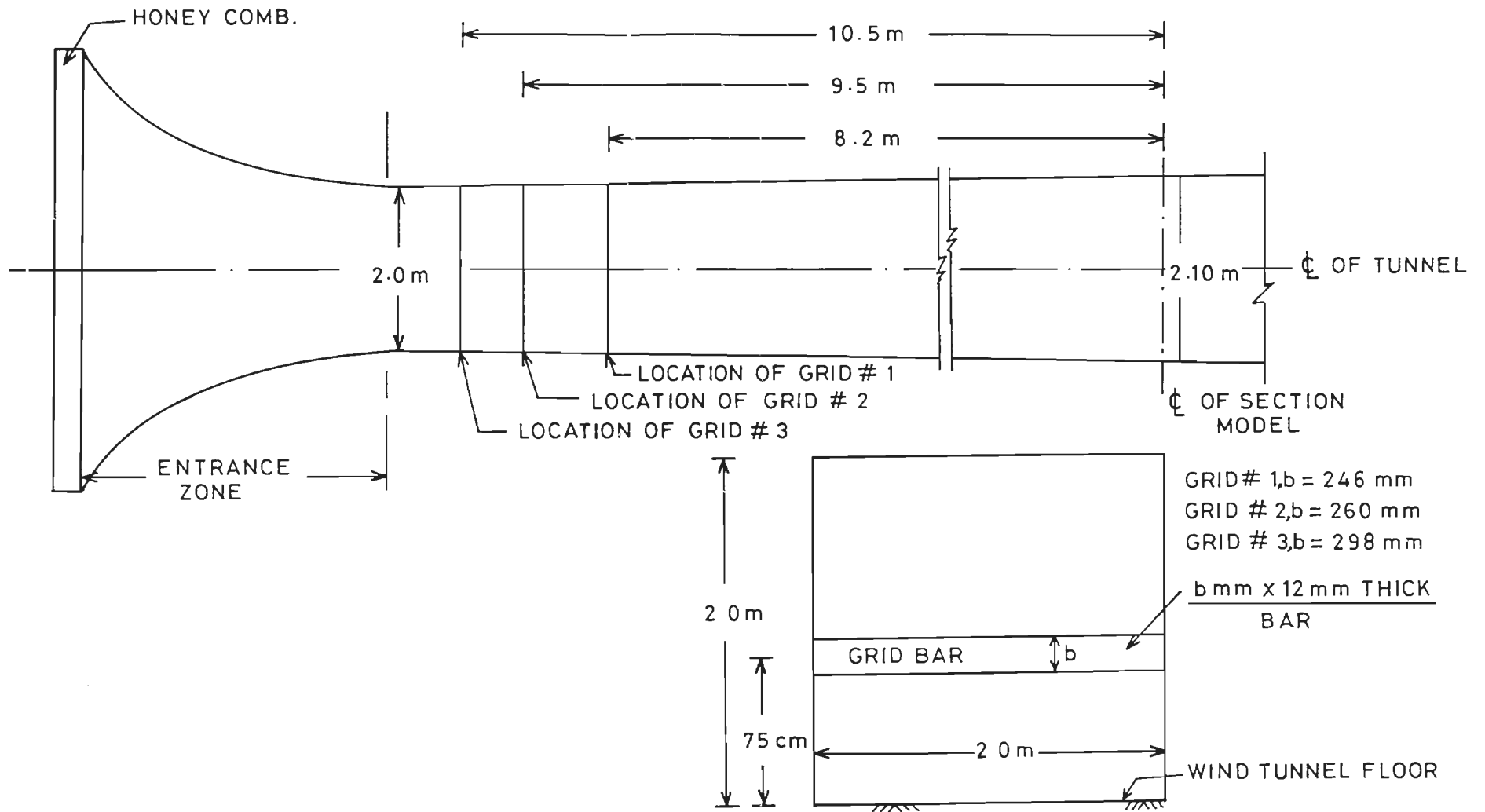
Fig.5.12 Details of grids and their location from the section model
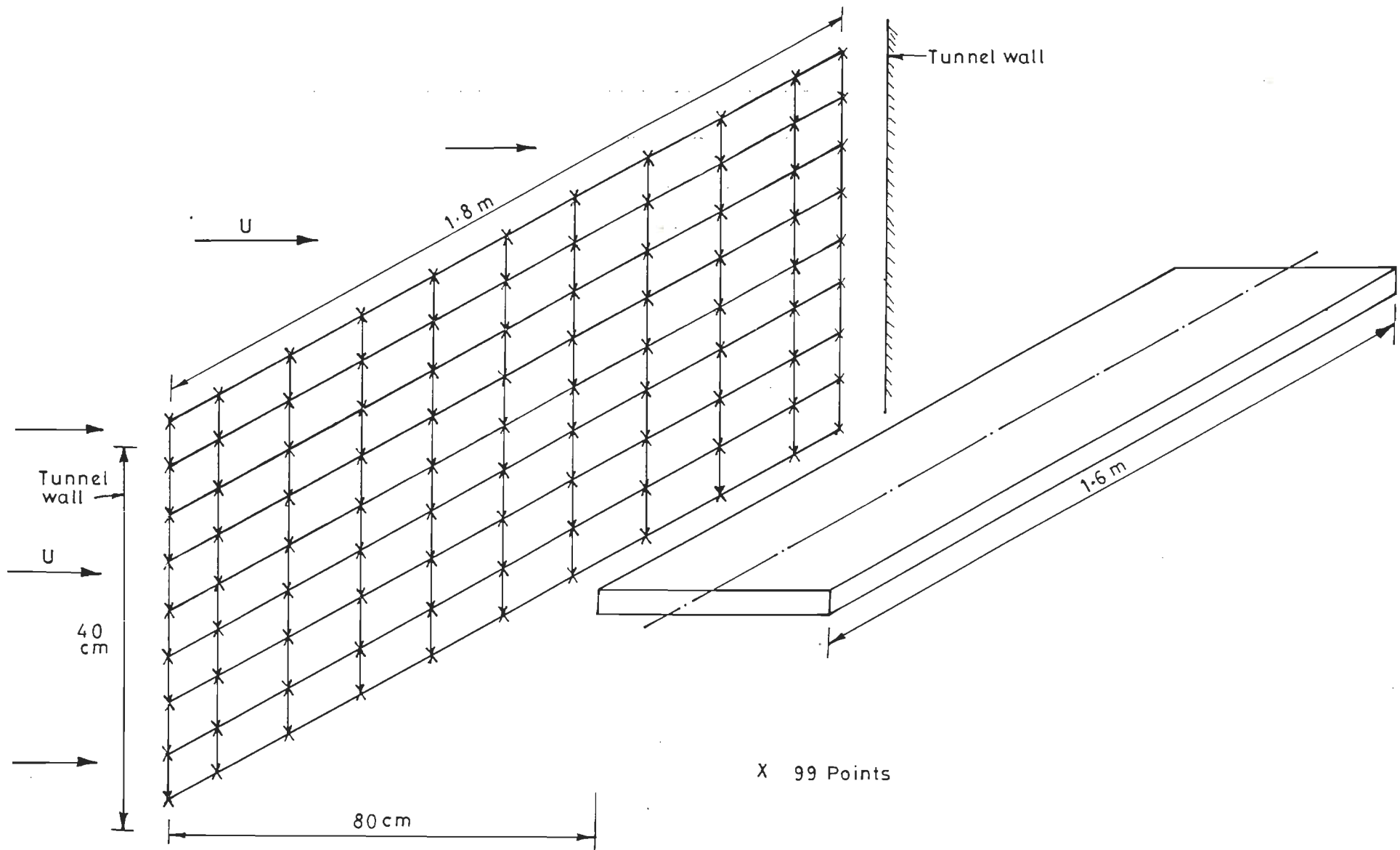
Fig. 5·13 Diagram showing points at which velocity measured
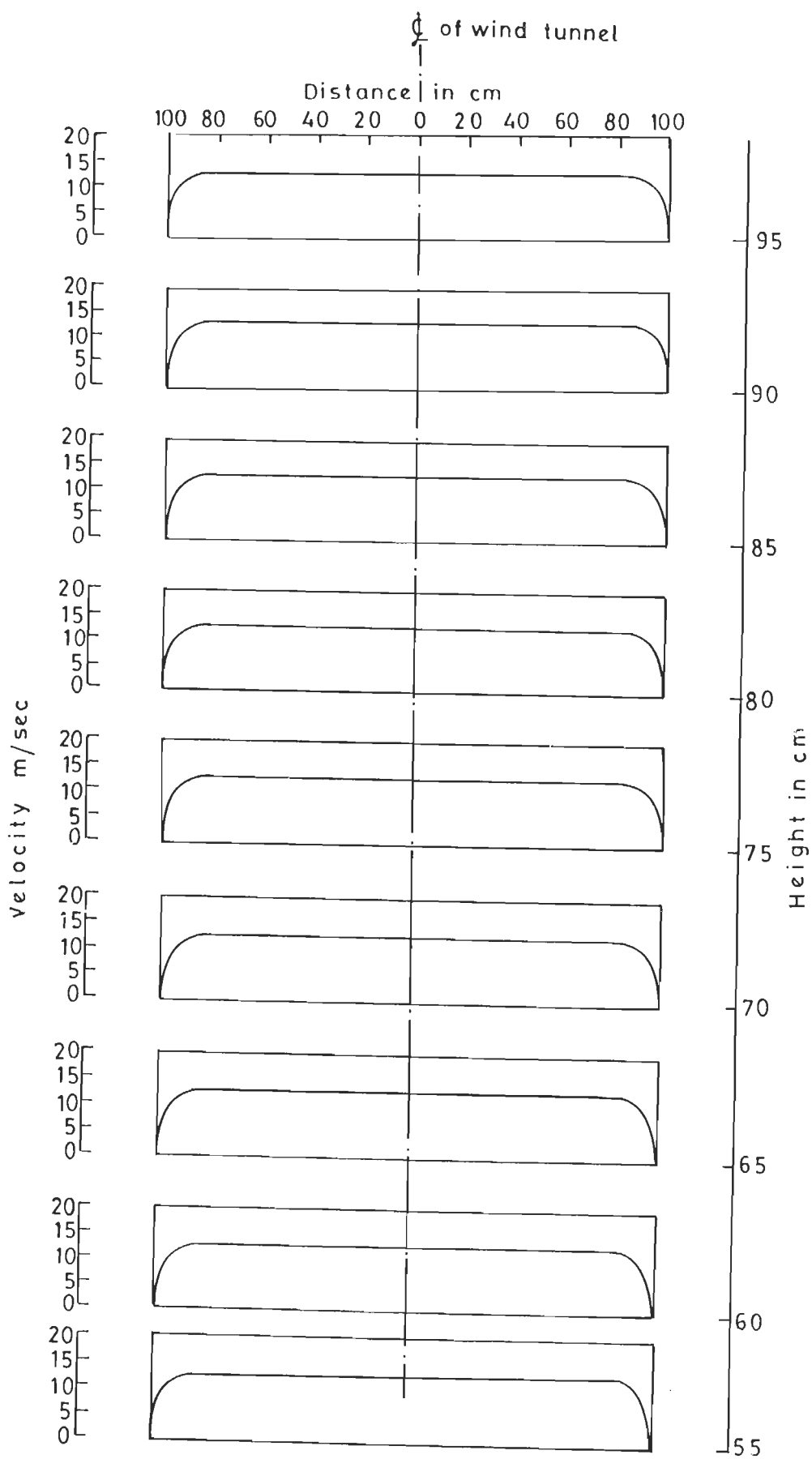
Fig. 5·14 Transverse velocity profiles at different heights under smooth flow condition

(a) Time history of U component

Velocity
Mean = 3.90 m/sec
Rms = 0.45 m/sec
Max. = 5.74 m/sec

Turbulence Intensity
I_u % = 11.45

Integral
Length Scale
L_{ux} = 0.44 m

(b) Non-dimensionalized spectrum plot

(c) Autocorrelation plot
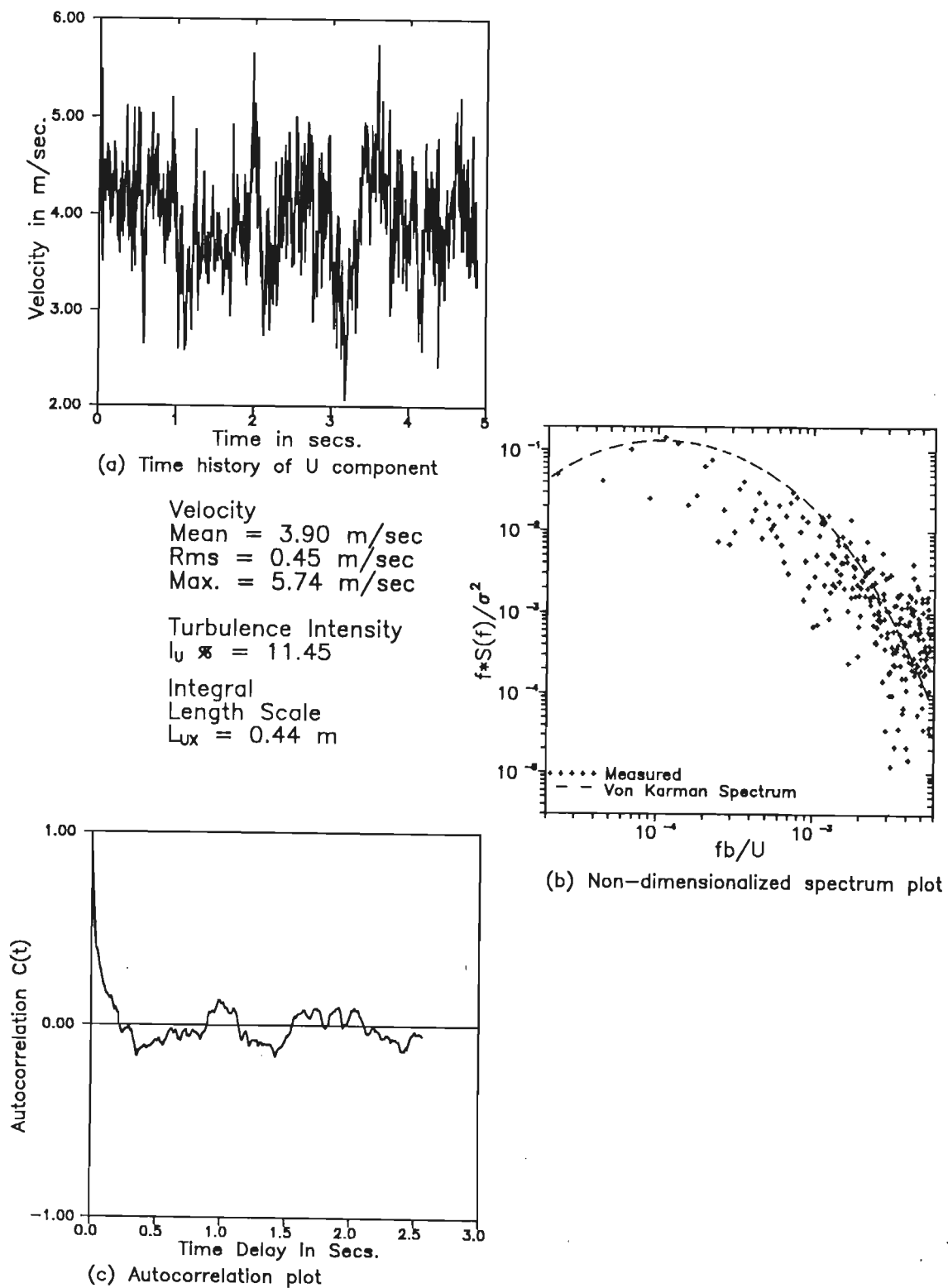
Fig. 5.15 Flow characteristics at 0.8 m upstream of the test section
at model height with Grid # 1 (U = 3.9 m/sec)
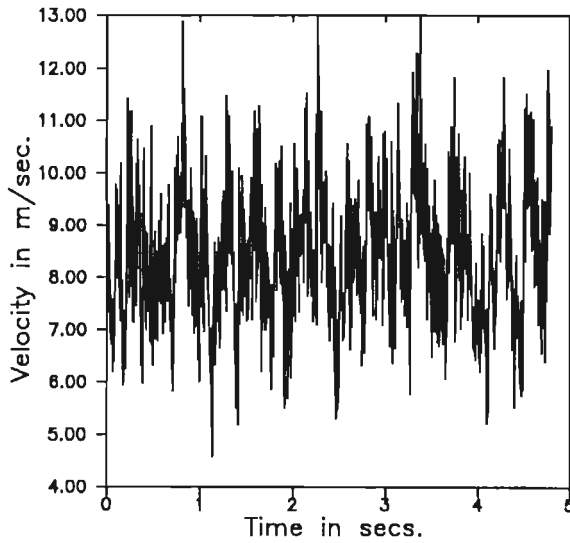
(a) Time history of U component

Velocity
Mean = 8.20 m/sec
Rms = 0.97 m/sec
Max. = 12.98 m/sec

Turbulence Intensity
I_U % = 11.44

Integral
Length Scale
L_{UX} = 0.42 m
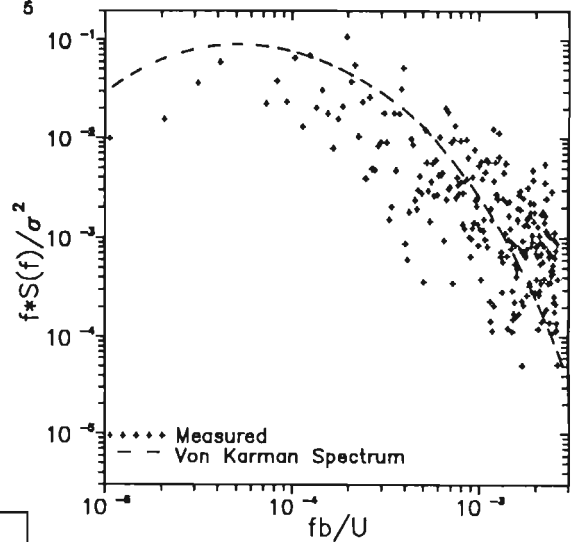
(b) Non-dimensionalized spectrum plot
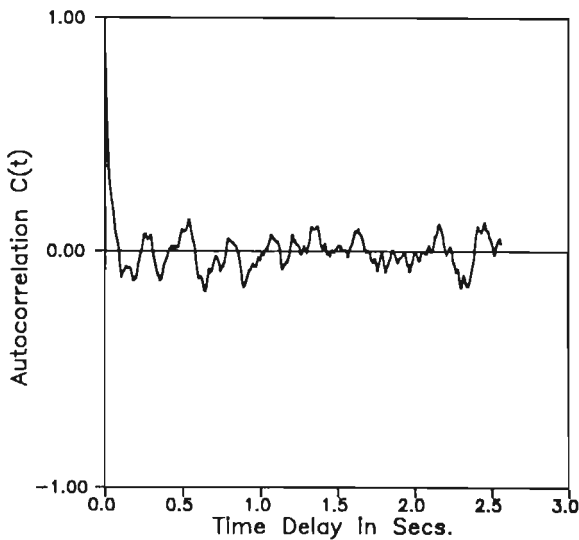
(c) Autocorrelation plot

Fig. 5.16 Flow characteristics at 0.8 m upstream of the test section
at model height with Grid # 1 (U = 8.2 m/sec)

(a) Time history of U component

Velocity
Mean = 3.90 m/sec
Rms = 0.42 m/sec
Max. = 5.68 m/sec

Turbulence Intensity
I_u % = 10.80

Integral
Length Scale
L_{ux} = 0.466 m

(b) Non-dimensionalized spectrum plot

(c) Autocorrelation plot
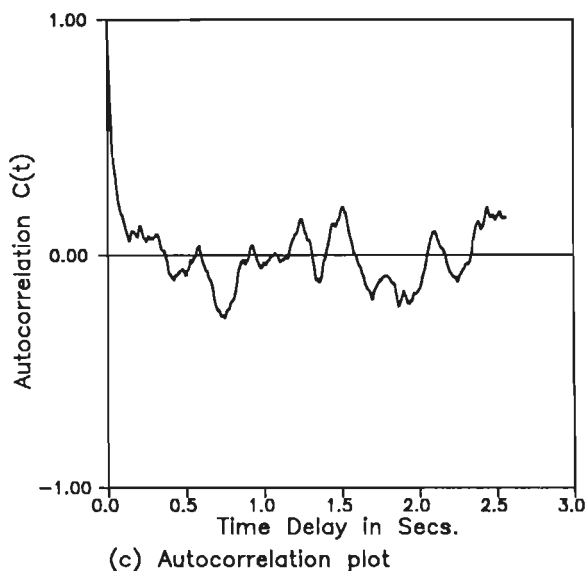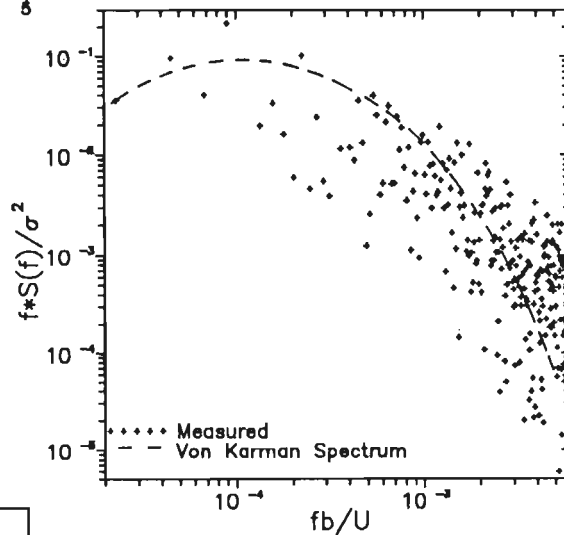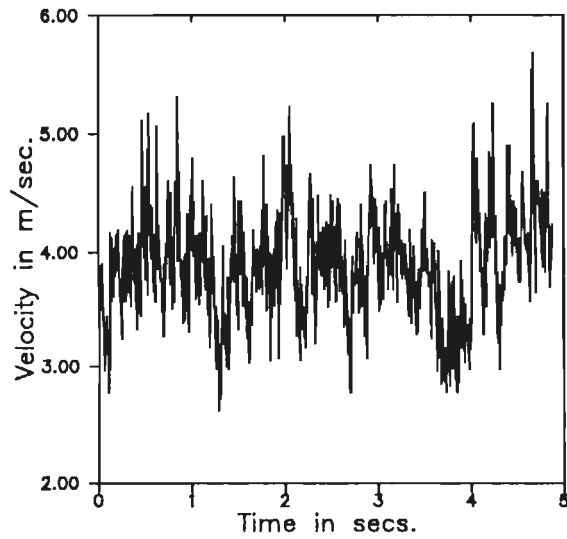
Fig. 5.17 Flow characteristics at 0.8 m upstream of the test section
at model height with Grid # 2 (U=3.9 m/sec)

(a) Time history of U component
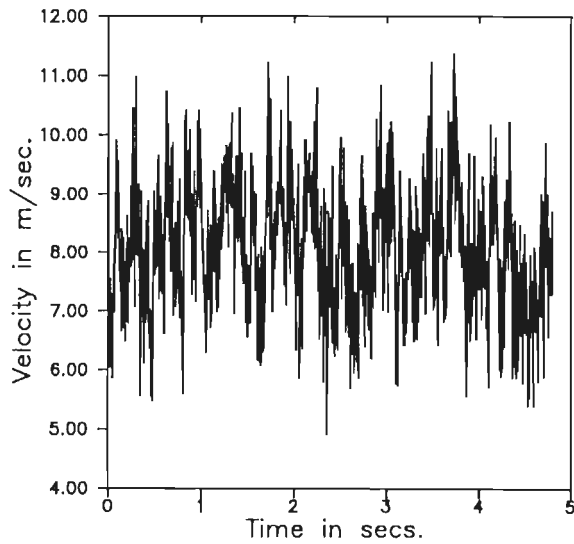
Velocity
Mean = 8.20 m/sec
Rms = 0.96 m/sec
Max. =11.37 m/sec

Turbulence Intensity
I_u % = 11.92

Integral
Length Scale
L_{ux} = 0.468 m

(b) Non-dimensionalized spectrum plot

(c) Autocorrelation plot
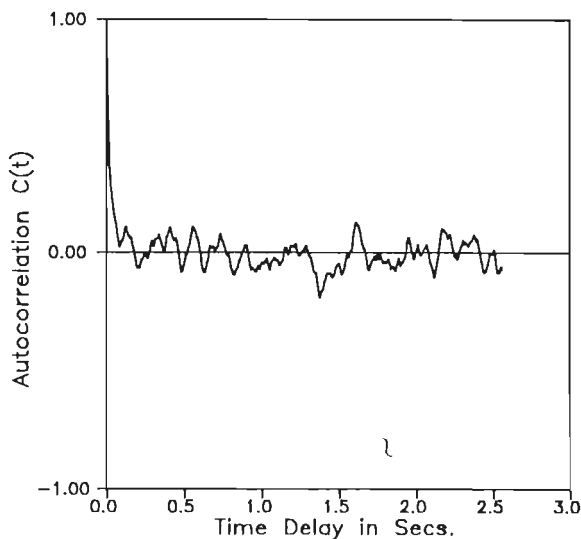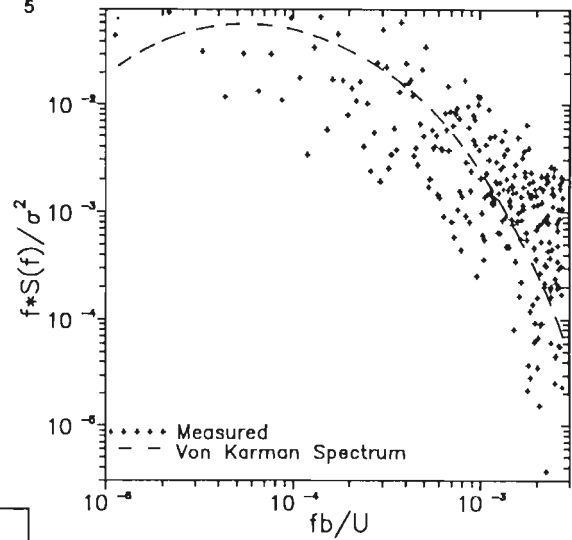
Fig. 5.18 Flow characteristics at 0.8 m upstream of the test section
at model height with Grid # 2 (U=8.2 m/sec)

(a) Time history of U component

Velocity
Mean = 3.90 m/sec
Rms = 0.47 m/sec
Max. = 5.48 m/sec

Turbulence Intensity
I_U % = 12.19

Integral
Length Scale
L_{UX} = 0.521 m

(b) Non-dimensionalized spectrum plot

(c) Autocorrelation plot
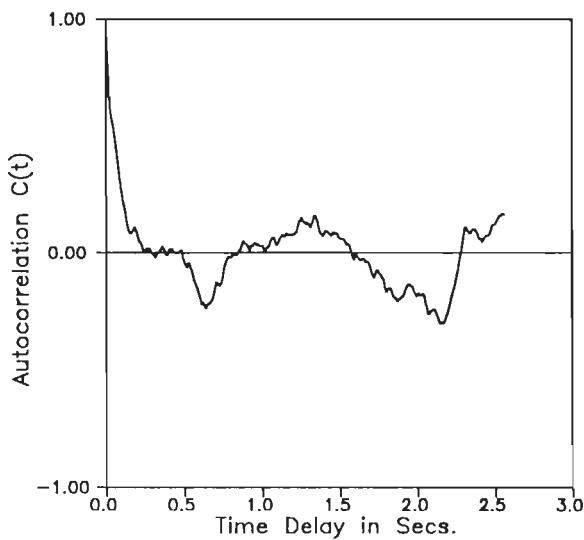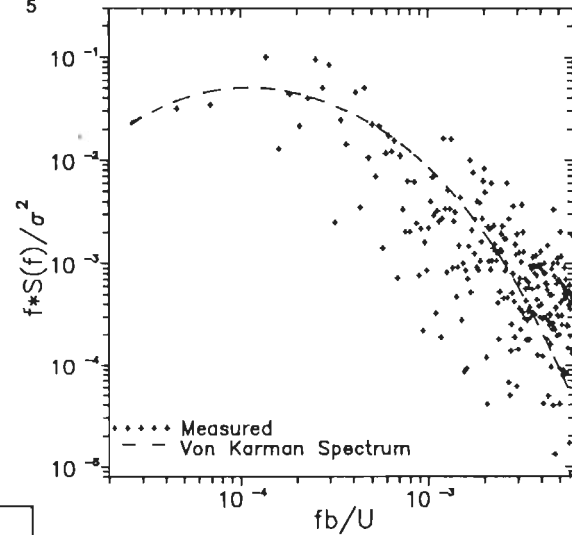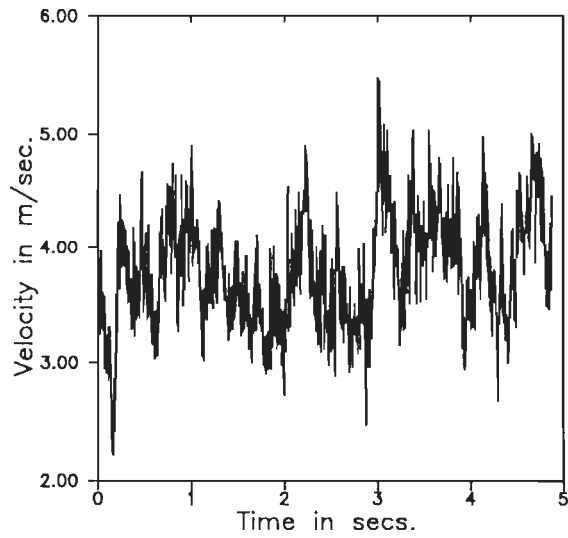
Fig. 5.19 Flow characteristics at 0.8 m upstream of the test section
at model height with Grid # 3 (U = 3.9 m/sec)

(a) Time history of U component
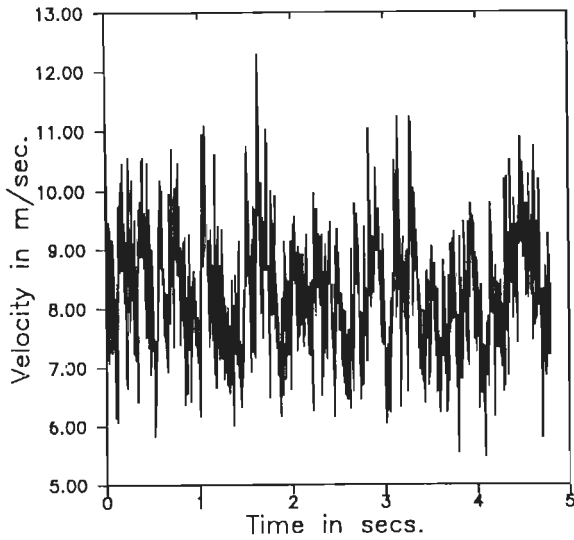
Velocity
Mean = 8.20 m/sec
Rms = 0.93 m/sec
Max. =12.28 m/sec

Turbulence Intensity
I_U % = 11.34

Integral
Length Scale
L_{UX} = 0.507m

(b) Non-dimensionalized spectrum plot

(c) Autocorrelation plot
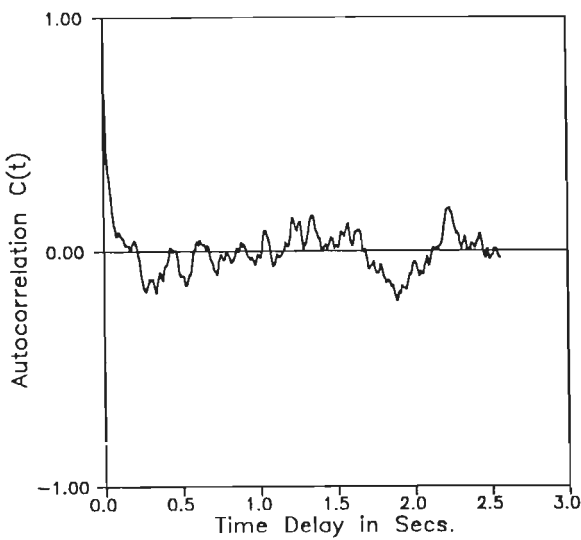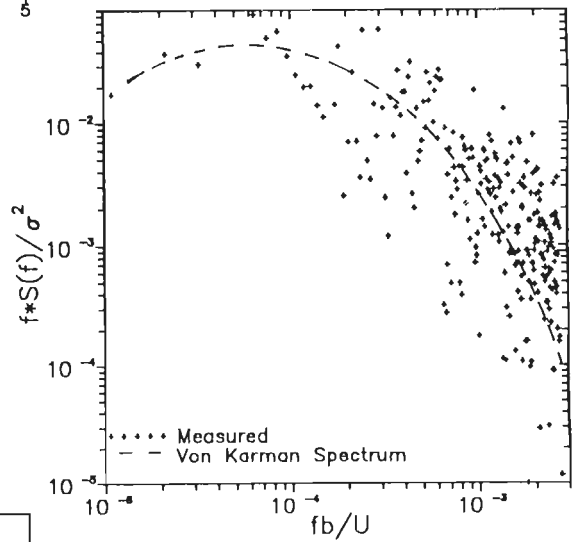
Fig. 5.20 Flow characteristics at 0.8 m upstream of the test section
at model height with Grid # 3 (U = 8.2 m/sec)

CHAPTER 6
EXPERIMENTAL RESULTS, ANALYSIS AND DISCUSSIONS

6.1 INTRODUCTION

This chapter discusses the extraction of flutter derivatives from the experimental data obtained from section model tests of the bridge deck with different configurations, and, under different flow conditions. With the aim of improving the aerodynamic behaviour of the bridge deck, different extents of fairings were attached to the deck. The flutter derivatives have been computed in each case and the results compared. Further, the use of flutter derivatives has been made in predicting the flutter instability of the bridges selected and also for the prediction of the buffeting response. The study has been made more comprehensive by considering different grid generated flows besides the smooth flow and varying the wind incidence angle over a practical range of -5^0 to $+5^0$.

6.2 EXTRACTION OF FLUTTER DERIVATIVES

The aeroelastic equations of motion for the two degrees of freedom section model, mounted with its centre of mass coincident with the centre of rotation, are written in the form as given by eqns.4.1 and 4.2.

The motion dependent bluff body aerodynamic lift and moment forces can be expressed in terms of the flutter derivatives as in eqns.4.15 and 4.16.

If either the torsional or the vertical degree of freedom is restrained, the aerodynamic lift and moment forces for the reduced single degree of freedom system will be given by

$$L = \frac{1}{2}\rho U^2 2B \left[KH_1^*(K)\frac{h}{U} + K^2 H_4^*(K)\frac{h}{B} \right] \qquad (6.1)$$

$$M = \frac{1}{2} \rho U^2 2B^2 \left[KA_2^*(K)\frac{B\alpha}{U} + K^2 A_3^*(K)\alpha \right]$$ (6.2)

The aeroelastic equations of motion (eqns.4.1 and 4.2) for each unrestrained degree of freedom can be written as:

$$\ddot{h} + 2\zeta_{h,E}\, \omega_{h,E}\, \dot{h} + \omega_{h,E}^2\, h = 0$$ (6.3)

$$\ddot{\alpha} + 2\zeta_{\alpha,E}\, \omega_{\alpha,E}\, \dot{\alpha} + \omega_{\alpha,E}^2\, \alpha = 0$$ (6.4)

where

$$2\zeta_{h,E}\, \omega_{h,E} = 2\zeta_h\, \omega_h - \frac{\rho U^2 B}{m}\left[(\frac{K}{U})H_1^*(K) \right]$$ (6.5)

$$\omega_{h,E}^2 = \omega_h^2 - \frac{\rho U^2 B}{m}\left[(\frac{K^2}{B})H_4^*(K) \right]$$ (6.6)

and

$$2\zeta_{\alpha,E}\, \omega_{\alpha,E} = 2\zeta_\alpha\, \omega_\alpha - \frac{\rho U^2 B^2}{I}\left[(\frac{KB}{U})A_2^*(K) \right]$$ (6.7)

$$\omega_{\alpha,E}^2 = \omega_\alpha^2 - \frac{\rho U^2 B^2}{I}\left[K^2\, A_3^*(K) \right]$$ (6.8)

The flutter derivative coefficients are usually extracted from experiments that measure the effective viscous damping ratio $\zeta_{h,E}$ and $\zeta_{\alpha,E}$ and the natural frequency $\omega_{h,E}$ and $\omega_{\alpha,E}$ of the aeroelastic section model system. The transient time history method explained in section 5.6 is adopted to measure the system properties. In this case the reduced frequency can be equated approximately to the natural frequency of the aeroelastic system in the concerned mode of vibration,as

$$K \cong \frac{\omega_{h,E}\, B}{U}$$ (6.9)

$$K \cong \frac{\omega_{\alpha,E}\, B}{U}$$ (6.10)

The single degree of freedom flutter derivative coefficients can now be expressed in terms of the effective aeroelastic system parameters and the zero velocity structural system parameters. Thus substituting from eqns.6.9 and 6.10 into eqns.6.5 through 6.8, we get

$$H_1^*(K) = \frac{2m}{\rho B^2}\left[\zeta_h\left(\frac{\omega_h}{\omega_{h,E}}\right) - \zeta_{h,E}\right] \qquad (6.11)$$

$$H_4^*(K) = \frac{m}{\rho B^2}\left[\left(\frac{\omega_h}{\omega_{h,E}}\right)^2 - 1\right] \qquad (6.12)$$

$$A_2^*(K) = \frac{2I}{\rho B^4}\left[\zeta_\alpha\left(\frac{\omega_\alpha}{\omega_{\alpha,E}}\right) - \zeta_{\alpha,E}\right] \qquad (6.13)$$

$$A_3^*(K) = \frac{I}{\rho B^4}\left[\left(\frac{\omega_\alpha}{\omega_{\alpha,E}}\right)^2 - 1\right] \qquad (6.14)$$

In the above eqns.6.11 through 6.14 the effective aeroelastic damping $\zeta_{\alpha,E}$ and $\zeta_{h,E}$ and the effective frequency $\omega_{\alpha,E}$ and $\omega_{h,E}$ are measured experimentally from the time history records.

6.3 TIME HISTORY RESULTS

The raw data acquired during experiments was processed to filter out unwanted signals and thus smoothened. The resultant time histories were stored for further analysis.

6.3.1 Torsional Vibrations

Several typical transient time history records of the torsional mode of the unmodified deck section under smooth and grid generated flows are shown in Figs.6.1(a) to 6.1(c). Some interesting results were obtained from these vibration records. Under smooth flow the model has a much greater tendency of destabilization as compared to the model under grid generated flow as it was observed by Scanlan et al.[7]. The same tendency can be observed for the fully faired deck section as well as the partially faired deck section (Figs.6.2 and 6.3). Over the entire velocity range (generally 2.0 m/sec to 10 m/sec) the fully faired deck model showed better stability so far as oscillations are concerned. It is clear from Figs. 6.1a, 6.2a and 6.3a that under smooth flow the model oscillations tend towards steady state vibrations at a wind velocity of about 9.6 to 9.9 m/sec. However, this condition is seen to occur at a somewhat higher wind velocity in the case of the fully faired model. Further increase in wind speed would thus lead to the flutter instability of

the model. This instance is shown in Fig.6.4, where the net damping of the system becomes negative. Further under smooth flow, the net damping of the model is seen to be much higher for wind velocity range between 4.0 m/sec and 5.0 m/sec (Figs.6.1(a)-ii, 6.2(a)-ii and 6.3(a)-ii). Interestingly this phenomenon was not observed in case of the grid generated flows. Otherwise the model showed stable vibrations under random exciting forces. The partially faired section model showed a tendency of self-excited vibrations at a mean velocity of 9.0-9.6 m/sec after the initial decay period in case of the grid generated turbulent flows (Figs.6.3(b)-ii to 6.3(d)-ii). In all such cases the flutter derivatives have been extracted using only the first phase of the time history records .

6.3.2 Vertical Vibrations

Figs. 6.5 through 6.7 show the typical time history records of the models under vertical mode of vibration. Unlike the torsional mode of vibration, here not much difference is found between the records of different model configurations and also under different flow conditions, except that there are self-excited vibrations in case of the grid generated flow conditions for all deck configurations. Typical records are shown in Figs.6.5(d)-ii, 6.6(b)-ii and 6.7(c)-ii.

6.4 FLUTTER DERIVATIVE RESULTS

Using the expressions given in section 6.2, the various flutter derivatives have been computed for the bridge deck section and for its modified configurations under smooth as well as different grid generated flows. The wind tunnel tests on the three model configurations have produced some interesting results. A computer program was developed for the post processing of the smoothened time history records in order to determine the governing parameters for the system, namely damping and natural frequency of vibration. Before feeding the data into the main program, a visual display of the time history records was seen on the P.C. monitor and the portion of the record with least disturbance was considered for processing in order to get an accurate value of the damping, since it is a sensitive parameters affecting the values of the flutter derivative. Since it is possible that amplitude of vibration may affect the values of the flutter derivatives, the initial

displacement was maintained constant at all the wind speeds and in all sets of experiments at 20 mm. Thus a constant range of peaks between 5 mm and 15 mm could be maintained to evaluate the dynamic characteristics of the model. To improve the accuracy it was evaluated for all the peaks in this range, which formed about 50 % of the record length. The average value was finally adopted. From all these records the four direct flutter derivative coefficients (H_1^*, H_4^*, A_2^* and A_3^*) were determined and used in the subsequent analysis.

6.4.1 Unmodified Section Model

The flutter derivative $H_1^*(K)$ has a tendency to decrease as the reduced velocity increases under smooth flow. This is evident from Fig.6.8(a). These plots (Fig.6.8(a)) show very little or no effect of wind incidence angle on $H_1^*(K)$. Further, the grid generated flows (Figs.6.8(b) to 6.8(d)) exhibit an enhancement in this trend in $H_1^*(K)$. Further decrease in negative values of $H_1^*(K)$ signifies that the grid generated turbulent flow tends to stabilize the vertical motion of the bridge deck. The trend of $H_1^*(K)$ in case of grid #2 is somewhat different from others. This difference could possibly be on account of the fact that the length scale of turbulence was equal to the deck width for this grid #2.

The flutter derivative $H_4^*(K)$ did not show any change with velocity in case of the smooth flow at zero angle of attack (Figs. 6.9(a) to 6.9(d)). But it showed some change as the angle of incidence changed from negative to positive at the higher reduced velocities. Furthermore, under the grid generated flows $H_4^*(K)$ shows considerable increase in magnitude. It thus appears that eddies present in the grid generated flow greatly influence the aerodynamic behaviour of bridge decks when the size of the eddies is close to the width of the bridge deck.

The torsional stability of a bridge deck, on the other hand, is mainly governed by the nature of $A_2^*(K)$, the aerodynamic damping derivative. Referring to eqn.4.43 an increase in the value of the derivative A_2^* (as also H_1^*) evidently reduces the stability of the system. Thus under smooth flow the curve for $A_2^*(K)$ (Fig.6.10(a)) shows a destabilizing trend. This positive trend gets reduced in case of the grid generated flows (Figs.6.10(b) and 6.10(c)). Besides turbulence, the wind incidence angle also plays a vital role in the

stability of the system. From Fig.6.10(a) it is also noticed that the negative wind incidence angles have an early destabilizing trend as compared to the positive wind incidence angles. The same trend is also seen for the grid generated flow.

The trend of the flutter derivative $A_3^*(K)$ (Figs.6.11(a) to 6.11(c)) does not change for either the wind incidence angle or for the grid generated flows. All plots have similar trends.

6.4.2 Fully Faired Section Model

To study the effect of fairings on the composite I-Girder deck section in an attempt to increase its stability, suitable fairings were designed and fabricated. The results of flutter derivatives are discussed here.

Plots of the derivative $H_1^*(K)$ under smooth flow are shown in Fig.6.12(a). The trends are similar to the unmodified deck section (Fig.6.8(a)) but the values of $H_1^*(K)$ are much lower indicating a substantial increase in stability compared to the unmodified deck section. However, under the grid generated flow conditions the $H_1^*(K)$ values are generally a little higher and at times even positive, (Fig.6.12(b), (c) and (d)) indicating a destabilizing trend. The fairing over the full length of the bridge deck, therefore, has not helped in reducing the vertical flutter oscillations of the deck. This effect is unusual and needs further investigation.

$H_4^*(K)$ derivatives for the smooth flow (Fig.6.13(a)) have a sharp reduction for the negative wind incidence angles which is observed over the entire range of the reduced velocities, while increasing with positive wind incidence angles for the higher reduced velocities beyond 6 to 8. It can thus be seen that, the natural frequency in the vertical mode of vibration gets largely affected by the wind incidence angle (eqn.6.12). The wind incidence angle can therefore have a significant effect on the stability of the system. However, under grid generated turbulent flows the derivative $H_4^*(K)$ does not show any specific trend (Figs.6.13(b), (c) and (d)).

The torsional flutter coefficient $A_2^*(K)$ shown in Fig 6.14(a) for the fully faired model under smooth flow indicates that there is an increase in the stability since the

reduced velocity at the point of change in sign from negative to positive value is higher compared to that for the unmodified section model. The wind incidence angle has a similar influence as for the unmodified section model. Further, the destabilizing positive trend is substantially reduced for the faired model under all wind incidence angles. The influence of fairings added to the deck is thus to improve the stability of the deck against torsional flutter. A similar nature of $A_2^*(K)$ was observed under the grid-generated flow conditions as well (Figs.6.14(b),(c) and (d)).

The derivative $A_3^*(K)$ shows a striking similarity in the trends with those of the unmodified deck section (Figs. 6.11 (a) to 6.11(c) and Figs. 6.15(a) to 6.15(c)) so it may be concluded that the fairings practically do not have any influence on the torsional frequency of oscillation of the model, which are responsible for the change in $A_3^*(K)$ (eqn.6.14).

6.4.3 Partially Faired Section Model

As it was observed in the preceding section, the fairings can influence the flutter derivatives substantially towards stabilizing the system. In order to achieve greater economy in the use of fairings it was decided to study further the effect of reduced length of fairings. Thus a reduction of 40 % was made in the fairings, providing them only over 60 % of the bridge span (evenly distributed with a length of 0.25m each).

Figs.6.16 through 6.19 show the plots of $H_1^*(K), H_4^*(K), A_2^*(K)$ and $A_3^*(K)$ for the partially faired model under various flow conditions. These plots compared with Figs. 6.8 through 6.11 and Figs.6.12 through 6.15 show that there is considerable change in the behaviour of the model -towards improved stability- as compared to the unmodified deck model. It is less stable, though only marginally, compared to the fully faired model.

6.4.4 Comparison with Other Deck Shapes

Although the deck geometry considered is different from other shapes for which the results are available, a comparison with the available results has been attempted to have some idea of the overall behaviour of the deck section.

Figs. 6.20 through 6.25 show some of the flutter derivatives for various deck shapes obtained by earlier investigators.

Comparing Fig. 6.12(a) with 6.20 [5], the variation of H_1^* in both cases follows a similar trend. The same behaviour can also be observed in Fig.6.21(a)[3]. The difference in the values, however, can be attributed to the difference in geometry and the dynamic characteristics of the models.

The variation of derivatives A_2^* with respect to wind incidence angles is shown in Fig.6.23 obtained from the 1:80 section model tests[1] of a concrete girder deck of cable stayed bridge. The trend shown in this figure confirms that the wind incidence angle has considerable influence on the flutter derivatives. This behaviour was also observed for the open composite girder deck studied (Fig.6.10). Further, the effect of positive wind incidence angles has been to contribute towards the stability of the bridge decks for both the deck types as is evident from Figs. 6.10 and 6.23.

Similarly, the effect of turbulence on the flutter derivatives obtained for Deer Isle[2] and Golden Gate[7] bridge decks is illustrated in Figs. 6.22 and 6.24 respectively. These plots do not show any significant change due to turbulence in the wind for which the study had been undertaken, whereas in the present study the turbulence present in the incident wind flow (Figs. 6.10(a) (b)and (c) for 0^0 angle of attack) showed considerable influence on the flutter derivatives. This apparent contradiction can be attributed to the levels of turbulence, the integral length scales of turbulence and also possibly to their methods of generation which were different in these cases.

The effect of fairings on the flutter derivatives is shown in Fig.6.25[4] obtained from the study on a modified unstable deck configuration. A comparison of Fig.6.25 with Figs.6.10 and 6.18 of the present investigation further confirms that the fairings can influence the flutter derivatives considerably and hence the stability of the deck.

6.5 FLUTTER CRITERIA

6.5.1 Criterion from Section Model Test Results

Based on the aerodynamic damping derivative $A_2^*(K)$ one can approximately determine the threshold velocity at which the flutter occurs, with torsional mode dominating. The point at which $A_2^*(K)$ changes its sign from negative to positive was considered as the point at which the onset of flutter may take place, i.e., the point where total damping of the structure becomes zero. This approach leads to conservatism since the influence of other derivatives and modes of vibrations of the full bridge are not considered, though one may utilize this data as first hand information in the preliminary design.

Table 6.1 shows the values of the threshold wind speed for the particular geometry of the deck at the zero wind incidence angle for various wind flow conditions. These values have been obtained directly from Figs. 6.10, 6.14 and 6.18 as the values where the derivative $A_2^*(K)$ changes sign from negative to positive.

Table 6.1

Critical Wind Speeds(threshold) in m/sec.

Particular	Smooth	Grid#1	Grid#2	Grid#3
Unmodified	46.79	59.51	63.60	-
Faired(100%)	58.58	72.81	79.61	72.81
Faired(60%)	50.55	70.06	70.06	72.81

The above reported values have been obtained from the reduced velocity and then converted for the prototype based on the frequency and deck width of bridge #1.

From Table 6.1 it is clear that the grid generated flow conditions increase the stability of the deck section. In addition the fairings provided to the deck are seen to influence the deck stability considerably. Also in case of the turbulent flow, a reduction of 40 % in the fairings is possible without much loss in the critical velocity, which affects the aerodynamic stability of the bridge, while attaining substantial economy in the deck.

Further, it is interesting to note that the wind incidence angle contributes much to the threshold velocity. Figs. 6.26 through 6.28 indicate the influence of the angle of

attack on the threshold velocity. From these figures it is clear that positive wind incidence angles enhance the threshold velocity of the deck and vice versa. In case of the unmodified deck section model under smooth flow the threshold velocity varies from 36 m/sec to 51 m/sec as the angle of incidence changes from -5 to +5 degrees respectively. For fully faired section the threshold velocity varies from 49 m/sec to 70.8 m/sec as the angle of incidence changes from -5 to +5 degrees respectively. However, in case of partially faired(60%) deck the trend is not definite with respect to the angle of wind incidence.

It is interesting to note that wind incidence angles within ±3 degrees do not have much influence on the threshold velocity, but angles outside this range cause much change in the behaviour.

The section model has been tested for 1.2% damping. However, analytical results presented in Fig.6.29 demonstrate how the threshold wind speed would increase for a horizontal wind as the net system damping is varied from 0 to 1.0% (i.e., total 1.2% to 2.2%). If the prototype bridge is expected to have 2.2 % damping, the threshold velocity would be 61.9 m/sec in case of unmodified deck, 77.37 m/sec in case of fully faired and 66.5 m/sec in case of partially faired deck. Critical velocities at other wind incidence angles similarly increase with damping (Fig.6.30). In all cases the negative wind incidence angles show more susceptibility towards flutter when compared with the positive wind incidence angles.

6.5.2 Full Bridge Flutter Criterion

With the utilization of free vibration results obtained for the prototype bridges (Section 3.6) and the flutter derivatives obtained from the section model tests the 'full bridge flutter criterion' could be computed using the formulation described in section 4.4.1.

Analysis has been carried out for the first 28 modes of vibration of the prototype structure to attain the 'full bridge flutter criterion' using all the four direct flutter derivatives. The first unsymmetrical torsional mode (mode no. 16) was found to have a tendency to enter into the flutter zone at a wind speed of 81.2 m/sec for bridge #1. This

wind speed is much higher than the values obtained in the preceding section, which shows the influence of other derivatives and possibly involvement of a higher mode of vibration(hence a different frequency) on the full bridge flutter criterion.

On adopting the faired deck section for the prototype, the critical wind velocity for the structure to enter into the flutter zone would increase from 81.2 m/sec to 92.4 m/sec.

For both the above cases the critical wind speed is very high and reflects the high stability of the bridge deck to flutter. This is obvious because the span length of bridge #1 is not very large and also the deck section along with the cable system is stiff enough to have rather high natural frequencies of vibration.

It is thus seen that bridge #1 with a composite I-Girder deck is quite stable against the aerodynamic flutter instabilities.

For bridge #2 the symmetrical torsional mode 7 was found to be critical and entered into the flutter zone at 46.5 m/sec. It is therefore seen that the same deck configuration as of bridge #1 will be susceptible to aerodynamic flutter instability at lesser wind speed when adopted for the much longer span of bridge #2 . This is because in case of longer spans the modal parameters have a dominant influence on the flutter criterion, besides the geometric configuration of the deck.

Another peculiarity observed in bridge#2 is that the addition of fairings has hardly any significant effect on the critical velocity which is attained at a value of 46.8 m/sec. It thus seems that the effect of geometrical changes in the deck section, brought about by the use of fairings, is specific not only to the deck type but it is also very sensitive to the total bridge characteristics such as the modifications in span.

Based on the design manual for highway bridges in Japan[9] the lowest critical wind speed is given by

$$U_r = U_{cf}/f_\Theta B$$

(6.15)

As per the manual the lowest reduced critical wind speed for solid deck is about 2.5.

Adopting this criterion the lowest reduced critical wind speed for bridge#1 is 3.96 and for bridge#2 it is 3.36.

These values indicates the composite I-girder type deck section studied here is expected to become unstable at a velocity higher than that for the solid deck.

6.6 BUFFETING RESPONSE OF FULL BRIDGES

The response of bridges #1 and #2 has been determined assuming the Simiu spectra for horizontal and vertical components [8] of wind and utilizing the flutter derivatives obtained for the deck section together with the modal parameters. The responses thus obtained are discussed in the following sub-sections.

6.6.1 Response of Bridge #1

Prediction of the bridge response has been made using the formulation described in section 4.4.2. Wind speeds upto 50 m/sec have been considered which are the normal wind speeds used in design. The responses have been estimated and cumulated for the first 10 bending and torsional modes of vibrations. The deformations obtained are further simplified to obtain the maximum/excursing edge deflections. A peak factor of 3.5 has been adopted [6] in all deflection computations. Further, the modal responses were cumulated for a particular section and the same are depicted for the quarter-span and mid-span points in Figs. 6.31(a) and 6.31(b) respectively. Here the flutter derivative data has been taken for the unmodified deck section. From these plots it is seen that the maximum response for a quarter-span point is about 0.8 m compared to 0.6 m at the mid-span, this is obvious since the response is dominated by torsional modes. From the plots one can observe that the major part of the response occurs in the first few modes of vibrations while the latter modes have much smaller contribution.

Figs. 6.32(a) and 6.32(b) show the plots of the maximum excursing edge deformations at the quarter-span and mid-span points for bridge #1 with the use of faired section model results. These figures show that there is no significant difference as compared to the results of the unmodified deck section. The two figures 6.31 and 6.32 illustrate that the fairing added to the section does not alter the buffeting response of the bridge in its bending mode of vibration.

Figs 6.33(a) and 6.33(b) show the variation of maximum edge excursing deformations with wind speed for the torsional mode of vibration. These responses have been obtained from the unmodified section model test results. Unlike in the vertical mode of vibration, here the maximum response is approximately same at both quarter-span and mid-span points.

Also the responses in the torsional mode are seen to reduce significantly with the addition of fairings to the deck section. The maximum excursing edge deformation at the quarter-span point reduces from 0.3m to 0.2 m. The reduction also happens to be equal at both quarter-span and mid-span points. The corresponding responses are depicted in Figs. 6.34(a) and 6.34(b).

In all the above cases the first six modes of vibration yielded the maximum response, with subsequent modes contributing insignificantly.

6.6.2 Response of Bridge #2

As discussed in section 2.3 the flutter derivative coefficients of the section model tested have been also utilized to predict the response of another bridge, bridge #2, of a much longer span.

Figs. 6.35(a) and 6.35(b) show the cumulative modal response in the form of maximum edge excursing deformations in pure bending at quarter-span and mid-span points of the main span of bridge #2. For this bridge the maximum edge deformation occurs at the mid- span point and is about 3.5 m, while it is only 1.5 m at the quarter-span point.

The response obtained using the flutter derivatives of the faired section model does not differ significantly from the response in pure bending and is depicted in Figs. 6.36(a) and 6.36(b) at the quarter-span and mid-span points respectively.

Figs. 6.37(a) and 6.37(b) show the response of bridge #2 in its torsional mode. The maximum edge deformation is seen to occur at the mid-span.

The use of fairings is found to have a considerable influence and reduces the response by about 25 %, i.e., from 3.5 m maximum edge deformation to 2.5 m. Figs. 6.38(a) and 6.38(b) again confirm that maximum deflection occurs around the mid-span point.

136

References

1. Bienkiewicz,B., J.E.Cermak, and J.A.Peterka, (1987), "Wind Tunnel Study of Aerodynamic Stability and Response of Cable Stayed Bridge Deck", Jnl. of Wind Engg. and Ind. Aero., Vol. 26, pp 341-352.

2. Bosch,H.R., (1990), "Section Model Studies of the Deer Isle Sedgwick Suspension Bridge", Jnl. of Wind Engg. and Ind. Aero., Vol. 34, pp 601-610.

3. Bosch,H.R., (1990), "Aerodynamic Stability of A Truss Stiffened Cable Stayed Bridge", Jnl. of Wind Engg. and Ind. Aero., Vol. 34, pp 1331-1340.

4. Houston,D.R., H.R.Bosch, and R.H.Scanlan, (1988), "The Effect of Fairings and Turbulence on Flutter Derivatives of a Notably Unstable Bridge Deck", Jnl. of Wind Engg. and Ind. Aero., Vol. 29, pp 339-349.

5. Sarkar,P.P., N.P.Jones, and R.H.Scanlan, (1992), "System Identification for Estimation of Flutter Derivatives", Progress in Wind Engineering, Jnl. Wind Engg. and Ind. Aero., Vol, 41-44, pp 1243-1254.

6. Scanlan,R.H., and R.H.Gade, (1977), "Motion of Suspended Bridge Spans under Gusty Wind", Jnl. of Structural Div., ASCE, Vol.103, ST9, September, pp 1867-1883.

7. Scanlan,R.H., and D.Houston, (1986), "Changes in Bridge Deck Flutter Derivatives Caused by Turbulence" Proc. of the Third Conf by Engg Mech Div. on Dynamic Response of Structures, ASCE, Los Angeles, U.S.A., Ed. G.C.Hart et al., pp 382-389.

8. Simiu,E., and R.H.Scanlan, (1986), "Wind Effects on Structures" II Ed., John Wiley and Sons, N.Y.

9. Sato,H., and R.Toriumi, (1994), "On the Wind Resistant Design Manual for Highway Bridges in Japan", National Seminar on Wind Loads- Codal Provisions, April 1994, Structural Engg. Research Centre, Ghaziabad, India, pp 13-1 to 13-15.

Notations

A_i^*	flutter derivatives (i=1,2,...)
B	deck width
H_i^*	flutter derivatives (i=1,2,..)
I	mass moment of inertia per unit span
K	reduced frequency
L	aerodynamic lift
M	aerodynamic moment
U	mean wind velocity
U_r	lowest reduced critical wind speed
U_{cf}	critical wind speed for flutter
f_Θ	natural frequency of the 1st torsional mode
h	vertical degree of freedom
m	mass per unit span
α	rotational degree of freedom
ρ	air density
ω_h	natural frequency of vibration in bending
ω_α	natural frequency of vibration in torsion
$\omega_{h,E}$	natural frequency of vibration in bending
$\omega_{\alpha,E}$	natural frequency of vibration in torsion
ζ_h	damping ratio in bending
ζ_α	damping ratio in torsion
$\zeta_{h,E}$	effective damping ratio in bending
$\zeta_{\alpha,E}$	effective damping ratio in torsion
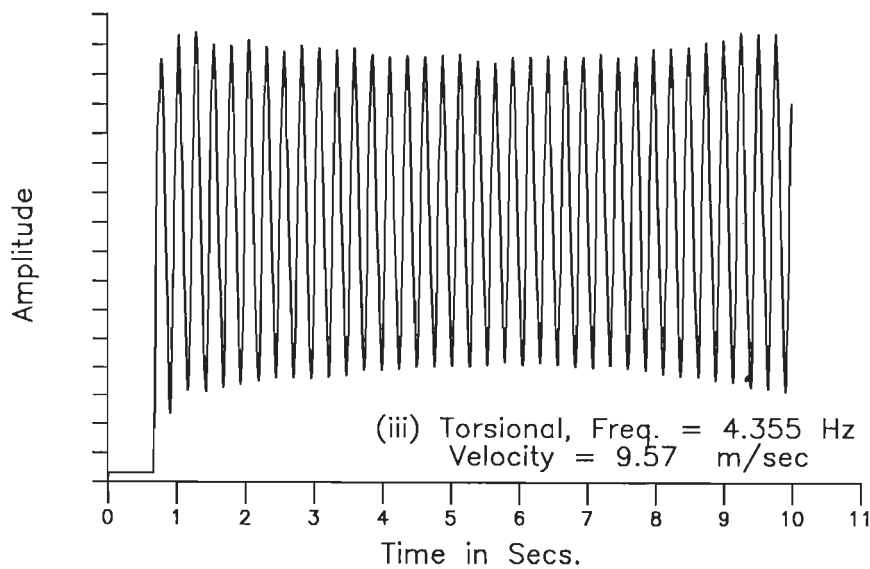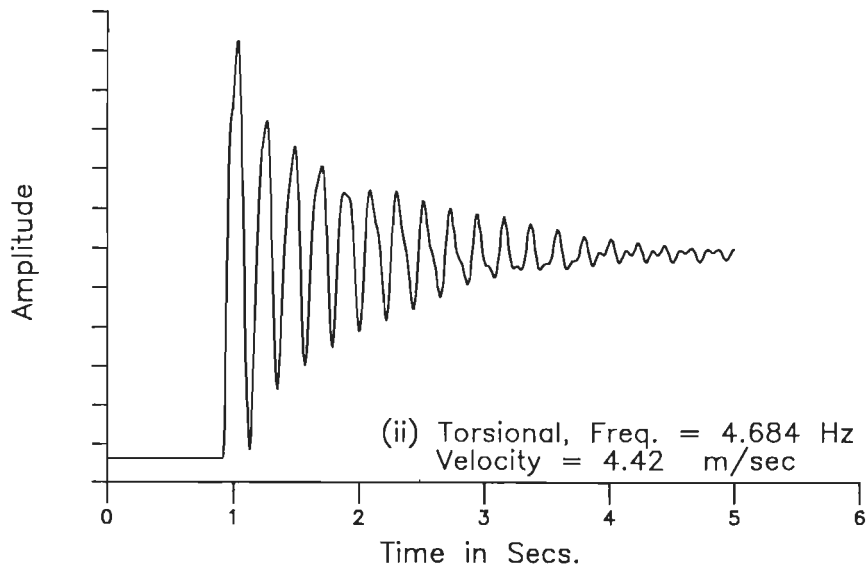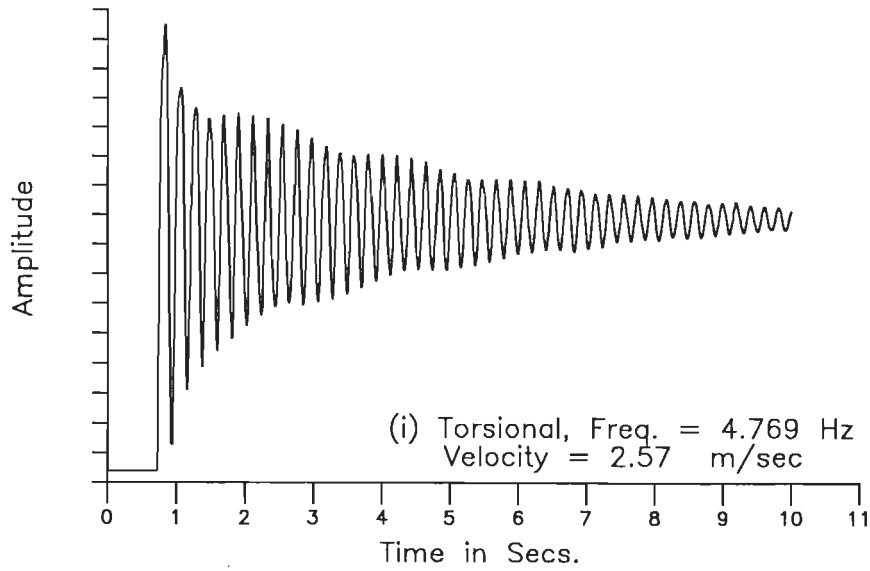
(i) Torsional, Freq. = 4.769 Hz
Velocity = 2.57 m/sec

(ii) Torsional, Freq. = 4.684 Hz
Velocity = 4.42 m/sec

(iii) Torsional, Freq. = 4.355 Hz
Velocity = 9.57 m/sec

Fig. 6.1(a) Time history record of unmodified section model in torsional mode of vibration under smooth flow.

(i) Torsional, Freq. = 4.71 Hz
Velocity = 2.57 m/sec

Time in Secs.

(ii) Torsional Freq. = 4.445 Hz
Velocity = 9.57 m/sec

Time in Secs.
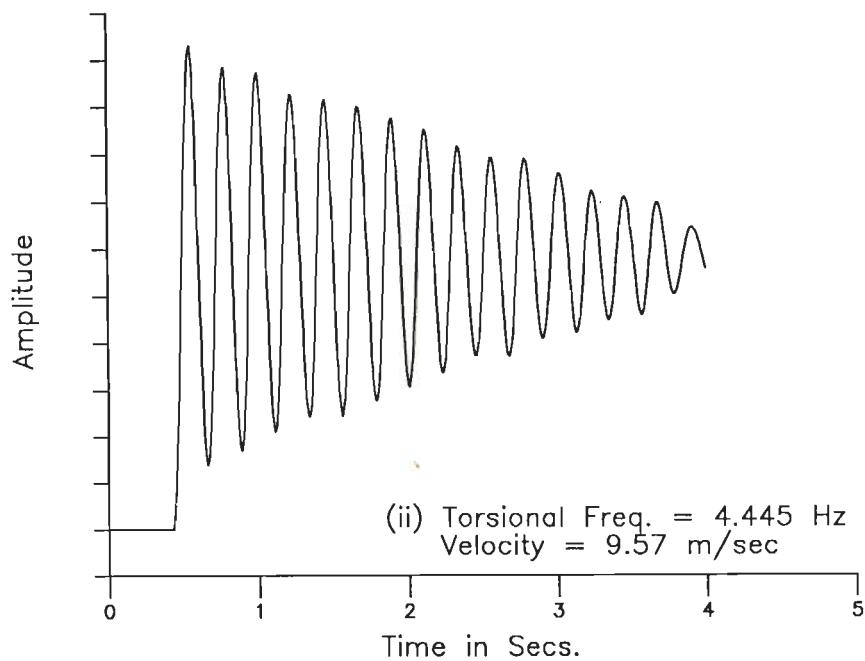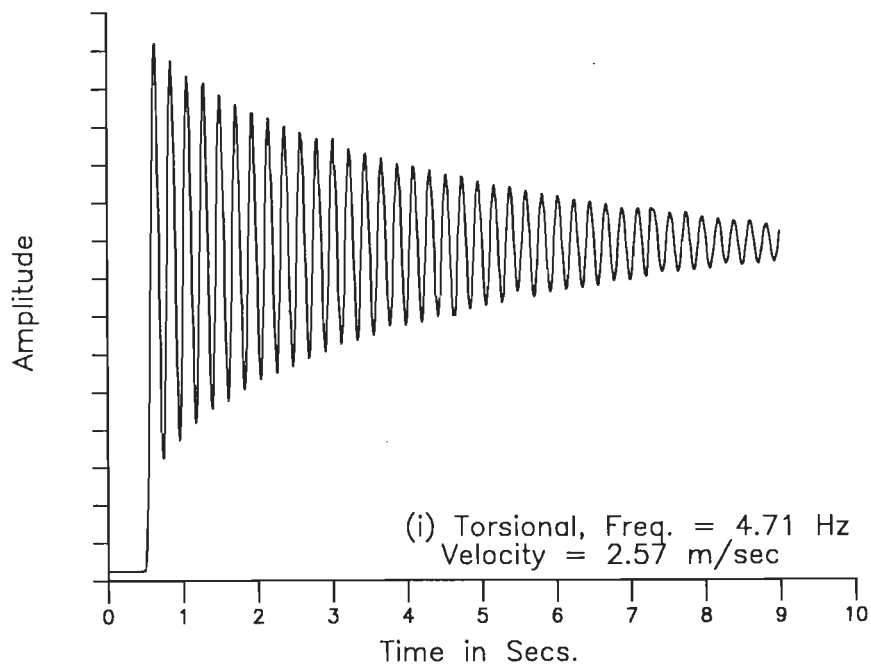
Fig. 6.1(b) Time history record of unmodified section model in torsional
mode of vibration under grid generated flow (Grid # 1).
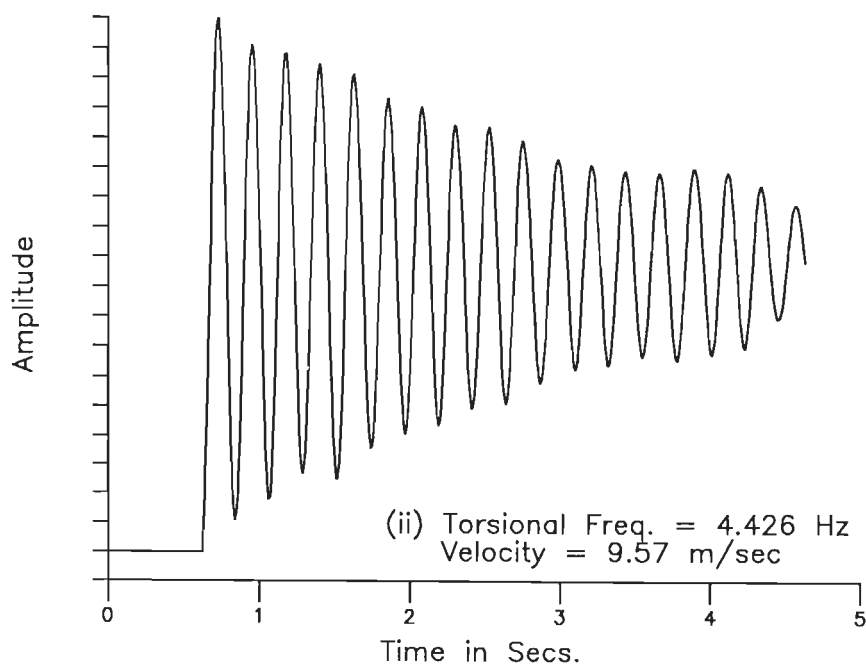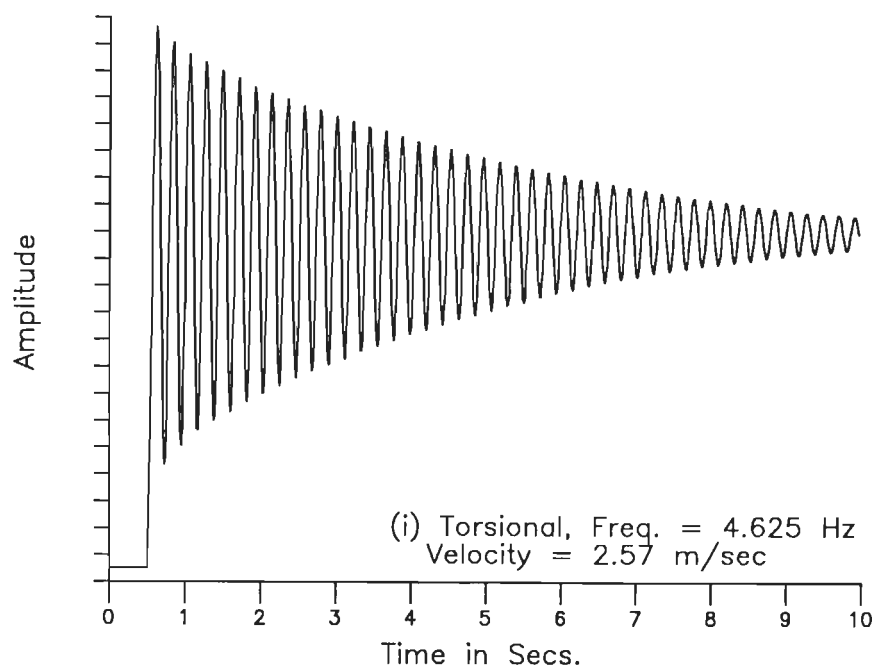
Fig. 6.1(c) Time history record of unmodified section model in torsional
mode of vibration under grid generated flow (Grid # 2).

Fig. 6.2(a) Time history record of faired section model in
torsional mode of vibration under smooth flow.

(i) Torsional, Freq. = 4.349 Hz
Velocity = 2.57 m/sec

Time in Secs.

(ii) Torsional Freq. = 4.149 Hz
Velocity = 9.57 m/sec

Time in Secs.
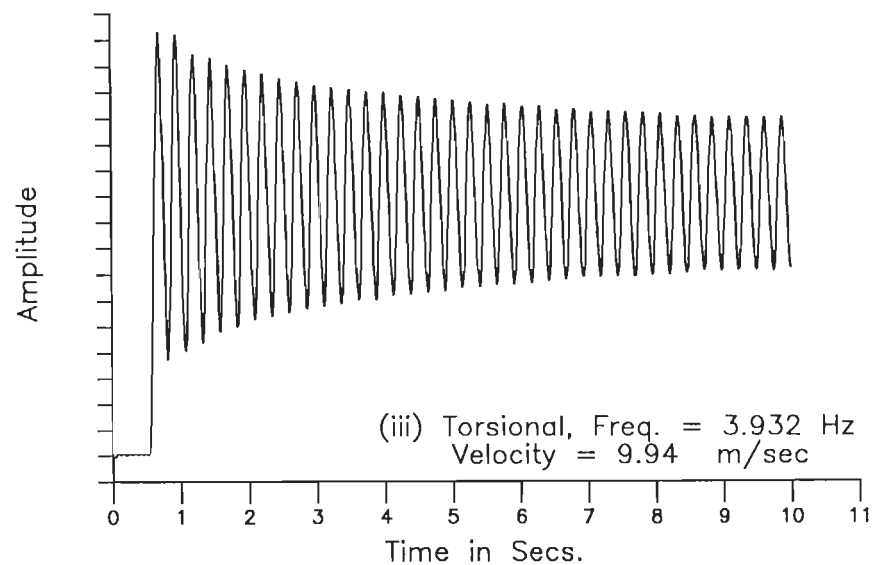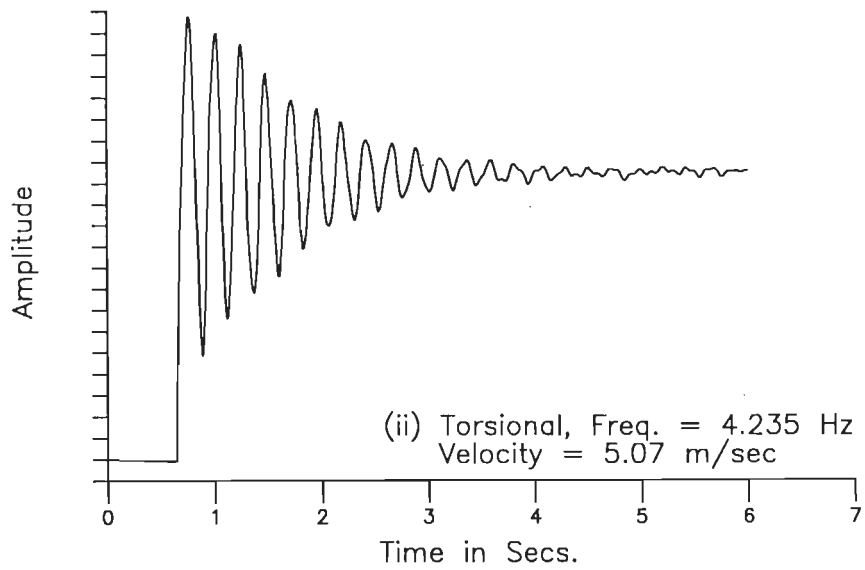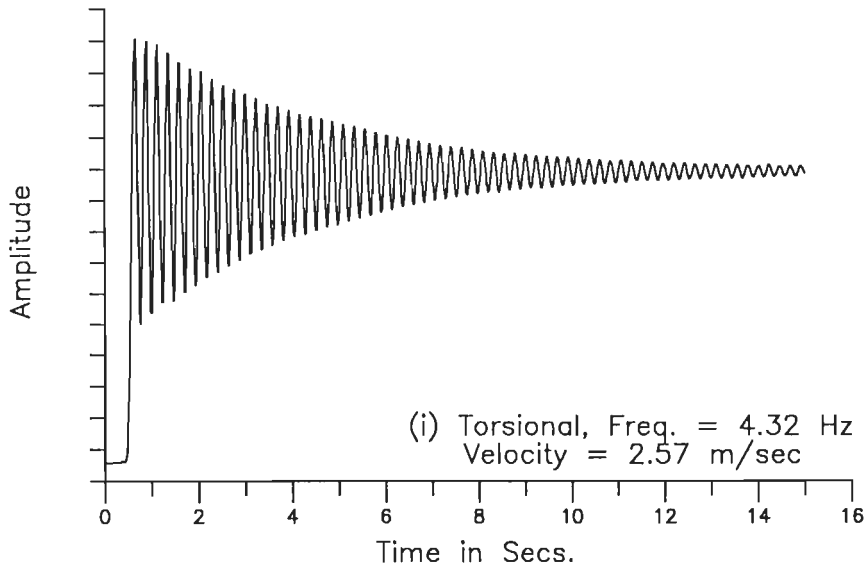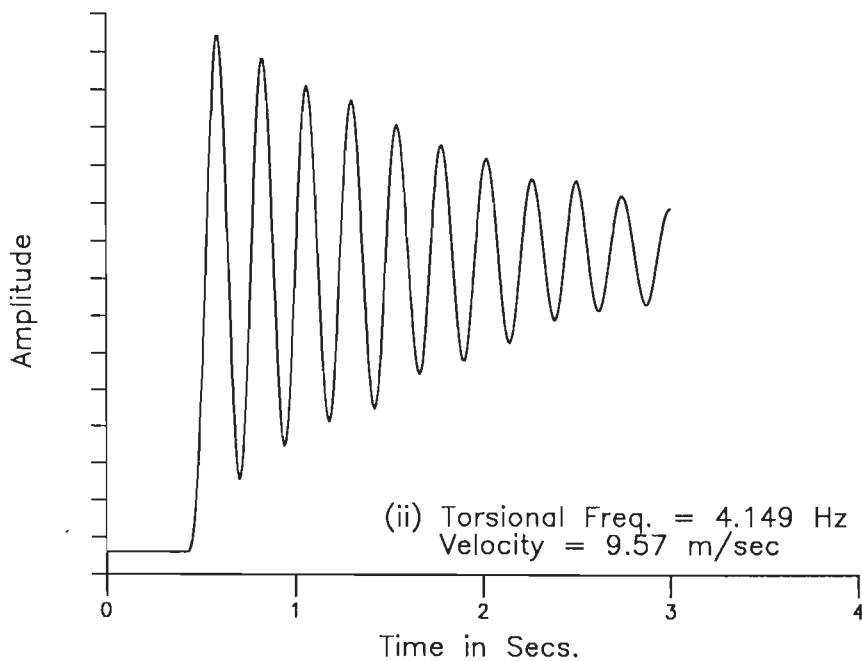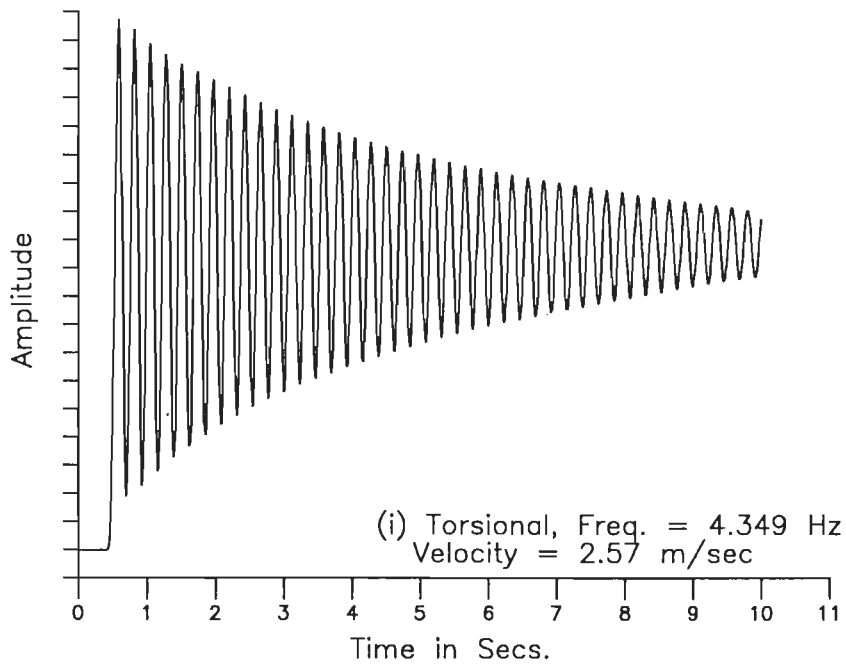
Fig. 6.2(b) Time history record of faired section model in torsional
mode of vibration under grid generated flow (Grid # 1).
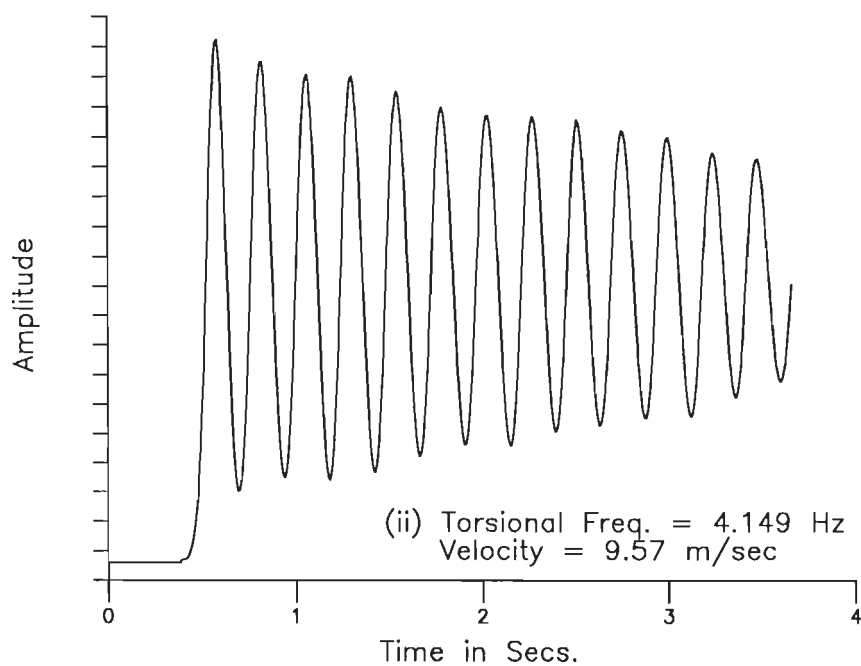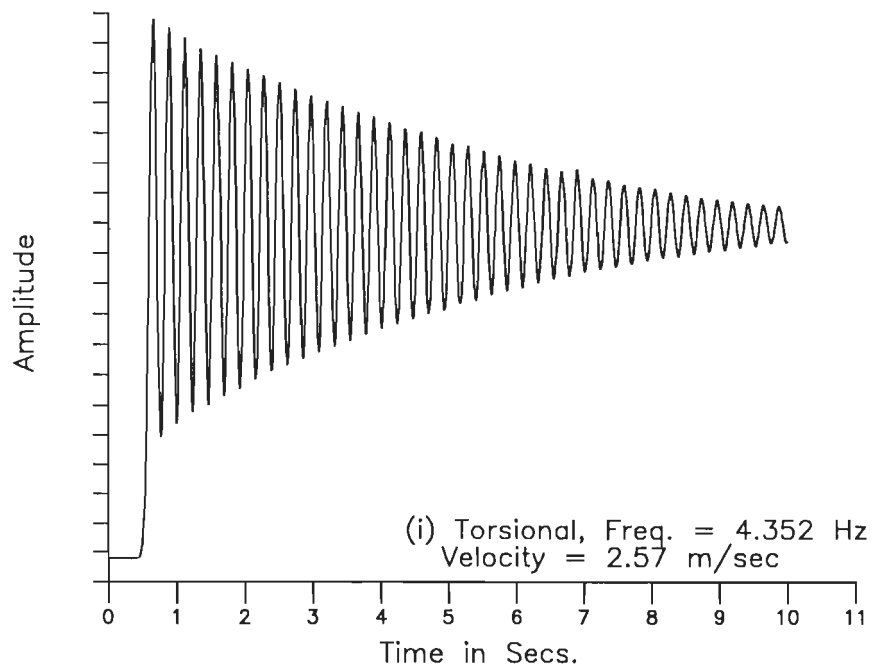
Fig. 6.2(c) Time history record of faired section model in torsional
mode of vibration under grid generated flow (Grid # 2).

Fig. 6.2(d) Time history record of faired section model in torsional mode of vibration under grid generated flow (Grid # 3).

(i) Torsional, Freq. = 4.407 Hz
Velocity = 2.57 m/sec

Time in Secs.

(ii) Torsional, Freq. = 4.323 Hz
Velocity = 5.07 m/sec

Time in Secs.

(iii) Torsional, Freq. = 4.142 Hz
Velocity = 9.94 m/sec

Time in Secs.
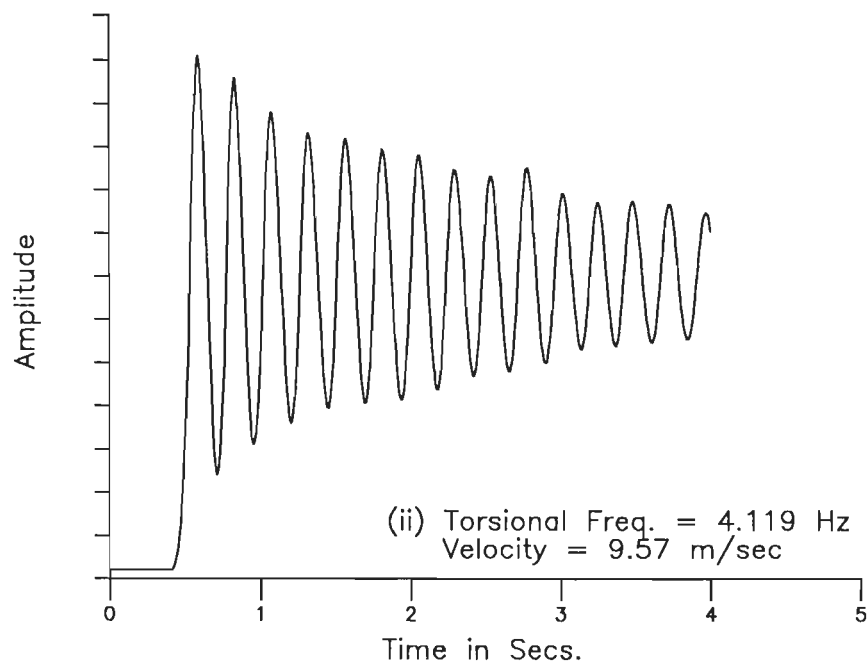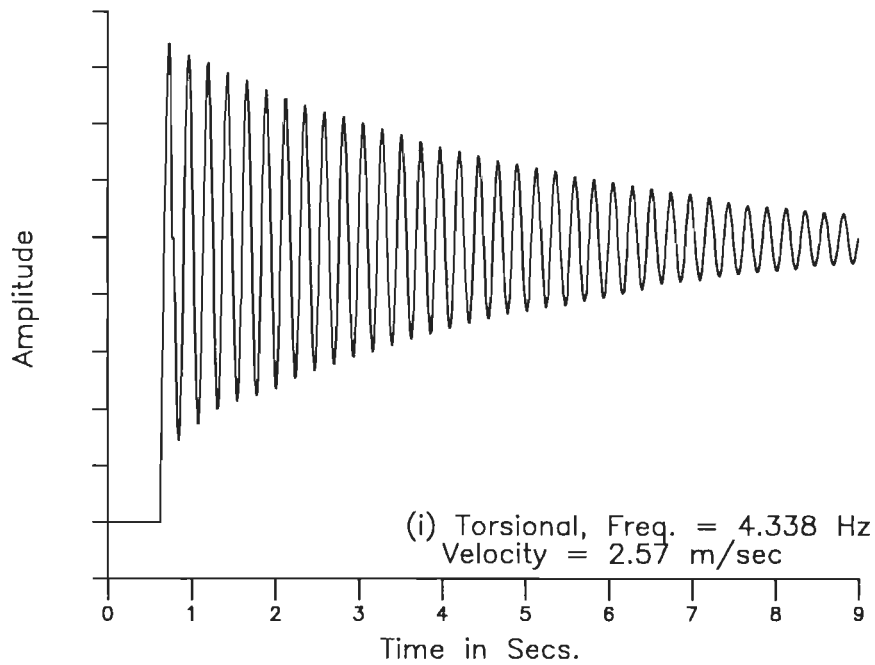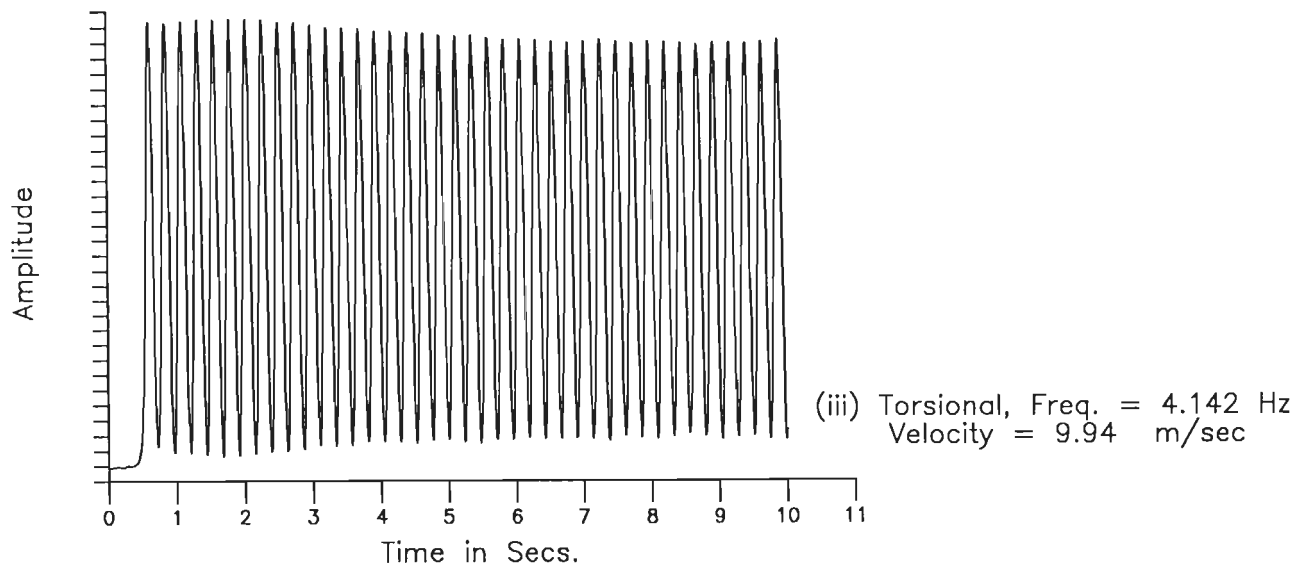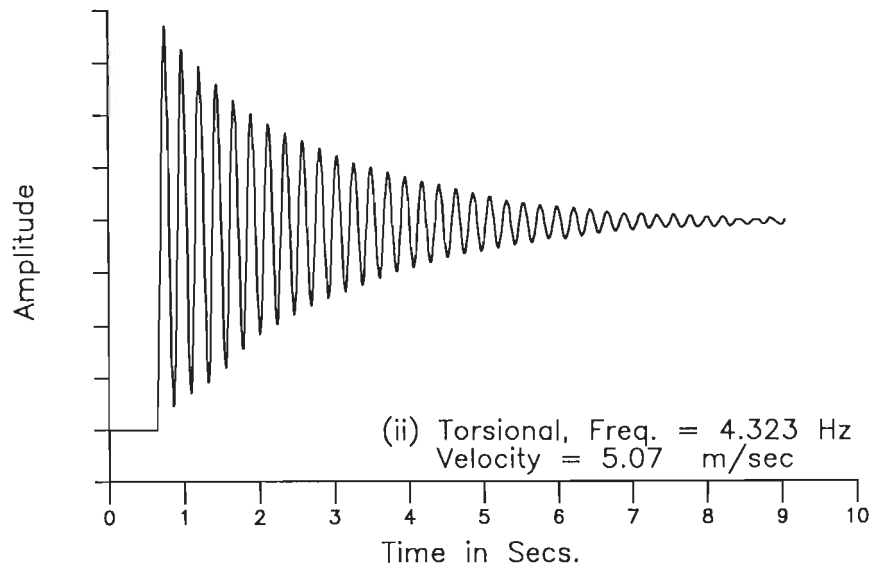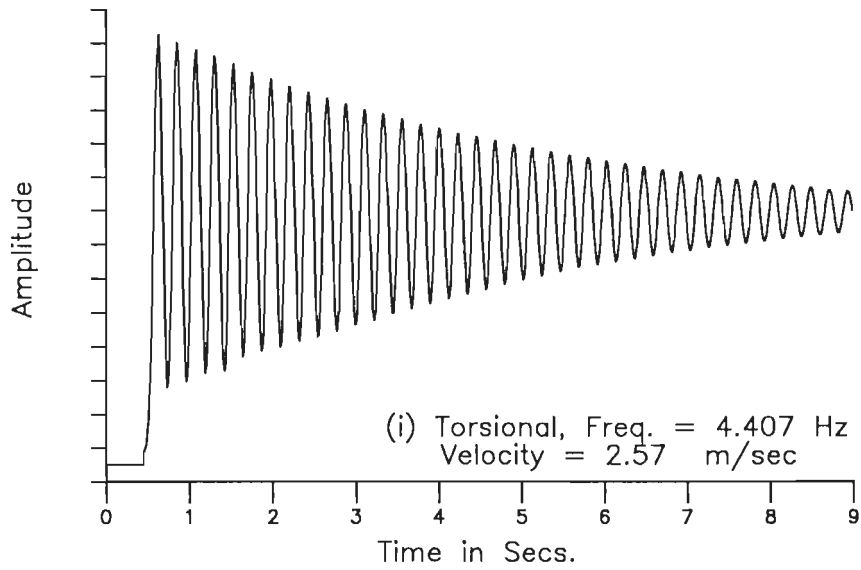
Fig. 6.3(a) Time history record of partially faired section model
in torsional mode of vibration under smooth flow.

Fig. 6.3(b) Time history record of partially faired section model in torsional mode of vibration under grid generated flow (Grid # 1).

(i) Torsional, Freq. = 4.464 Hz
Velocity = 2.57 m/sec

(ii) Torsional Freq. = 4.301 Hz
Velocity = 8.97 m/sec
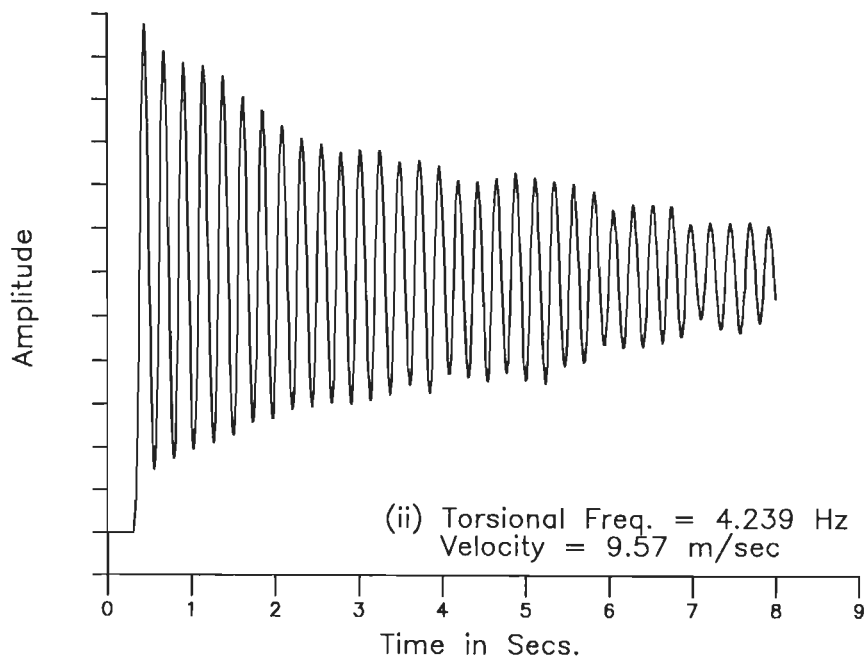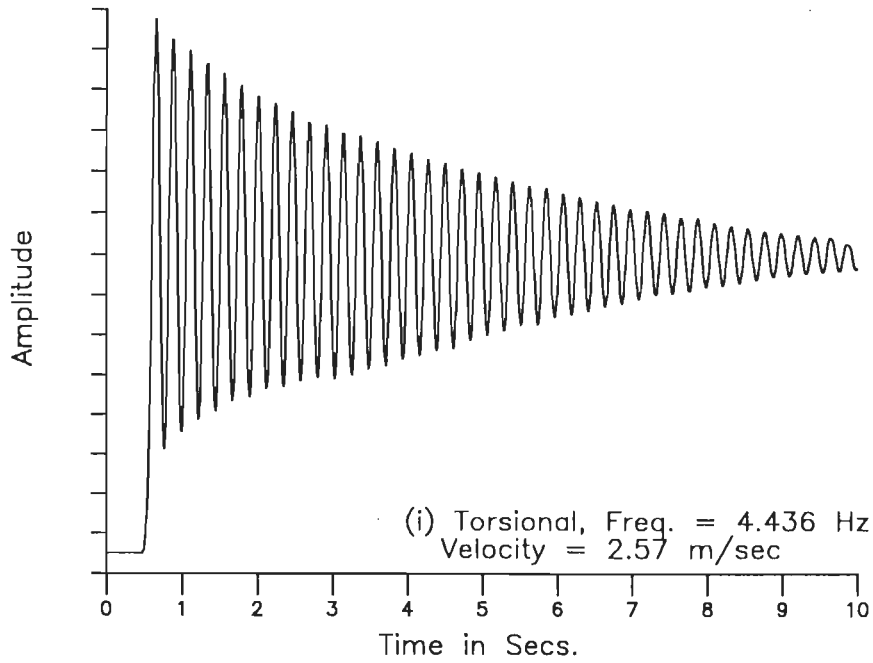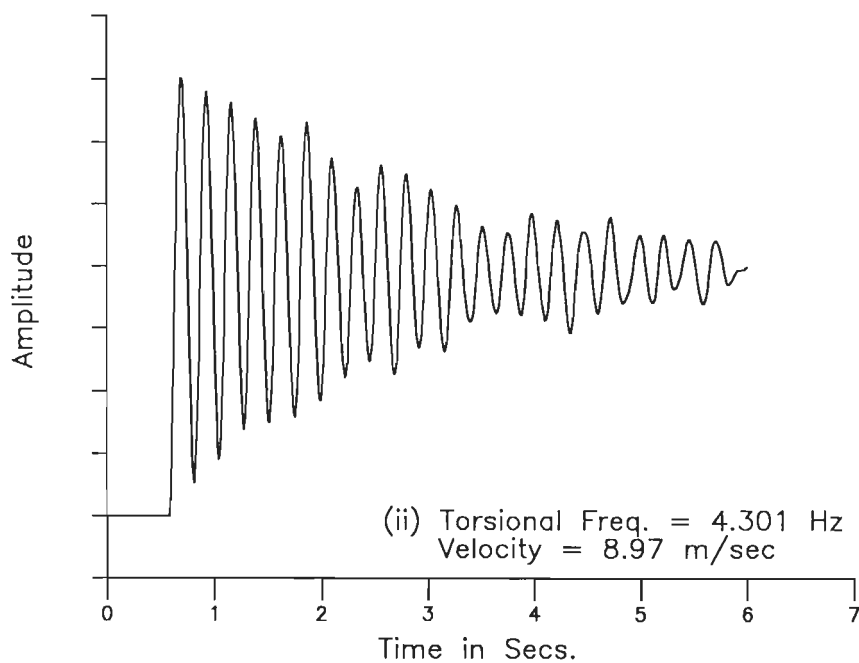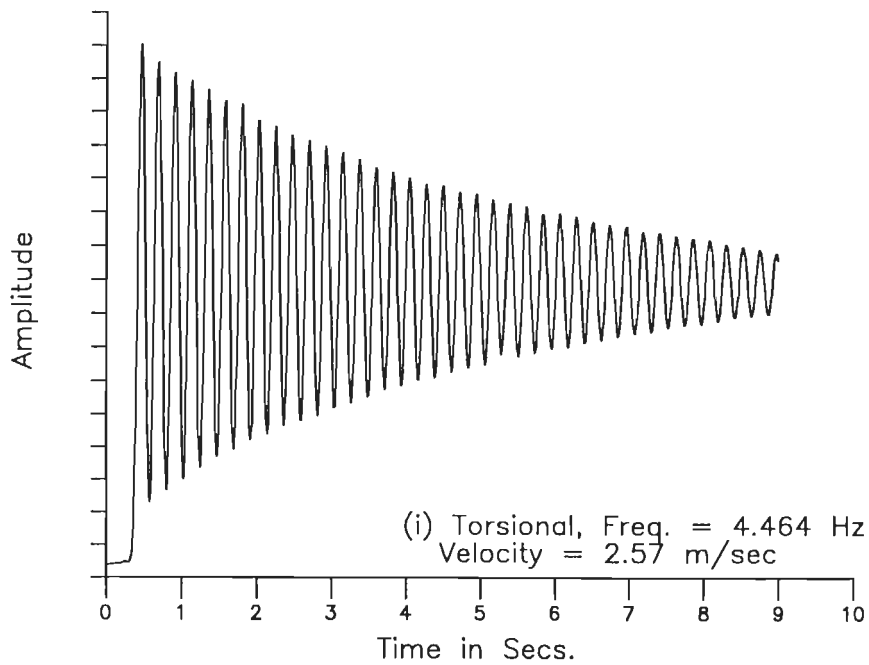
Fig. 6.3(c) Time history record of partially faired section model in torsional
mode of vibration under grid generated flow (Gird # 2).

(i) Torsional, Freq. = 4.464 Hz
Velocity = 2.57 m/sec

(ii) Torsional Freq. = 4.267 Hz
Velocity = 9.57 m/sec
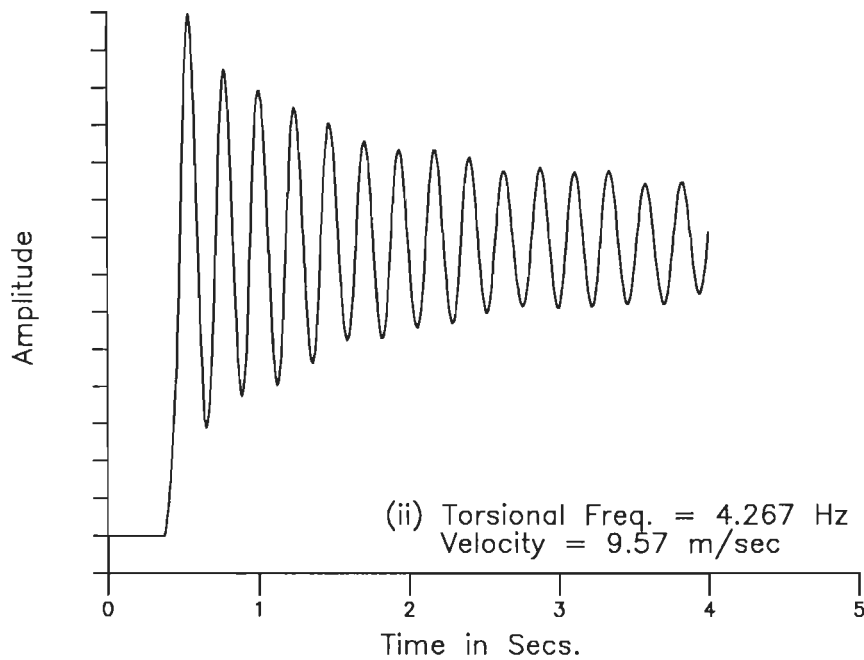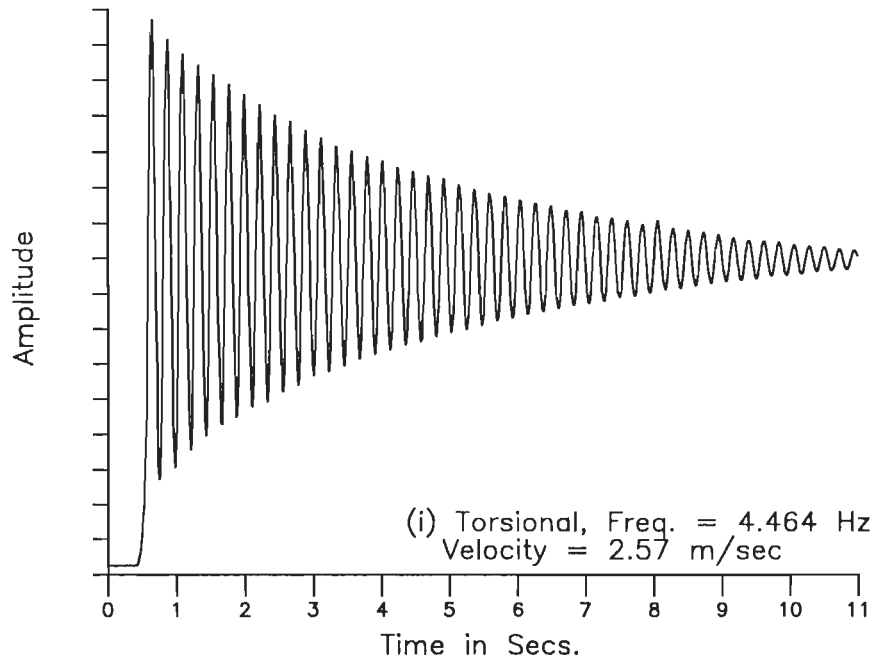
Fig. 6.3(d) Time history record of partially faired section model in torsional mode of vibration under grid generated flow (Grid # 3).
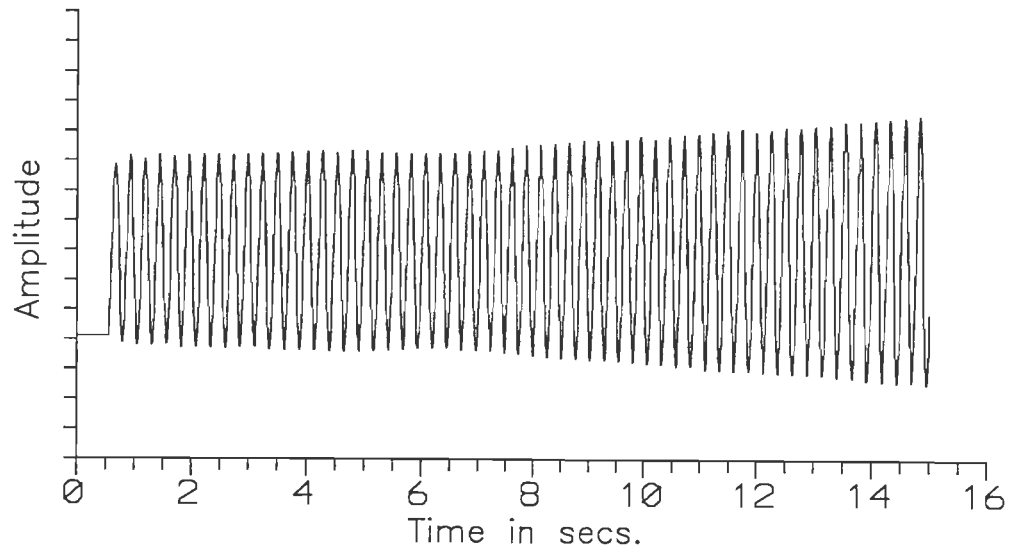
Fig. 6.4   Time   history   record showing the phenomenon of
           flutter occurence (Unmodified deck section model,
           mean velocity = 12.6 m/sec, torsional mode
           under smooth flow condition)
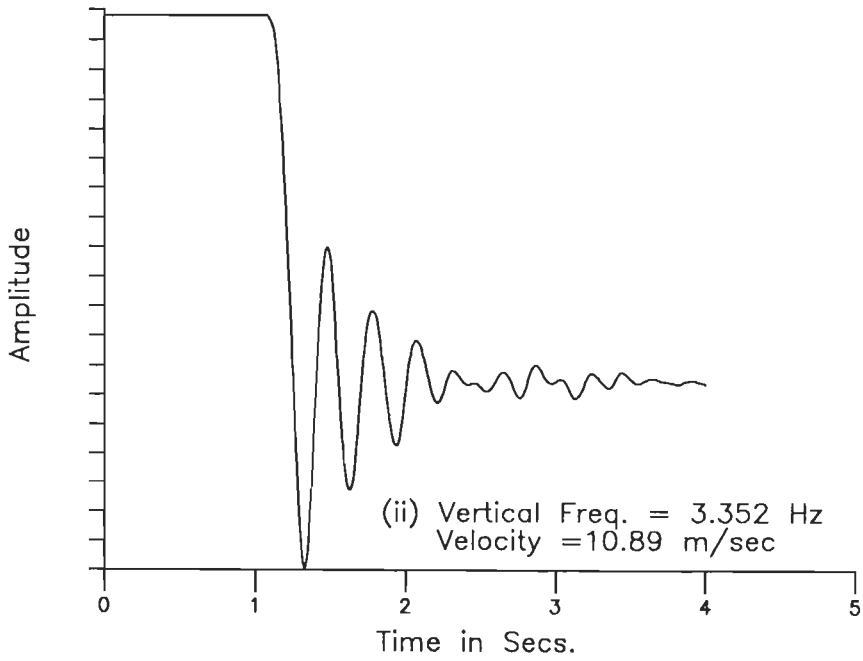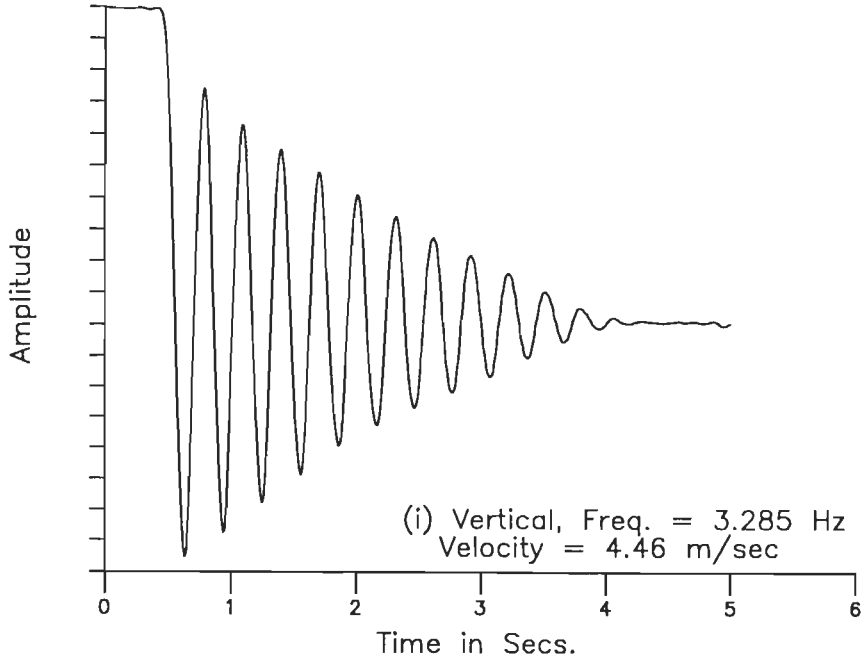
(i) Vertical, Freq. = 3.285 Hz
Velocity = 4.46 m/sec

(ii) Vertical Freq. = 3.352 Hz
Velocity =10.89 m/sec

Fig. 6.5(a) Time history record of unmodified section model in vertical mode of vibration under smooth flow.

(i) Vertical, Freq. = 3.200 Hz
Velocity = 2.57 m/sec

(ii) Vertocal Freq. = 3.293 Hz
Velocity = 8.64 m/sec
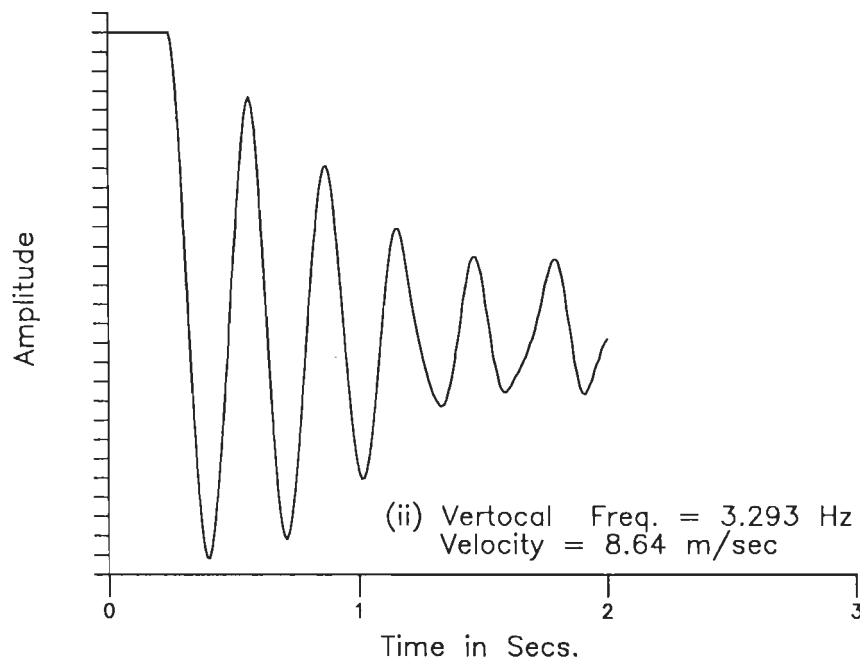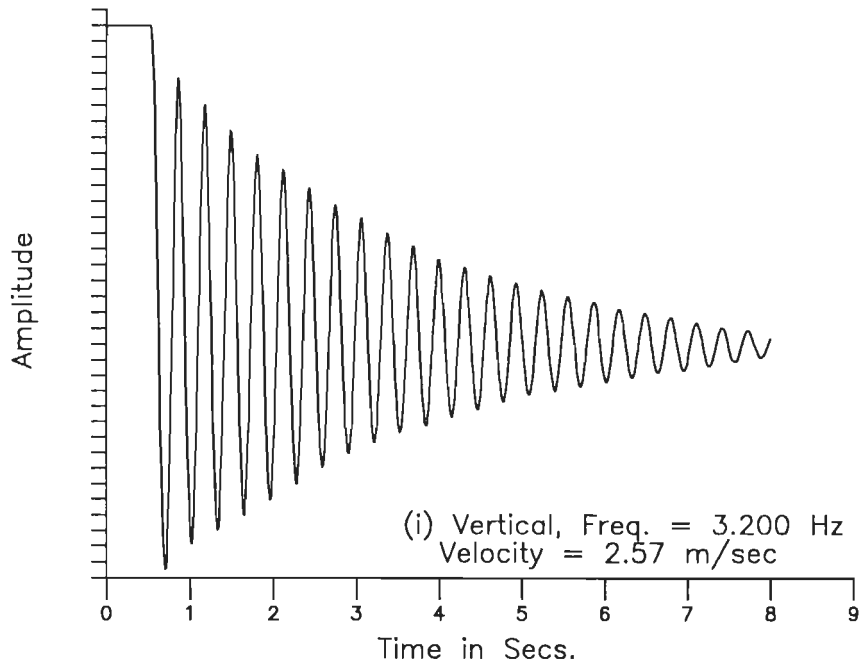
Fig. 6.5(b) Time history record of unmodified section model in vertical
mode of vibration under grid generated flow (Grid # 1).
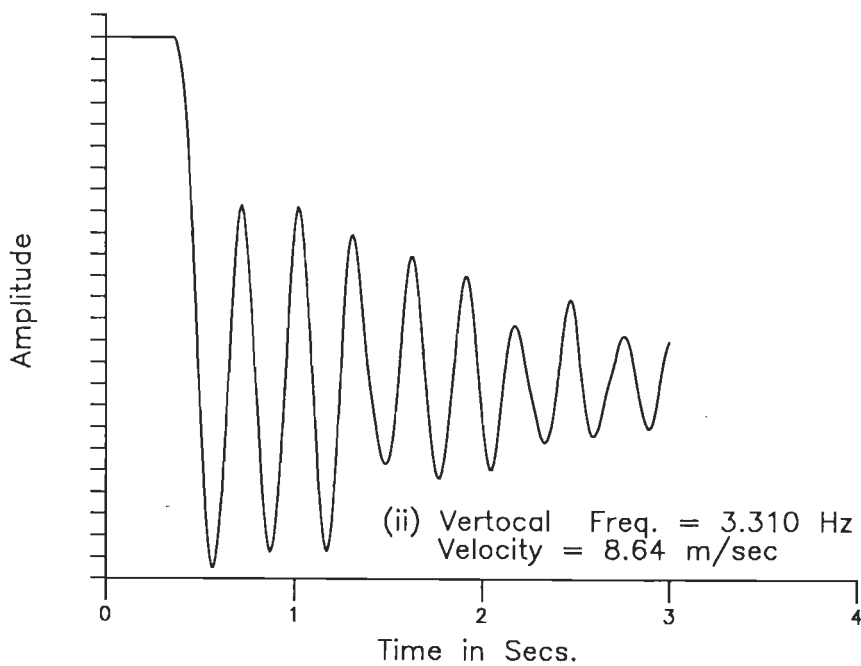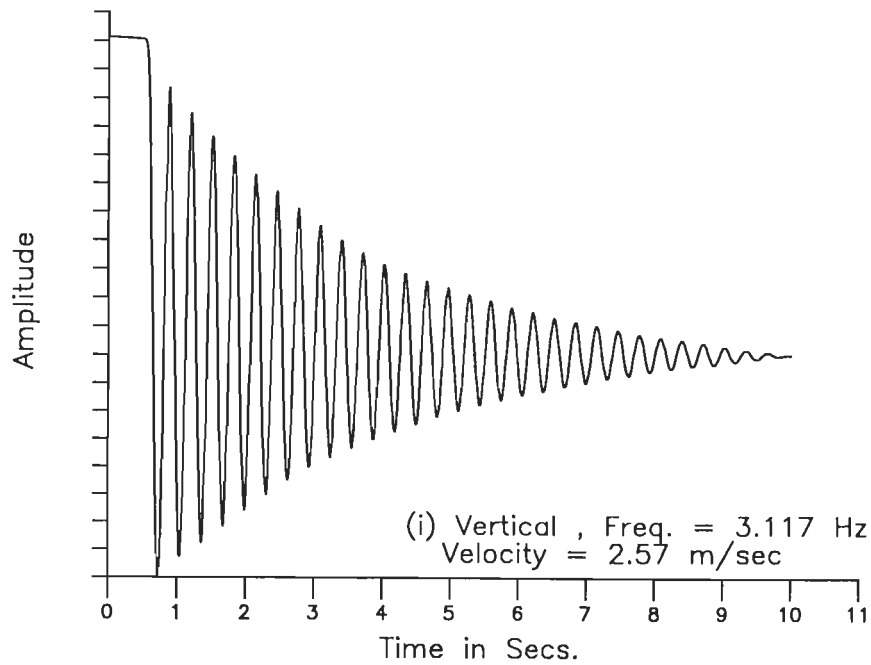
Fig. 6.5(c) Time history record of unmodified section model in torsional
mode of vibration under grid generated flow (Grid # 2).
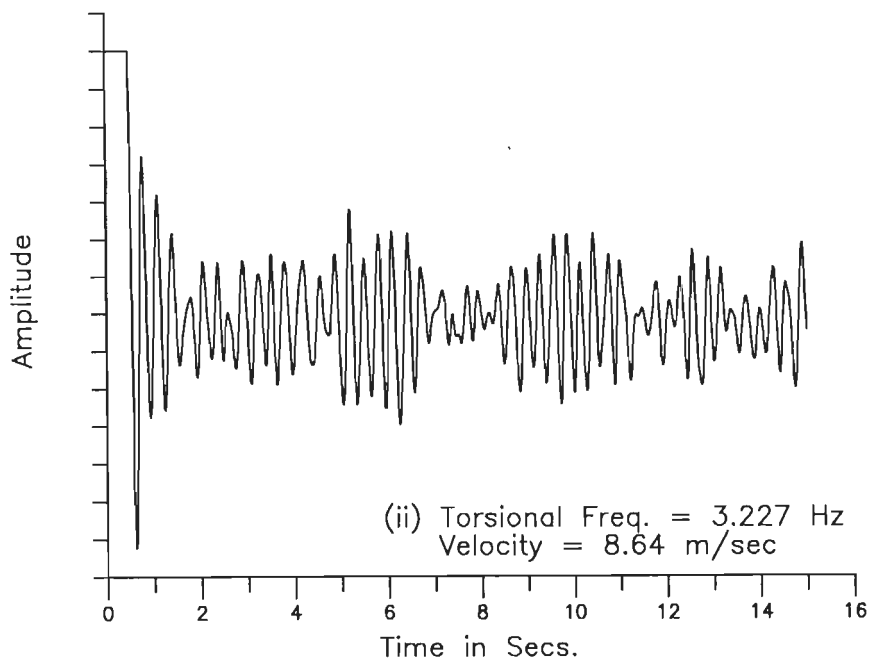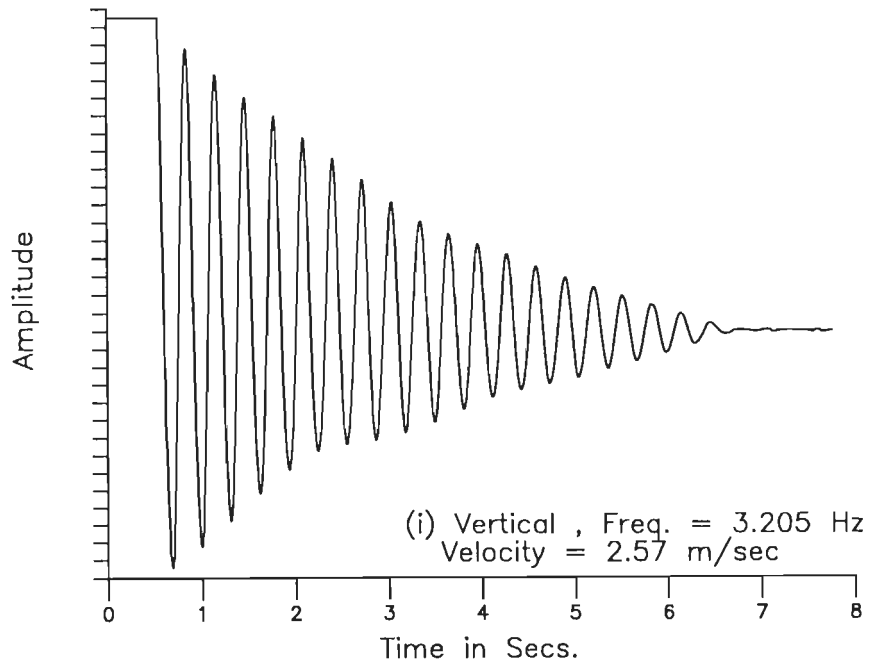
Fig. 6.5(d) Time history record of unmodified section model in vertical mode of vibration under grid generated flow (Grid # 3).

Fig. 6.6(a) Time history record of faired section model in
vertical mode of vibration under smooth flow.

(i) Vertical , Freq. = 3.087 Hz
Velocity = 2.57 m/sec

Time in Secs.

(ii) Vertical ,Freq. = 3.142 Hz
Velocity = 8.64 m/sec

Time in Secs.
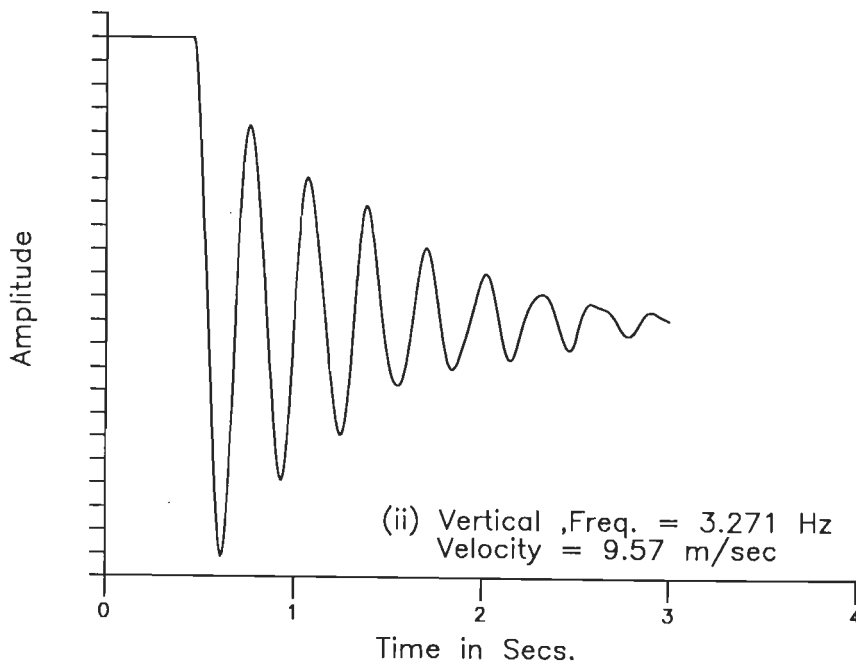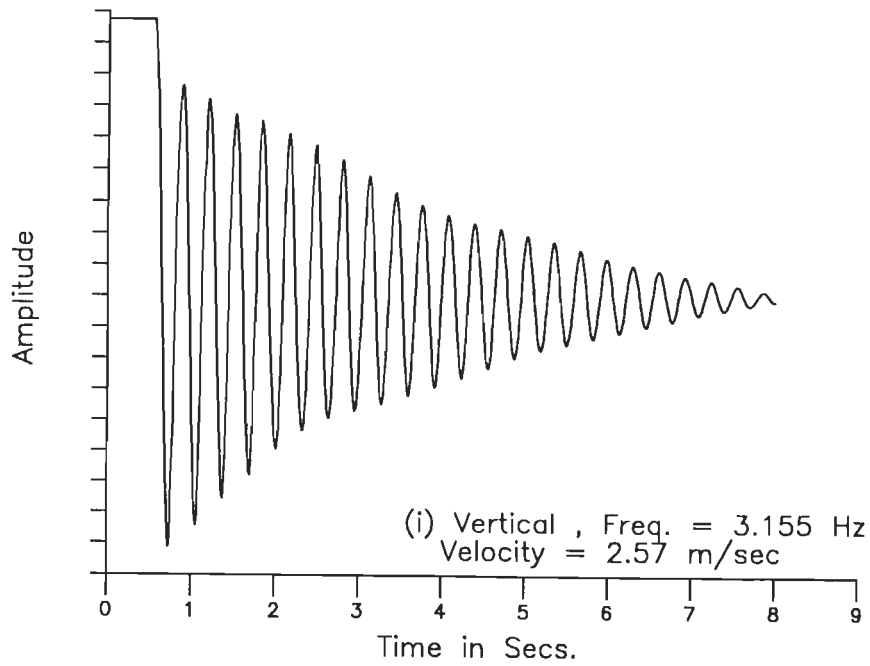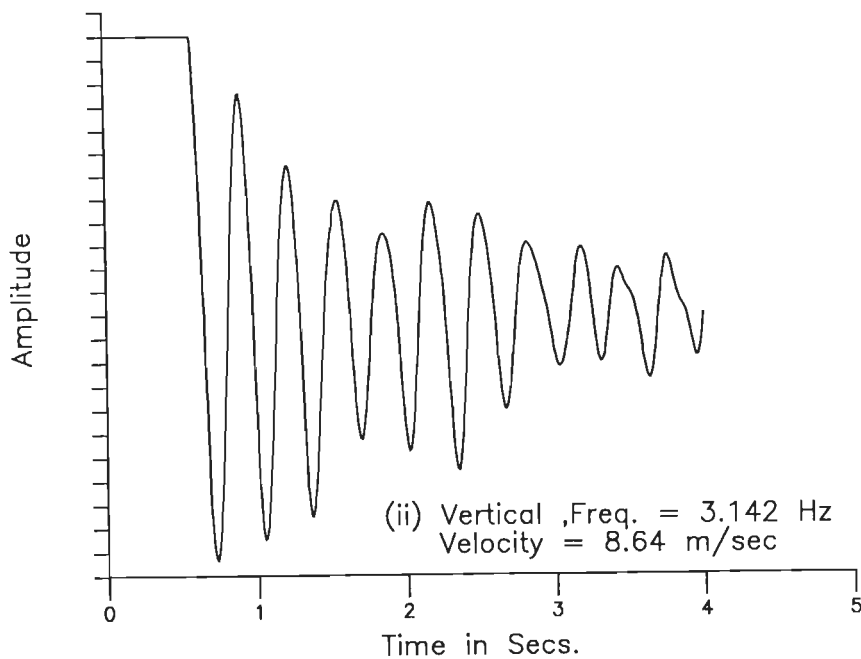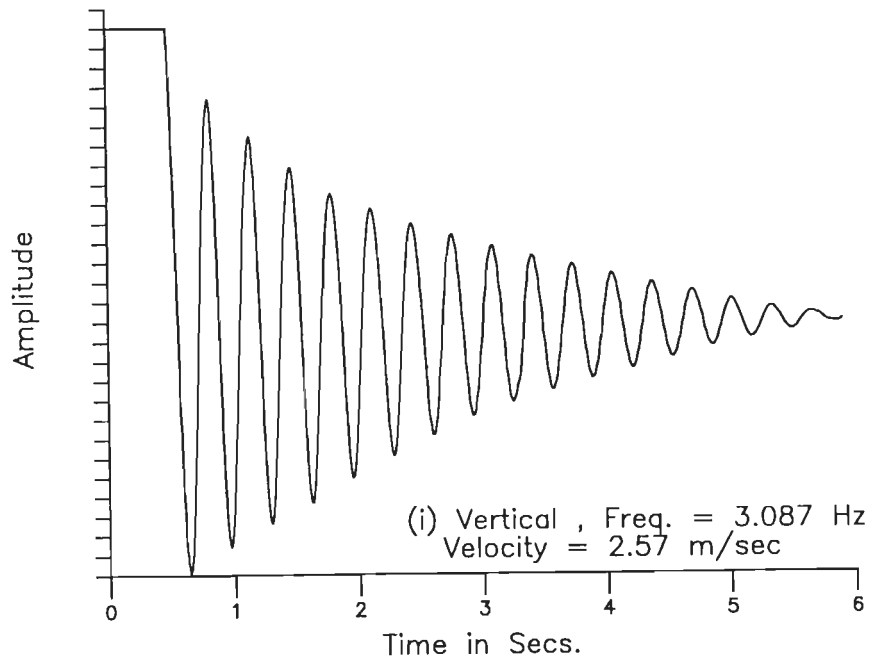
Fig. 6.6(b) Time history record of faired section model in vertical
mode of vibration under grid generated flow (Grid #1).

Fig. 6.6(c) Time history record of faired section model in vertical
mode of vibration under grid generated flow (Grid # 2).

(i) Vertical, Freq. = 3.082 Hz
Velocity = 2.57 m/sec

Amplitude

Time in Secs.

(ii) Vertical, Freq. = 3.209 Hz
Velocity = 8.64 m/sec

Amplitude

Time in Secs.
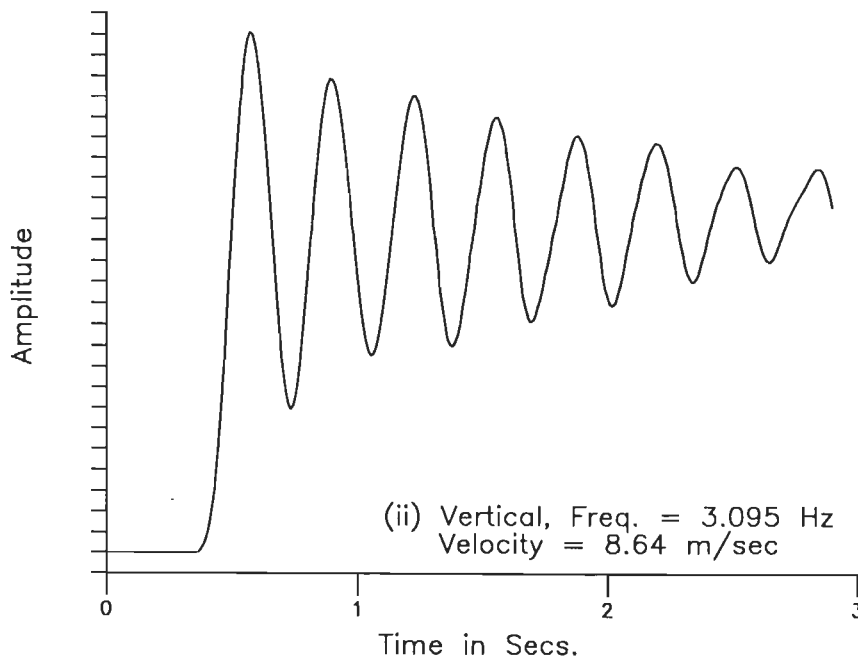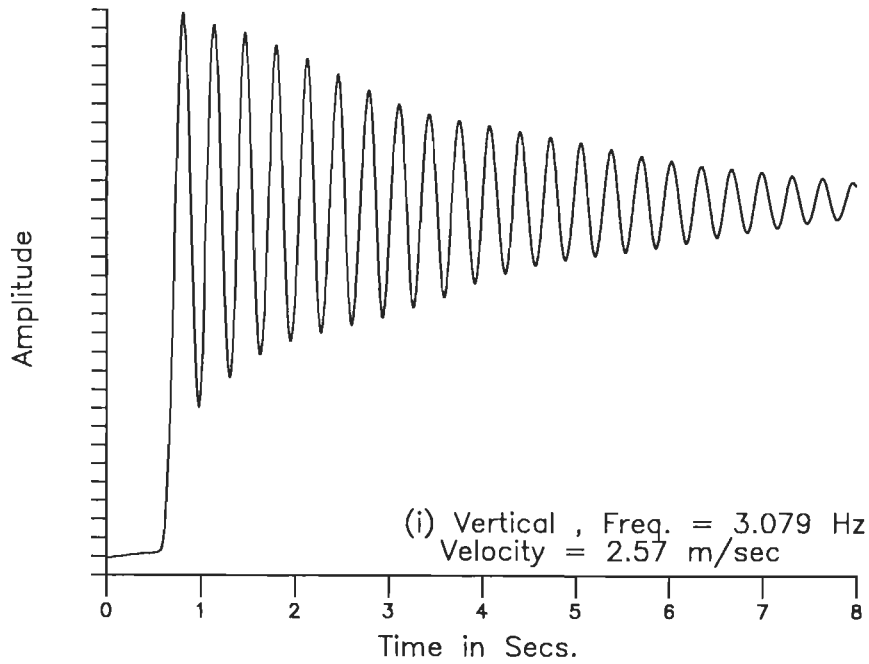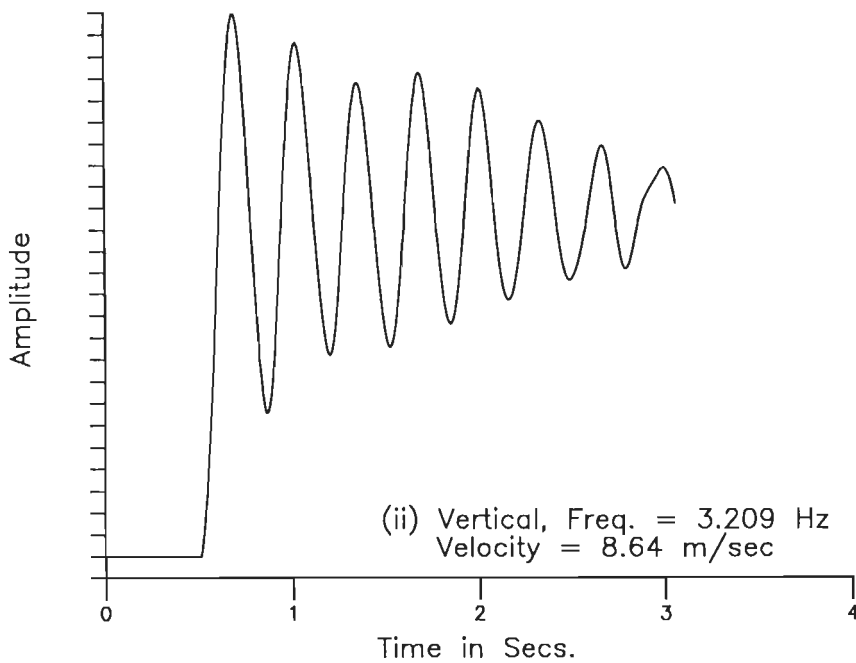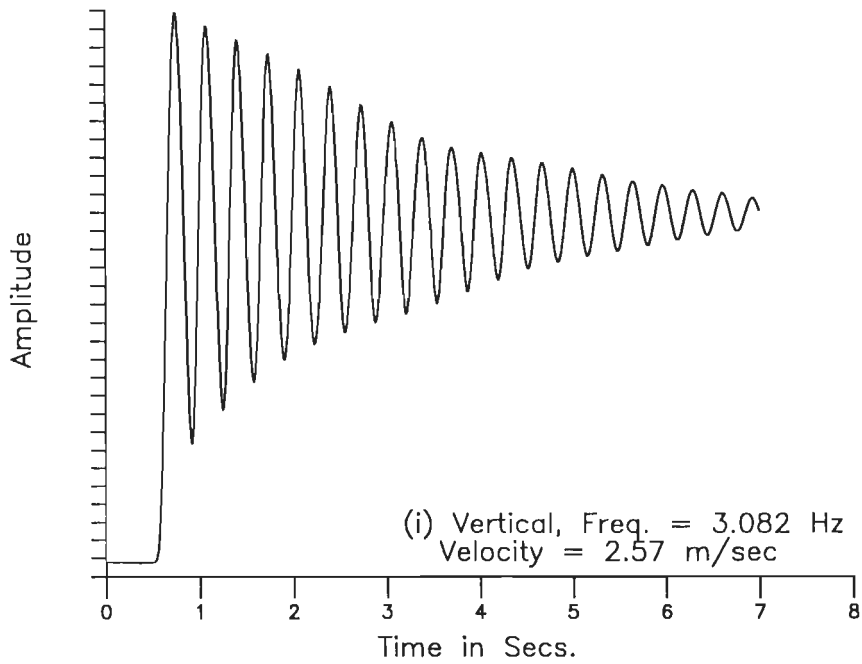
Fig. 6.6(d) Time history record of faired section model in vertical
mode of vibration under grid generated flow (Grid # 3).

Fig. 6.7(a) Time history record of partially faired section model in vertical mode of vibration under smooth flow.

(i) Vertical , Freq. = 3.129 Hz
Velocity = 2.57 m/sec

Time in Secs.

(ii) Vertical, Freq. = 3.167 Hz
Velocity = 8.64 m/sec

Time in Secs.
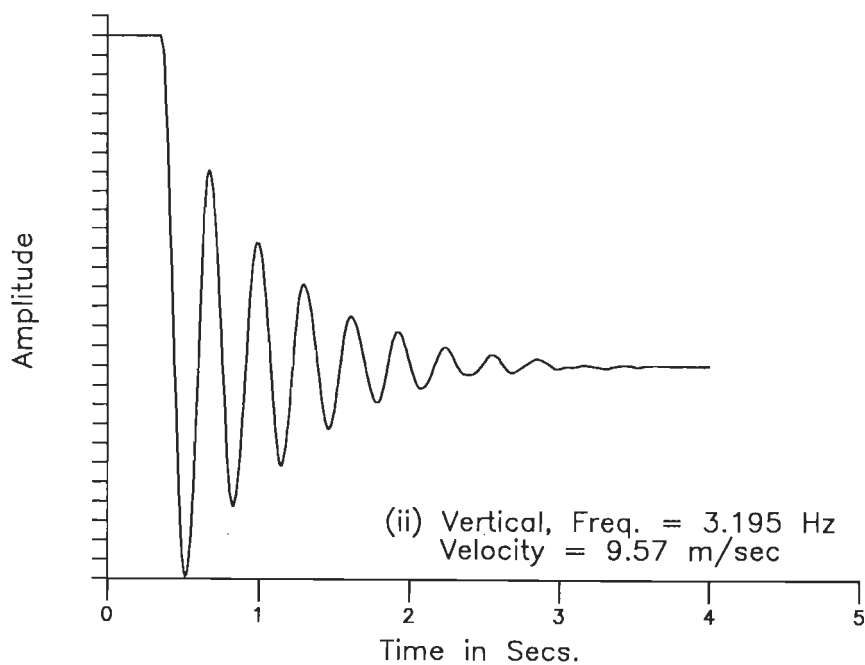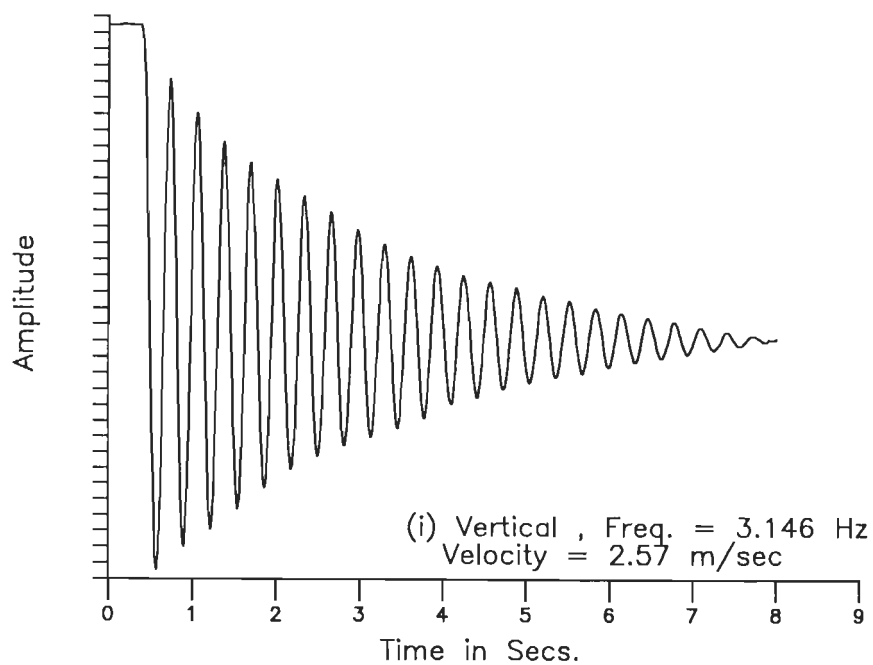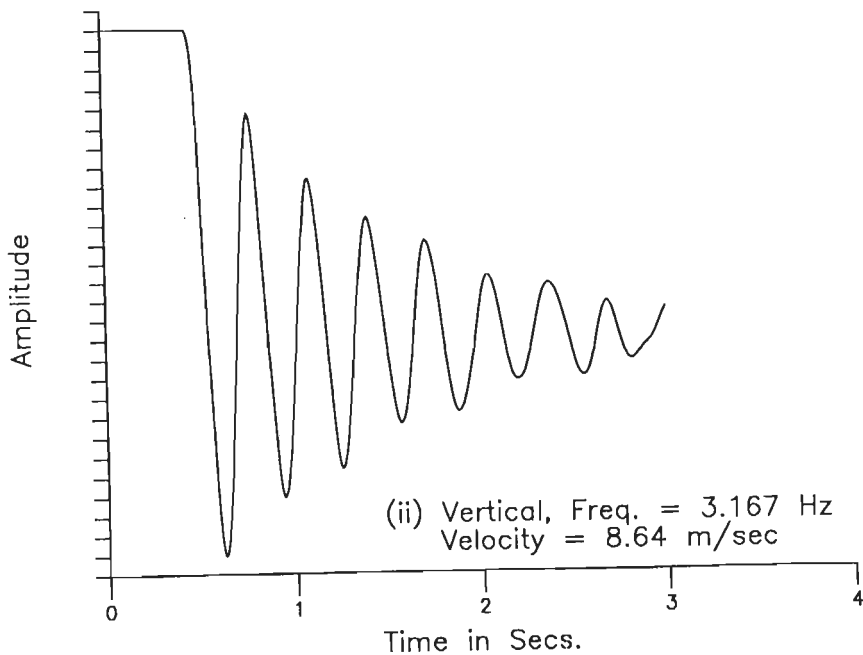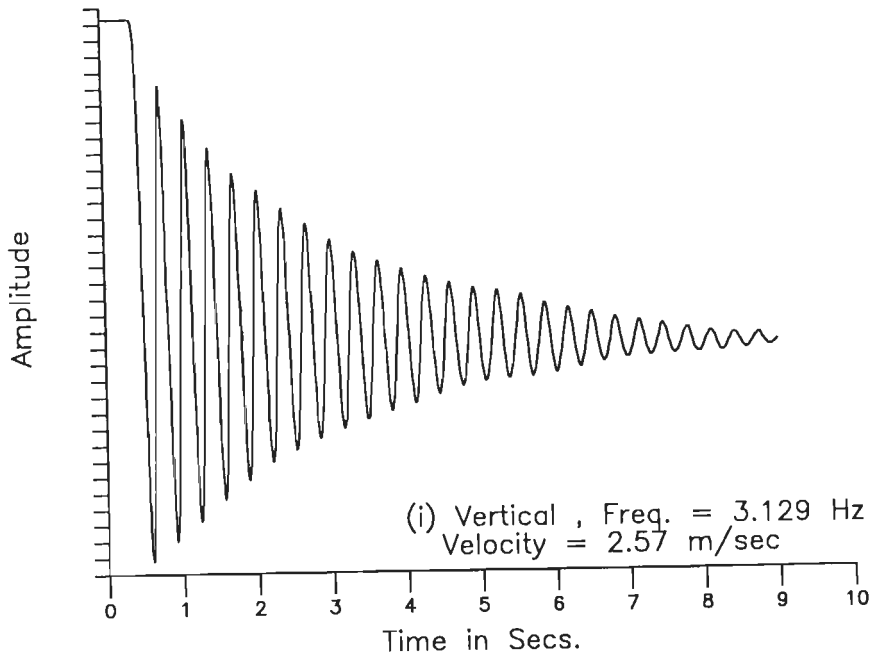
Fig. 6.7(b) Time history record of partially faired section model in vertical
mode of vibration under grid generated flow (Grid # 1)

Fig. 6.7(c) Time history record of partially faired section model in vertical
mode of vibration under grid generated flow (Grid # 2).

(i) Vertical , Freq. = 3.162 Hz
Velocity = 2.57 m/sec

Time in Secs.

(ii) Vertical, Freq. = 3.145 Hz
Velocity = 8.64 m/sec

Time in Secs.
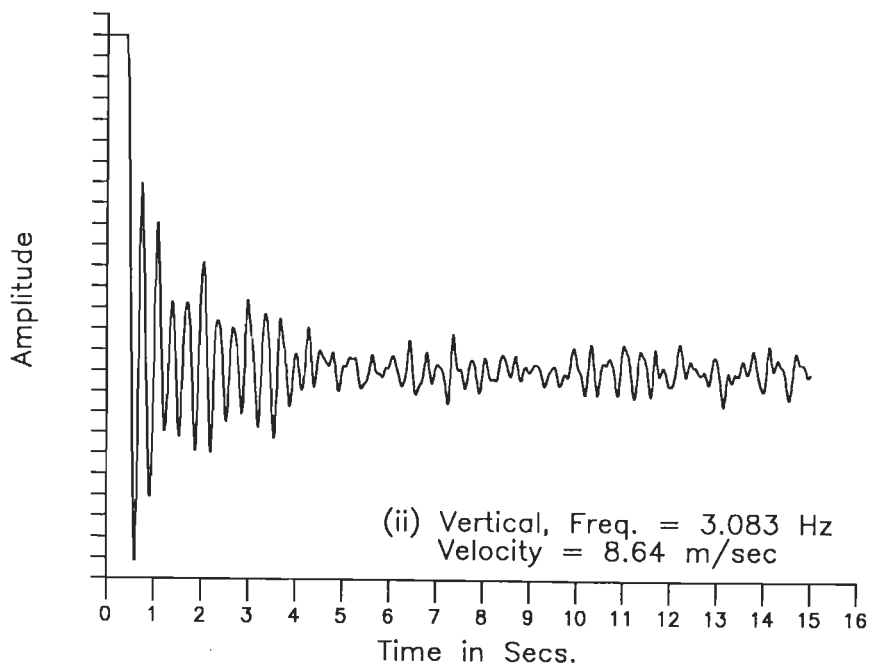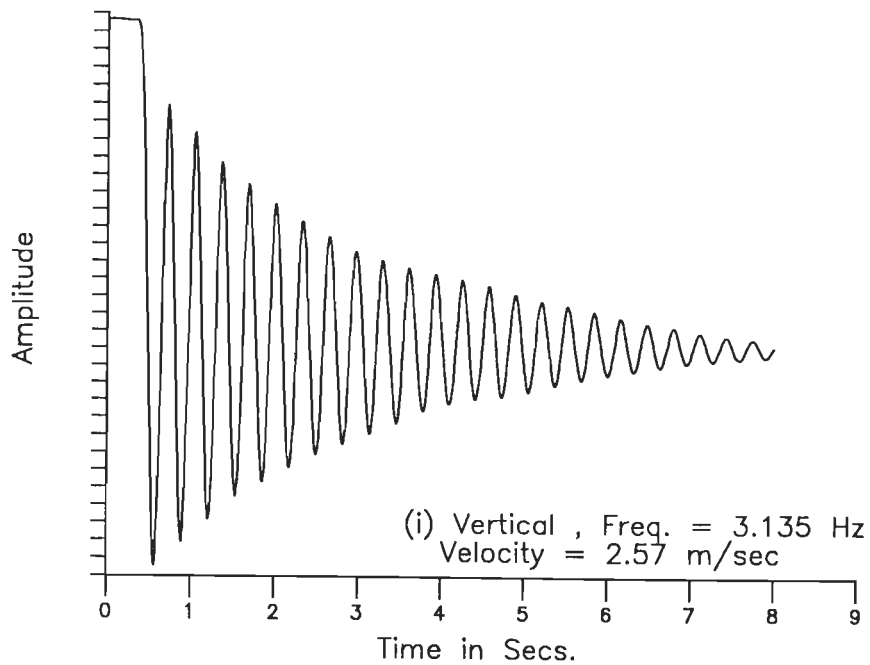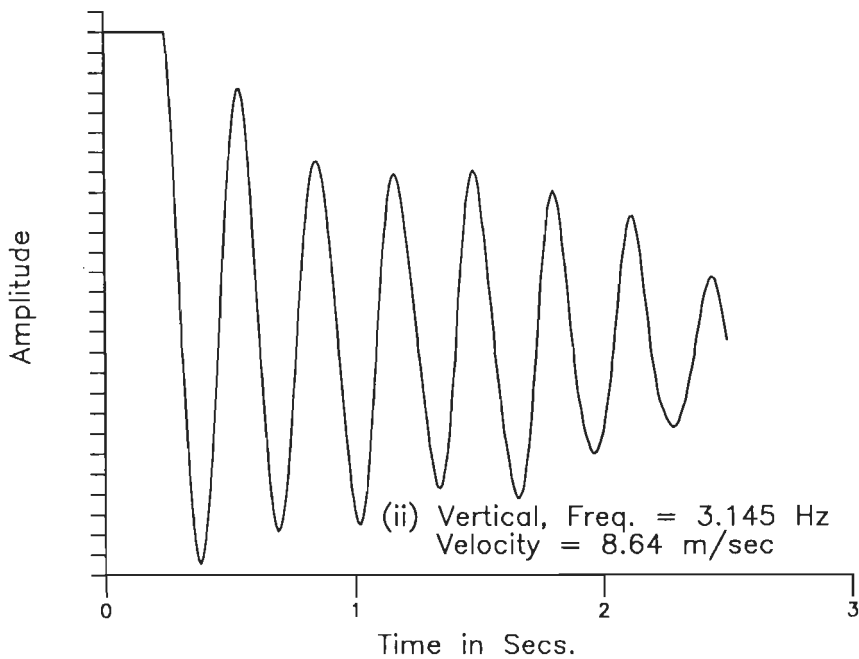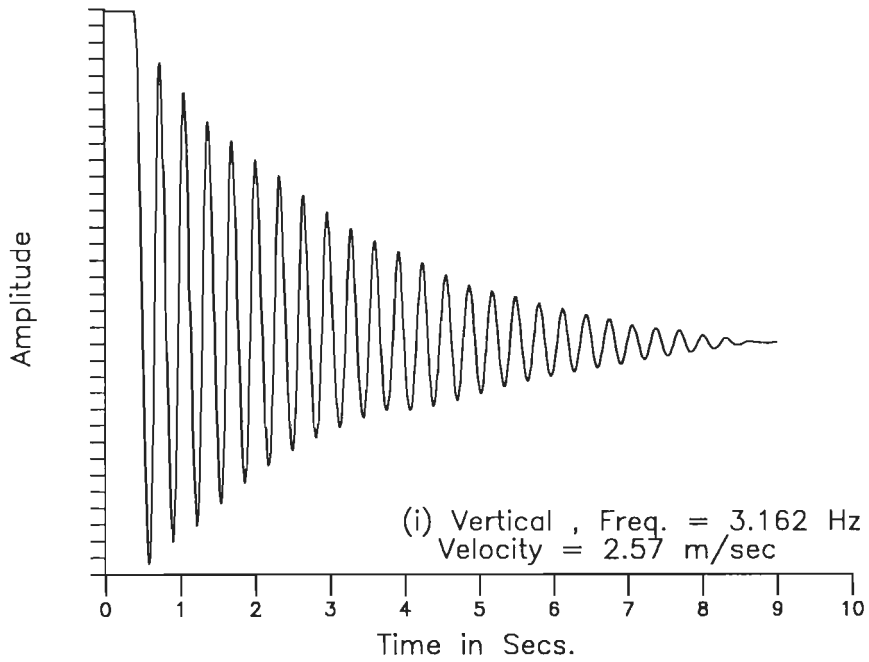
Fig. 6.7(d) Time history record of partially faired section model in vertical
mode of vibration under grid generated flows (Grid # 3).
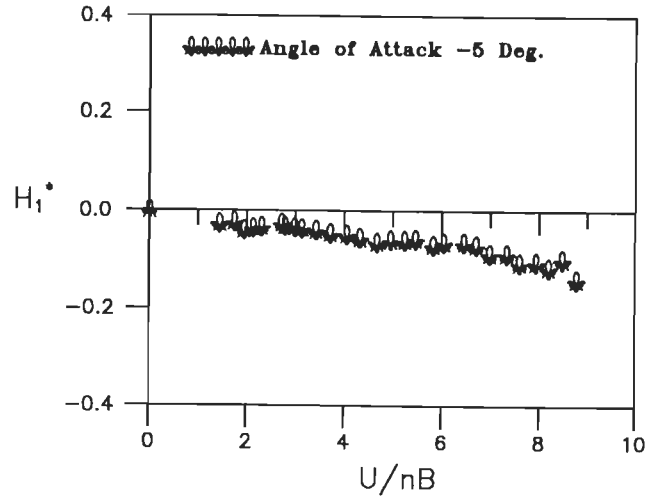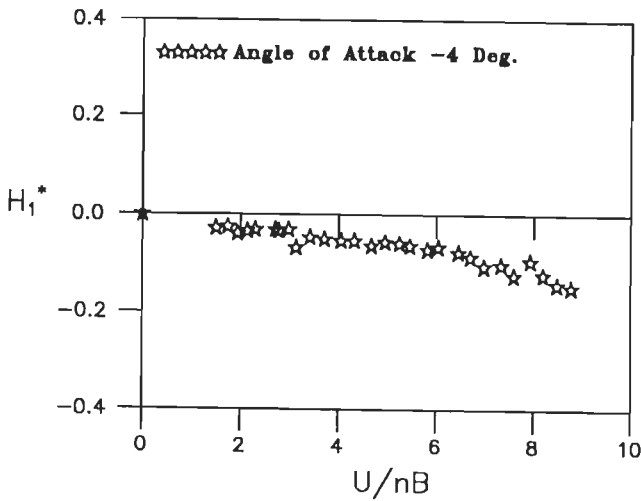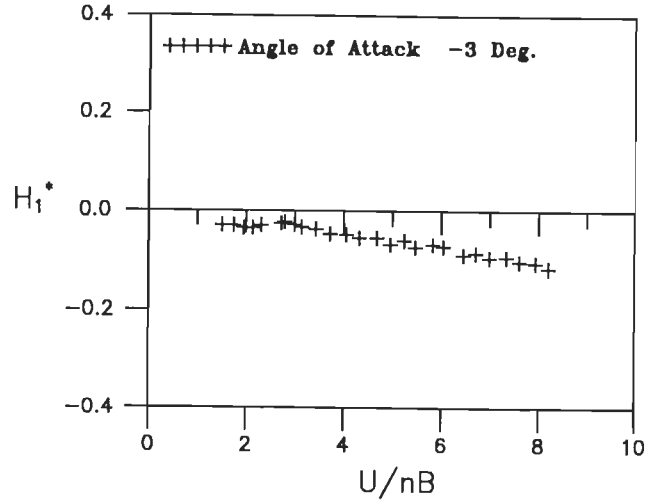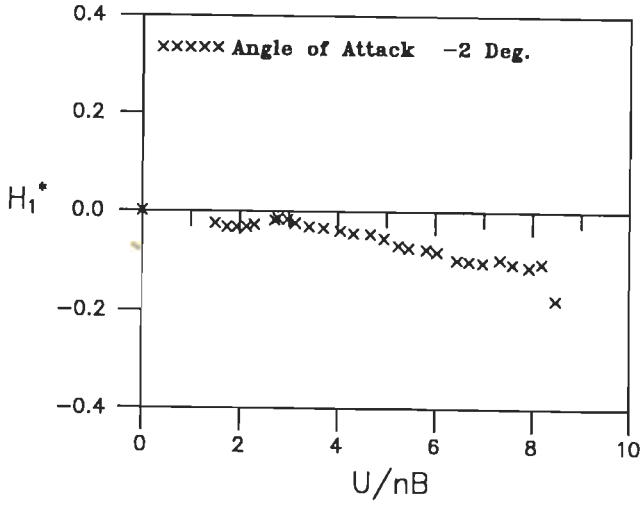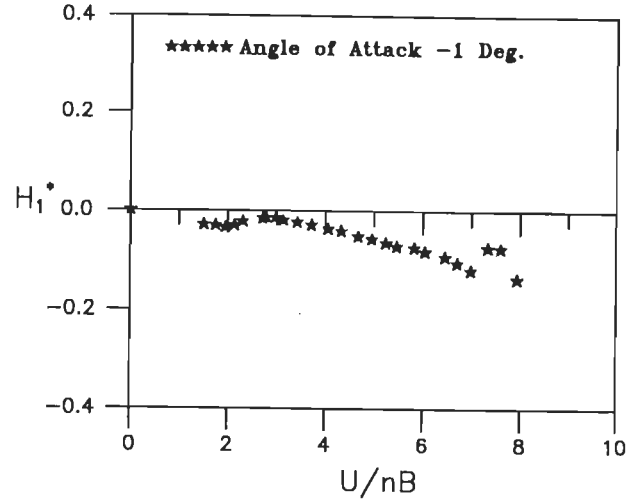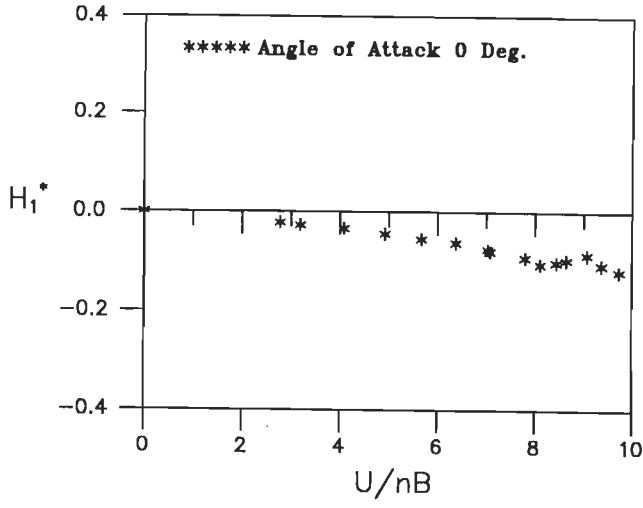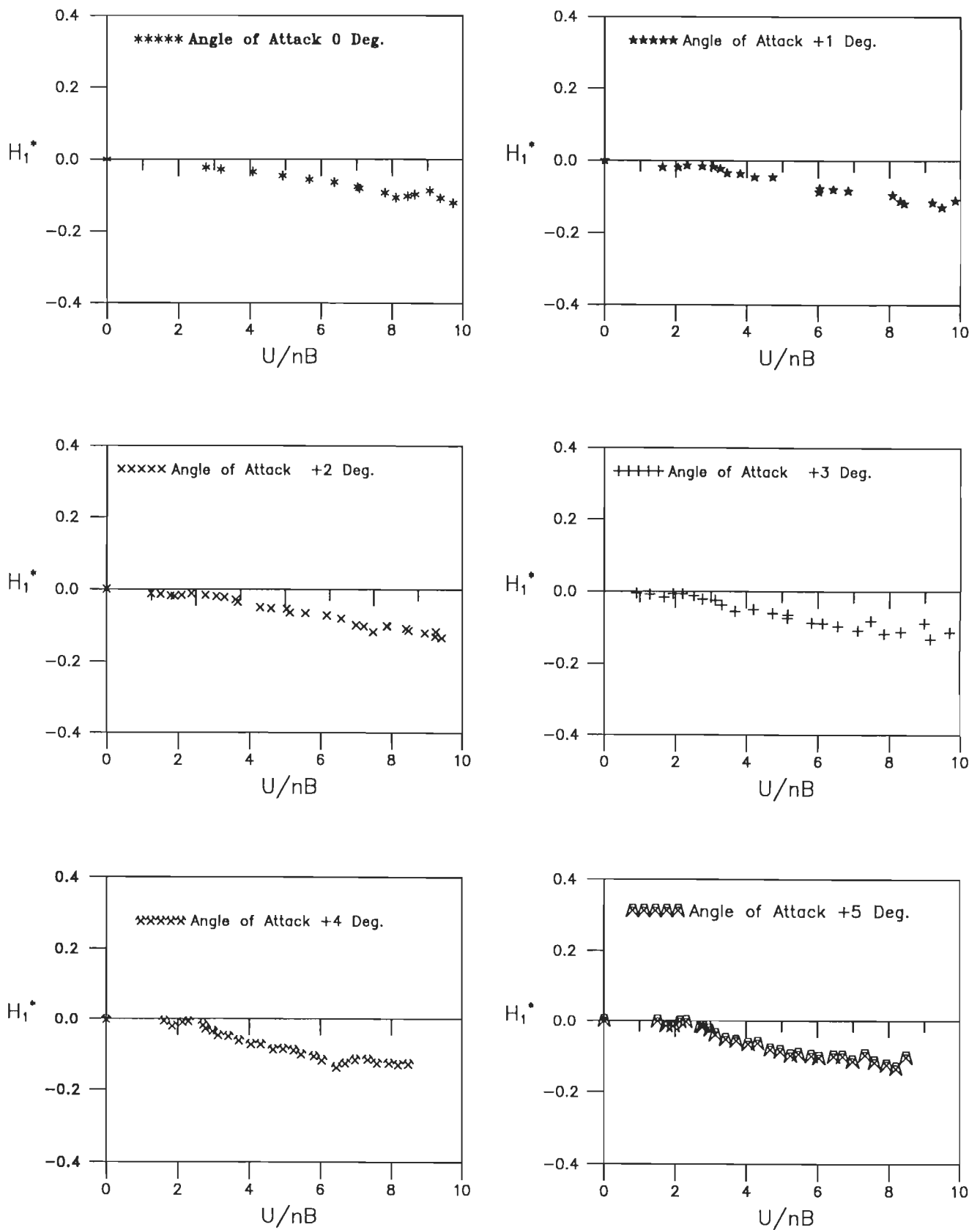
Fig.6.8(a)   Variation of flutter derivative(H_1^*) with wind incidence
           angles for unmodified   section model under smooth flow.
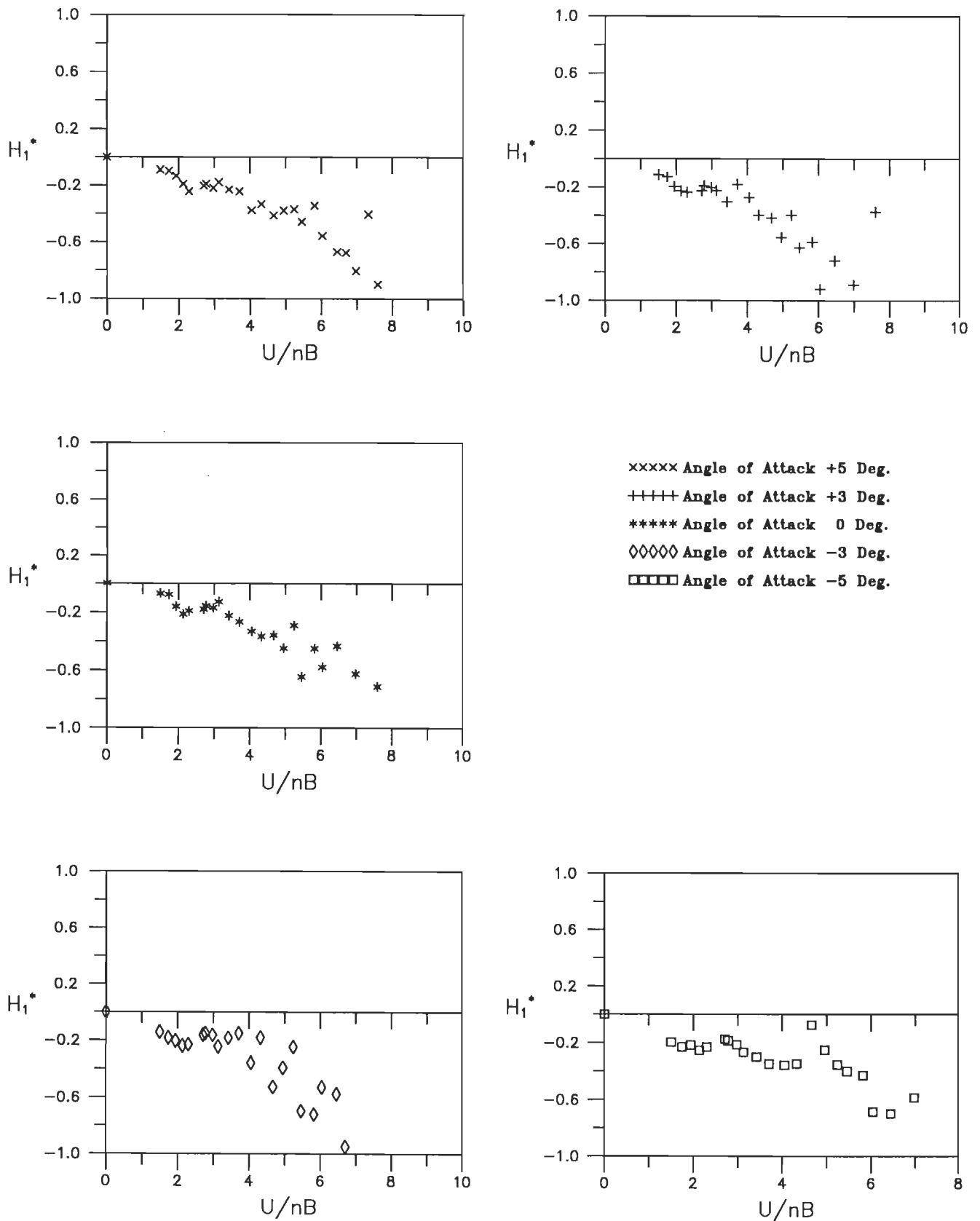
Fig. 6.8(b) Variation of flutter derivative (H₁*) with wind incidence angles
for unmodified section model under grid generated flow(Grid # 1).
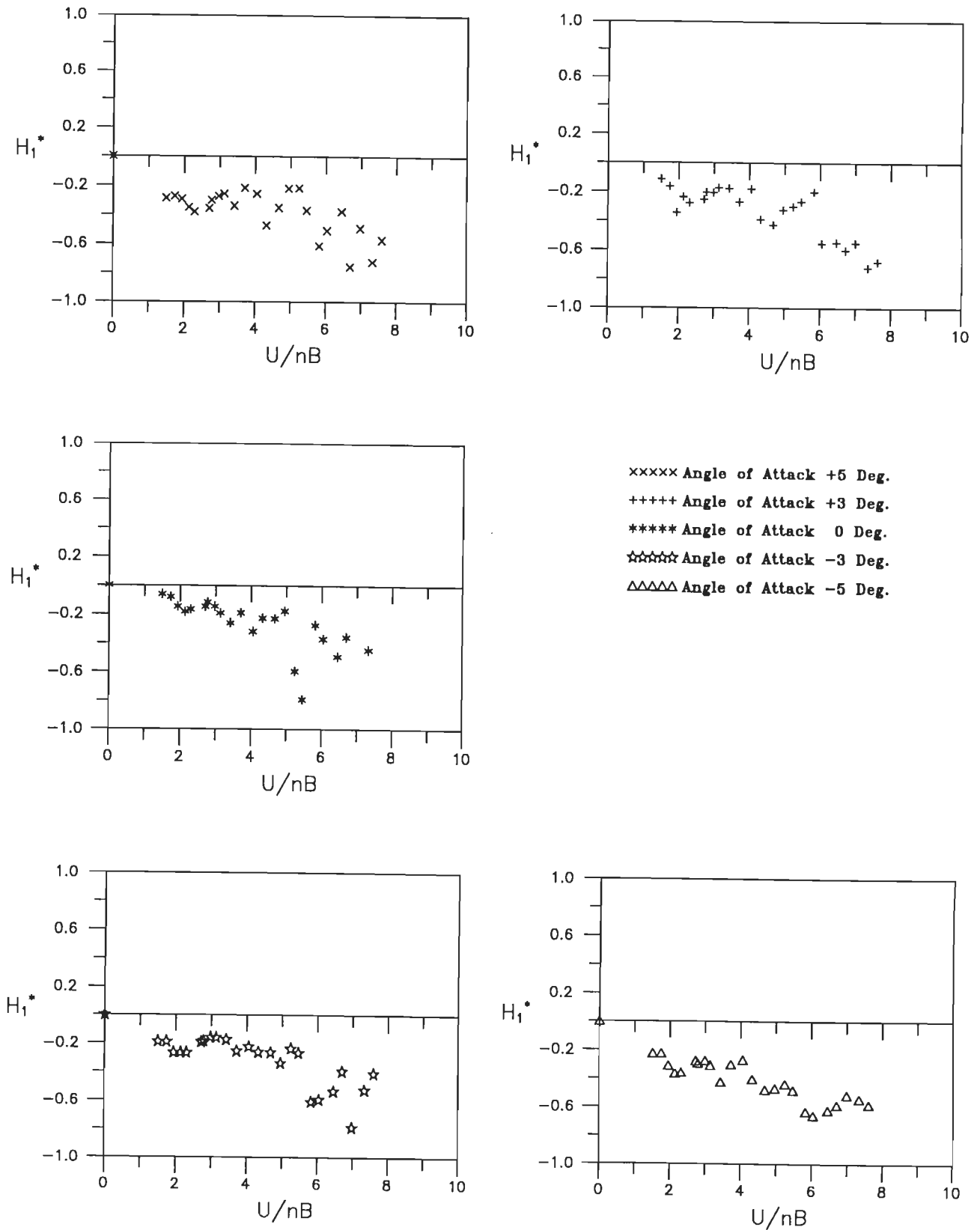
Fig. 6.8(c) Variation of flutter derivative (H_1^*) with wind incidence angles for unmodified section model under grid generated flow (Grid # 2).
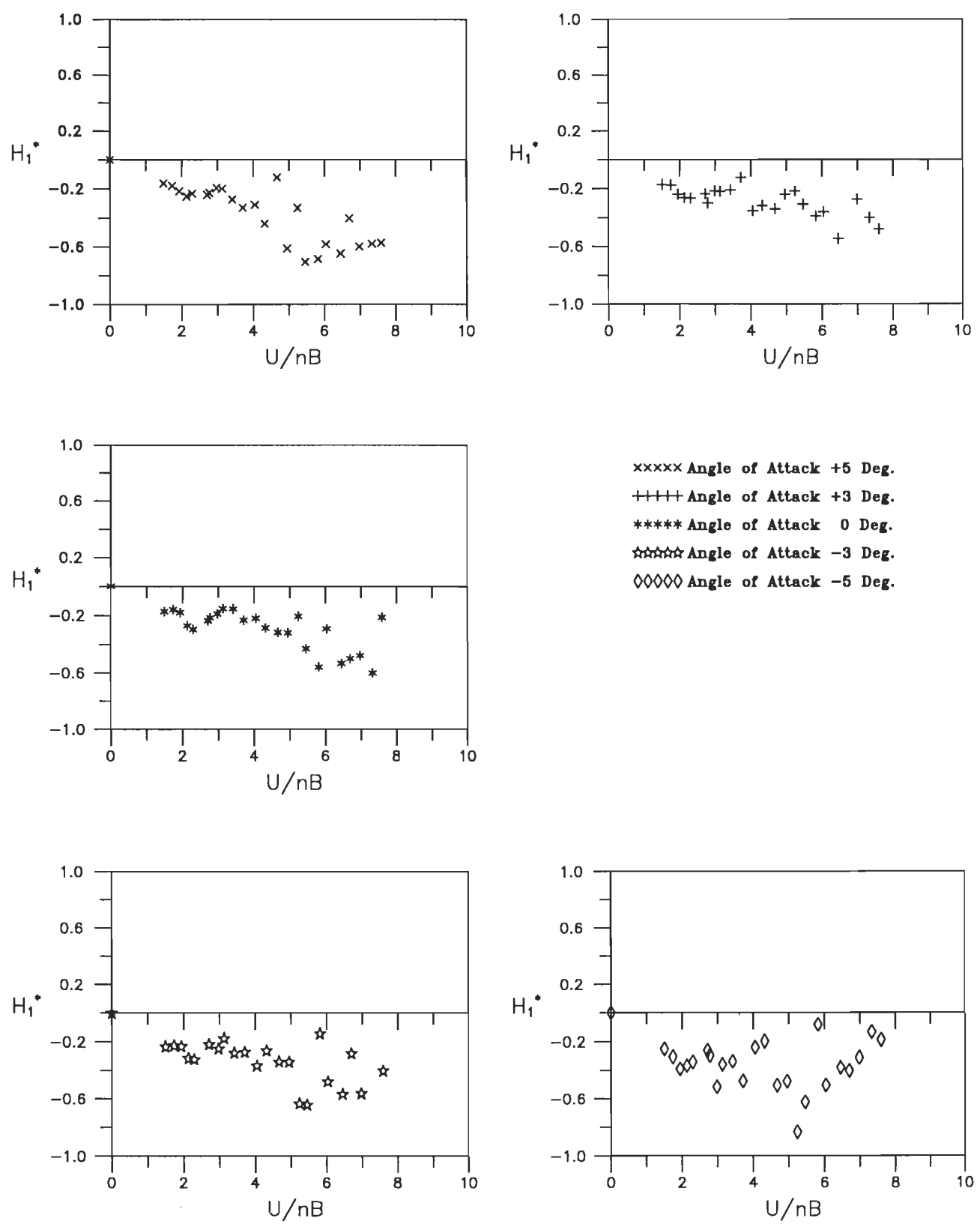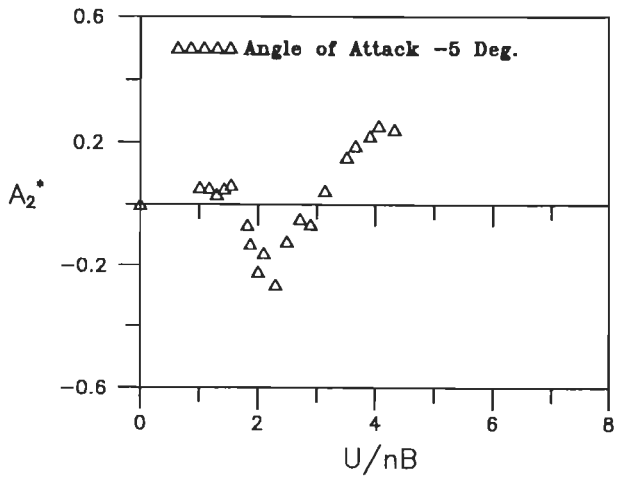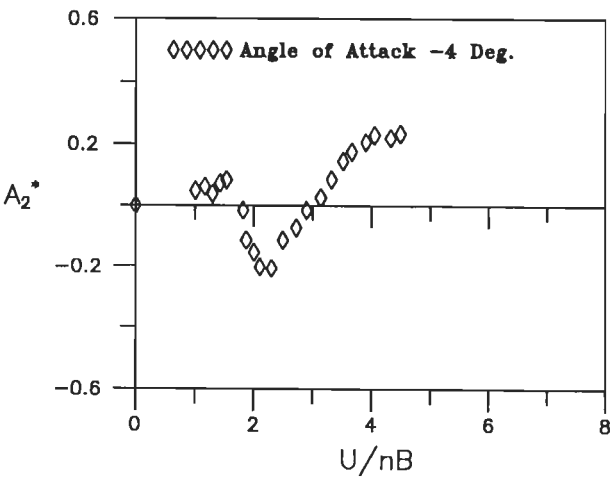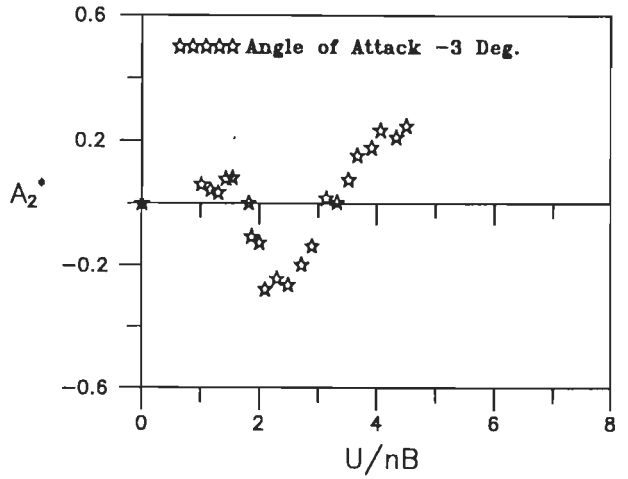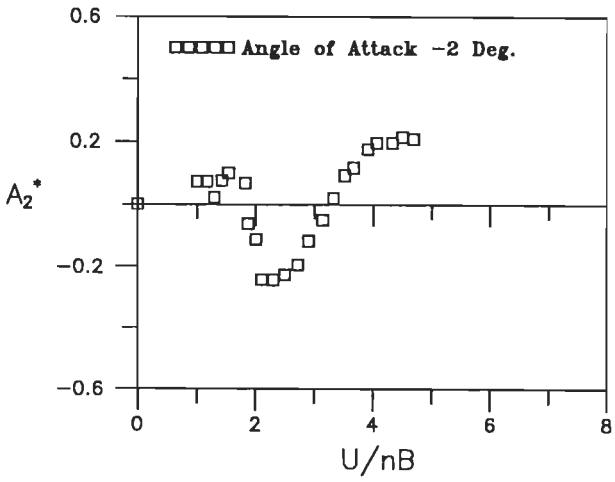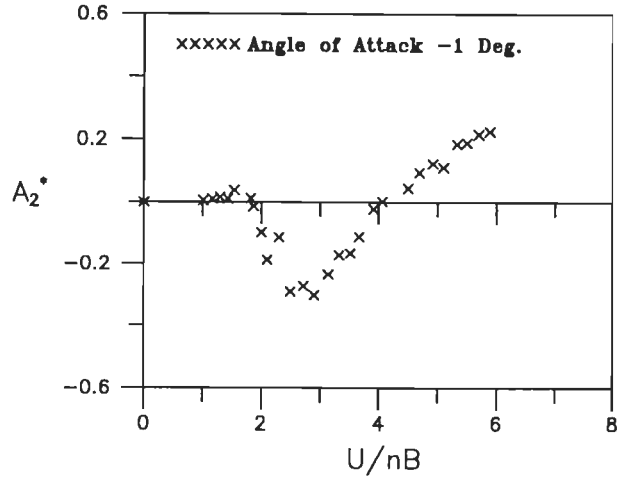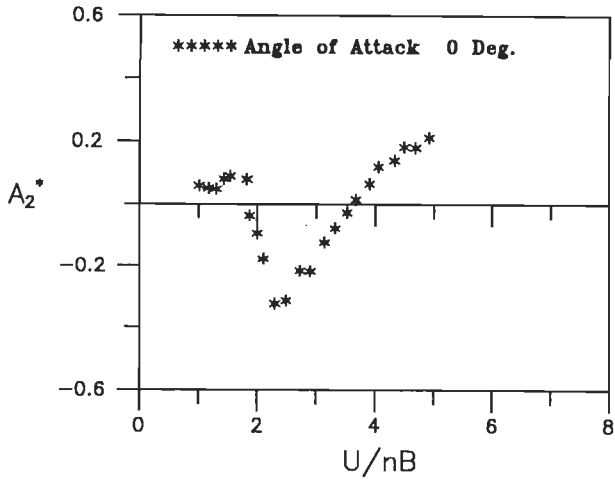
Fig.6.8(d) Variation of flutter derivative (H_1^*) with wind incidence angles for unmodified section model under grid generated flow (Grid # 3).
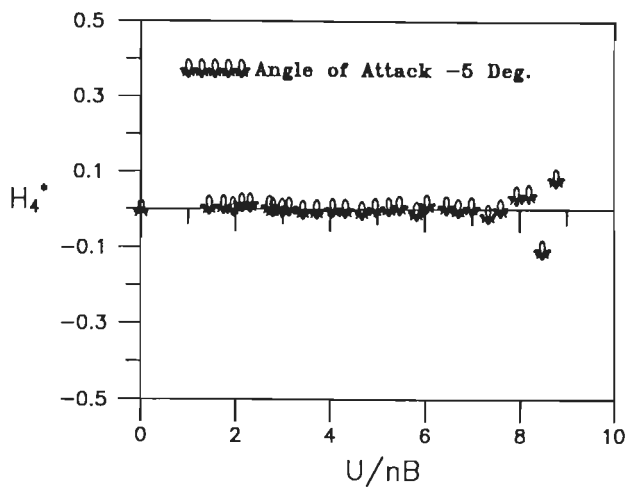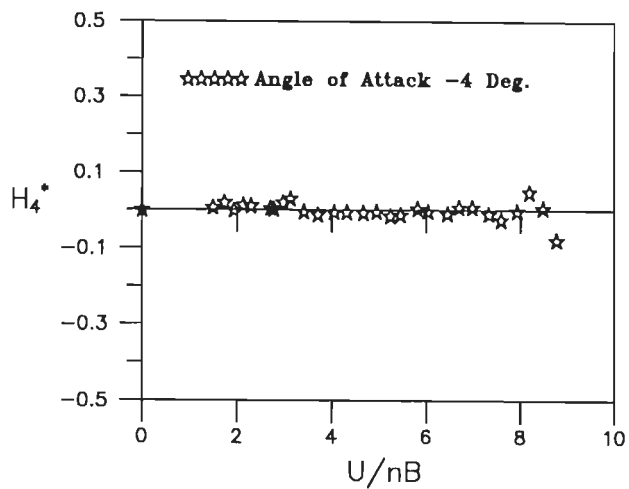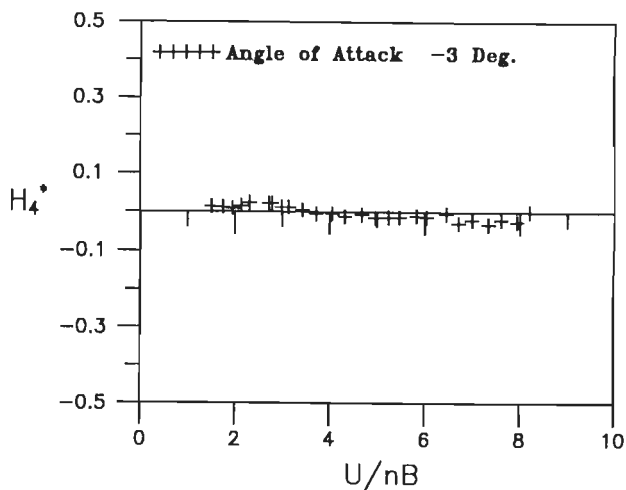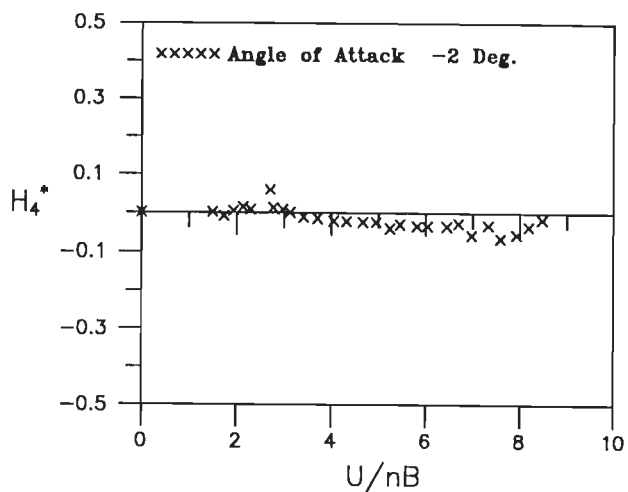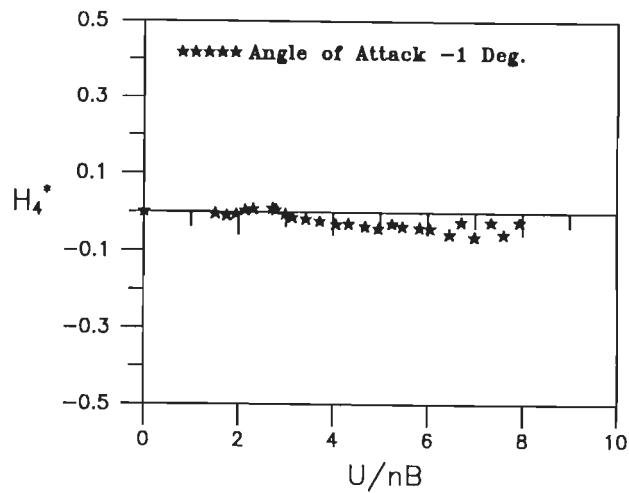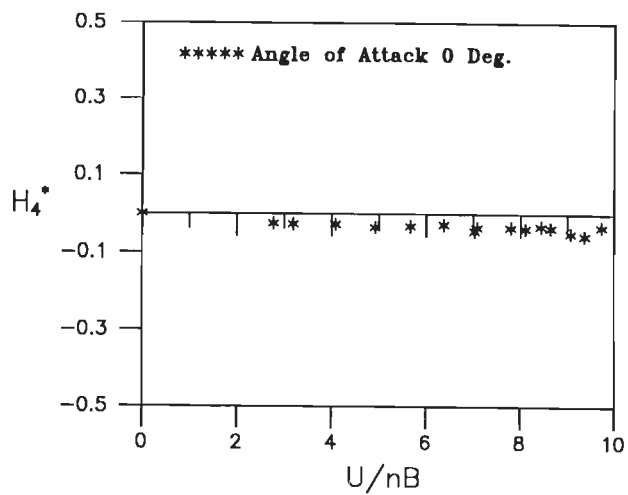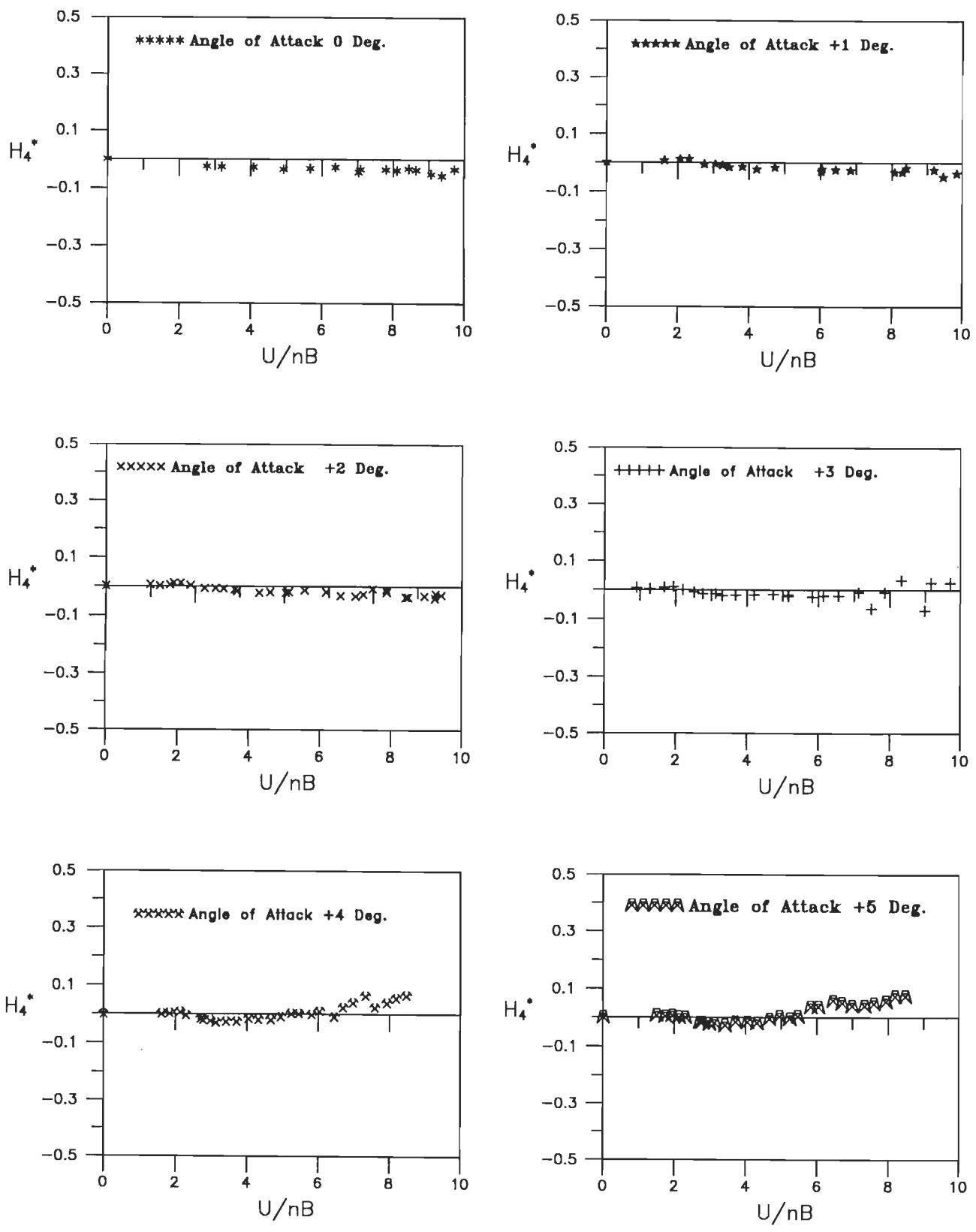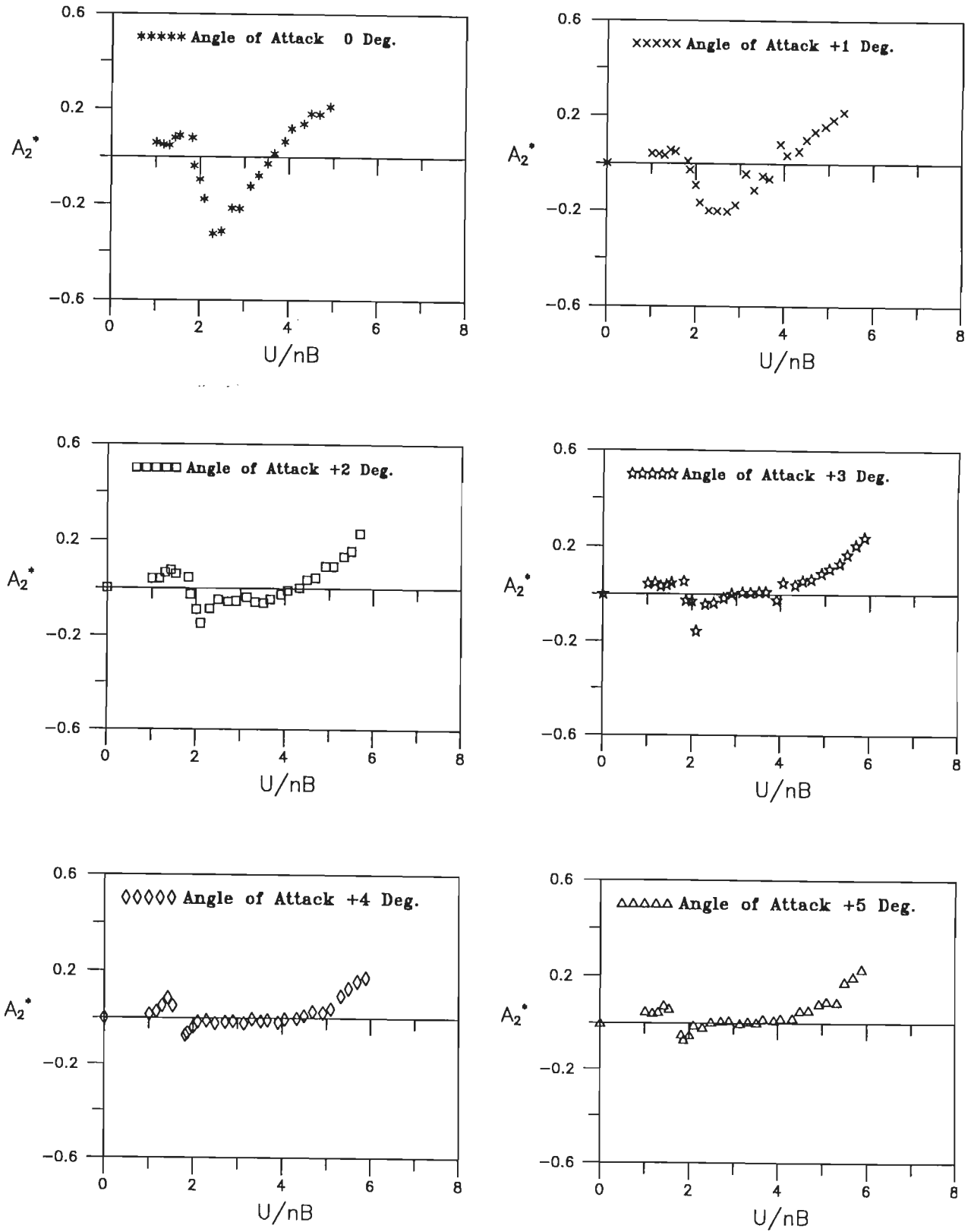
Fig.6.9(a) Variation of flutter derivative (H_4^*) with wind incidence angles for unmodified section model under smooth flow.
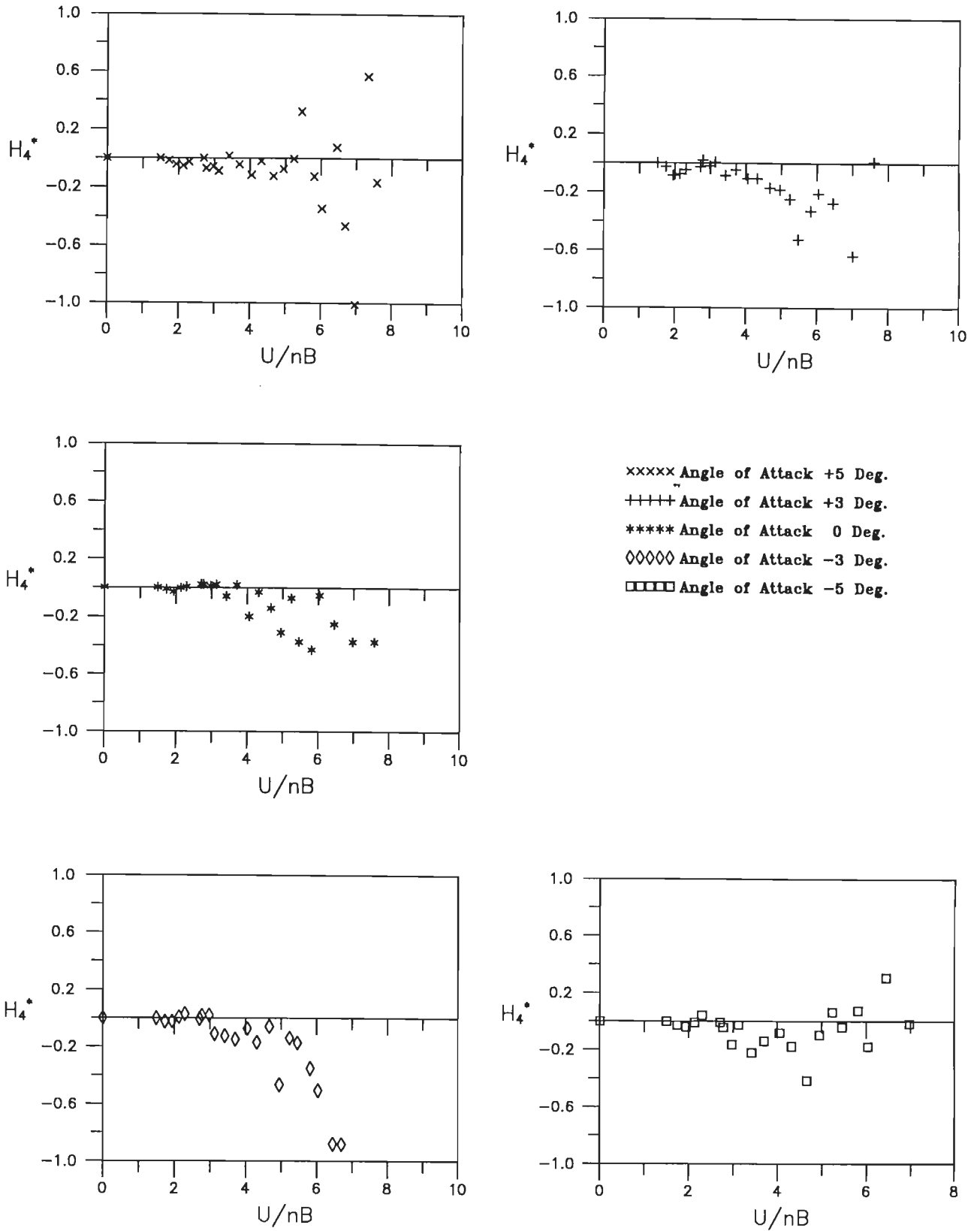
Fig. 6.9(b) Variation of flutter derivative (H_4^*) with wind incidence angles for unmodified section model under grid generated flow (Grid # 1)
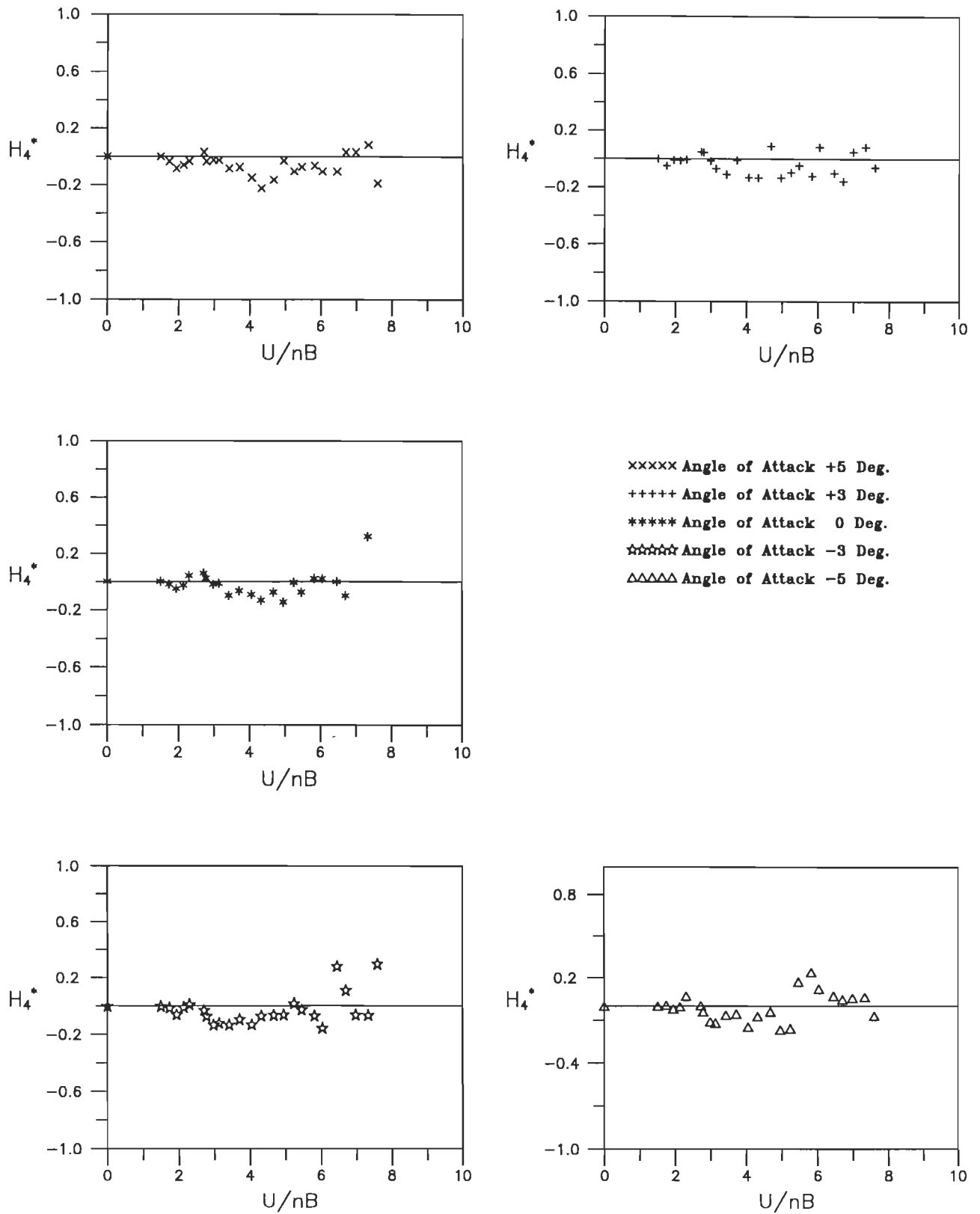
Fig. 6.9(c) Variation of flutter derivative (H_4^*) with wind incidence angles
for unmodified section model under grid generated flow (Grid # 2)
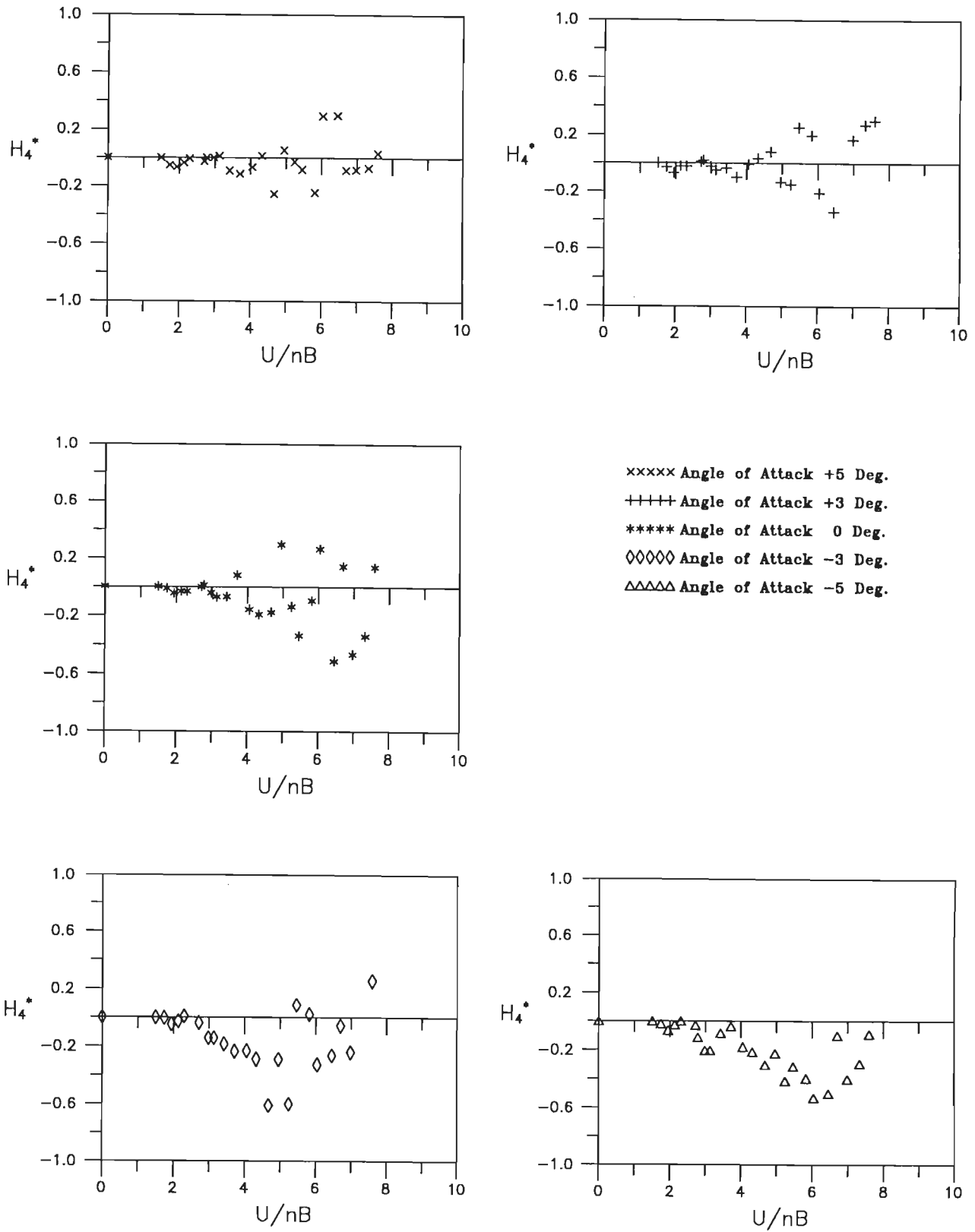
Fig. 6.9(d) Variation of flutter derivative (H_4^*) with wind incidence angles for unmodified section model under grid generated flow (Grid # 3)
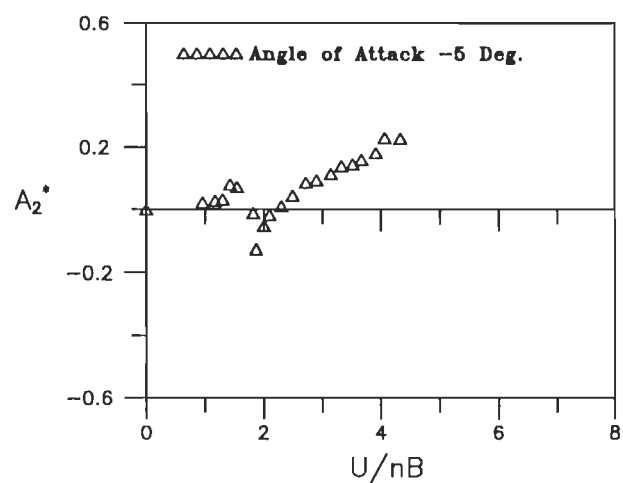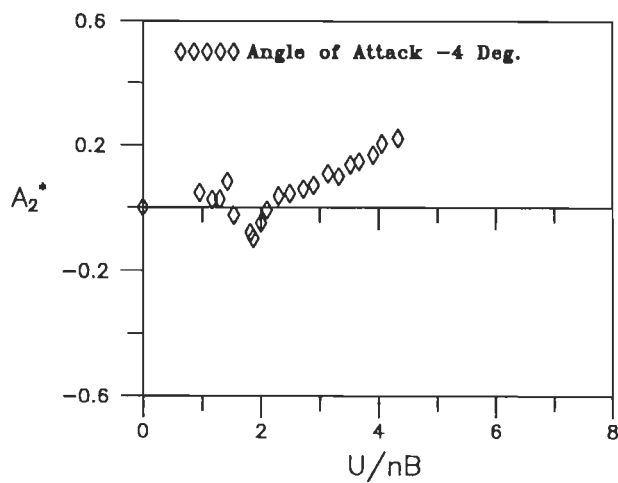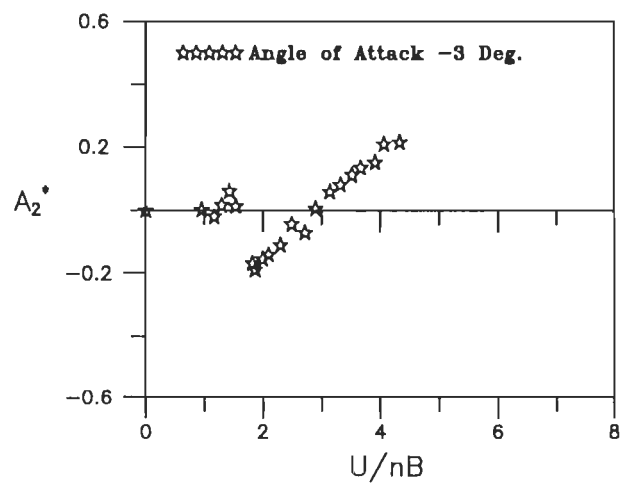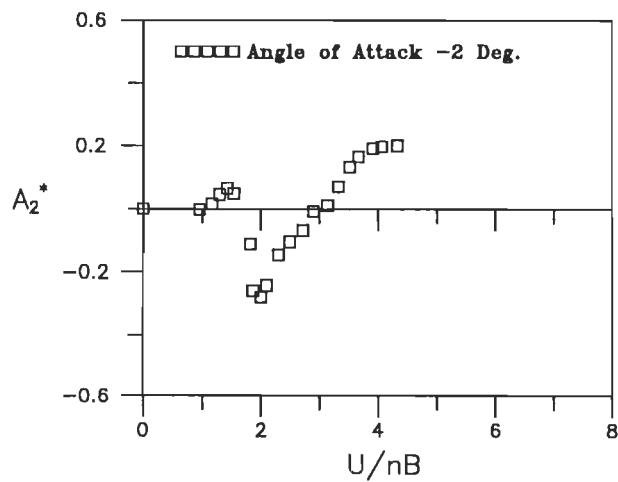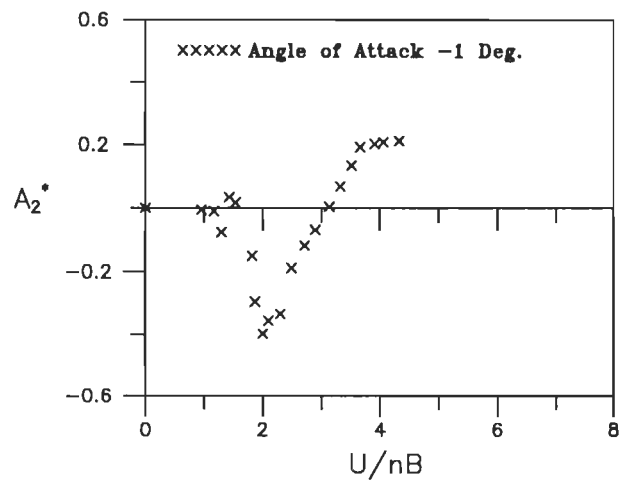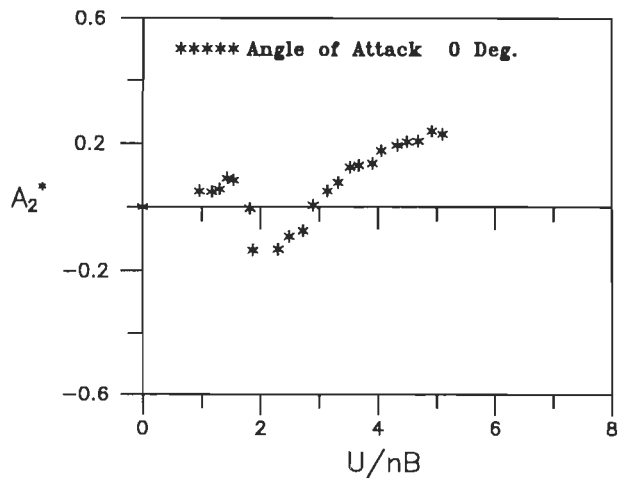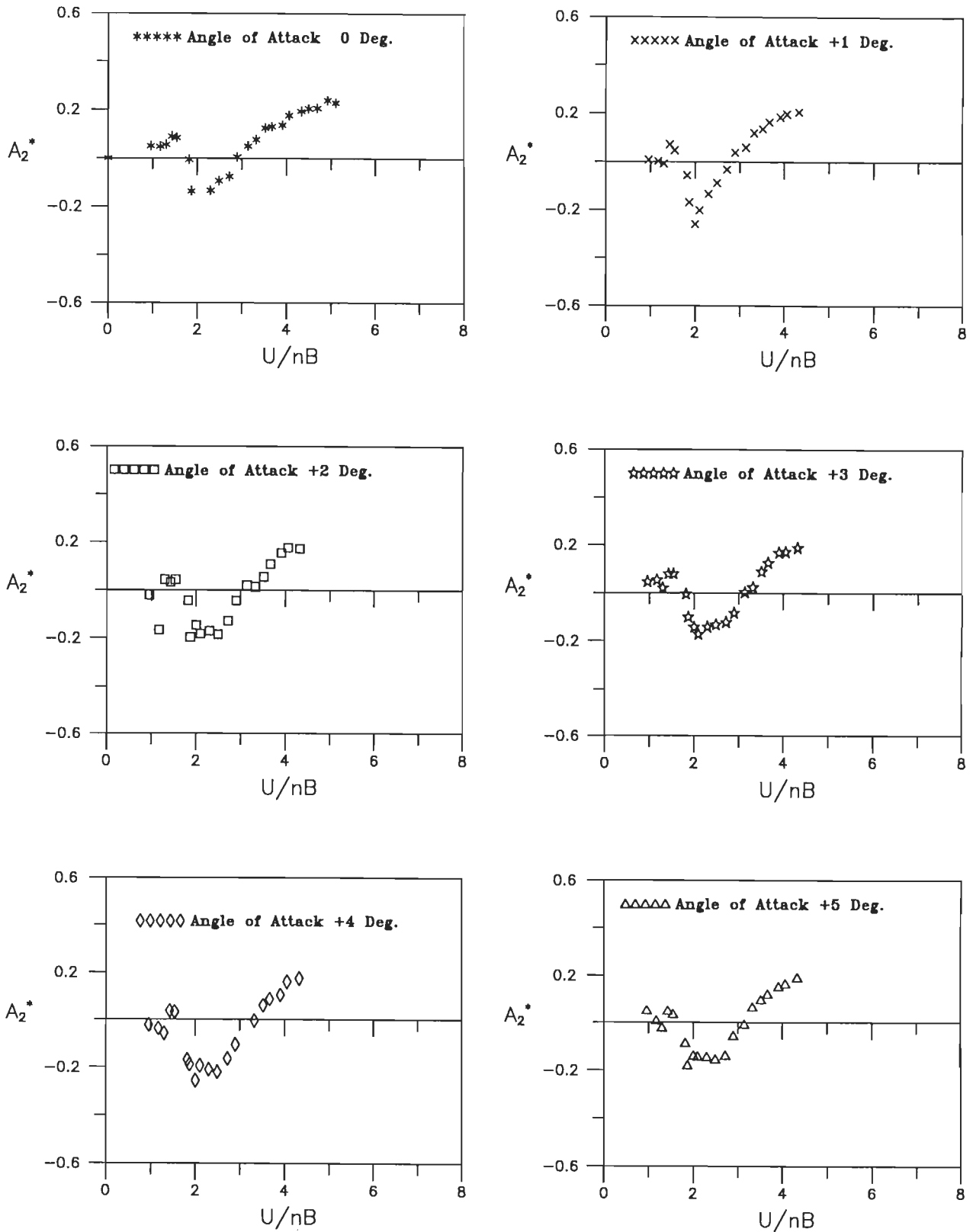
Fig.6.10(a) Variation of flutter derivative (A_2^*) with wind incidence angles for unmodified section model under smooth flow.
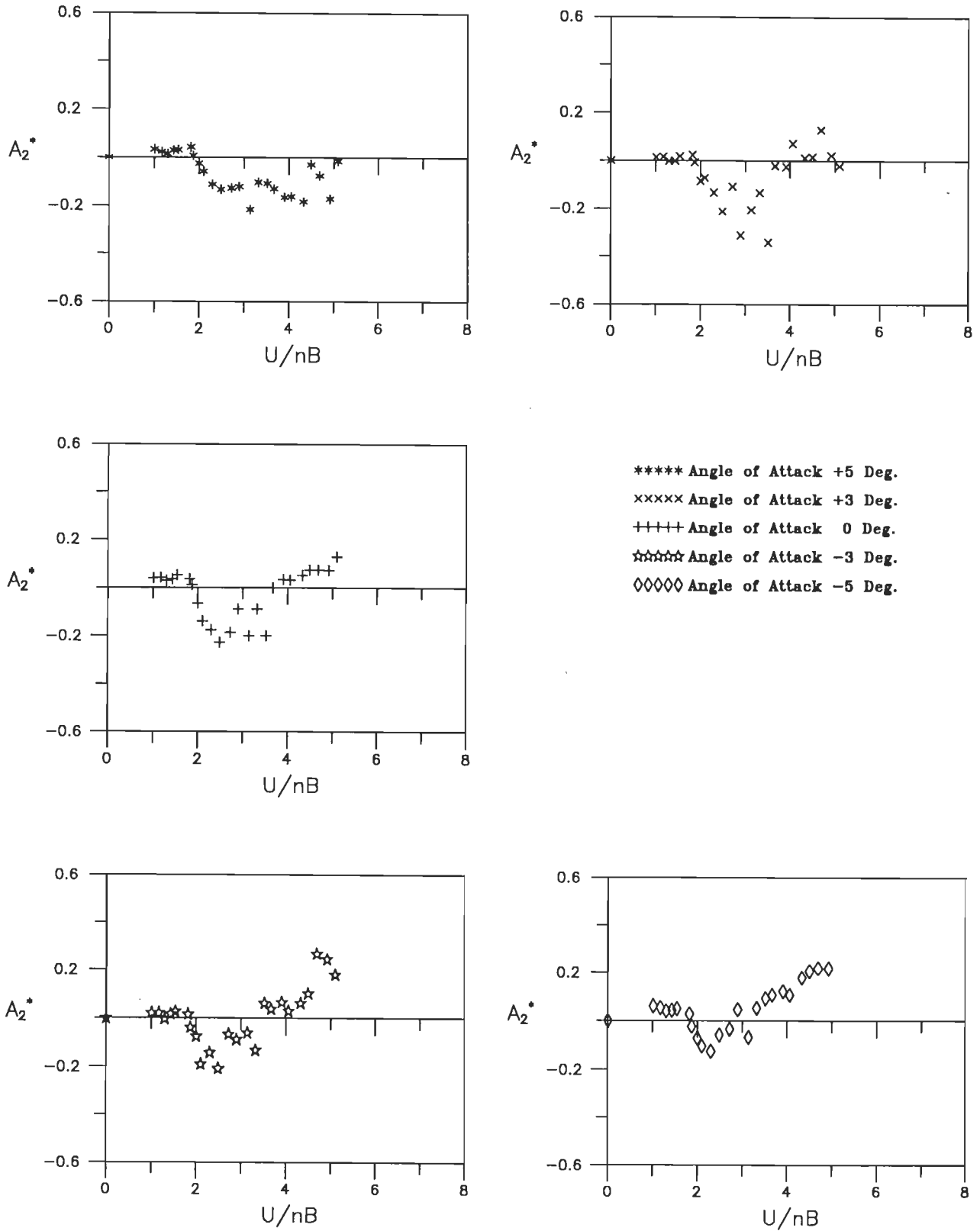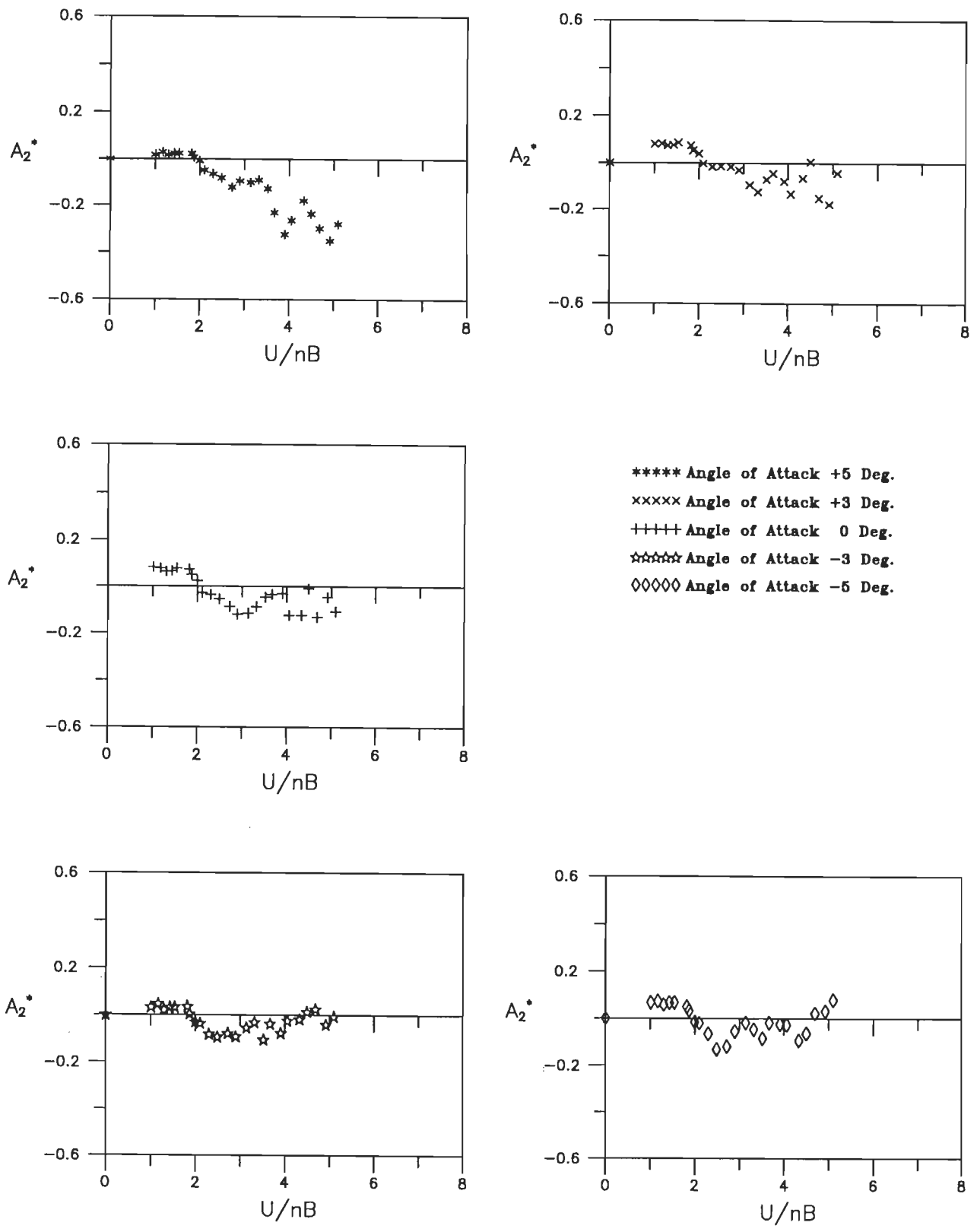
Fig.6.10(b) Variation of flutter derivative (A_2^*) with wind incidence angles for unmodified section model under grid generated flow (Grid # 1).
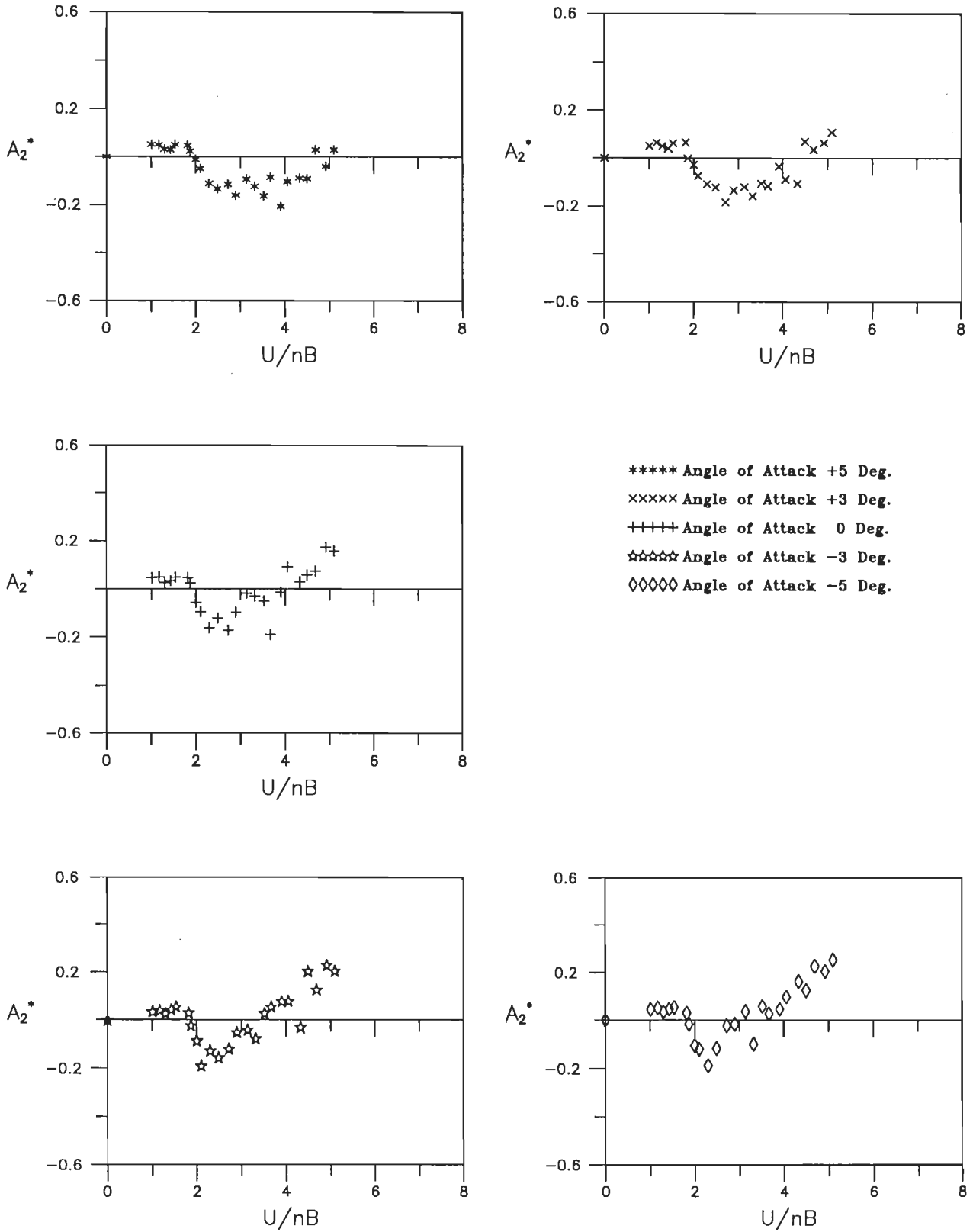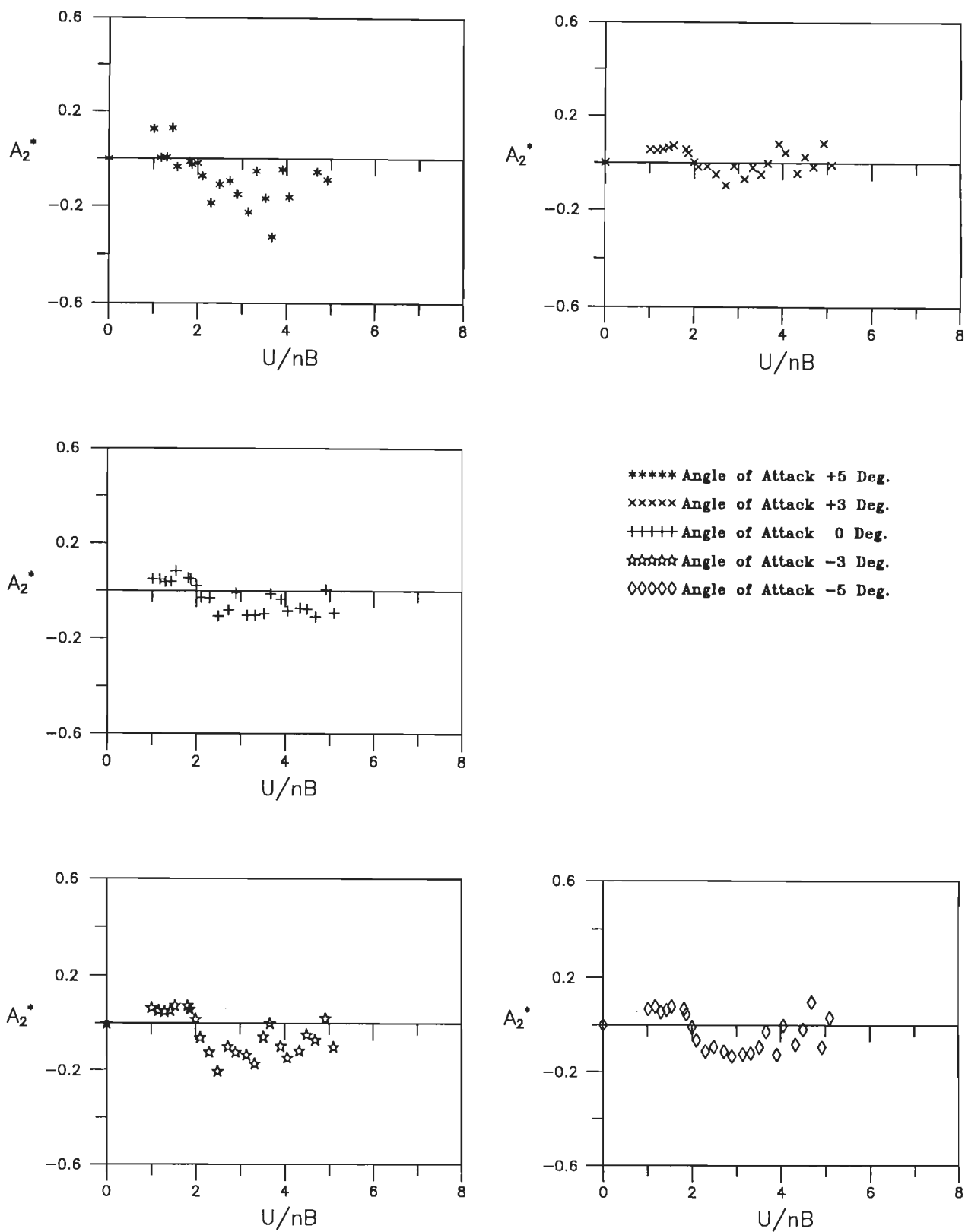
Fig. 6.10(c) Variation of flutter derivative (A₂*) with wind incidence angle for unmodified section model under grid generated flow (Grid # 2).
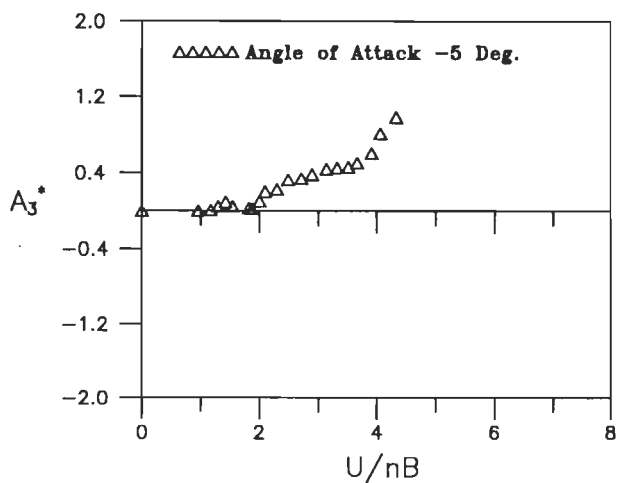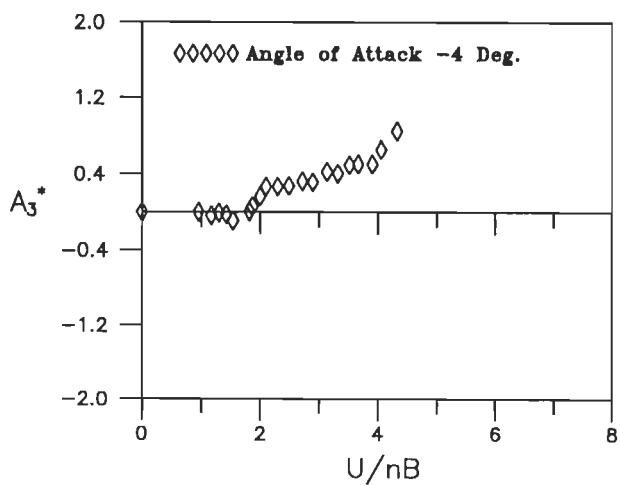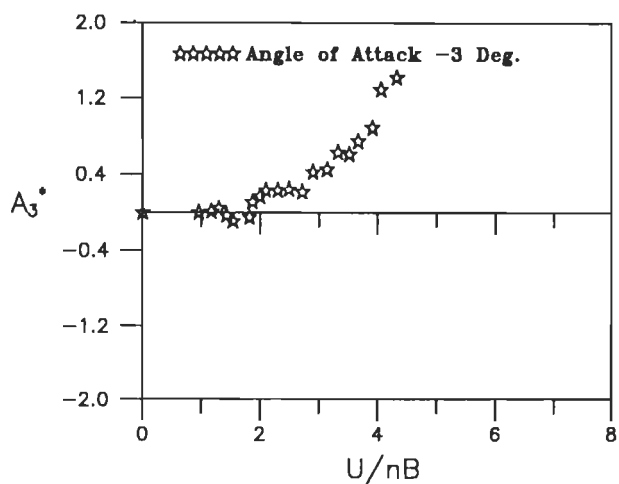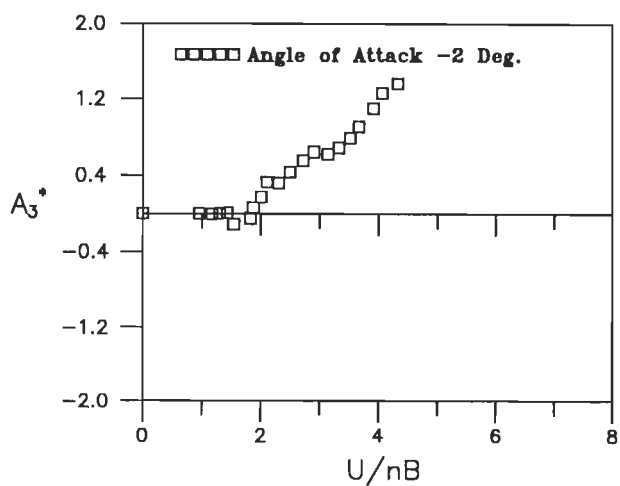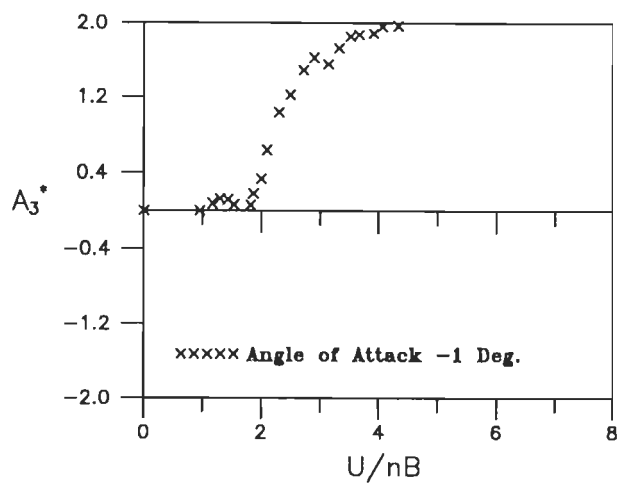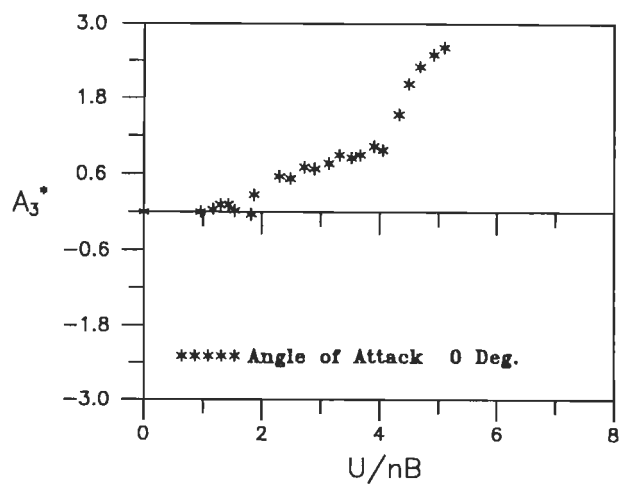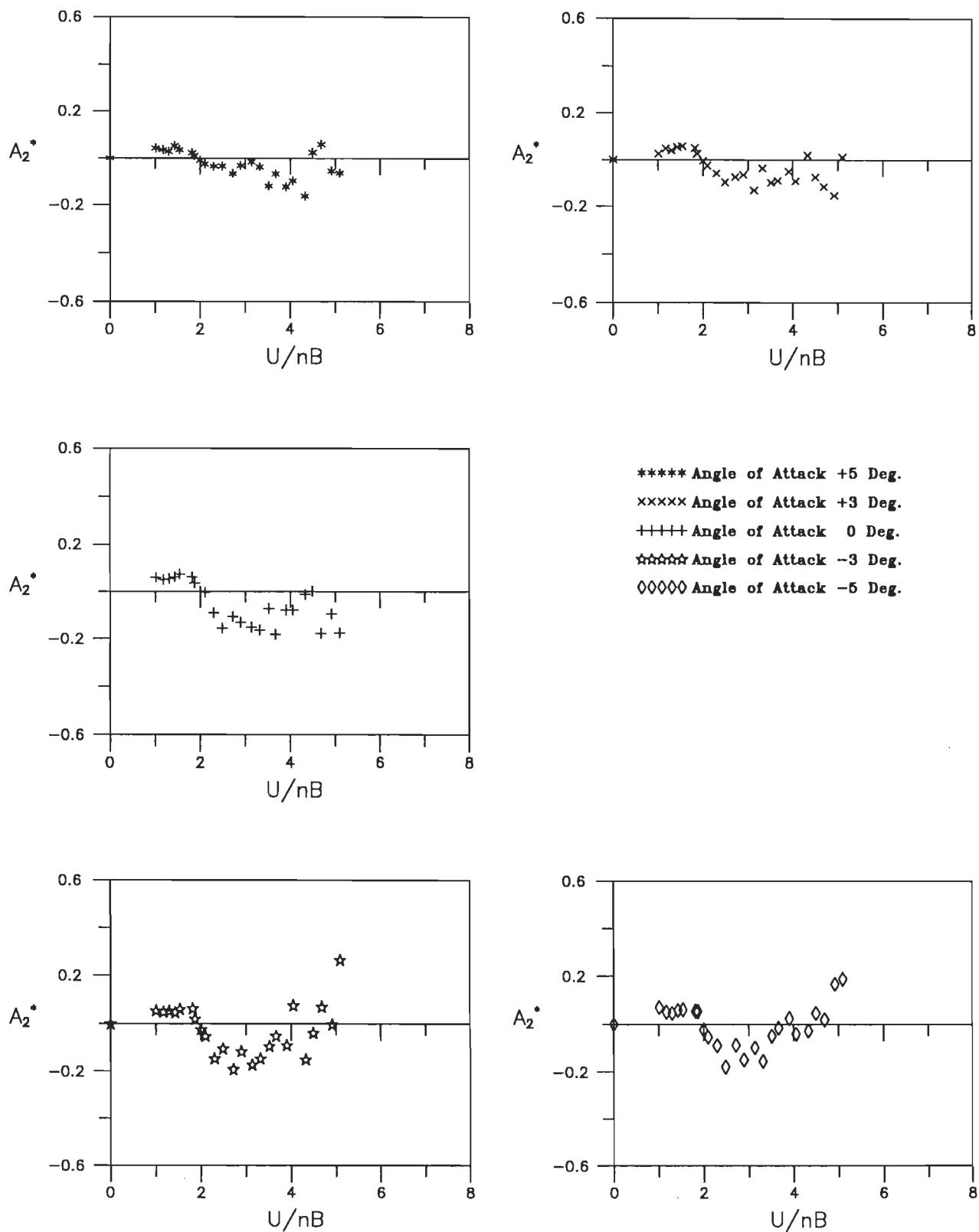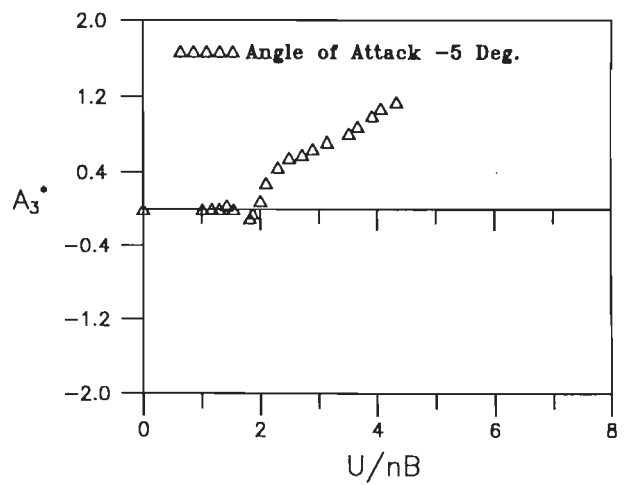
Contd.,
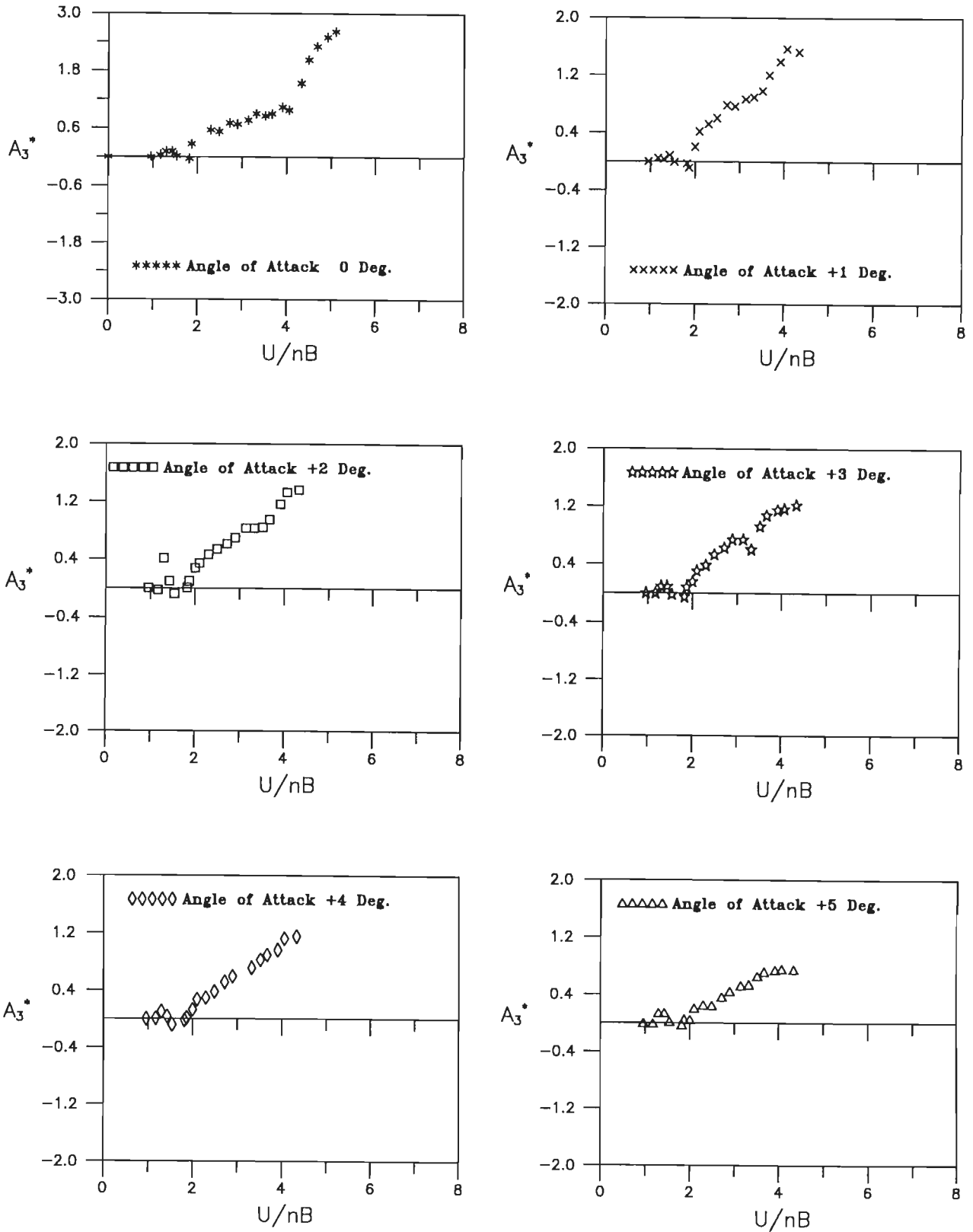
Fig.6.11(a) Variation of flutter derivative A_3^* with wind incidence angles for unmodified section model under smooth flow.
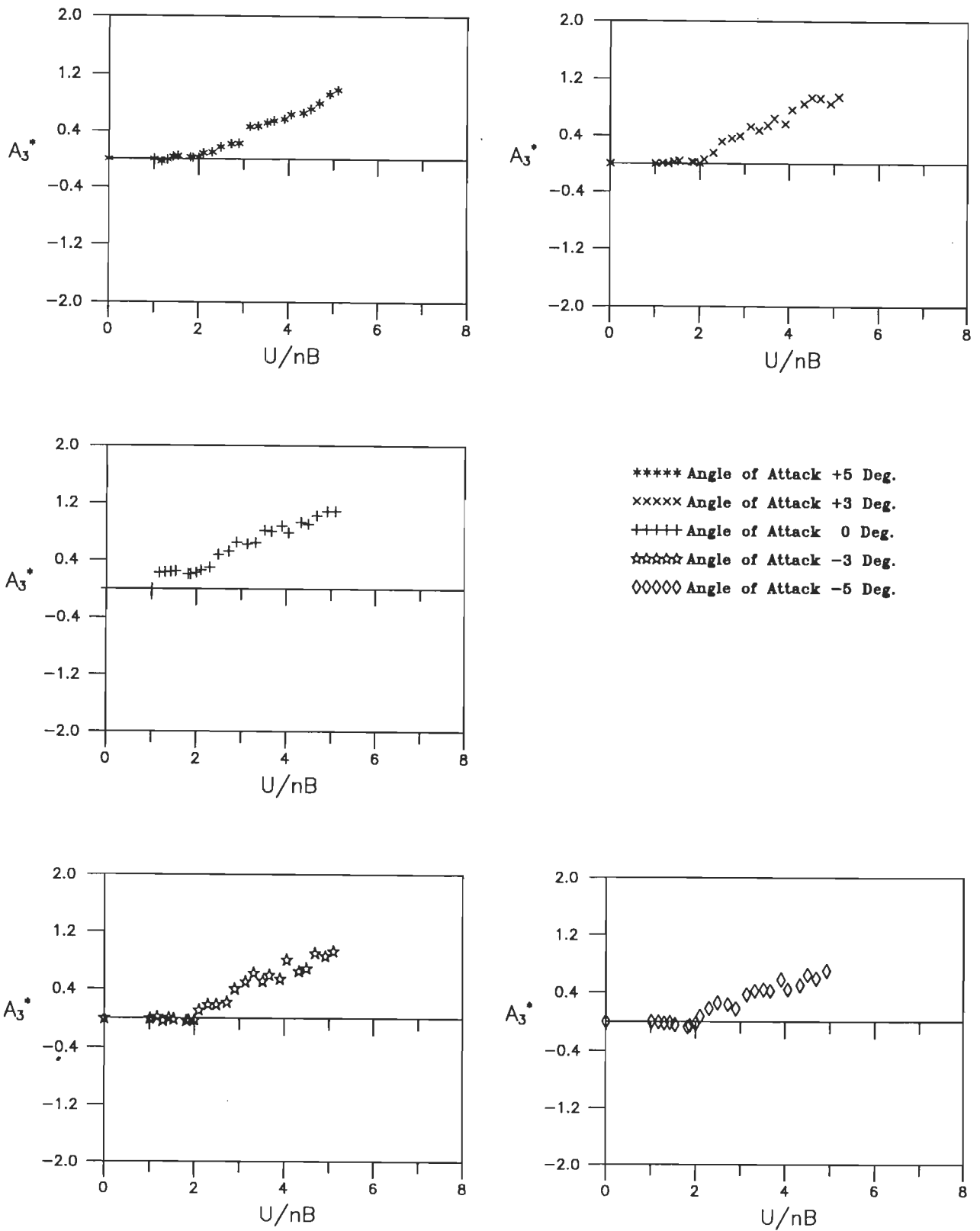
Fig.6.11(b) Variation of flutter derivative A_3^* with wind incidence angles
for unmodified section model under grid generated flow (Grid # 1).
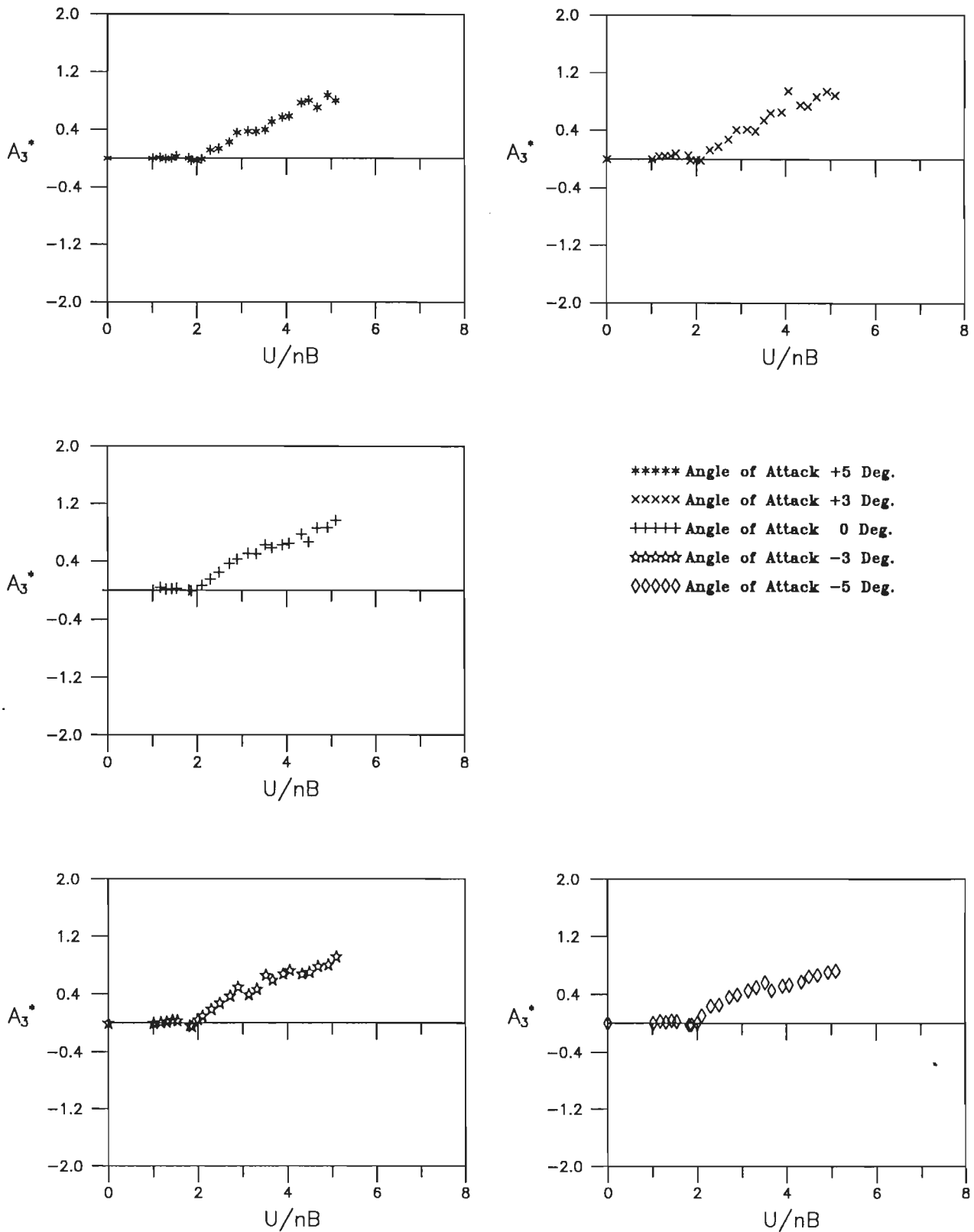
Fig.6.11(c) Variation of flutter derivative A_3^* with wind incidence angles for unmodified section model under grid generated flow (Grid # 2).
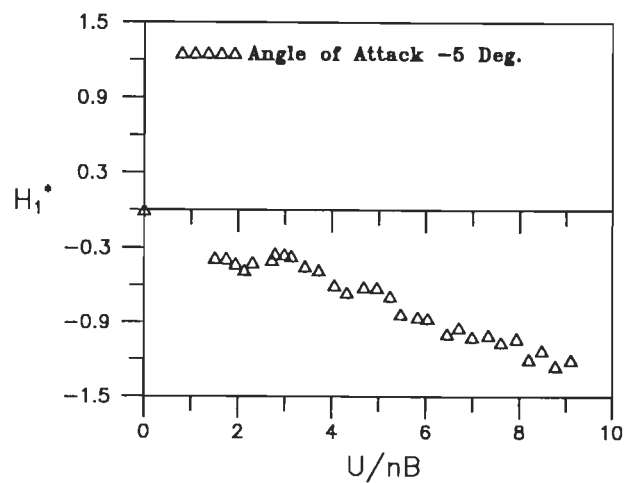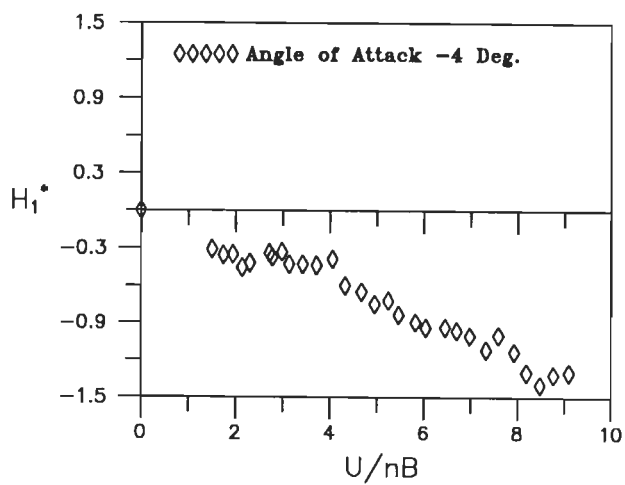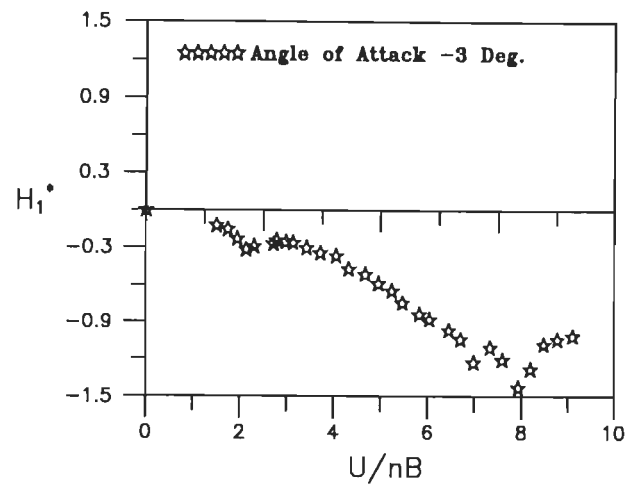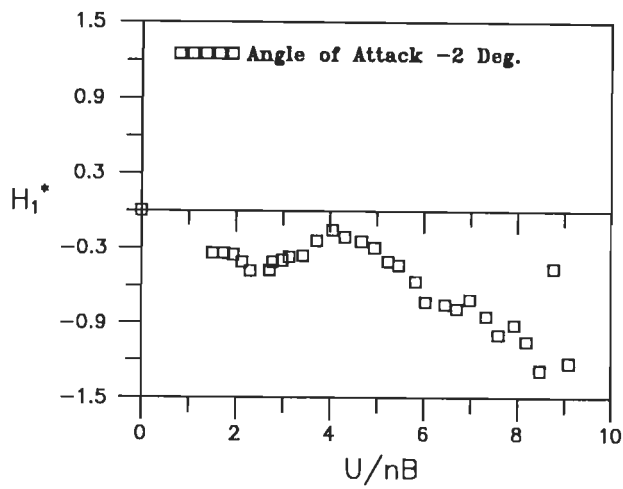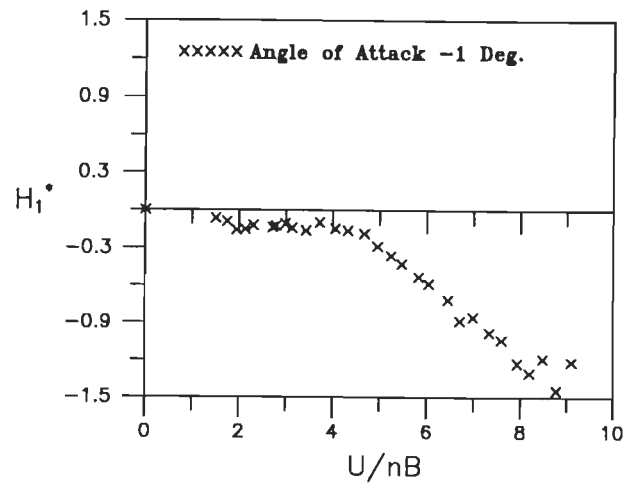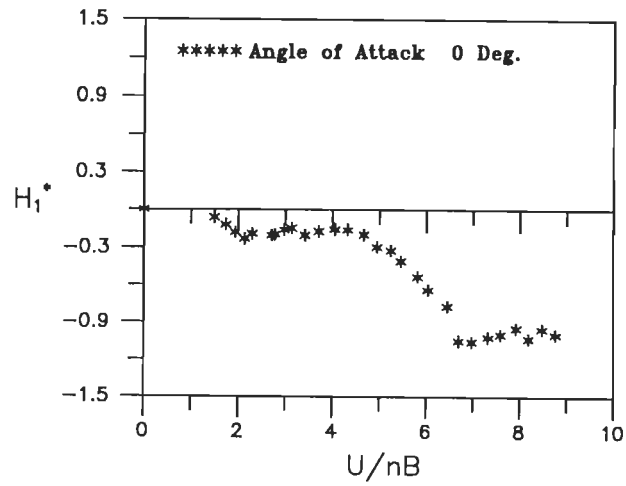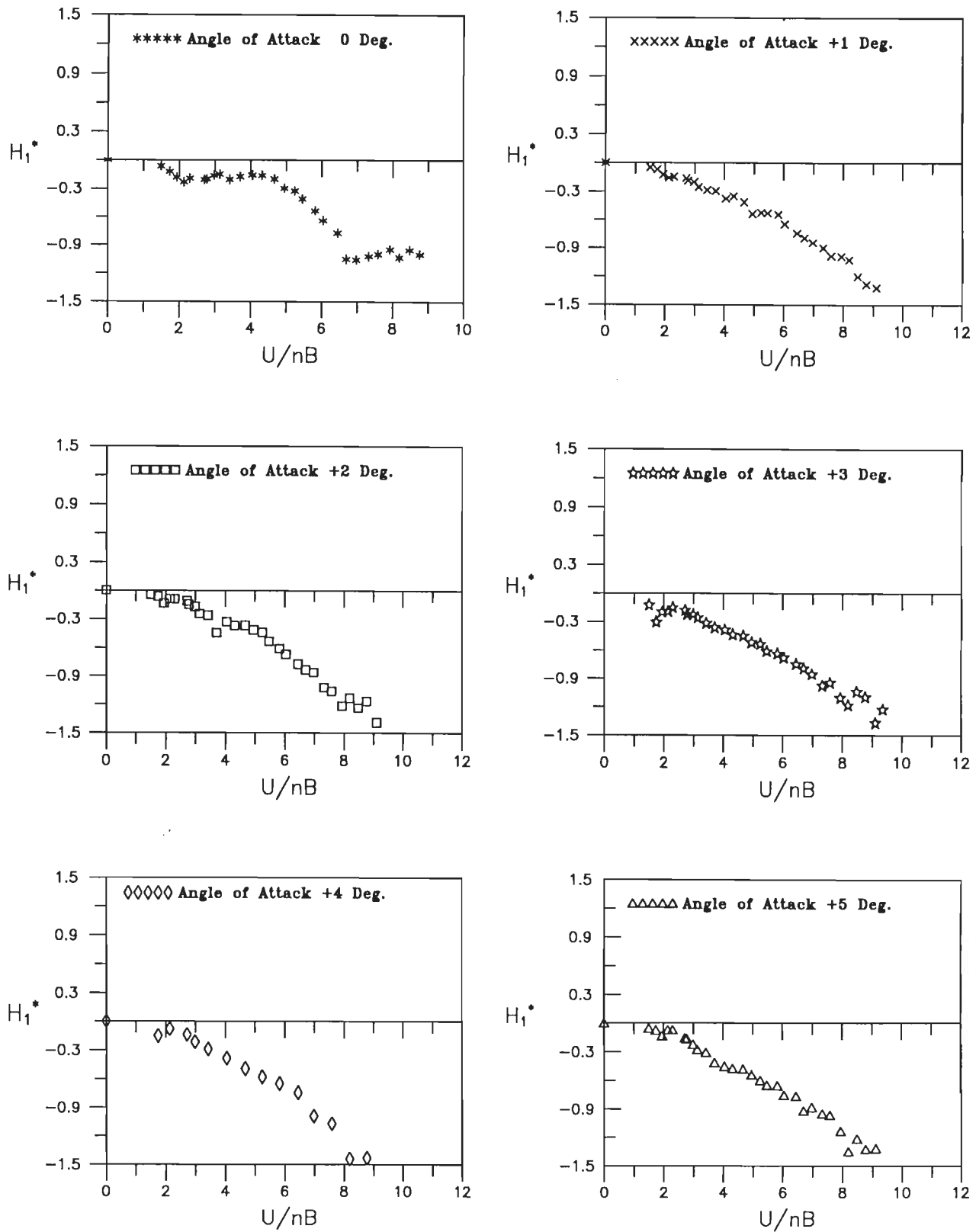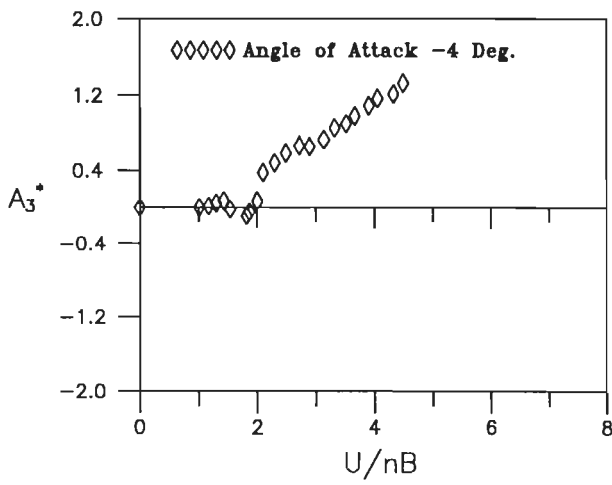
Fig. 6.12(a) Variation of flutter derivative (H_1^*) with wind incidence angles for faired section model under smooth flow .
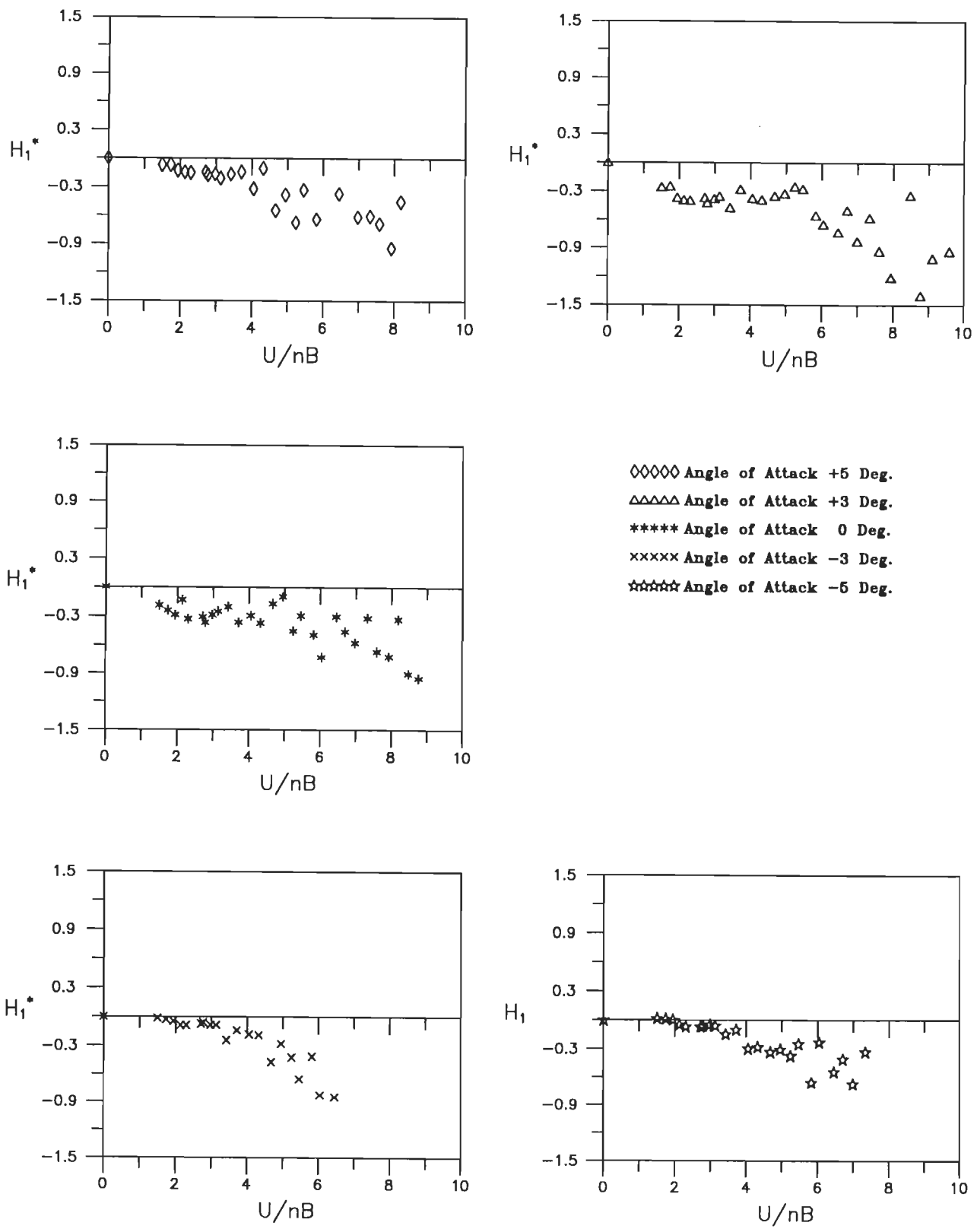
Fig. 6.12(b) Variation of flutter derivative (H_1^*) with wind incidence angles for faired section model under Grid Generated flow (Grid # 1)
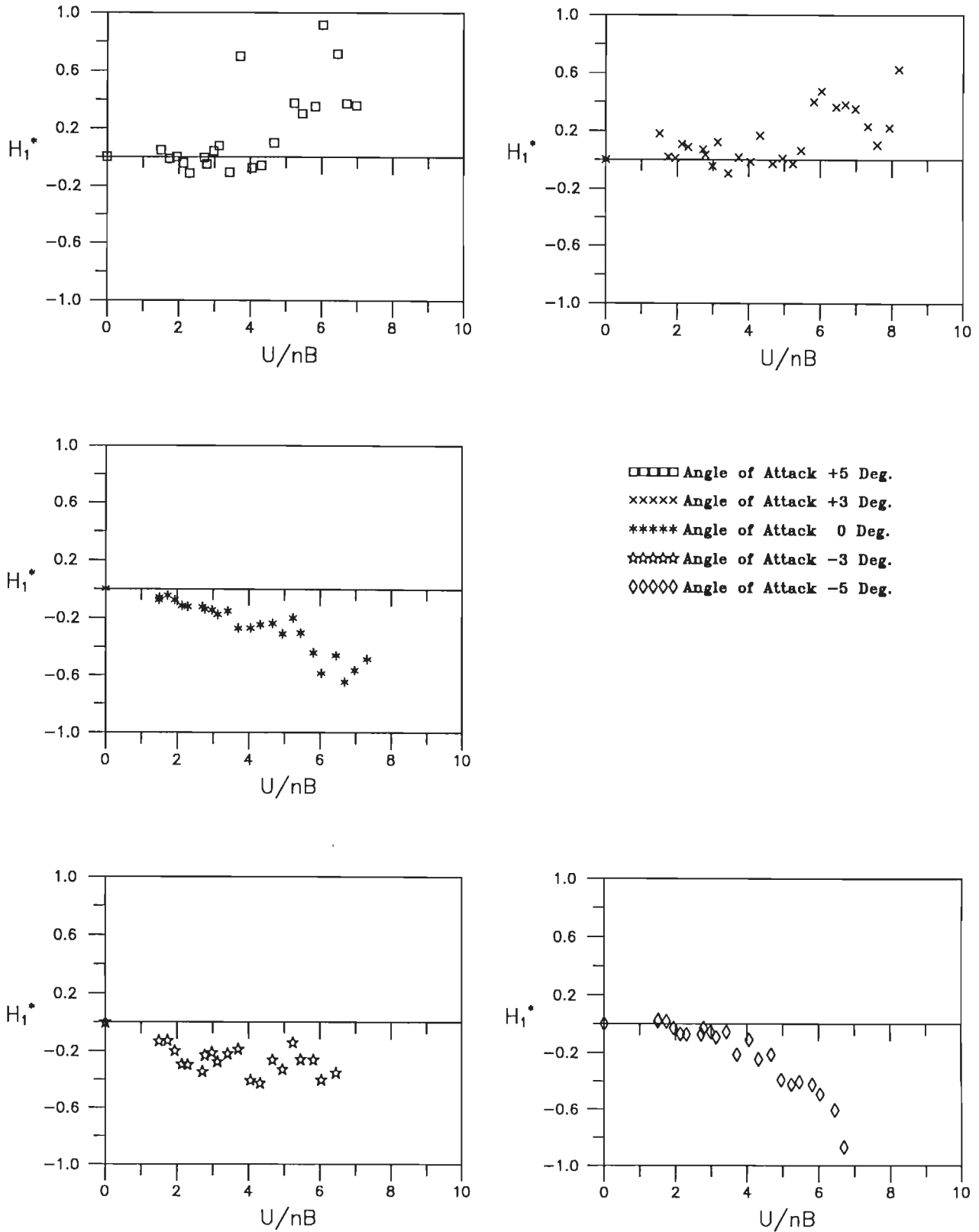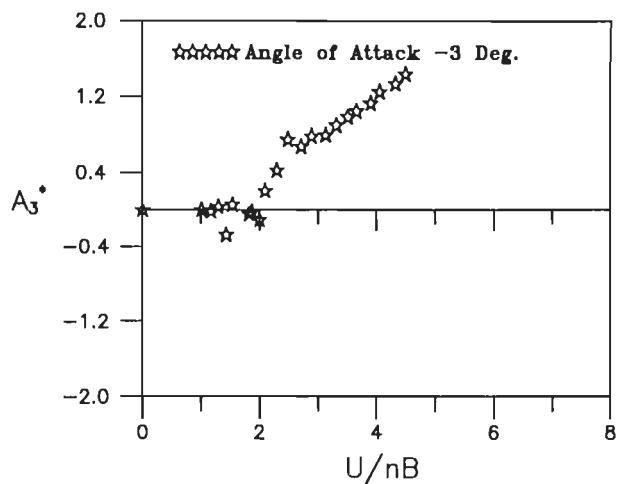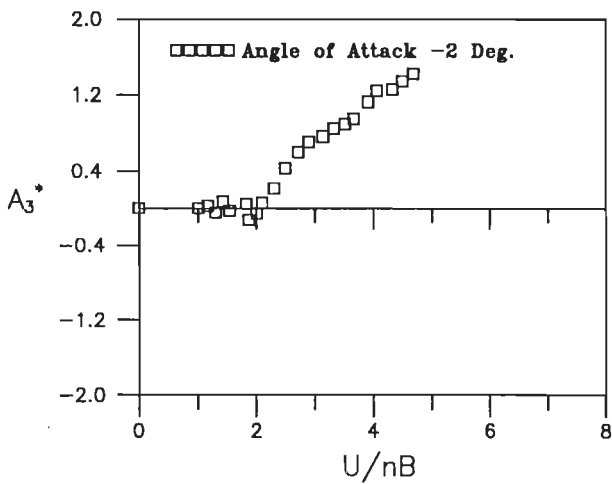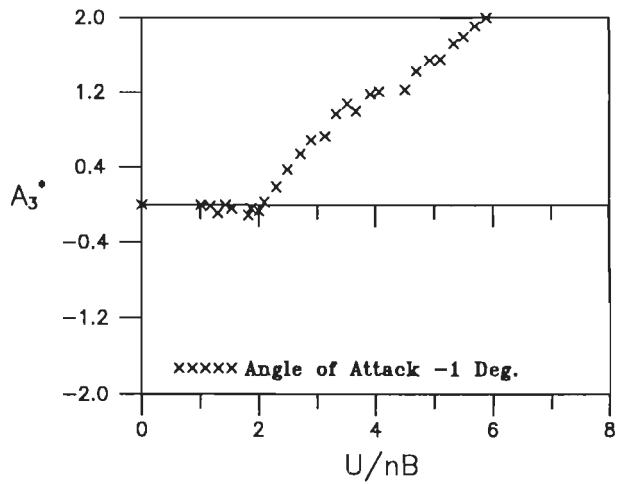
Fig. 6.12(c) Variation of flutter derivative (H_1^*) with wind incidence angles for faired section model under grid generated flow (Grid # 2)
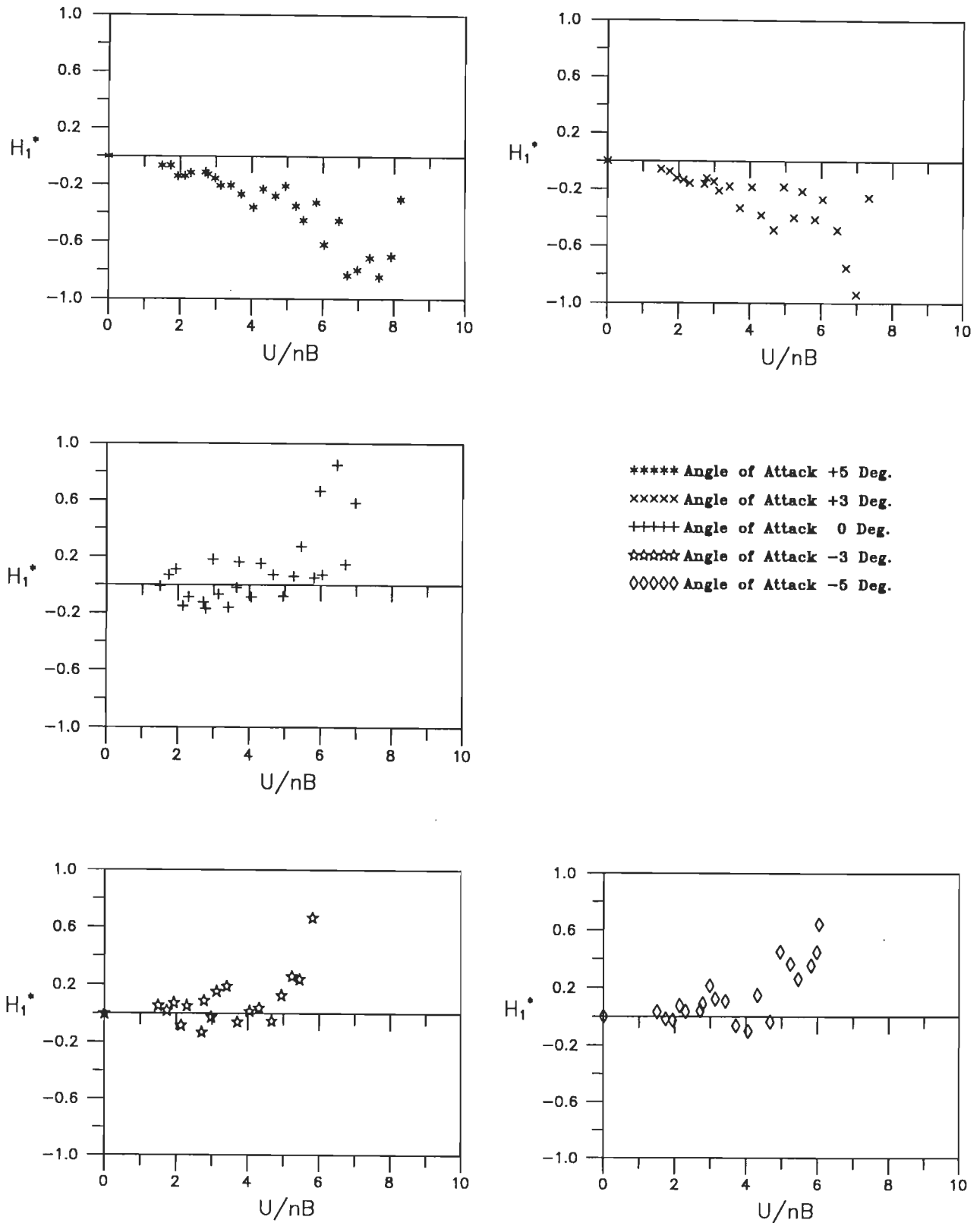
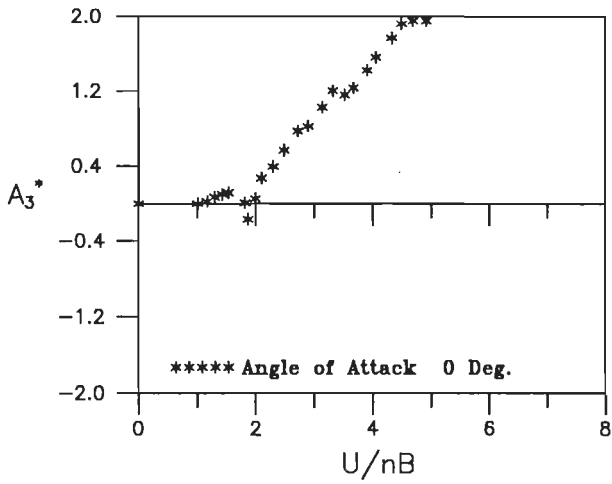Fig. 6.12(d) Variation of flutter derivative (H_1^*) with wind incidence angles for faired section model under grid generated flow (Grid # 3).
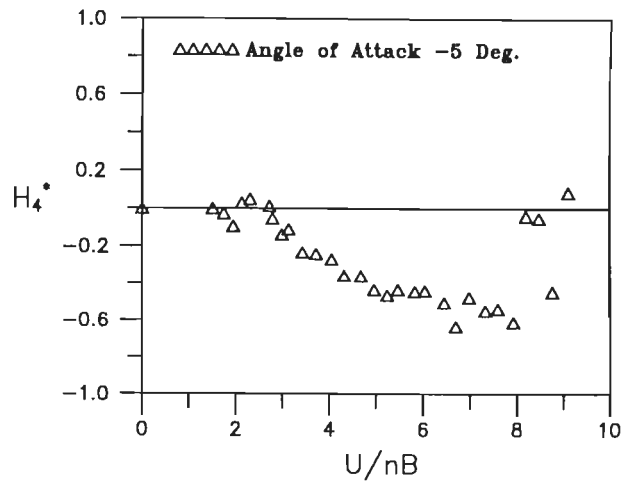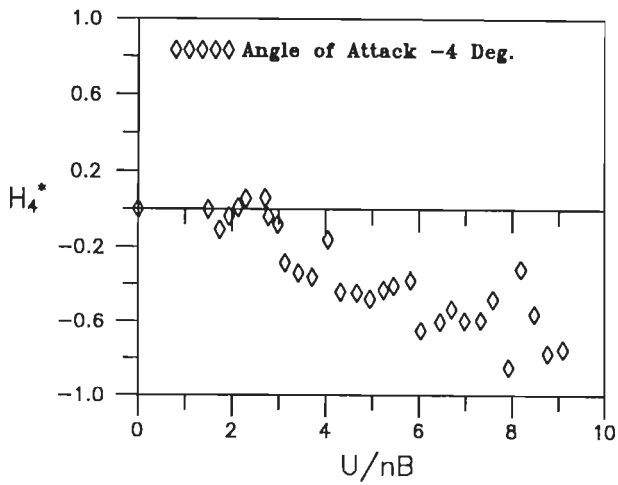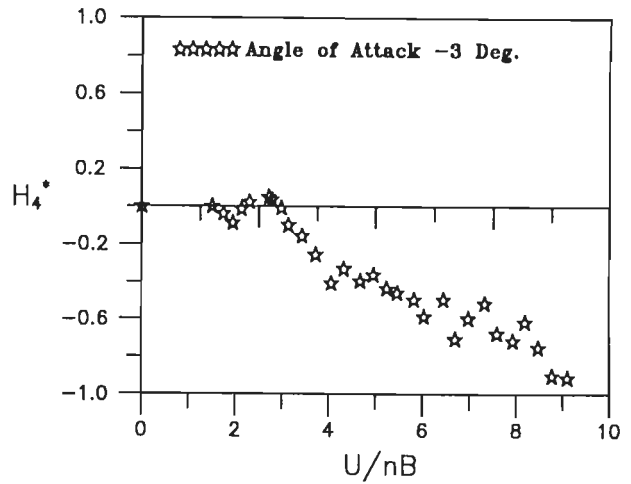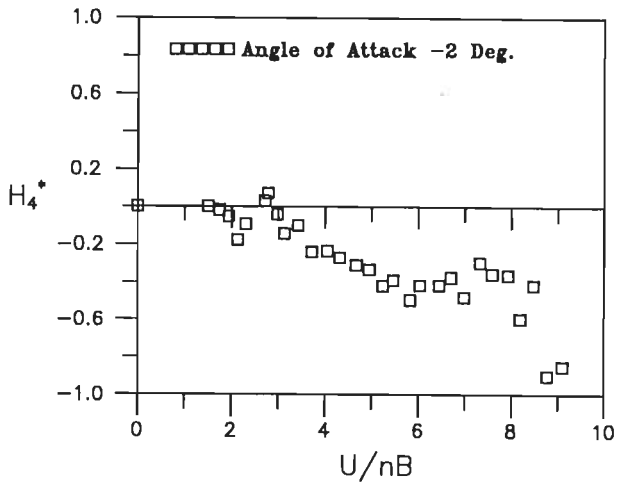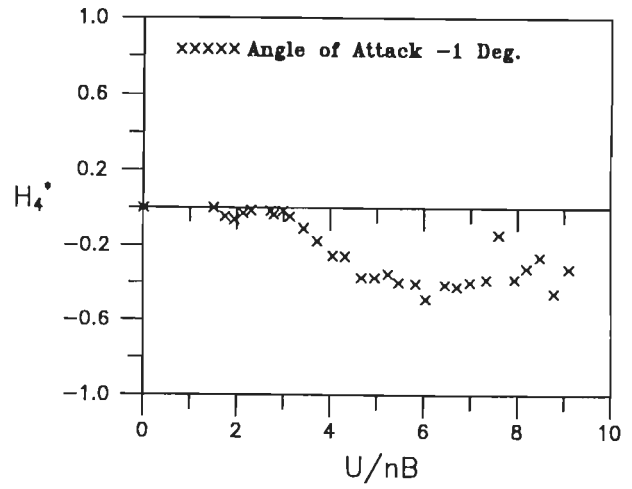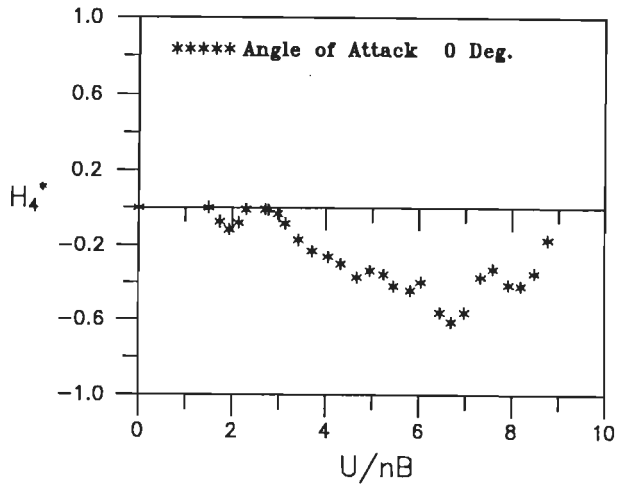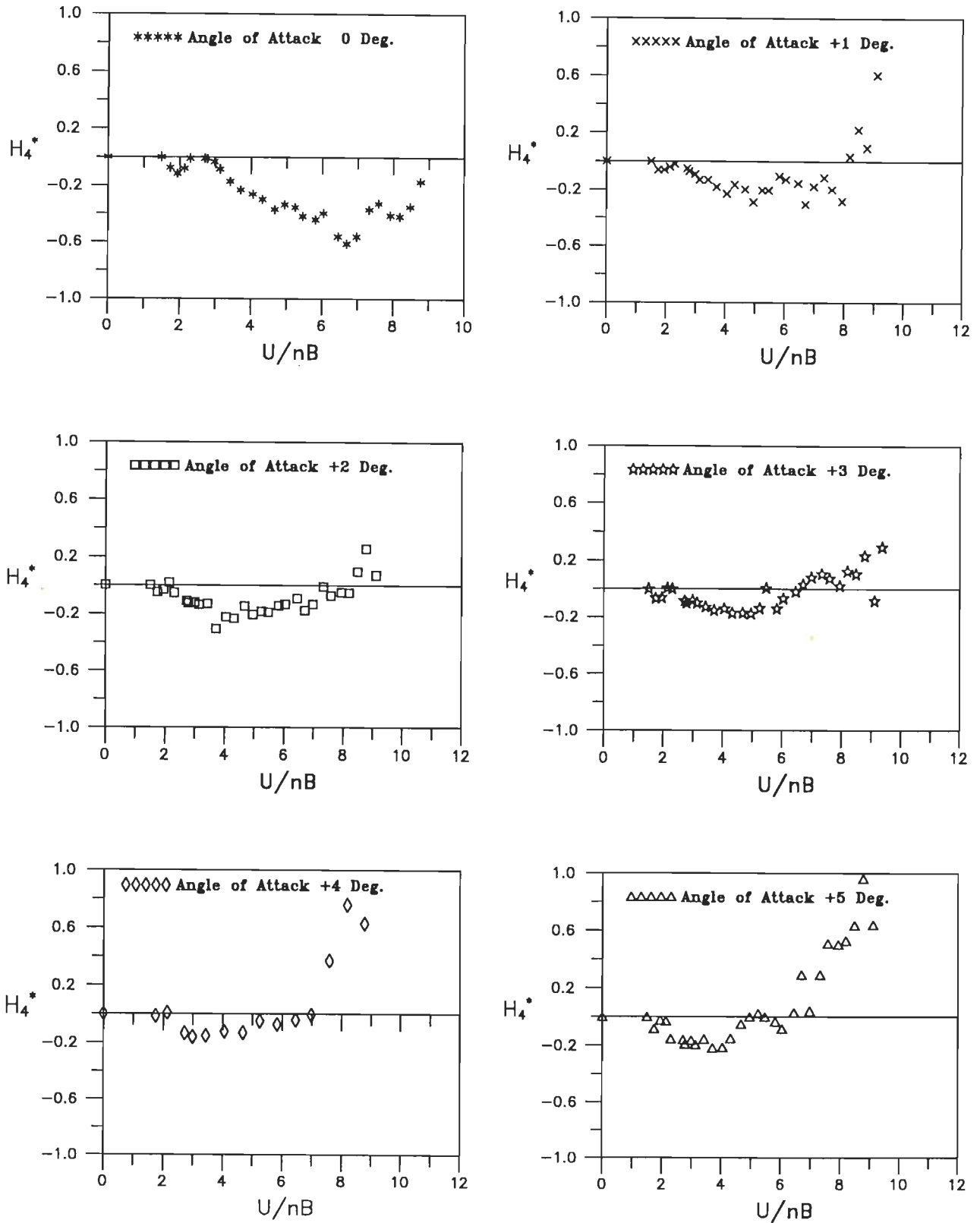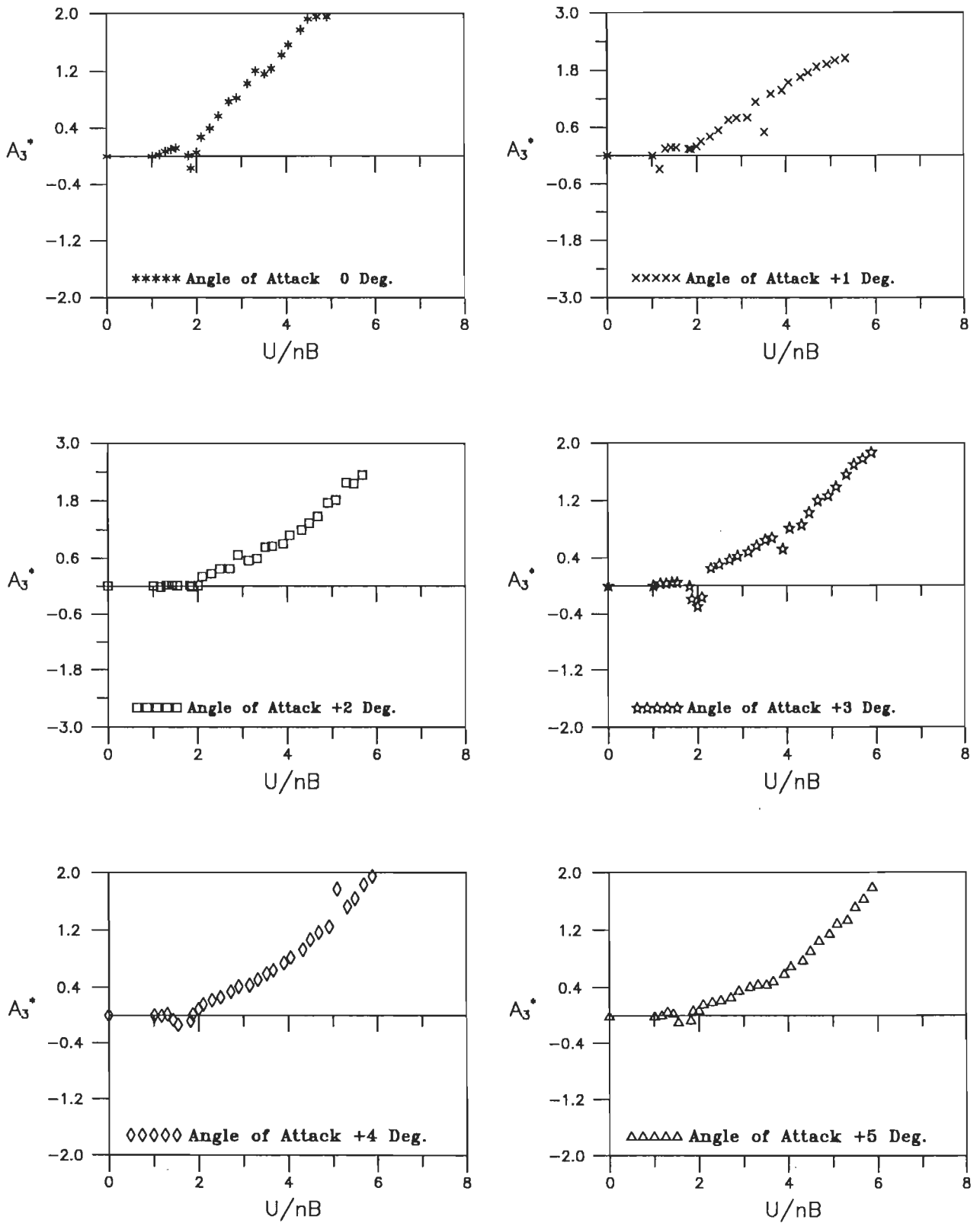
Fig. 6.13(a) Variation of flutter derivative (H_4^*) with wind incidence
angles for faired section model under smooth flow .
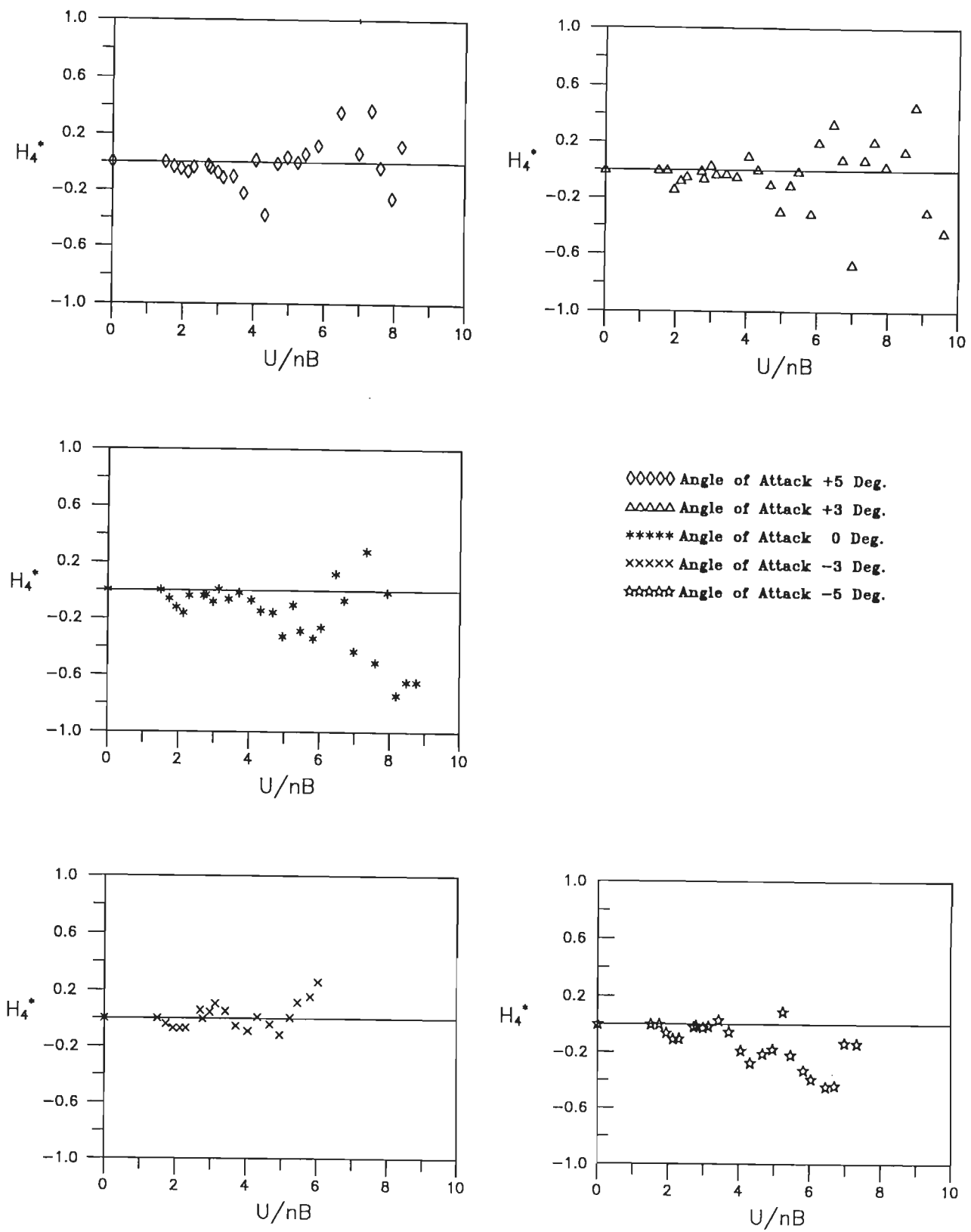
Fig.6.13(b) Variation of flutter derivative (H_4^*) with wind incidence angles for unmodified section model under grid generated flow (Grid # 1).
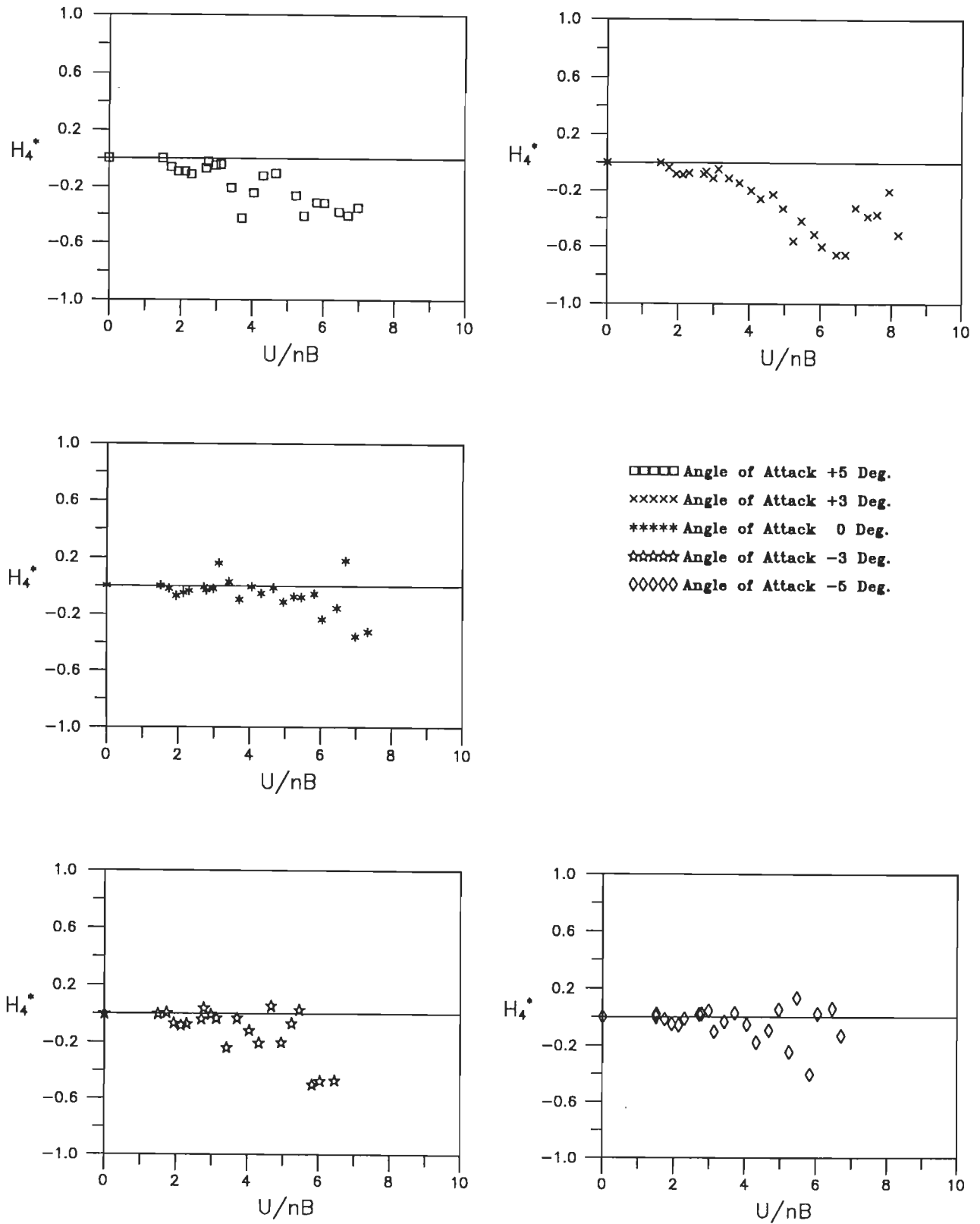
Fig. 6.13(c) Variation of flutter derivative (H_4^*) with wind incidence angles for faired section model under grid generated flow (Grid # 2).
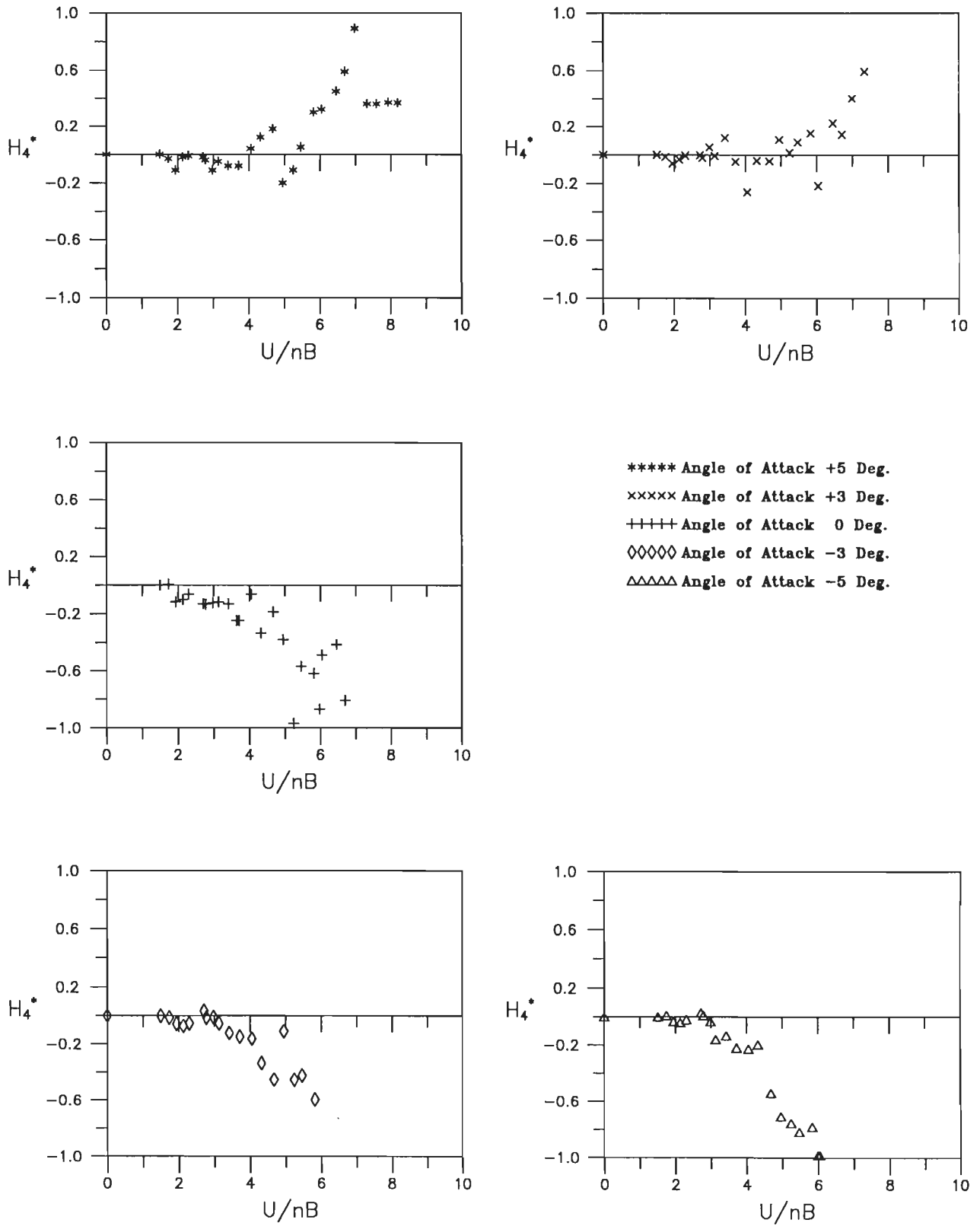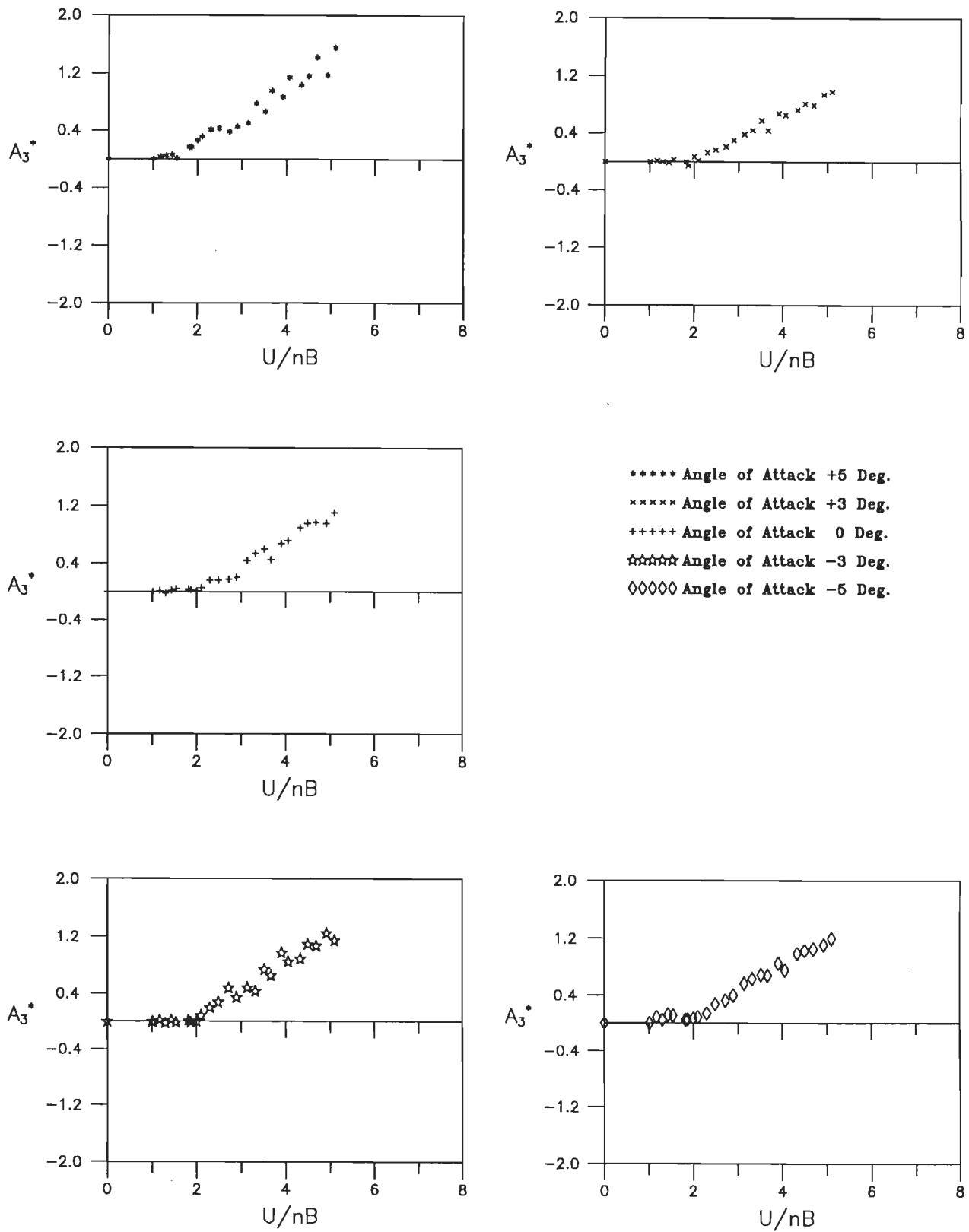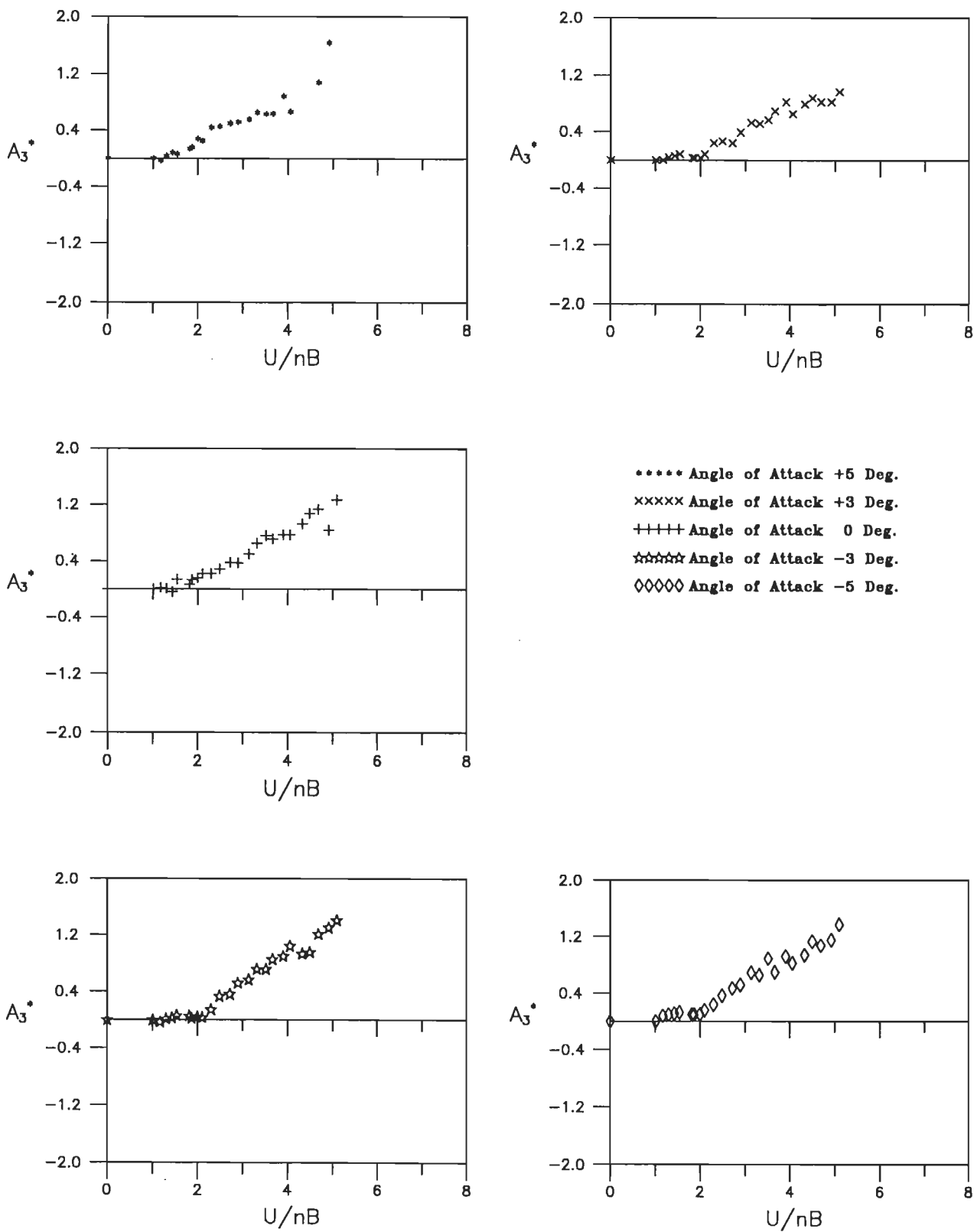
Fig. 6.13(d) Variation of flutter derivative H_4^* with wind incidence angles for faired section model under grid generated flow (Grid # 3).

Fig.6.14(a) Variation of flutter derivative(A_2^*) with wind incidence angles for faired section model under smooth flow.

Fig.6.14(b) Variation of flutter derivative(A_2^*) with wind incidence angles for faired section model under grid generated flow (Grid # 1).
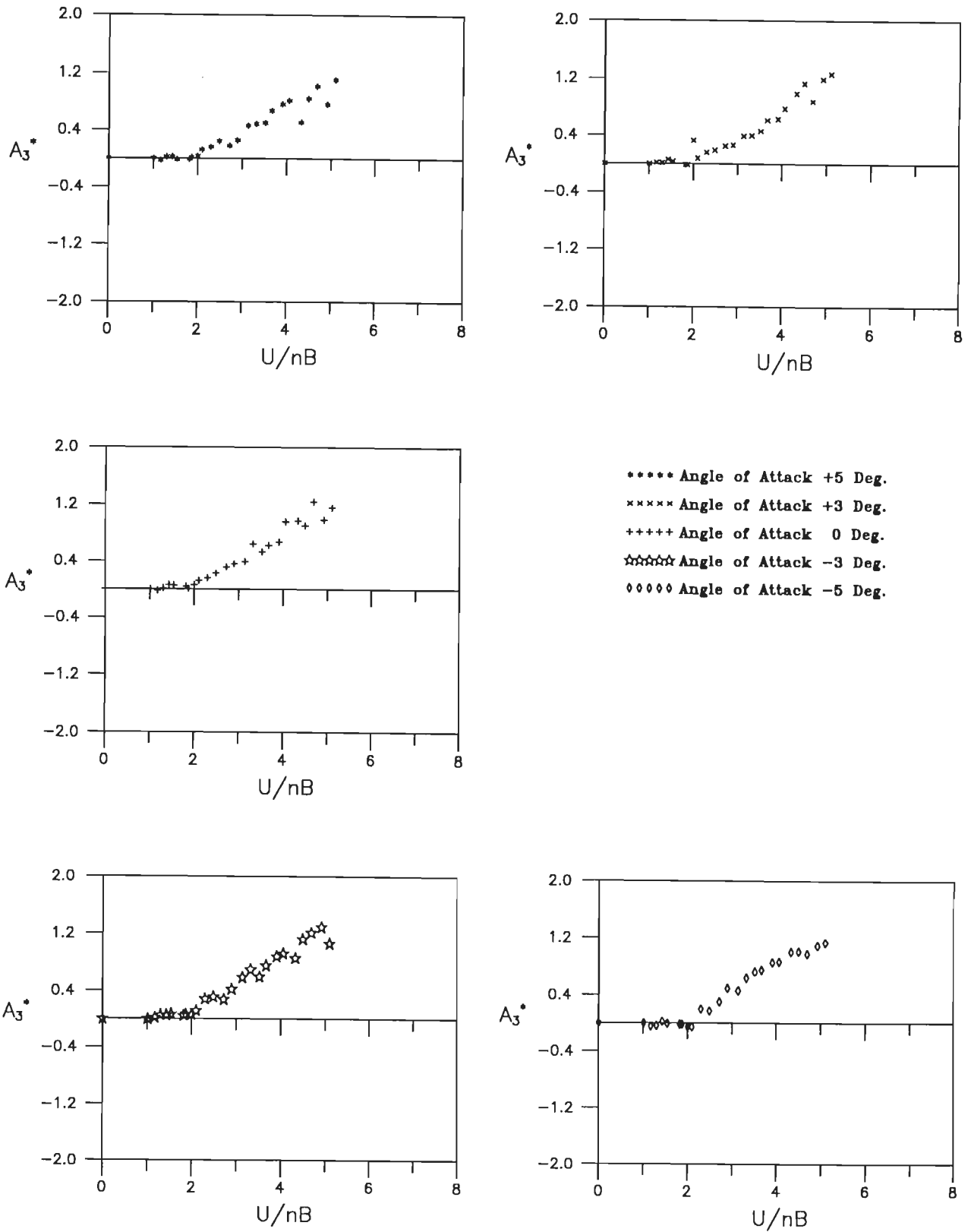
194

Fig.6.14(C) Variation of flutter derivative A_2^* with wind incidence angles for faired section model under grid generated flow (Grid # 2).

Fig. 6.14(d) Variation of flutter derivative A_2^* with wind incidence angles for faired section model under grid generated flow (Grid # 3).
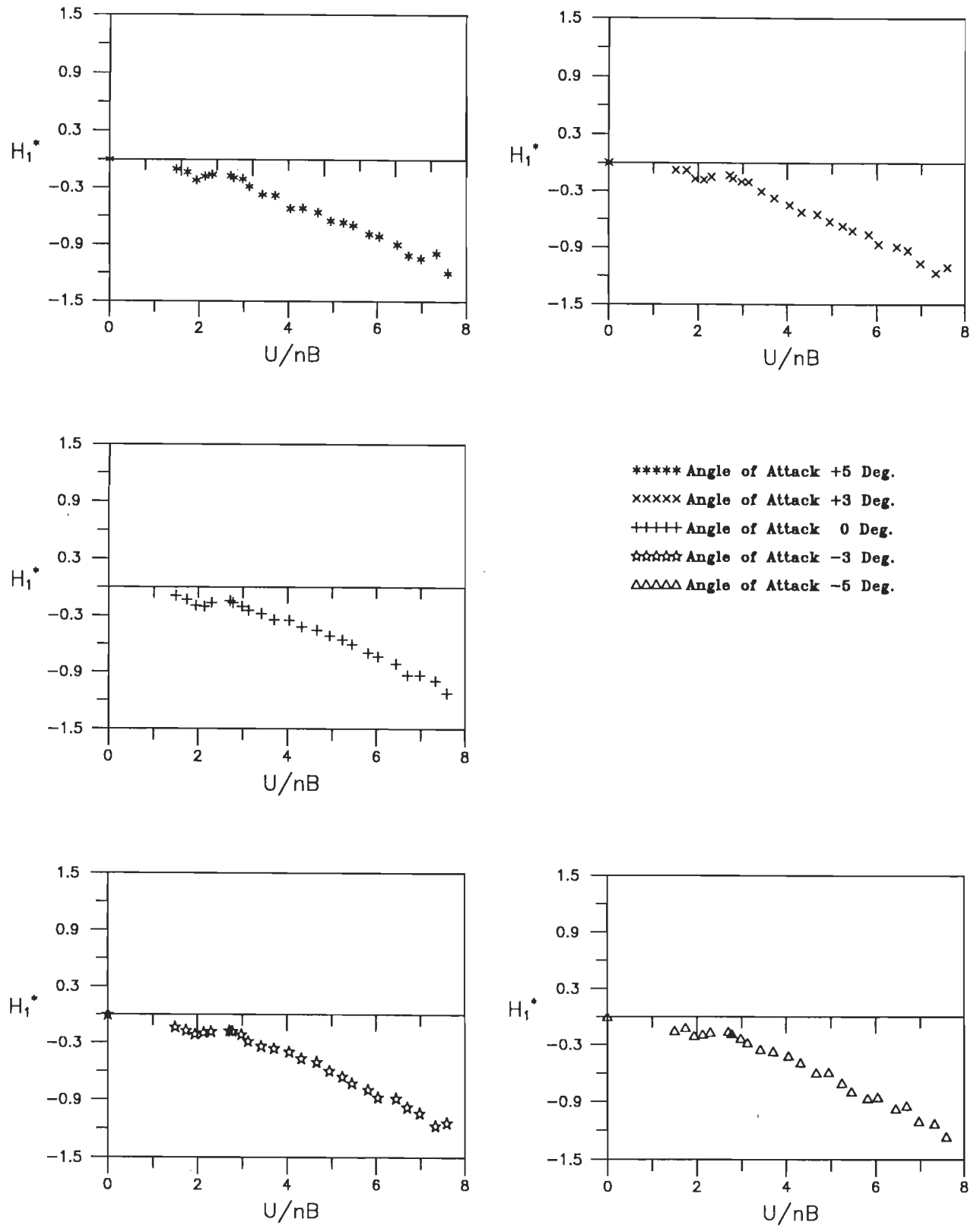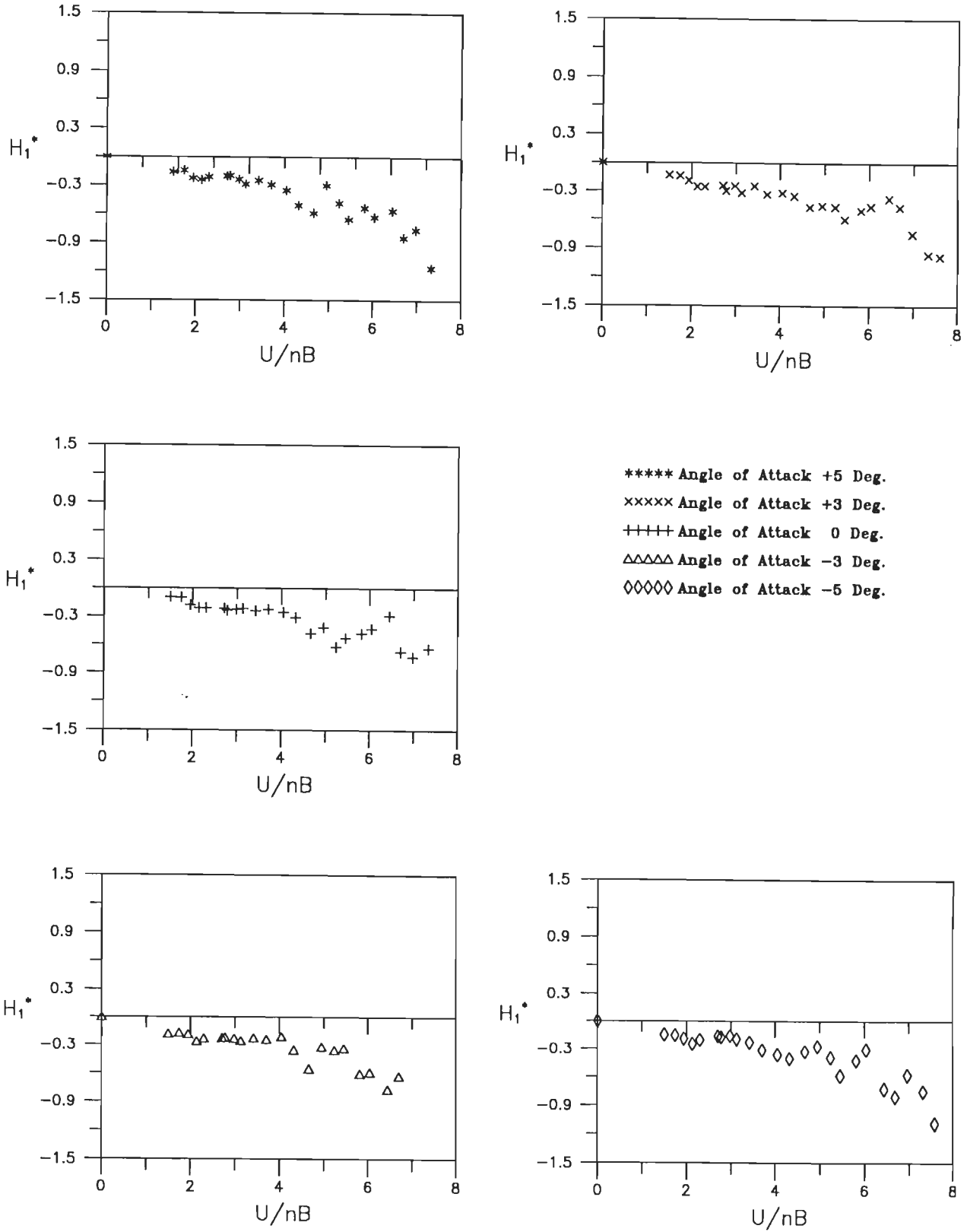
Contd.,

Fig.6.15(a) Variation of flutter derivative A_3^* with wind incidence angles for faired section model under smooth flow.

198

Fig.6.15(b) Variation of flutter derivative A_3^* with wind incidence angles for faired section model under grid generated flow (Grid # 1).
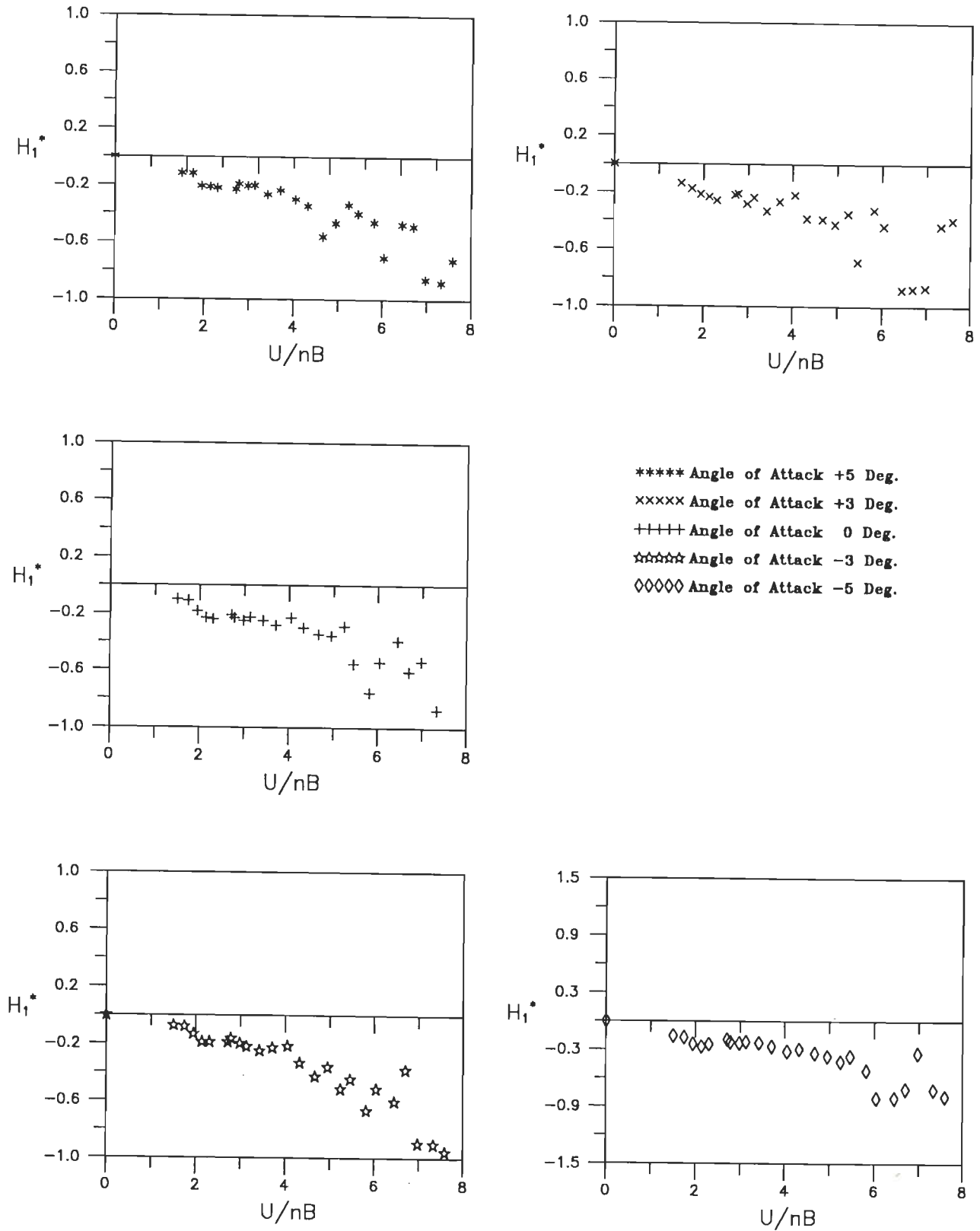
Fig.6.15(c) Variation of flutter derivative A_3^* with wind incidence angles for faired section model under grid generated flow (Grid # 2).

Fig.6.15(d) Variation of flutter derivative A_3^* with wind incidence angles for faired section model under grid generated flow (Grid # 3).

***** Angle of Attack +5 Deg.
××××× Angle of Attack +3 Deg.
+++++ Angle of Attack 0 Deg.
☆☆☆☆☆ Angle of Attack −3 Deg.
△△△△△ Angle of Attack −5 Deg.

Fig. 6.16(a) Variation of flutter derivative (H_1^*) with wind incidence
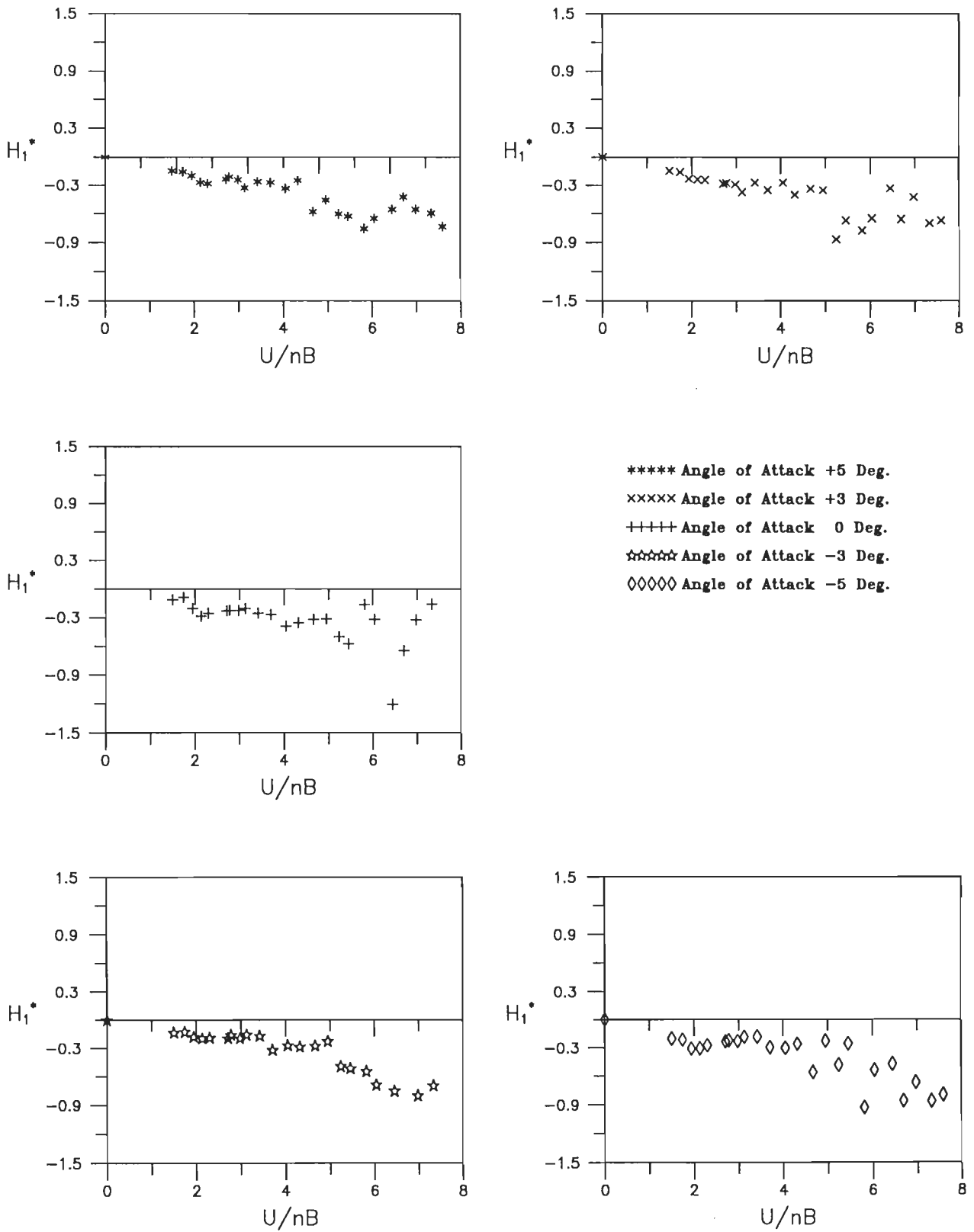angles for partially faired section model under smooth flow

Fig. 6.16(b) Variation of flutter derivative (H_1^*) with wind incidence angles for partially faired section model under grid generated flow (Grid # 1).
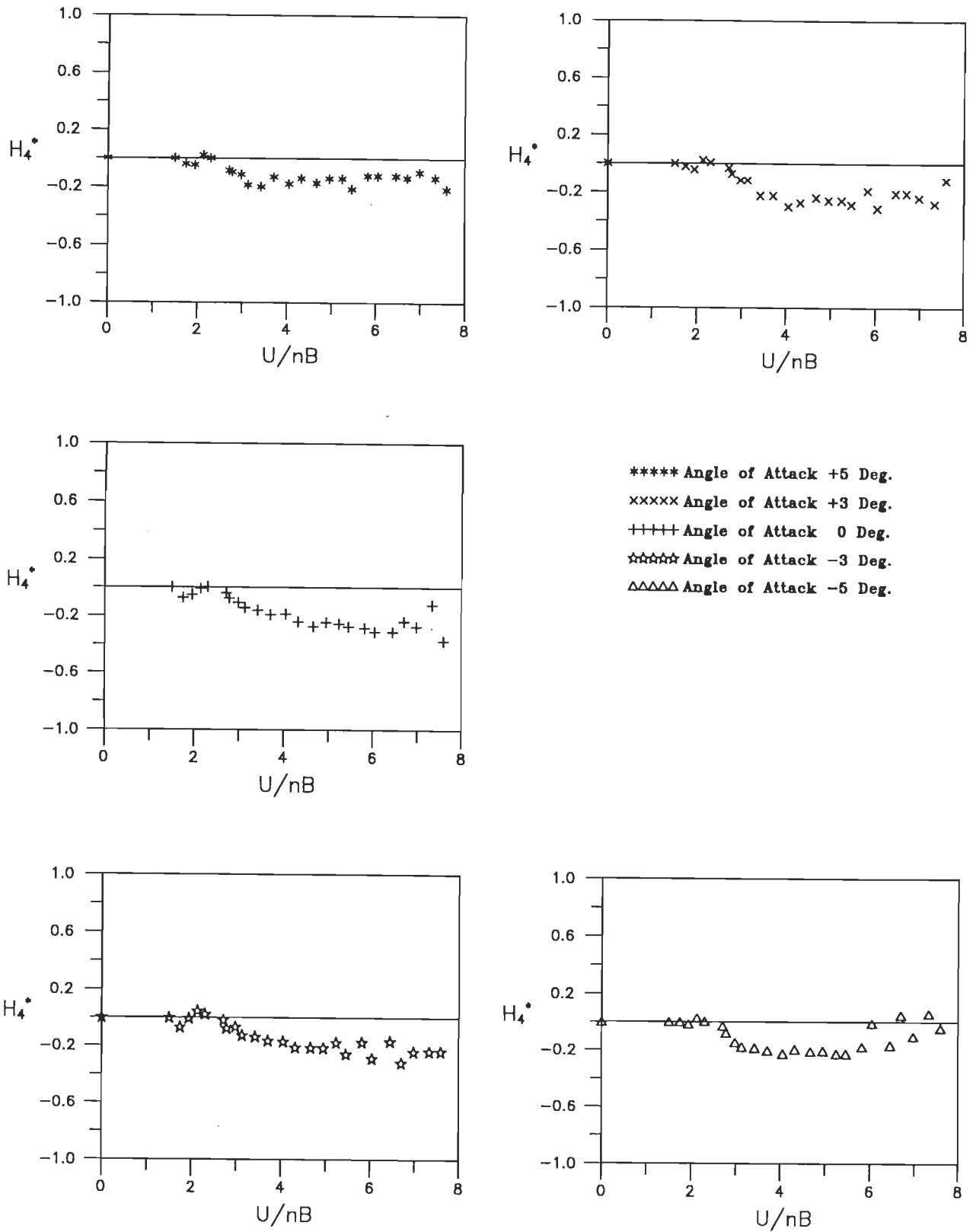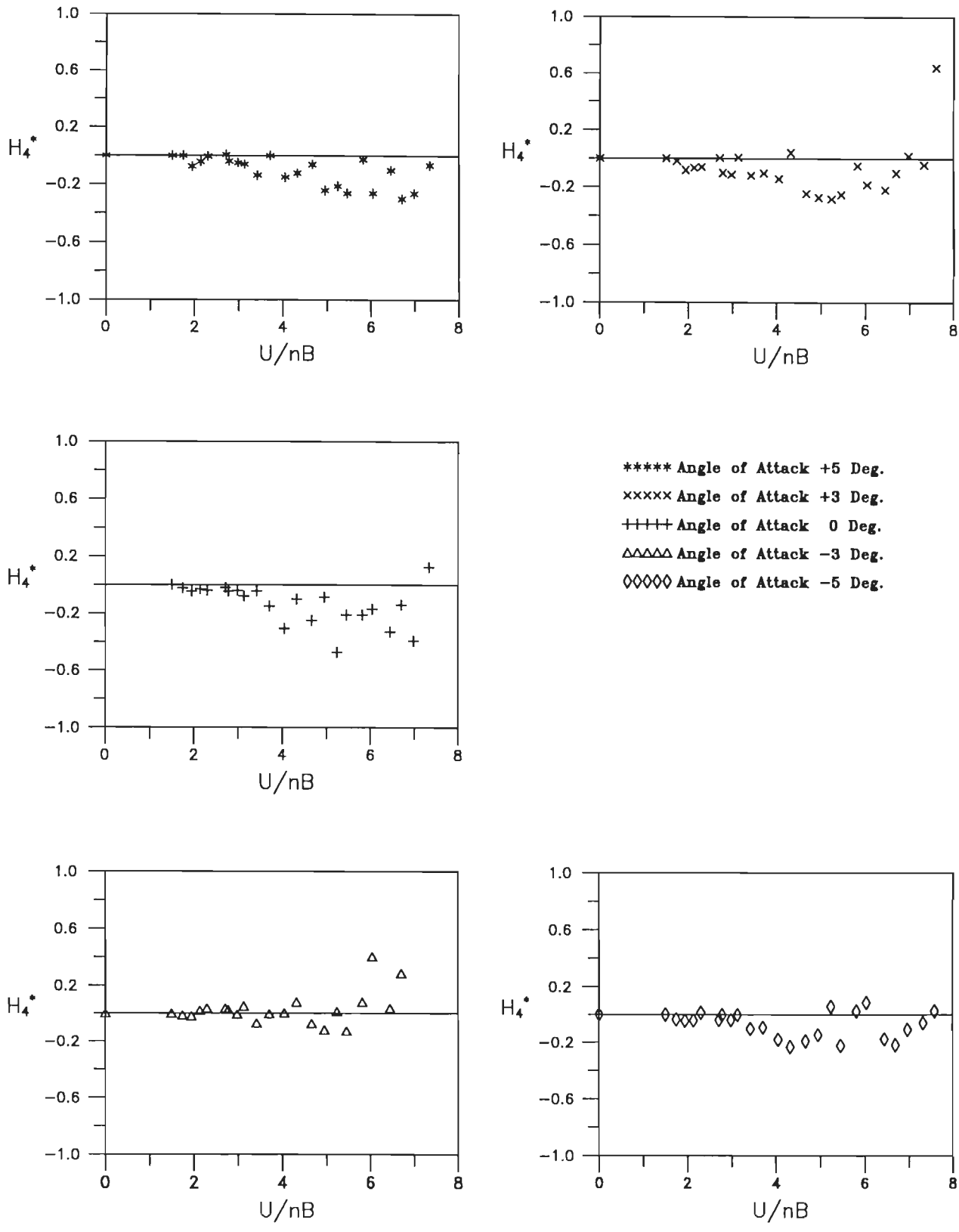
Fig. 6.16(c) Variation of flutter derivative (H_1^*) with wind incidence angles for partially faired section model under grid generated flow (Grid # 2).

Fig. 6.16(d) Variation of flutter derivative (H_1^*) with wind incidence
angles for partially faired section model under grid generated flow
(Grid # 3).

Fig.6.17(a) Variation of flutter derivative (H_4^*) with wind incidence angles
for partially faired section model under grid generated flow(Grid # 1)

Fig.6.17(b) Variation of flutter derivative (H_4^*) with wind incidence angles for partially faired section model under grid generated flow (Grid # 1).
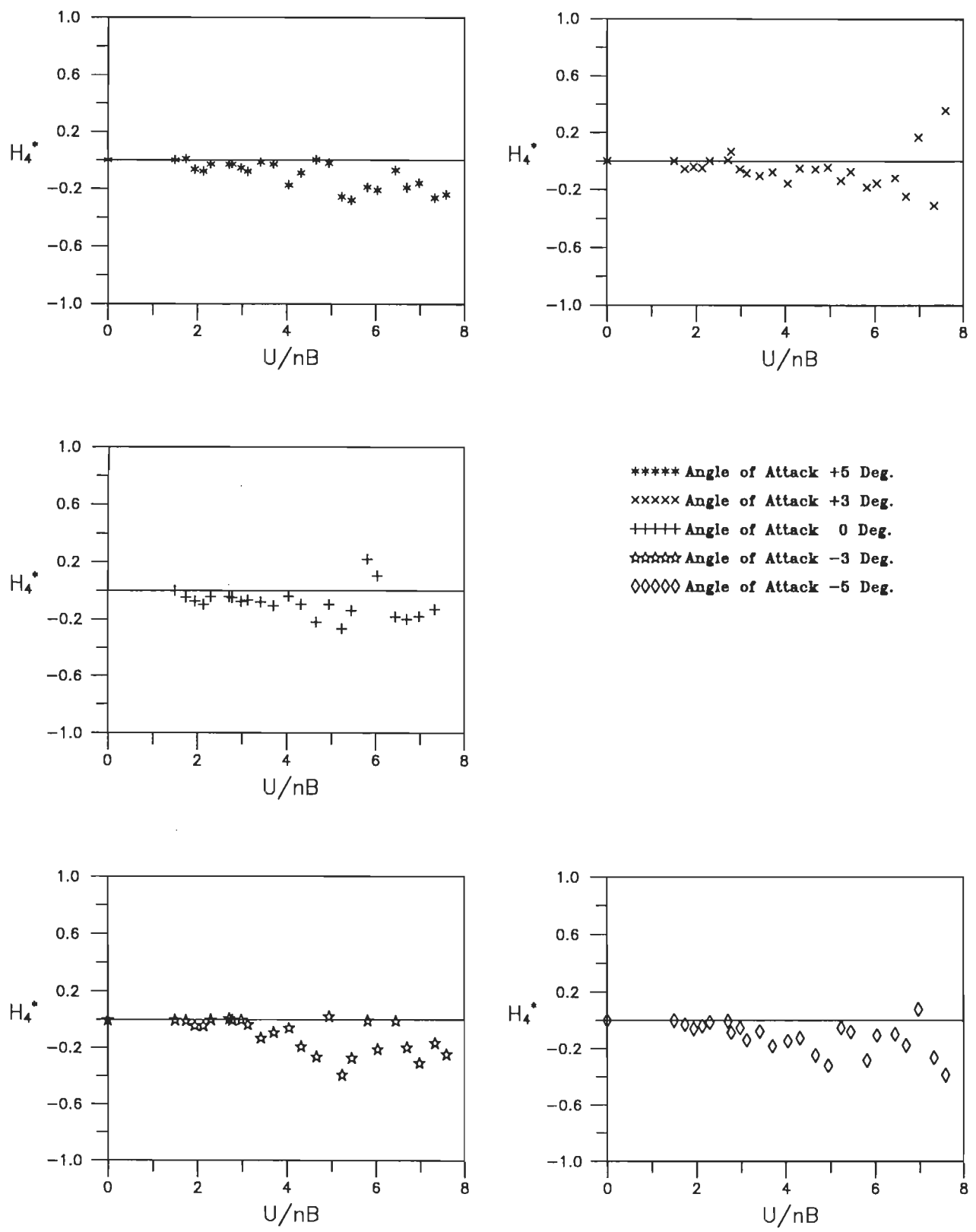
Fig.6.17(c) Variation of flutter derivative (H_4^*) with wind incidence angles for partially faired section model under grid generated flow (Grid # 2)
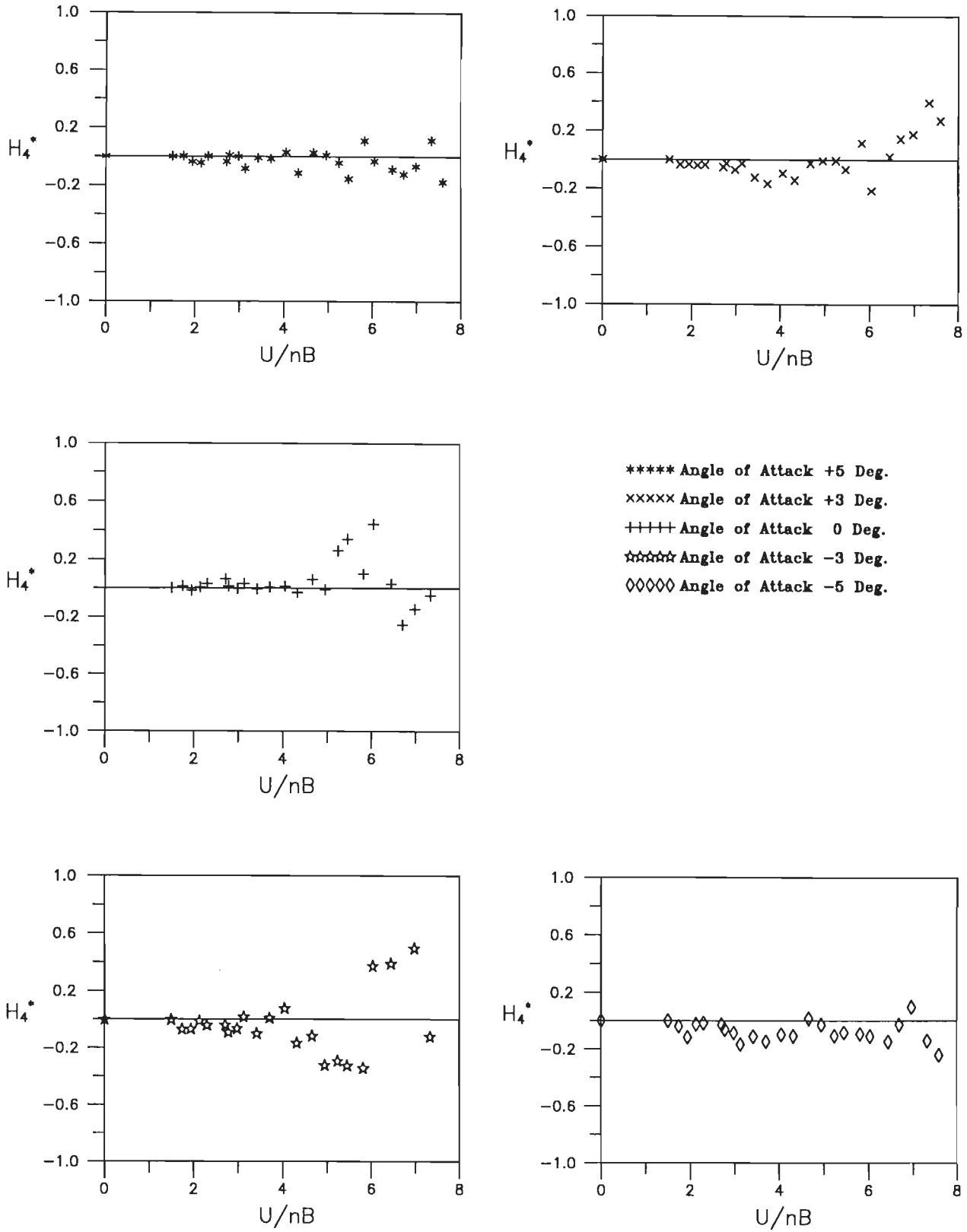
Fig.6.17(d) Variation of flutter derivative (H_4^*) with wind incidence angles
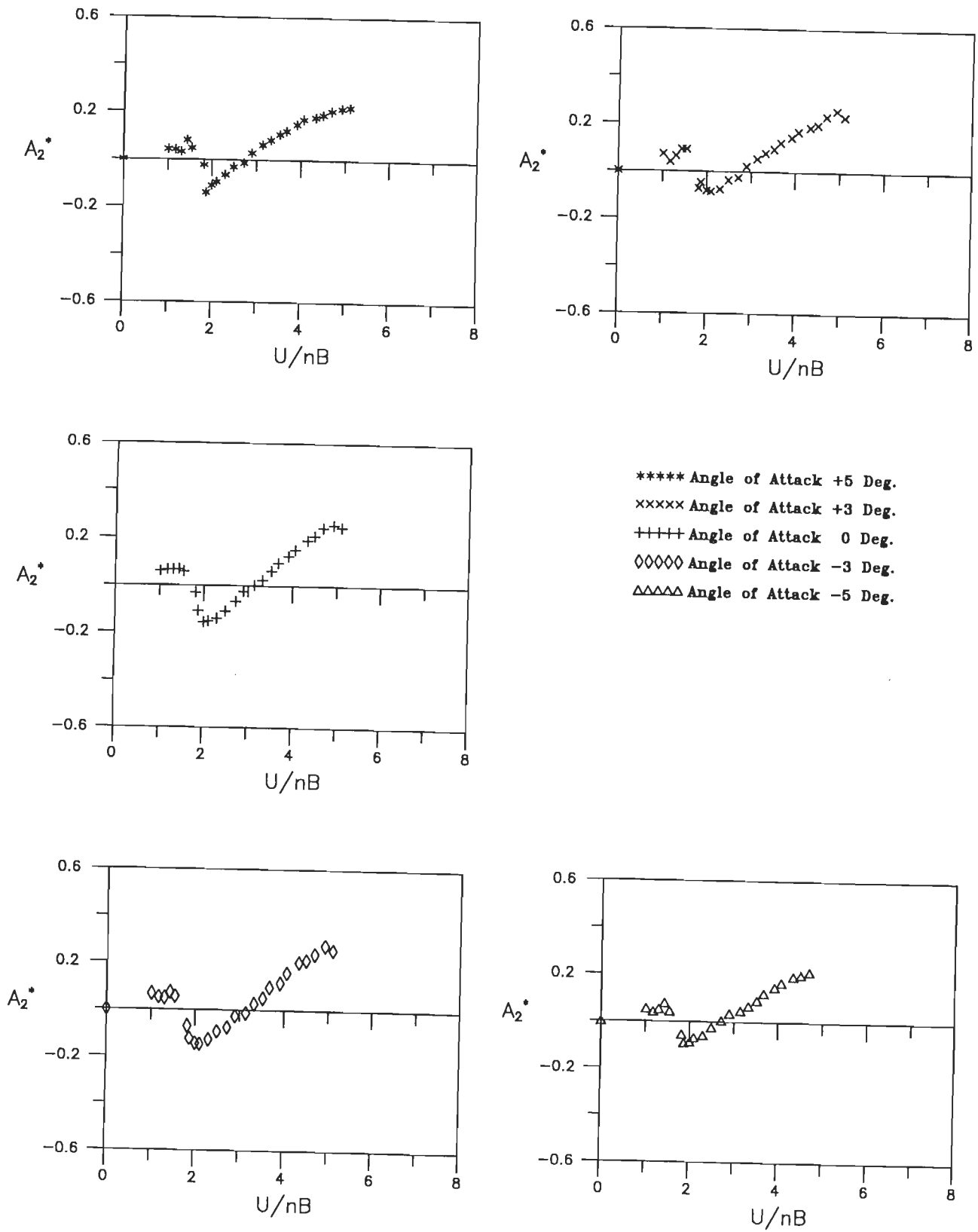for partially faired section model under grid generated flow (Grid # 3).

209

Fig.6.18(a) Variation of flutter derivative A_2^* with wind incidence angles for partially faired section model under smooth flow.
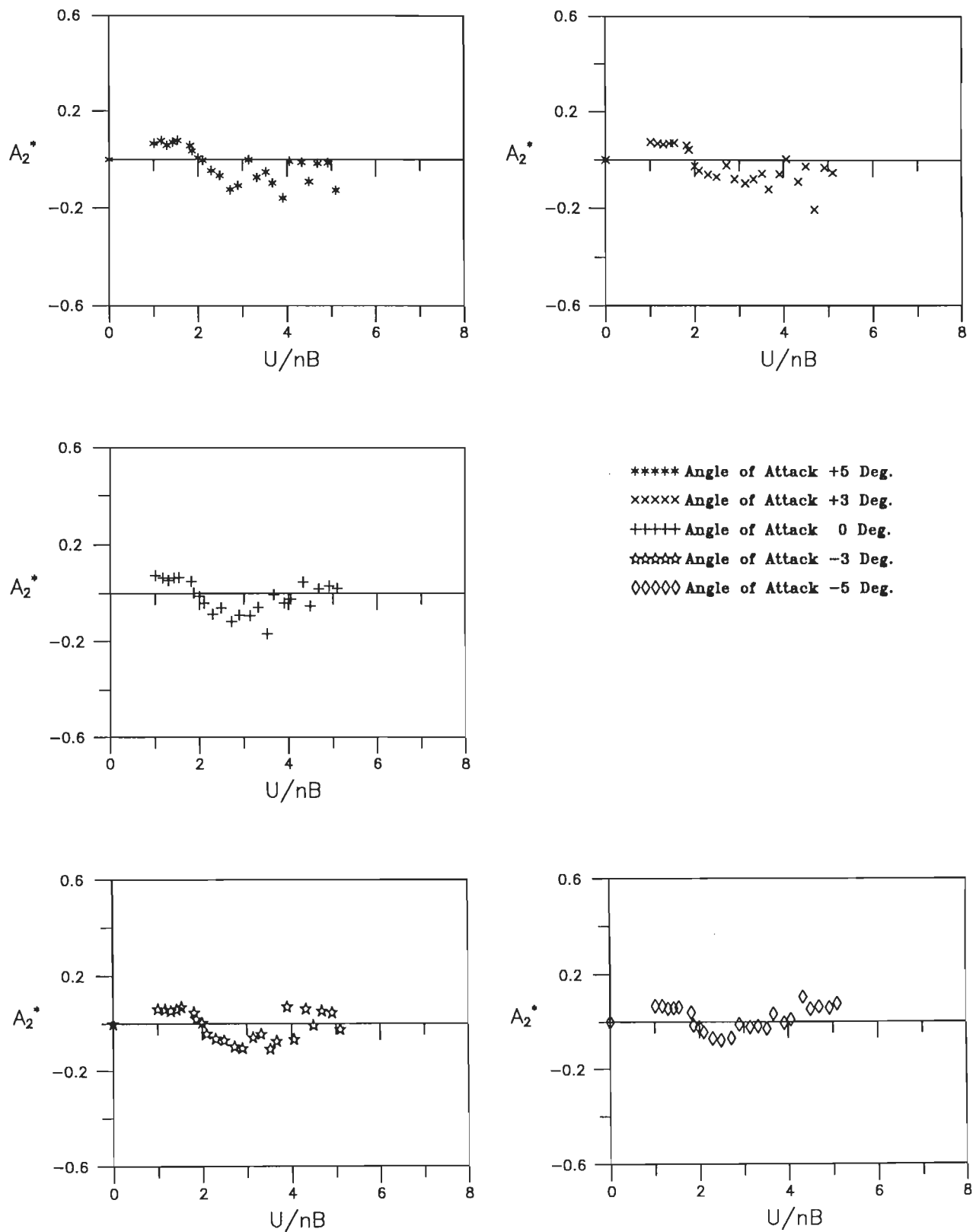
Fig.6.18(b) Variation of flutter derivative A_2^* with wind incidence angles for partially faired section model under grid generated flow (Grid # 1)
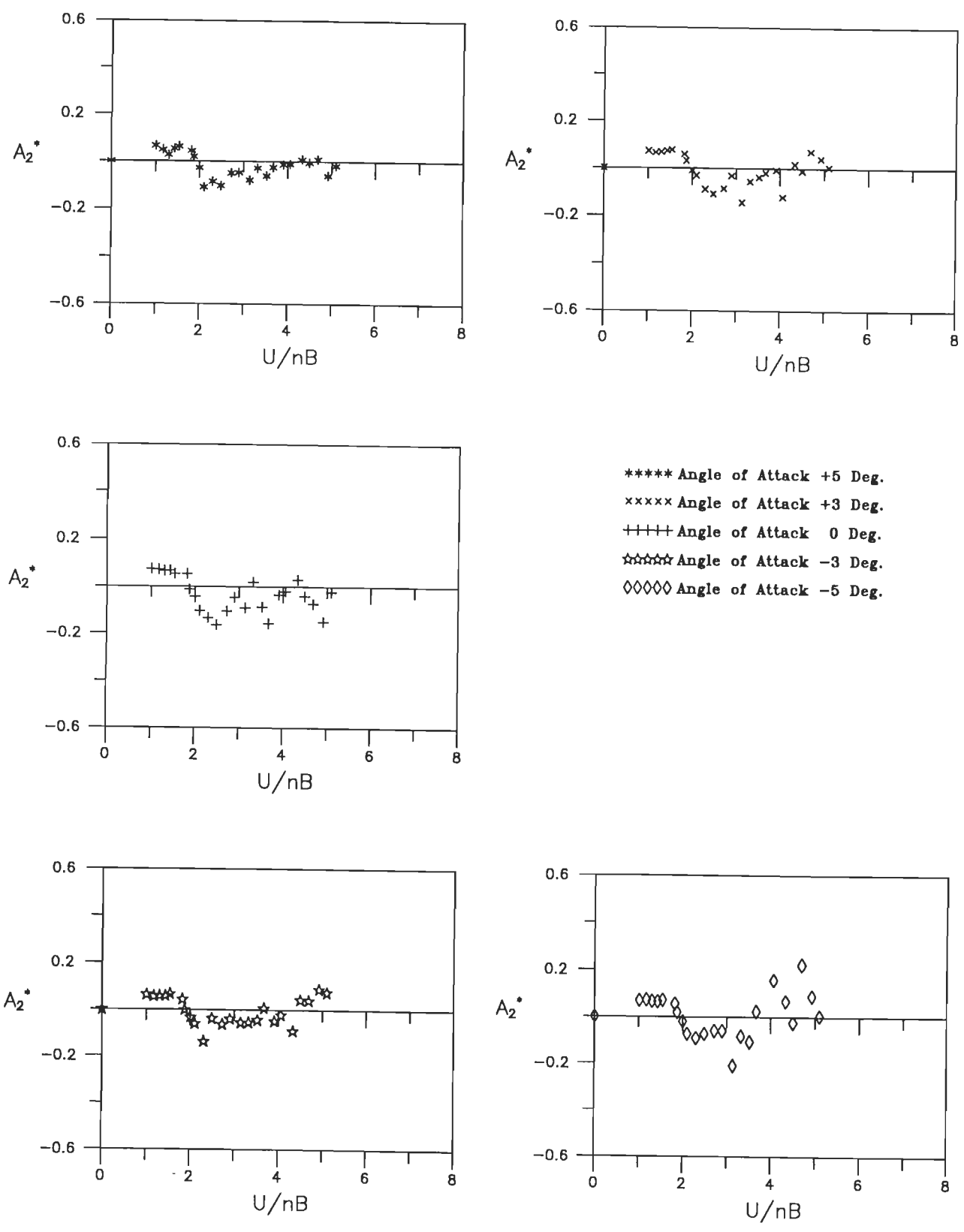
Fig.6.18(c) Variation of flutter derivative A_2^* with wind incidence angles
for partially faired section model under grid generated flow (Grid # 2).

Fig.6.18(d) Variation of flutter derivative A_2^* with wind incidence angles
for partially faired section model under grid geneated flow (Grid # 3)

Fig.6.19(a) Variation of flutter derivative A_3^* with wind incidence angles for partially faired section model under smooth flow.

214

Fig.6.19(b) Variation of flutter derivative A_3^* with wind incidence angles
for partially faired section model under grid generated flow (Grid # 1).

Fig.6.19(c) Variation of flutter derivative A_3^* with wind incidence angles for partially faired section model under grid generated flow (Grid # 2).
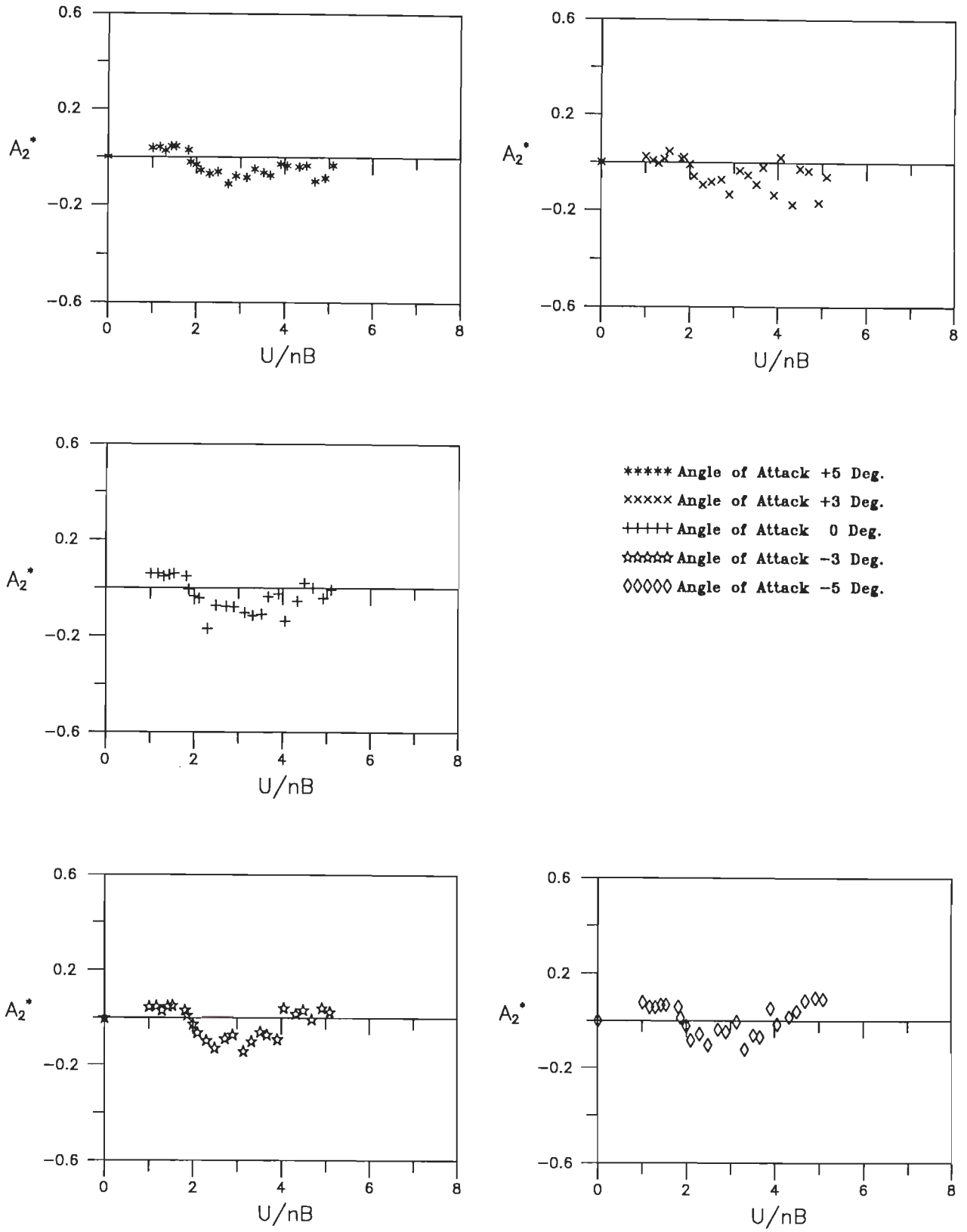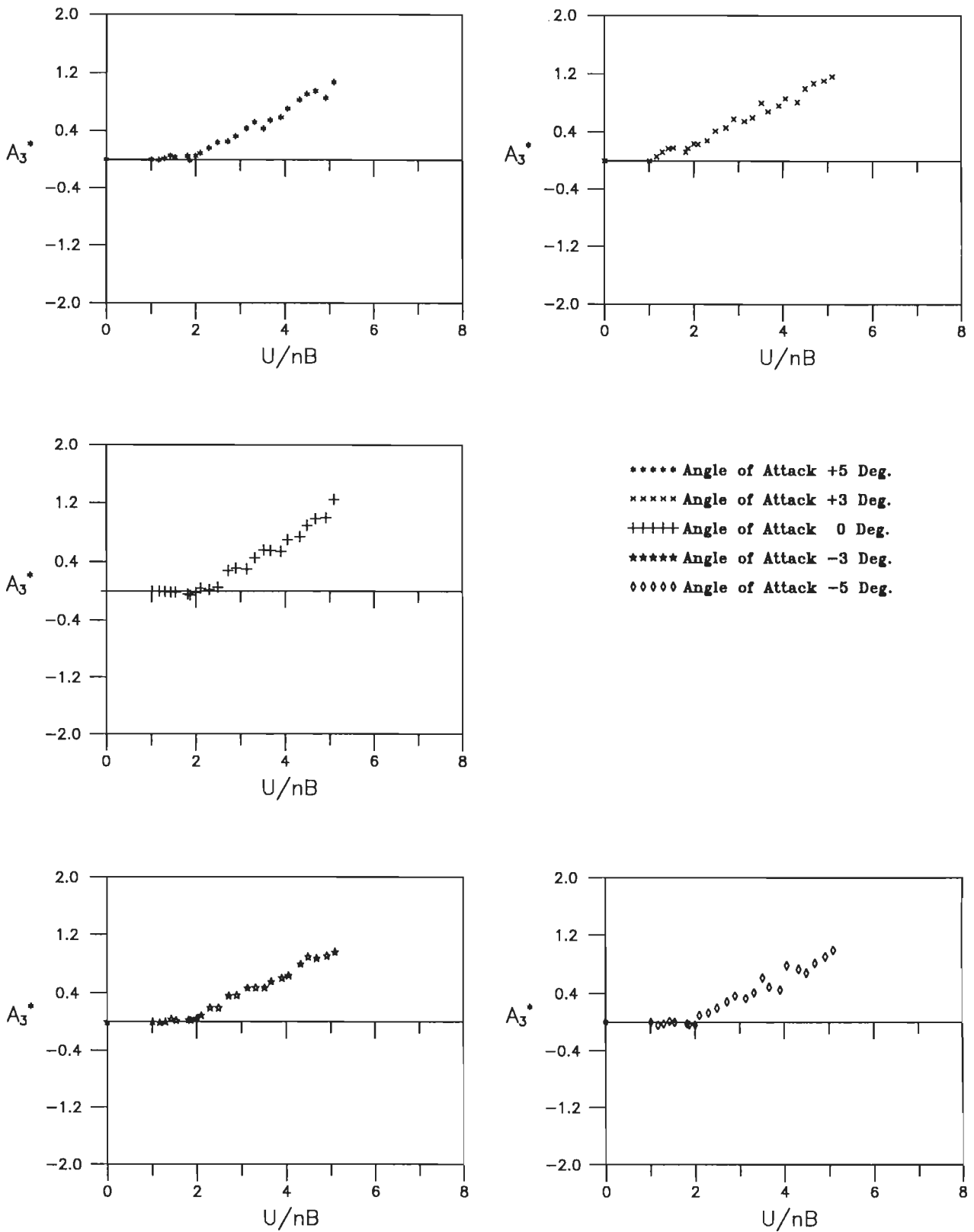
Fig.6.19(d) Variation of flutter derivative A_3^* with wind incidence angles
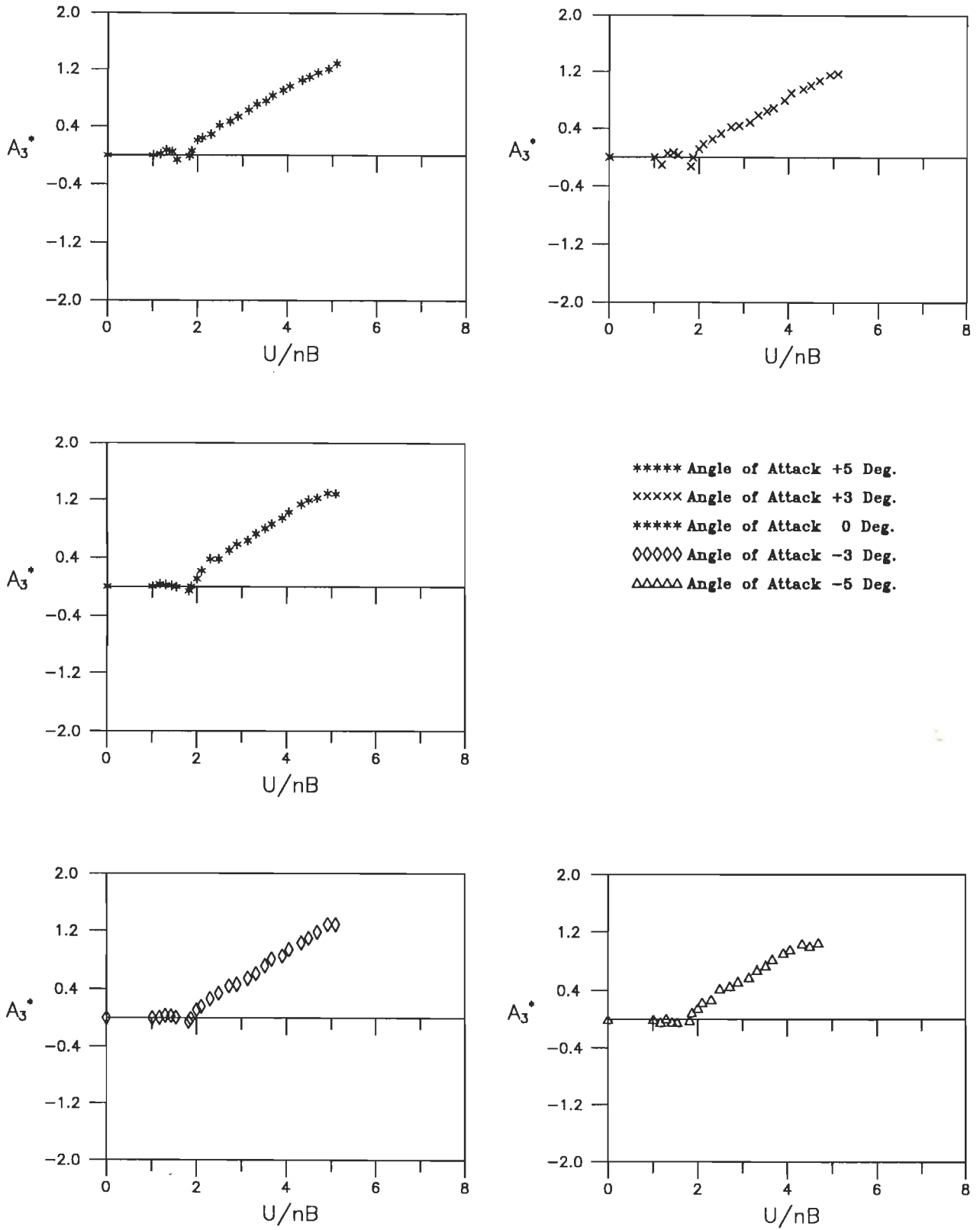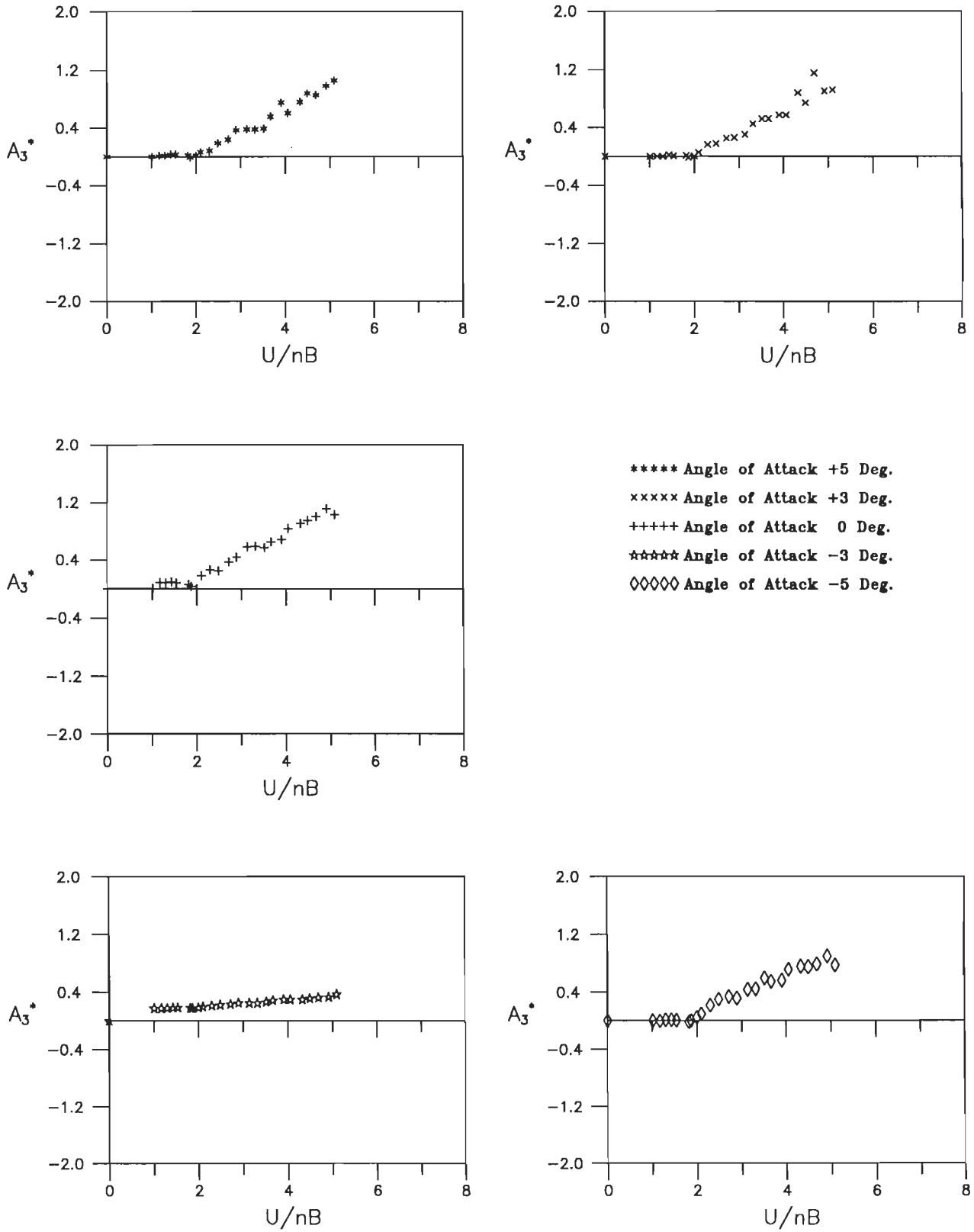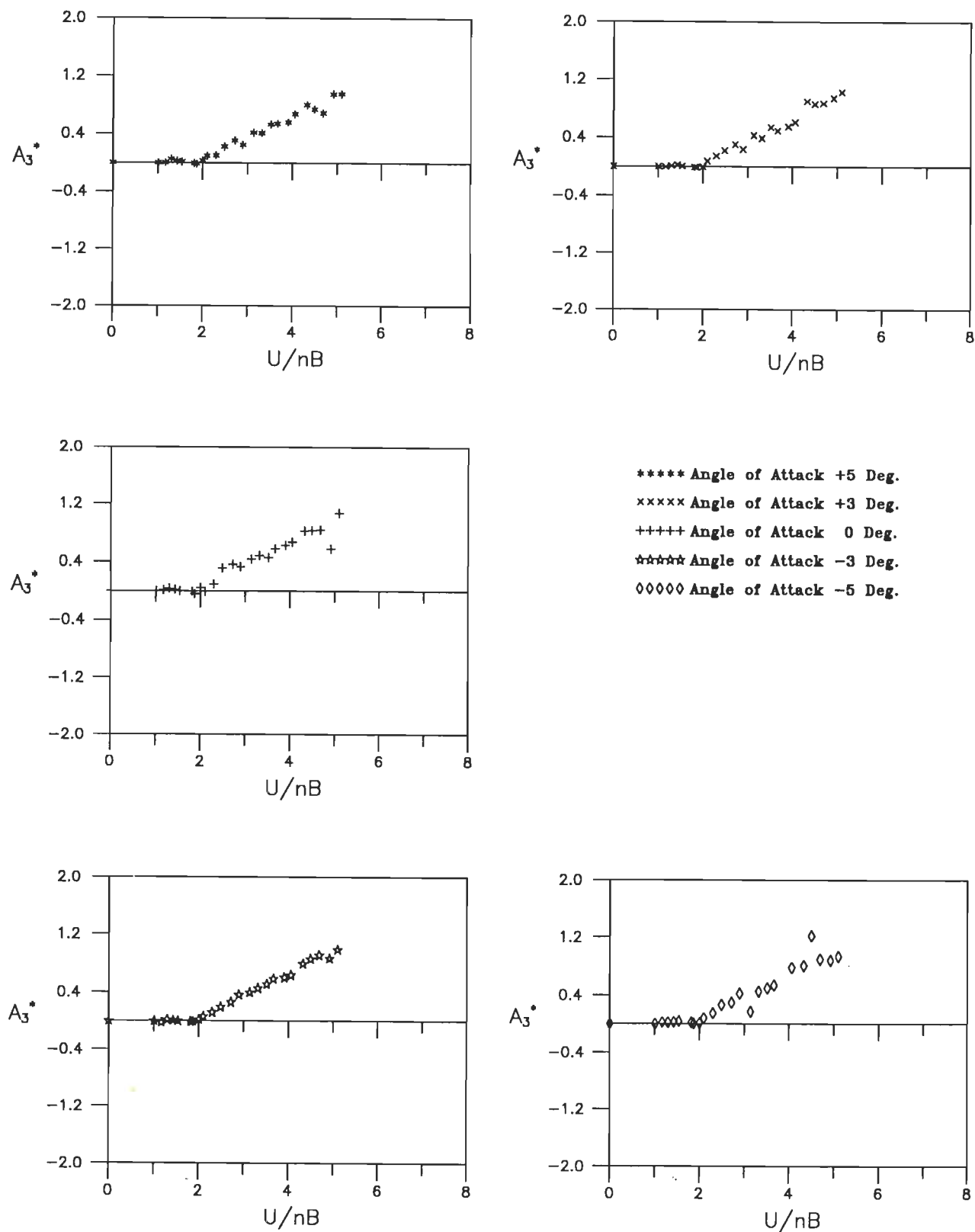for partially faired section model under grid generated flow (Grid # 3)
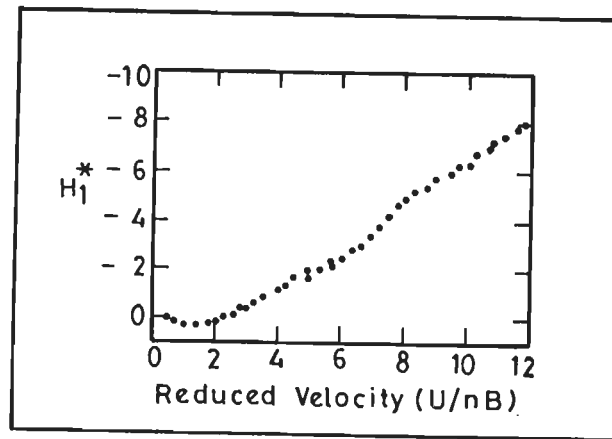
Fig.6.20 Variation of H_1 with reduced velocity for streamlined steel box girder deck (Sarkar et al.[5])
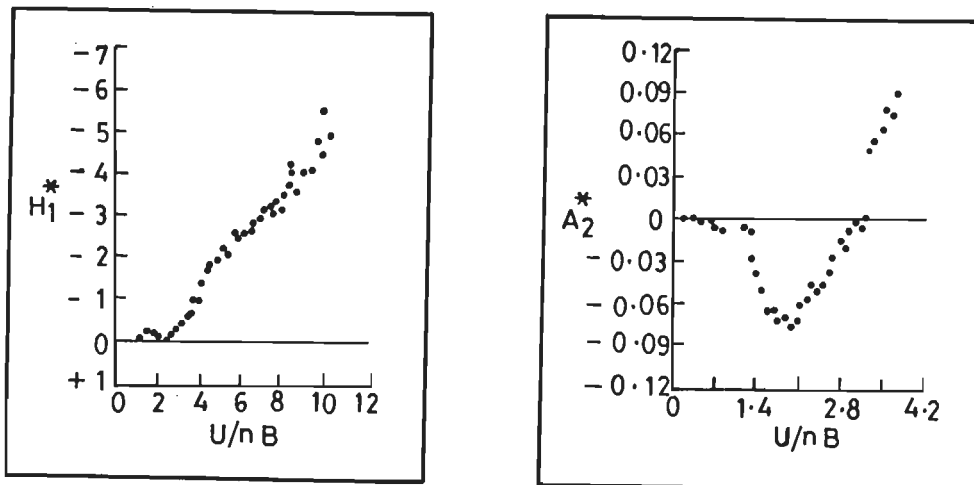
Fig.6.21 Variation of flutter derivatives for truss stiffened deck (Bosch[3])
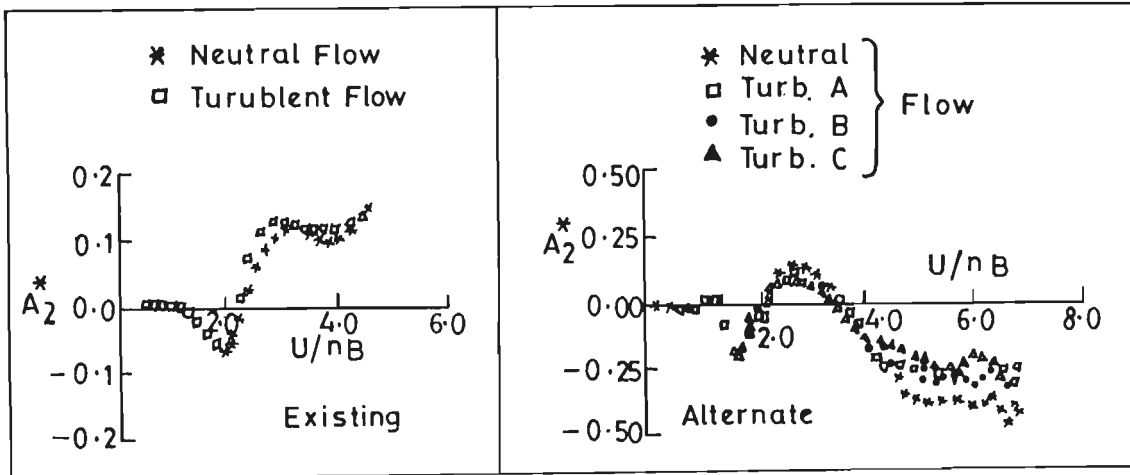
Fig.6.22 Derivatives of Deer Isle Sedgwick bridge composite deck (Bosch[2]).
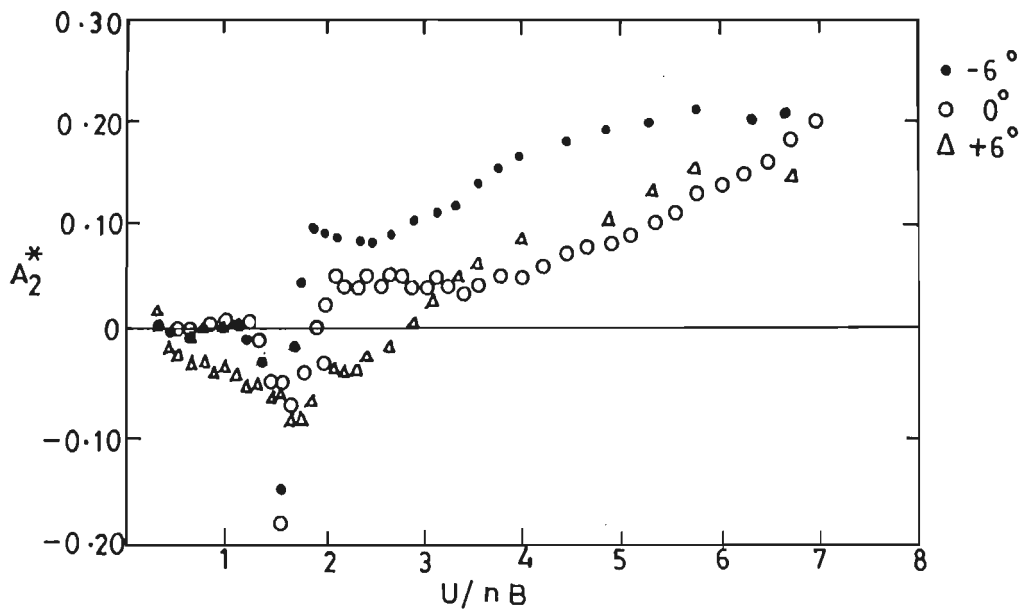
Fig.6.23 Variation of flutter derivative with wind incidence angle for 1:80 section model of concrete girder of a cable stayed bridge(Bienkiewicz et al.[1]).
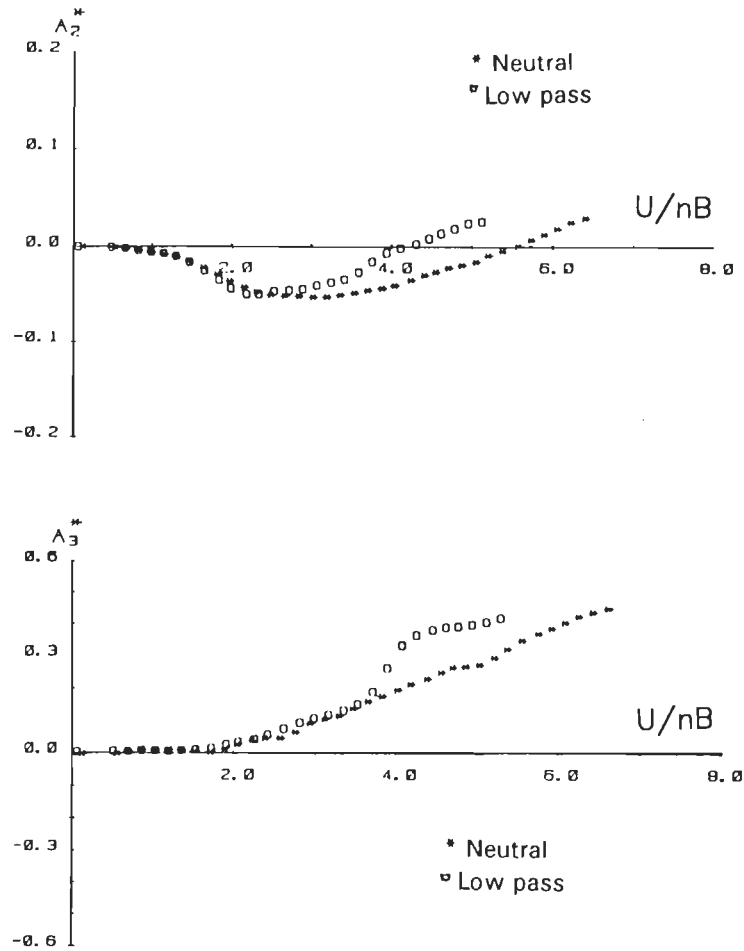
Fig.6.24 Derivatives of Golden Gate bridge deck (Houston et al.[4]).
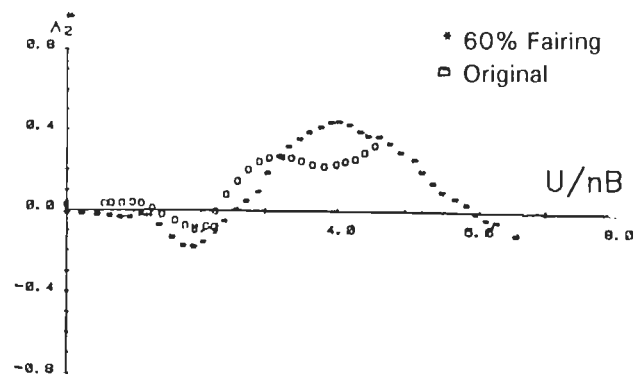
Fig.6.25 Plot showing the effect of fairing on the
flutter derivative (Houston et al.[4]).
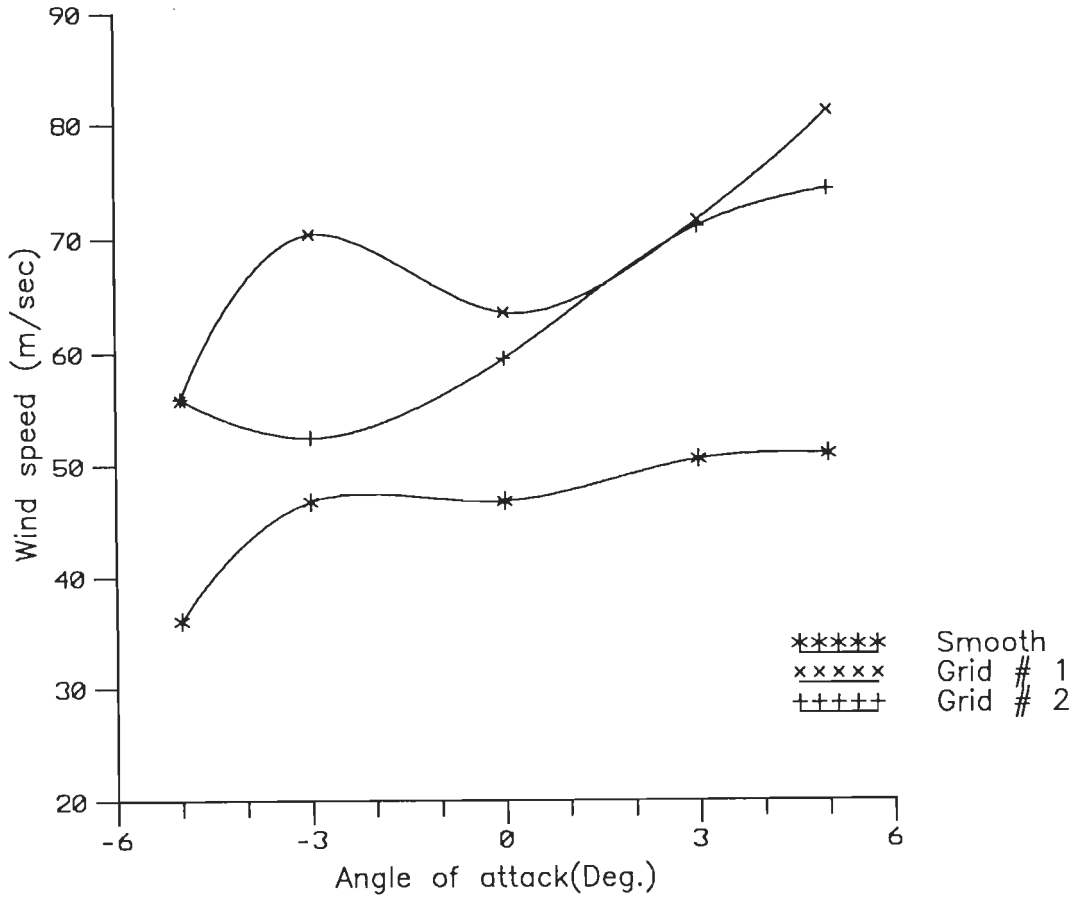
Fig. 6.26 Variation of threshold velocity with wind incidence angles under different flow conditions for unmodified deck section.
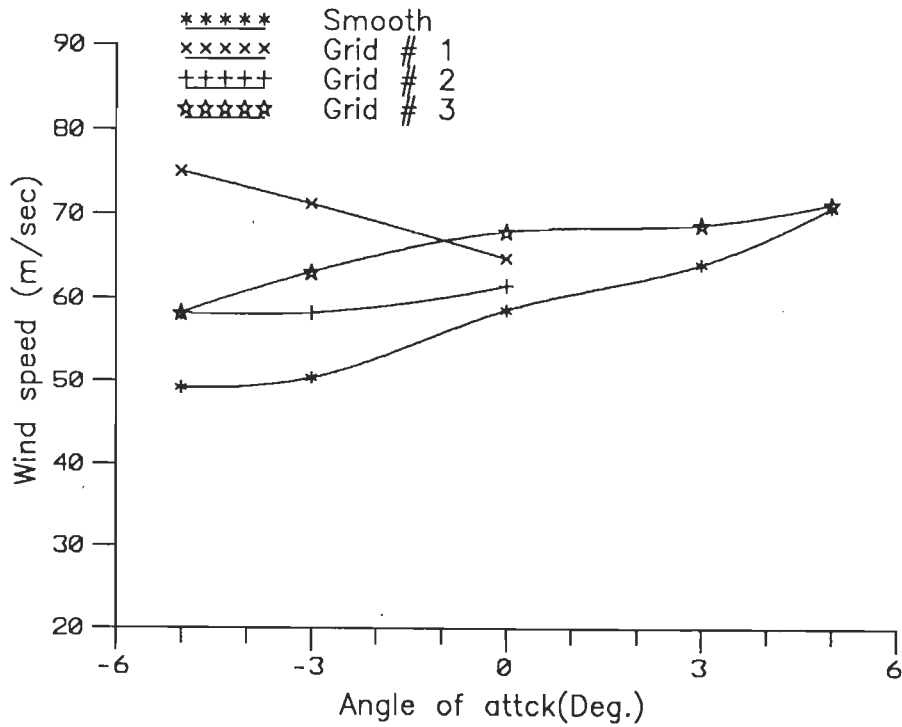
Fig. 6.27 Variation of threshold velocities with wind incidence angles under different flow conditions for fully faired deck section.
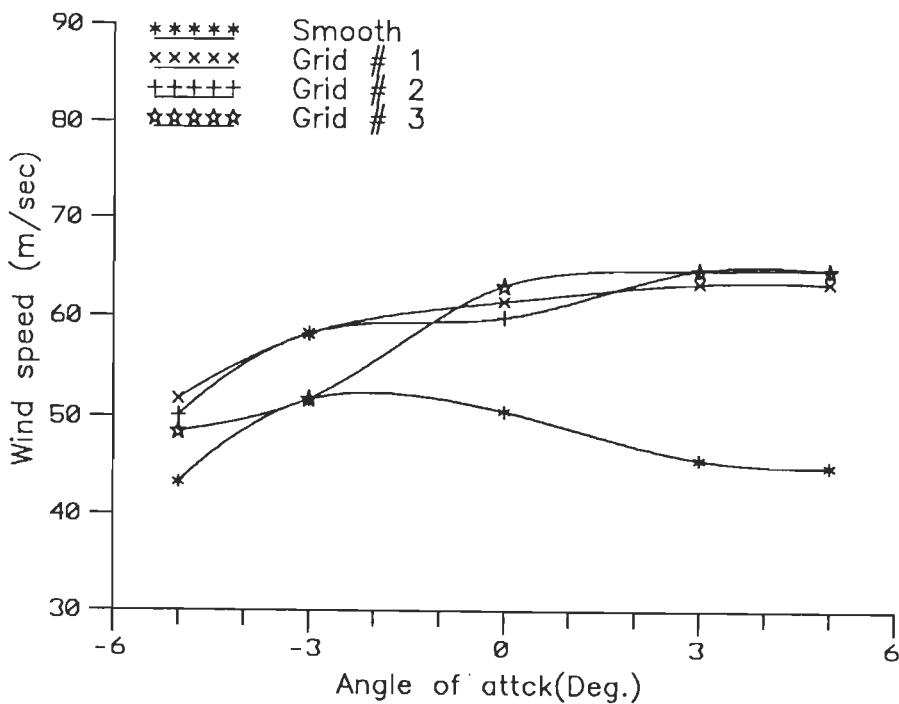
Fig. 6.28 Variation of threshold velocities with wind incidence angles under different flow conditions for partially faired deck section
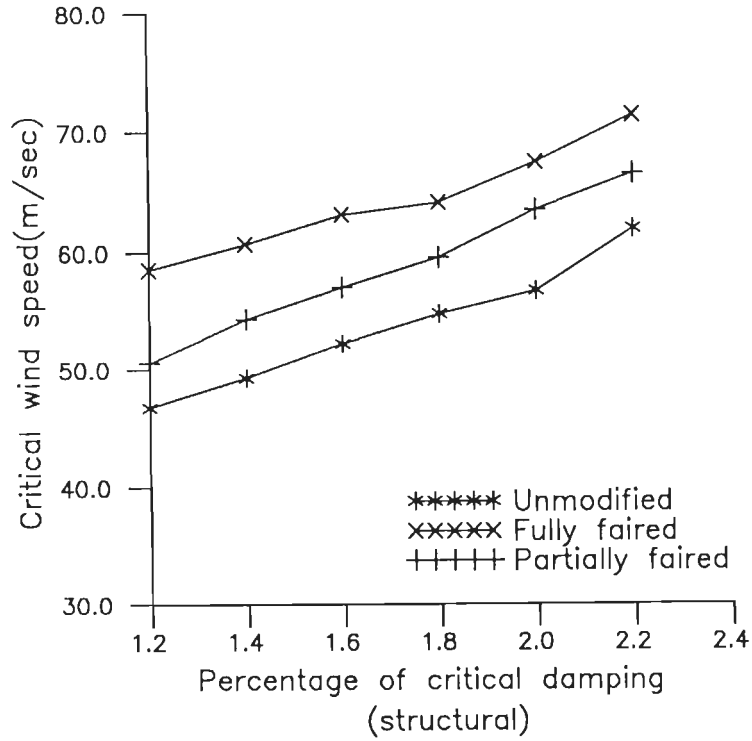
Fig.6.29 Variaton of critical wind speed with damping for prototype bridge under smooth flow condition at 0 degree angle of attack.
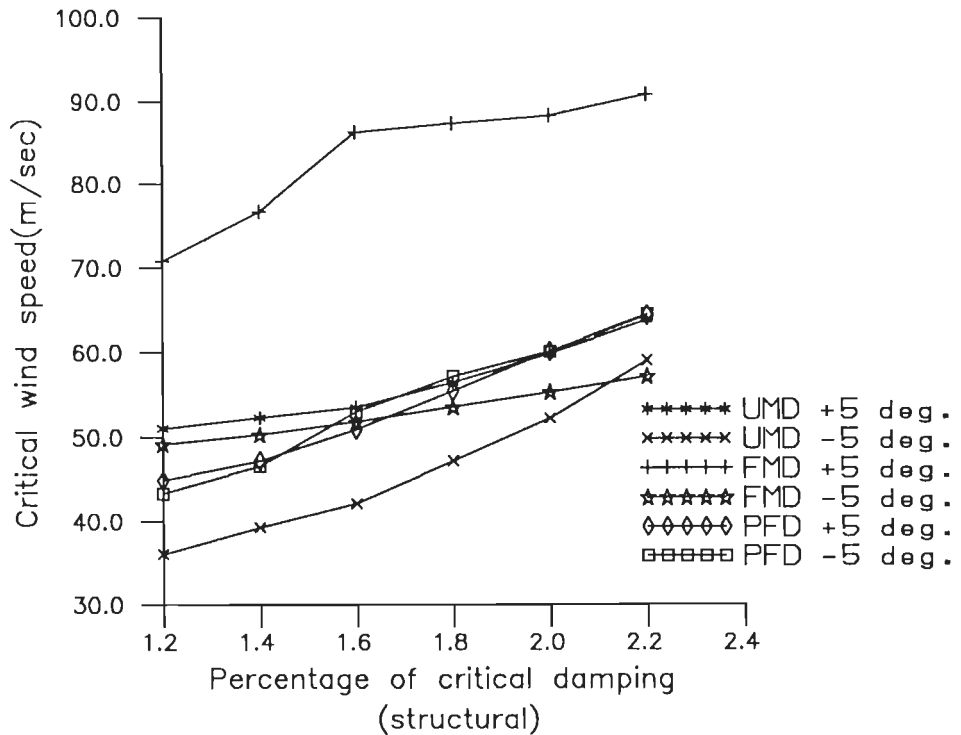
Fig. 6.30 Variation of critical wind speed with damping for prototype bridge under smooth flow for different angle of attacks (UMD — Unmodified deck, FMD — Fully faired deck, PFD — Partially faired deck)

Fig.6.31(a) Cumulative modal response of the main span of Bridge # 1 in pure bending at quarter span. (Unmodified deck section)

Fig.6.31(b) Cumulative modal response of the main span of Bridge # 1 in pure bending at mid span. (Unmodified deck section)

Fig.6.32(a) Cumulative modal response of the main span of Bridge # 1 in pure bending at quarter span. (Faired deck section)

Fig.6.32(b) Cumulative modal response of the main span of Bridge # 1 in pure bending at quarter span. (Faired deck section)

Fig.6.33(a) Cumulative modal response of the main span of
Bridge # 1 in pure torsion at quarter span.
(Unmodified deck section)

Fig.6.33(b) Cumulative modal response of the main span of
Bridge # 1 in pure torsion at mid span.
(Unmodified deck section)

Fig.6.34(a) Cumulative modal response of the main span of
Bridge # 1 in pure torsion at quarter span.
(Faired deck section)

Fig.6.34(b) Cumulative modal response of the main span of
Bridge # 1 in pure torsion at mid span.
(Faired deck section)
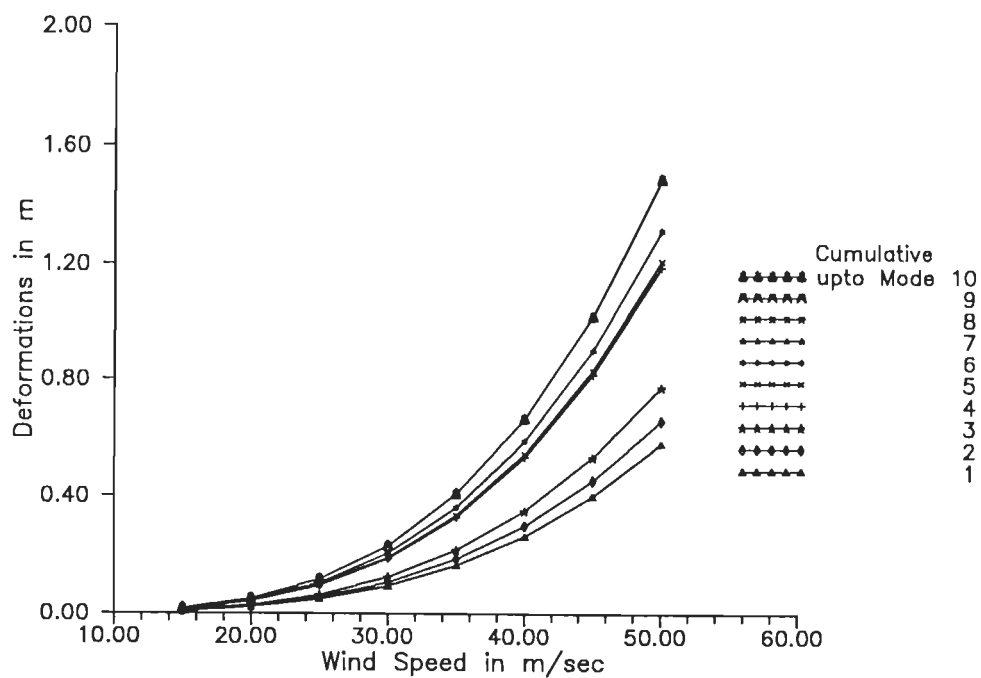
Fig.6.35(a) Cumulative modal response of the main span of Bridge # 2 in pure bending at quarter span. (Unmodified deck section)
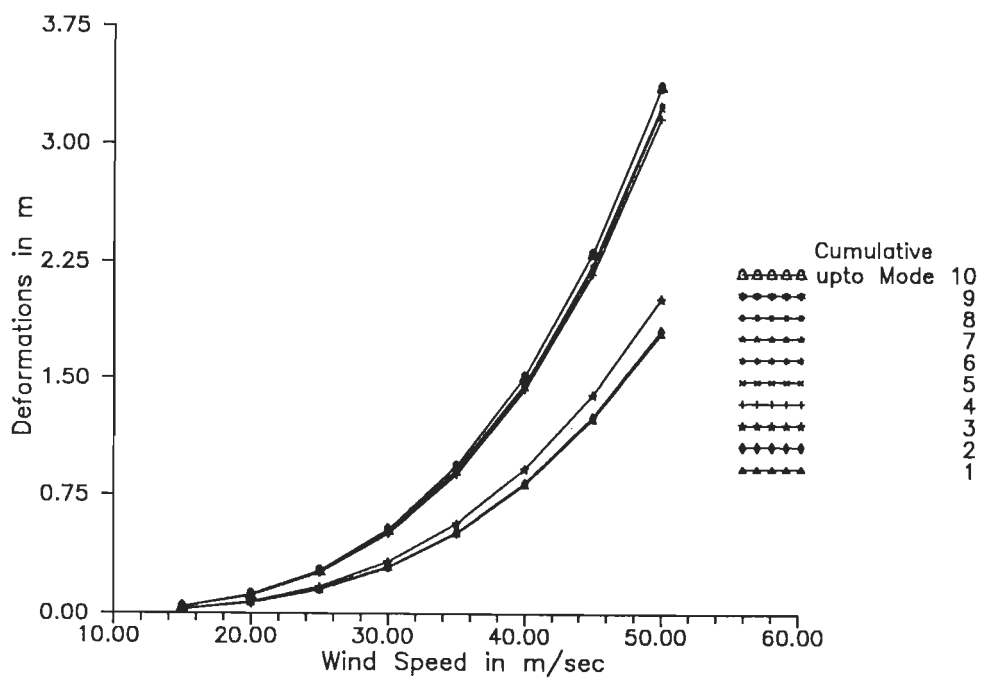
Fig.6.35(b) Cumulative modal response of the main span of Bridge # 2 in pure bending at mid span. (Unmodified deck section)
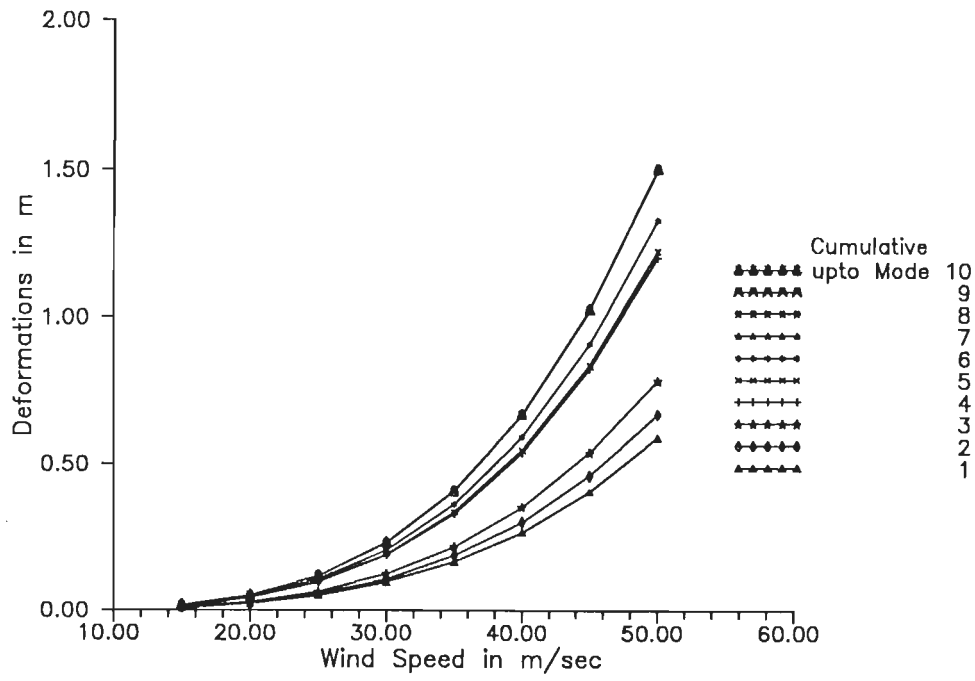
Fig.6.36(a) Cumulative modal response of the main span of Bridge # 2 in pure bending at quarter span. (Faired deck section)
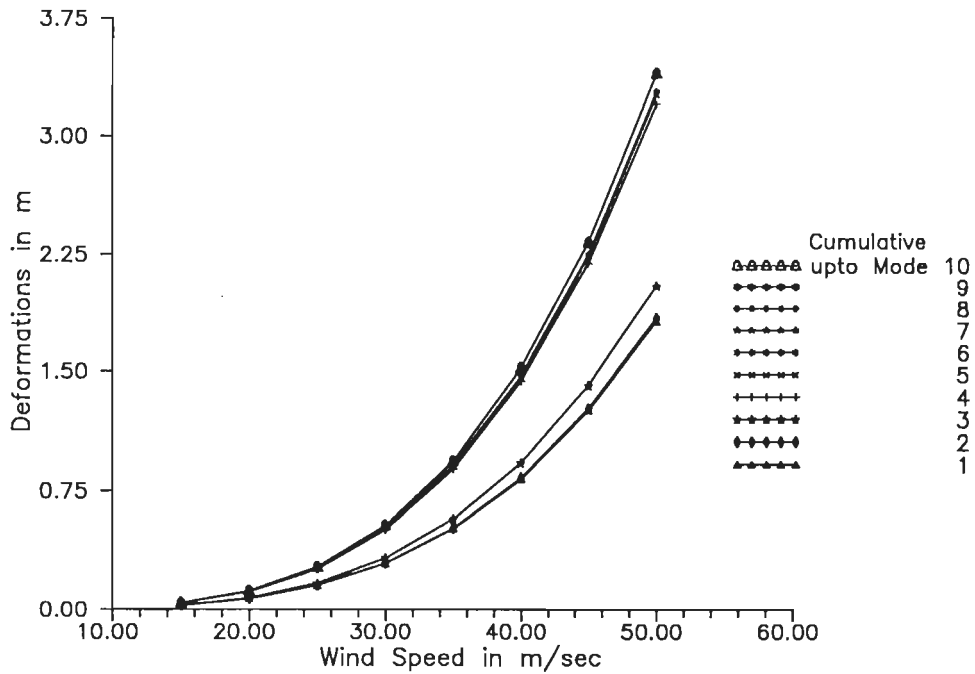
Fig.6.36(b) Cumulative modal response of the main span of Bridge # 2 in pure bending at mid span. (Faired deck section)
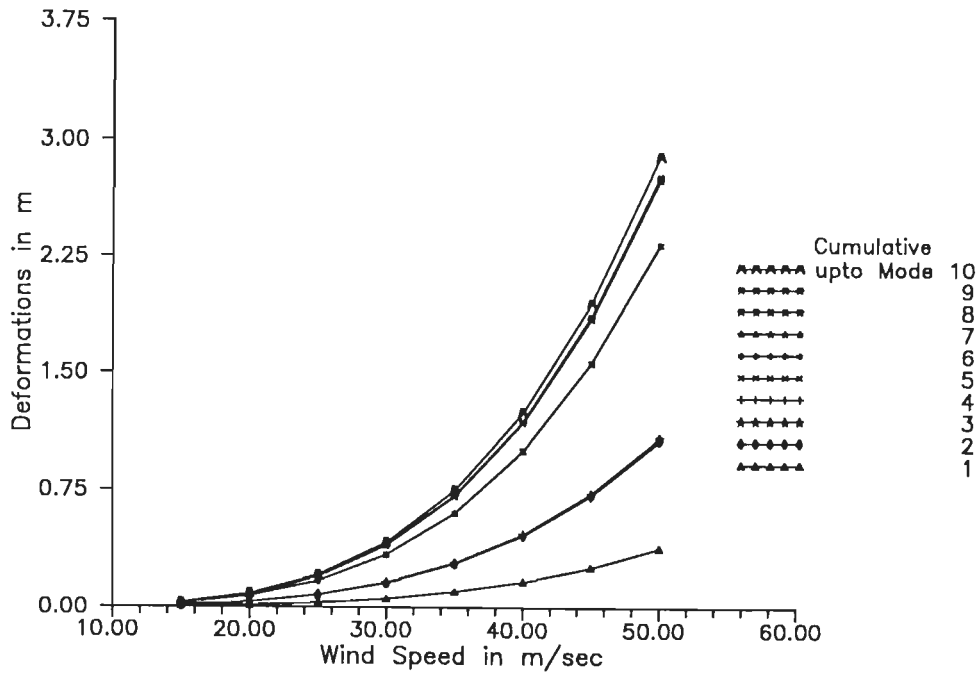
Fig.6.37(a) Cumulative modal response of the main span of Bridge # 2 in pure torsion at quarter span. (Unmodified deck section)
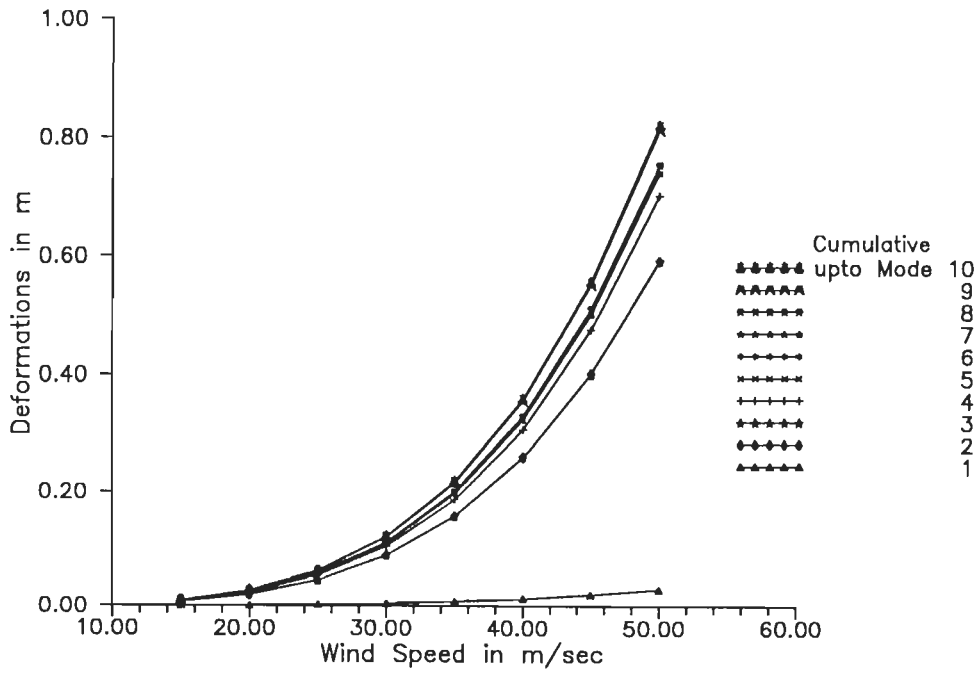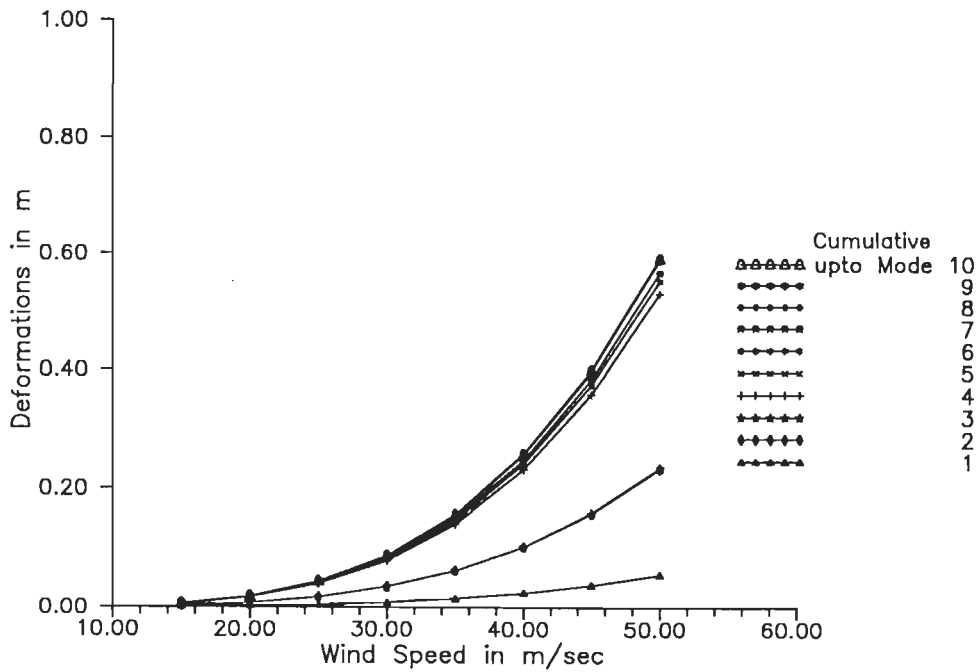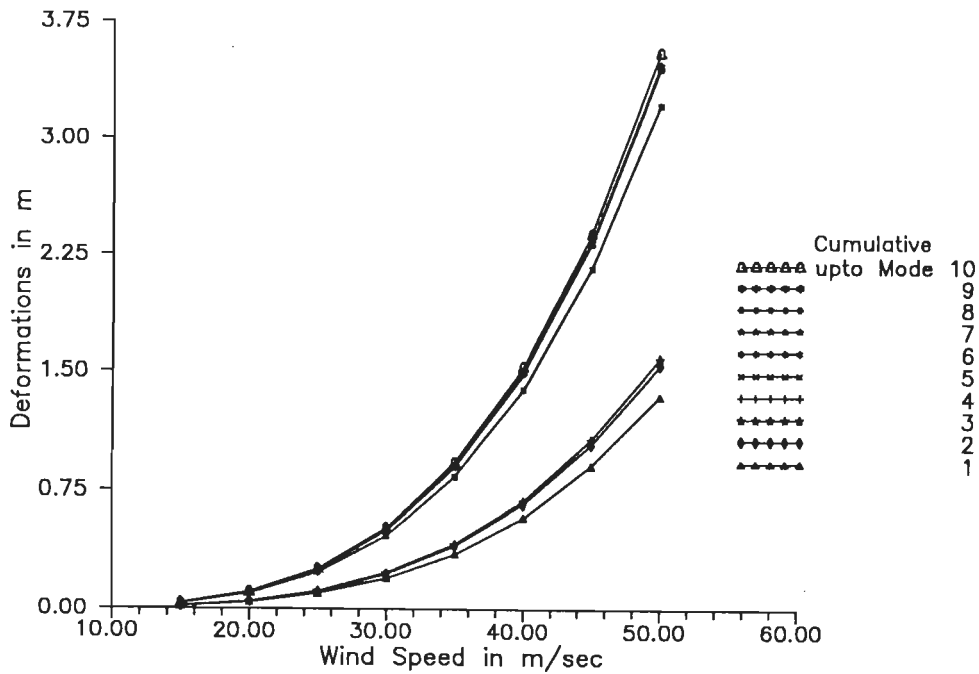

Fig.6.37(b) Cumulative modal response of the main span of Bridge # 2 in pure torsion at quarter span. (Unmodified deck section)
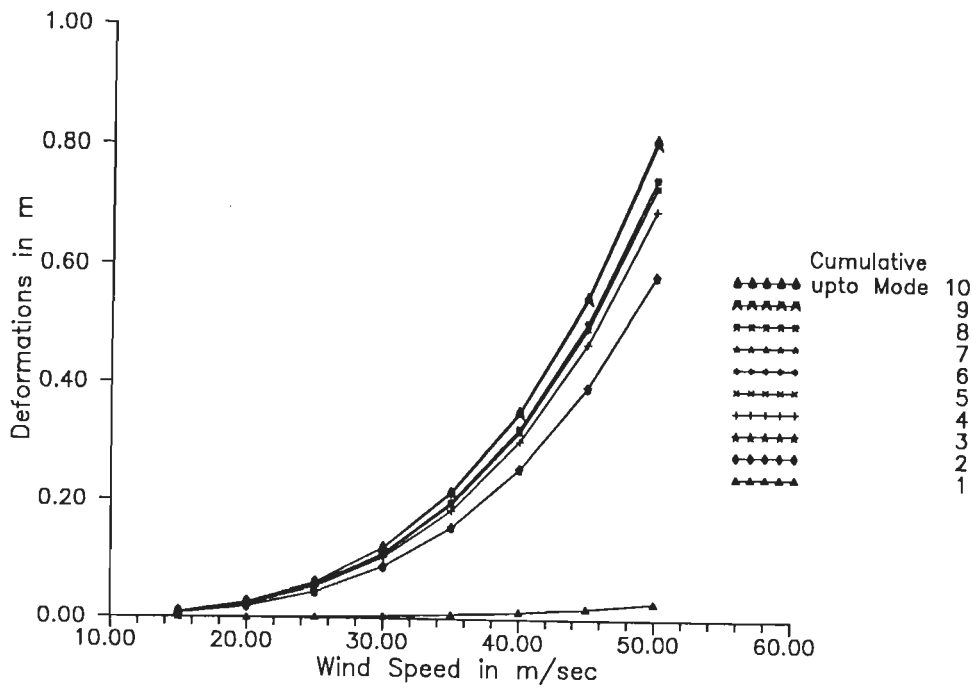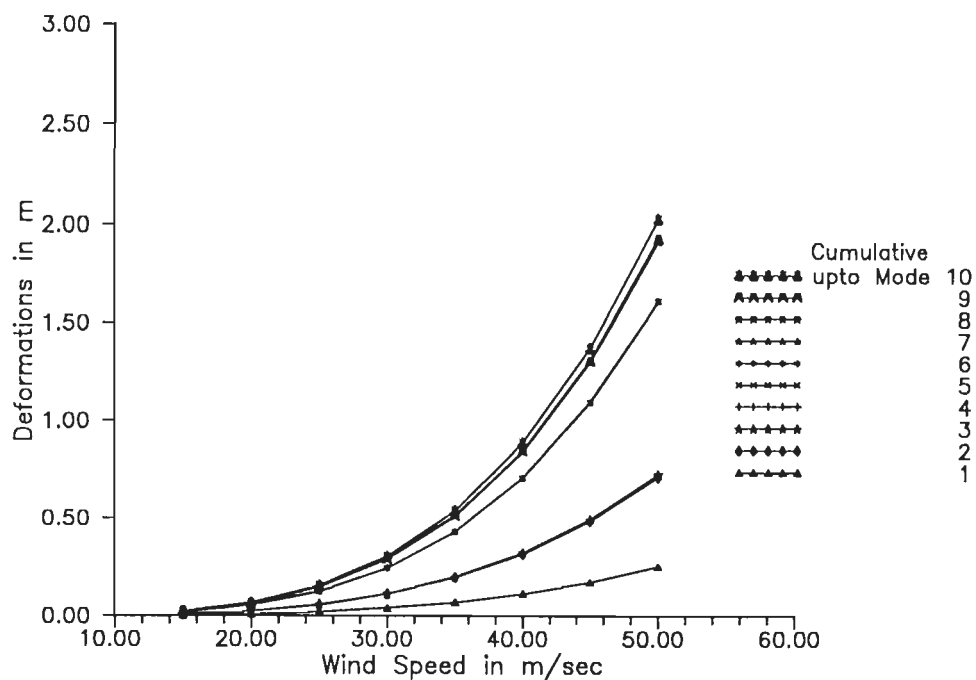
Fig.6.38(a) Cumulative modal response of the main span of Bridge # 2 in pure torsion at quarter span. (Faired deck section)
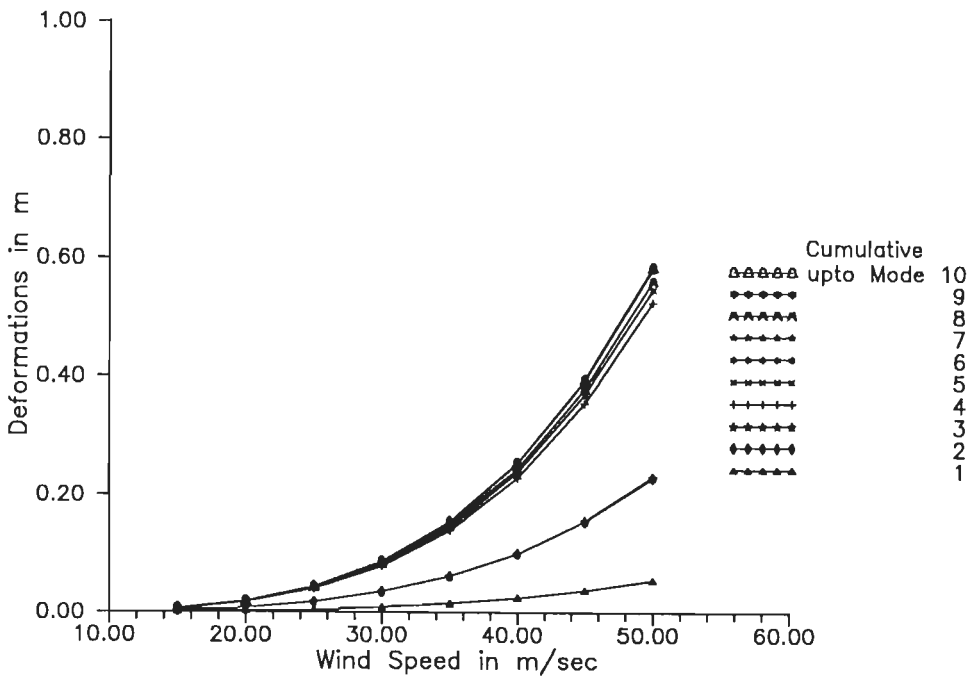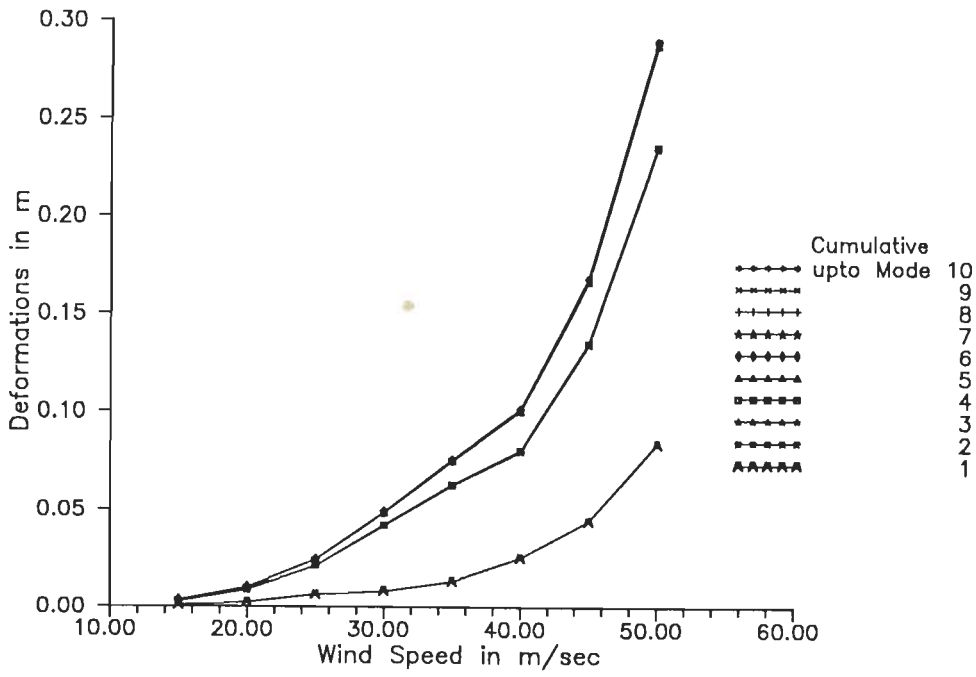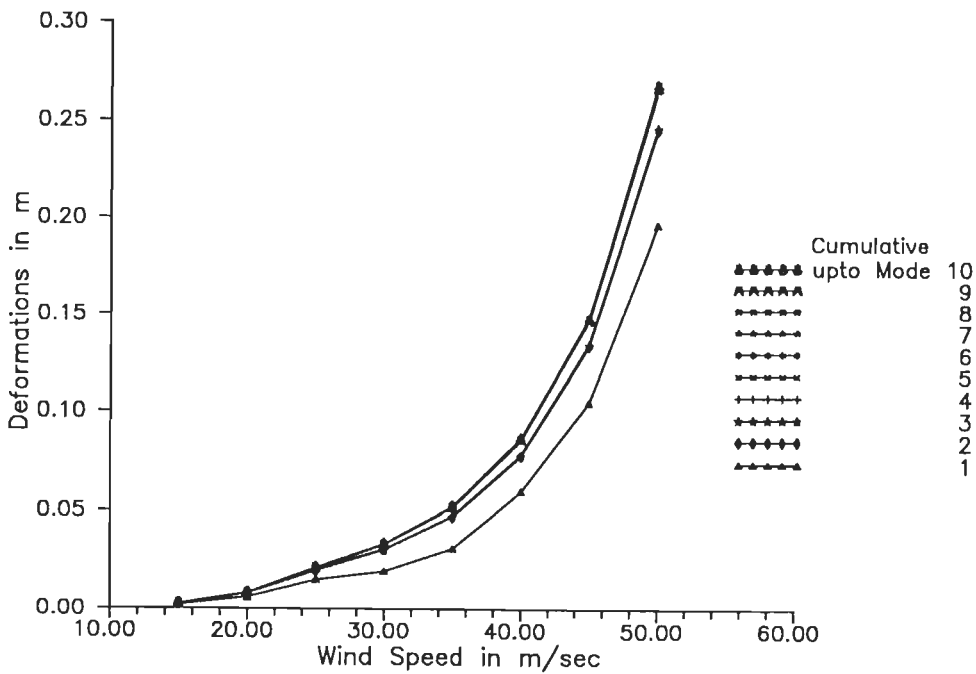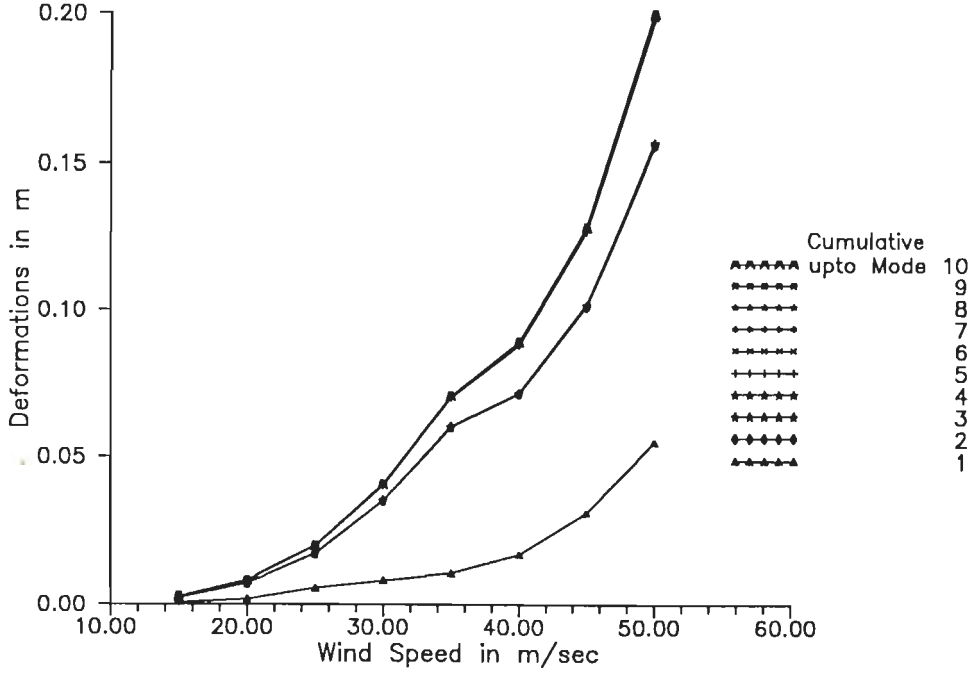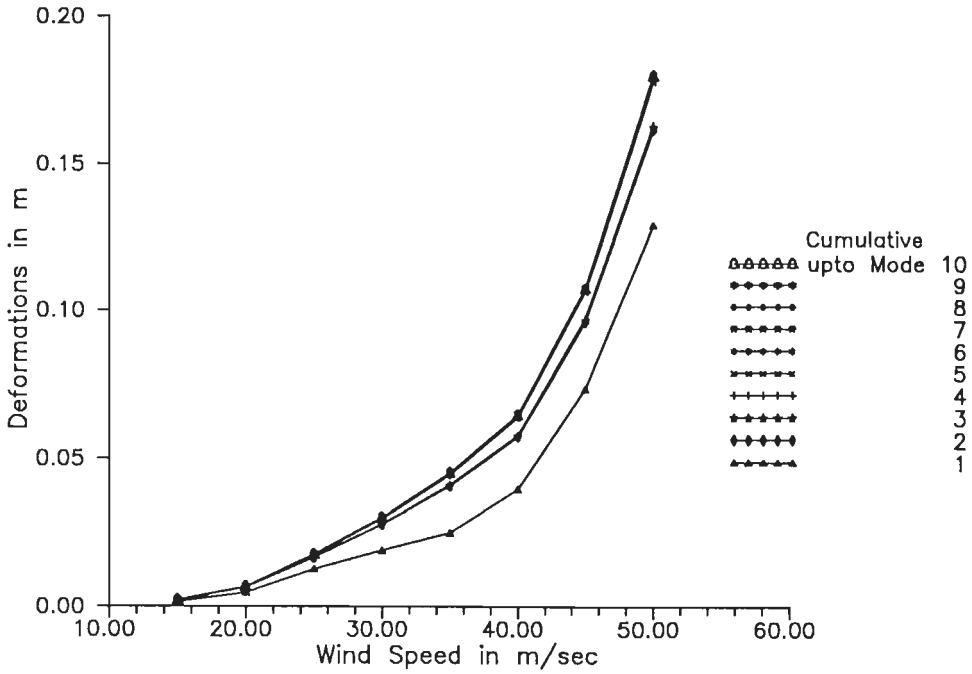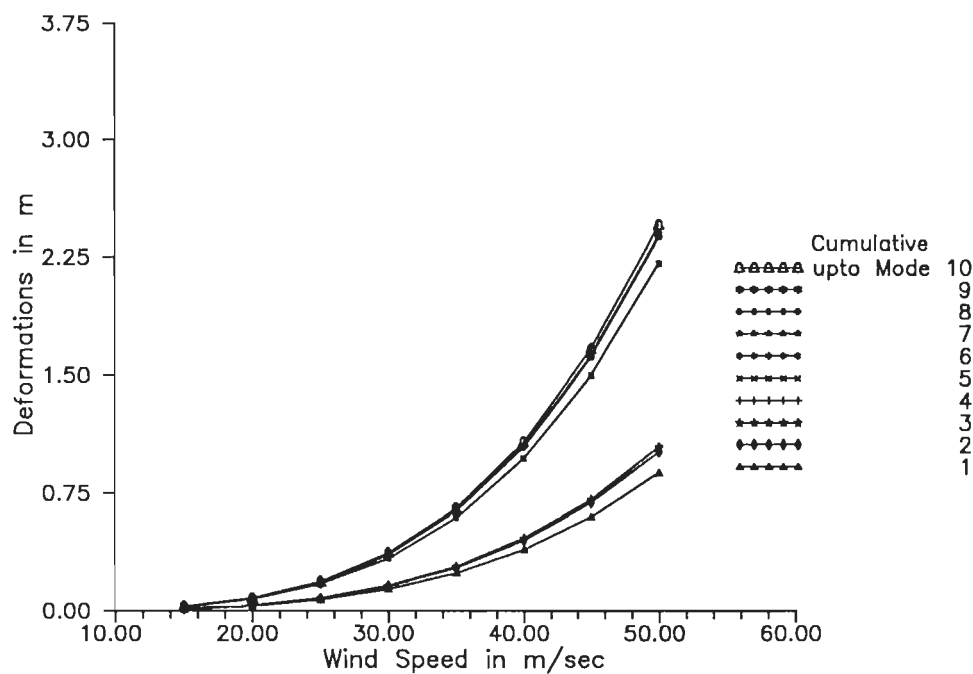

Fig.6.38(b) Cumulative modal response of the main span of Bridge # 2 in pure torsion at mid span. (Faired deck section)

CONCLUSIONS AND SCOPE FOR FUTURE RESEARCH

7.1 OVERVIEW

The work carried out in this thesis is a study on the behaviour of composite girder deck cable stayed bridges under smooth and turbulent winds. The approach of using the flutter derivative coefficients pertaining to a deck section for estimating the response of the bridge, has been adopted in the present study, after necessary considerations as explained in the first chapter. In this method, the flutter derivatives of the bridge deck system are the essential coefficients needed for computing the bridge responses to wind and these can only be obtained experimentally from wind tunnel tests on the 'section model' of the bridge deck.

Provision of fairings is often needed for longer spans as it helps to streamline the deck section and improve its aerodynamic stability. Therefore in this study the deck section with part and full length fairings was included.

The purpose of this study has been to (i) enrich data bank of flutter derivatives with the deck section studied and (ii) to understand the aerodynamic stability of bridges using this type of deck (with the possible improvements in its shape) which has gained popularity in the recent years. Parameters like bridge span, wind incidence angle and integral length scale of turbulence have also been studied.

Using the flutter derivatives, theoretical analysis of the full bridge system could be carried out to predict its response in the stable region and also to evaluate the flutter criteria which defines the aerodynamic instability of the system. The theoretical responses have been obtained by superposition of the response of the system in its various modes of

vibrations. The eigenvalue problem of the 3-D bridge system was therefore solved and the dynamic characteristics of the system, like natural mode shapes, modal integrals, generalised mass, and generalised mass moment of inertia, etc., were determined and used in the analysis.

The results of this study will be of interest to a wide section of the profession including the research community engaged in analysis and design of cable stayed bridges of composite I-girder deck sections.

7.2 CONCLUSIONS

Conclusions drawn from the experimental and theoretical study carried out in this work, though not comprehensive, are yet a step forward in understanding the aerodynamic instability of cable stayed bridges. The results would be of greater value on substantiation from prototype studies and possibly also 'full model' studies. The main conclusions of the study are summarised as follows :

7.2.1 Flow Characteristics

The nature of the upstream turbulence as expressed by the length scale, the intensity of turbulence and the spectral density of fluctuating components of the wind velocities, play a vital role in the flow pattern generated around the deck section. Hence it can greatly affect the resulting aerodynamic forces which govern the behaviour of the bridge deck section and therefore that of the total bridge system.

Also the flow characteristics generated by passive means in the wind tunnel through grids were found to corroborate with the desired atmospheric wind characteristics, ensuring properly simulated wind environment in the tests.

7.2.2 Section Model Results

From the extensive measurement of flutter derivatives determined from section model tests it was observed that the upstream turbulence has considerable effect on the values of the flutter derivatives, the grid generated turbulence improving the bridge deck stability for aerodynamic vibrations.

Another aspect of the wind effect on bridge decks is the wind incidence angle.

Extensive measurements carried out for this parameter showed that there is a significant influence on the flutter derivatives for wind incidence angles exceeding 3 degrees on either side of the deck. It is observed that for the positive wind incidence angles above 3 degrees, the aerodynamic stability of the section improves in the torsional modes of vibration, the vertical modes remaining unaffected.

Addition of fairings influenced the flutter derivatives A_2^* and H_1^* of the section model significantly and favourably, while the derivatives A_3^* and H_4^* did not show any significant change, the former affects the dominant modes of vibration influencing the aerodynamic response. The type of fairing as used can be of much help in improving the aerodynamic stability of the bridge.

7.2.3 Flutter Criteria

The analysis for the flutter criteria showed that only the first few torsional modes of vibration of the structure are critical for single degree flutter in torsion.

The typical cable stayed bridge with composite I-girder deck having a main span of 199 m is seen to be fully stable against flutter, the instability occurring at a high wind speed of 82 m/sec. The addition of fairings produced a further improvement in the aerodynamic stability of the bridge. Thus cable stayed bridges of similar form and spans upto about 200 m may be expected to remain aerodynamically stable even in severe winds.

Extending the analysis to a bridge of span 457 m, it has been been found that the flutter occurred at a wind speed of 46 m/sec. Hence it may be said that bridges with fairly large main span may exhibit flutter at much lower wind speed which may lie within the design wind speeds. Interestingly there is not much change in the critical wind speed with the use of fairings added to the deck. Hence it may be concluded that for longer spans(of the range studied) the dynamic characteristics influence the flutter criteria besides the geometric shape.

7.2.4 Buffeting Response

From the performance of the bridge for buffeting response under turbulent wind conditions the following conclusions may be drawn:

(i) For small span bridges the response will be higher at or around quarter-span points compared to the middle of the span.

(ii) For fairly large span bridges the maximum response occurs around mid-span of the bridge.

(iii) Among the 28 modes analysed the first six modes of vibration yield the maximum response, with subsequent modes contributing insignificantly. This is true for both the rotational and the vertical modes of vibration.

(iv) Fairing added to the deck reduces the response of the bridge deck in its torsional modes of vibration significantly but it has much less effect in the vertical modes of vibration.

7.3 SCOPE FOR FUTURE RESEARCH

The aeroelastic study of cable bridges reported in this thesis is based on the single mode response of the section model tests hitherto used by research workers in this field. Very recent works have extended the analysis for buffeting and flutter to more sophisticated multi-mode forced vibration excitations. These and some other earlier works have revealed that the flutter derivatives may depend upon the amplitude of motion of the structure in a manner which may affect the buffeting response and the aerodynamic bridge stability. However, the linear flutter derivative model of deck response may be considered to have reasonable accuracy, since the local(non-linear) pressure variations are likely to get averaged out over the width and length of the deck. Moreover, the structural restoring and inertia forces shall dominate over the motion dependent fluid forces. The future work may thus be planned to throw more light on this issue besides investigating the following aspects:

(i) Though with special grid sizes, the required integral length scales of turbulence could be achieved in this study, it is generally not possible to simulate this flow parameter by the passive means. Hence there is a need to develop devices for generating large integral scales by active mechanical means.

(ii) More detailed experimental and theoretical studies are justifiably needed to understand the behaviour of the section model for various wind incidence angles. It is felt that recording of the flow patterns and the pressures over the section of the deck would be of great help in this direction.

A.1 DATA ACQUISITION SYSTEM

The Keithley model 500A is a general purpose data aquisition and control device-an interface between the computer and the physical system. This model is a 'data-acquisition-and -control-main-frame' system for bench, portable or rock mounted applications. This data acquisition platform consists of a ten-slot mother board to house modules like strain gauge, thermocouple, LVDT/RVDT, etc., a power supply, and an interface logic unit housed in a rugged case.

Modules are available for A/D conversion, multiplexing, analog and digital input and output and other functions. The system is linked to the PC via a specialised bus extension interface which resides inside the host computer.

500A model supports Keithley data acquisition software (KDAC500) which handles all fore-ground/back-ground acquisition, engineering unit conversion, arrays and memory management. It also provides real time graphing. Also it has a file management system which permits easy export of data to other packages for analysis.

In the present study the following modules have been utilized for the acquisition of strain gauge data.

A.1.1 Master Analog Measurement Module(AMM2)

This module is having an option of external 16 single ended or 8 differential ended inputs (input mode progammably selected) in addition to analog inputs from other modules. The signal acquired through other modules is fed to a global multiplexer of AMM2 for further processing. AMM2 conditions the signals and filters the unwanted signals of 50

Hz to 60 Hz frequency generated by the power source and finally converts the signal into 16 bit digital values. The Fig.A.1 shows the signal conditioning steps adopted in AMM2 module.

A.1.2 Strain Gauge and DC Amplifier Module(AIM8)

The AIM8 is a highly versatile module used to measure data from strain gauge based transducers. The following are some of the important features of the module utilized during the data acquisition

Gain: The AIM8 module offers software programmable local gains of 1,10,100 or 1000, and it can be combined with the global gain to obtain a total gain upto 10,000.

Sensitivity: The AIM8 module provides usable measurement sensitivity in the micro volt region.

Transducer Compatibility: AIM8 accepts transducers which include resistive and semiconductor strain gauges with the values of resistance from 120 Ω to several thousand ohms.

Bridge completion facilities: AIM8 has spring loaded pin sockets for quick installation of jumpers and bridge completion resistors directly on the module.

Adjustable excitation: AIM8 provides regulated independently adjustable excitation of 0 V to 10 V.

Selectable low pass filter: AIM8 offers 10 Hz, 1 KHz and 3 KHz filter selectable through configuration.

In the present setup full bridge circuit (Fig.A.2) has been used to acquire the data from strain gauge based transducers fixed on to an A-frame which helped measure the vibrations of the section model. At an excitation of 3 V, and using the 3 KHz low pass filter, the raw data was acquired through by writing a program in BASIC and invoking the functions of KDAC500 software. The flow chart in Fig.A.3 shows the steps involved in the process.

The processing of data was carried out using **Asystant**[+] software. This software helped to further smoothen the acquired (raw) data by eliminating the high frequency unwanted noise. Finally, the filtered and smoothened data was fed to the software developed for determining the dynamic parameters of the system (frequency and log decrement).
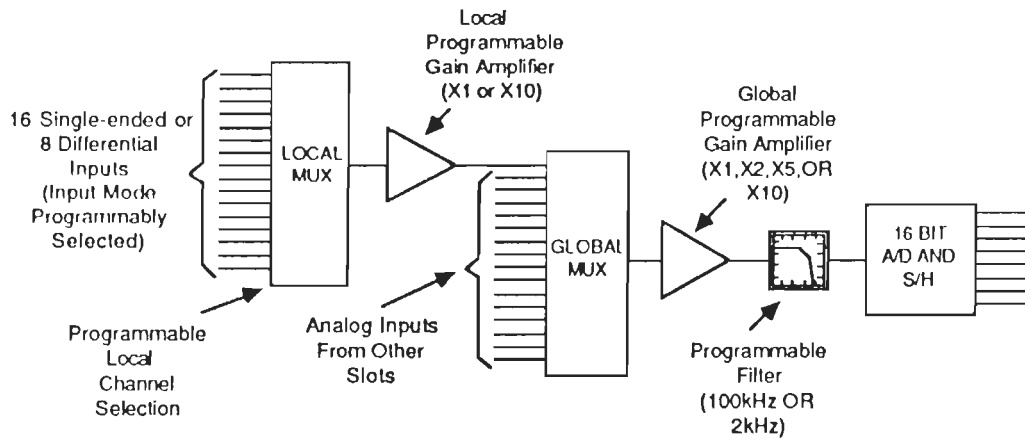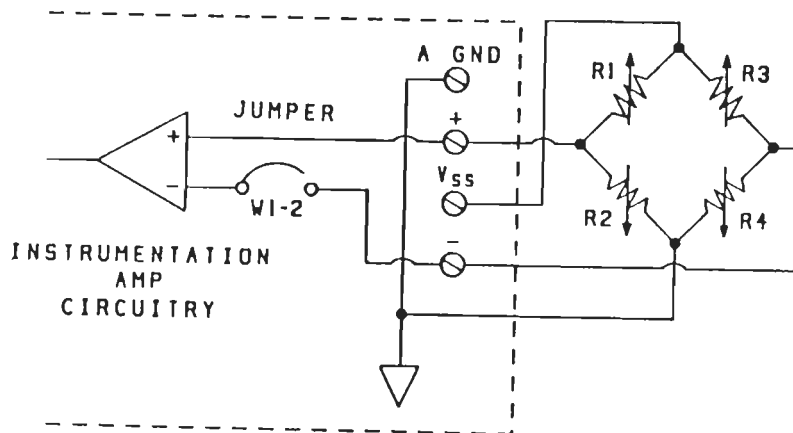
Fig.A.1 AMM2 signal conditioning steps

Fig.A.2 Full bridge circuit and jumpers

```
┌───────┐
│ Start │
└───────┘
    │
┌──────────────────────────────────────┐
│ Connect the transducer bridge circuit │
│ to AIM8 module on 500A model DAS       │
└──────────────────────────────────────┘
    │
┌────────────────────────────┐
│ Switch on the DAS 500A and  │
│ the corresponding P.C       │
└────────────────────────────┘
    │
┌────────────────────────────┐
│ Configure the module for the │
│ required specifications     │
└────────────────────────────┘
    │
┌──────────────────────────────────────┐
│ Trigger the module through program    │
│ and set the excitation voltage        │
└──────────────────────────────────────┘
    │
┌──────────────────────────────┐
│ Invoke for initialization     │
│ and set the offset voltage    │
└──────────────────────────────┘
    │
┌──────────────────────────────┐
│ Give the section model its initial │
│ displacement and release      │
└──────────────────────────────┘
    │
┌──────────────────────────────────────┐
│ Trigger the module to acquire the     │
│ data at the specified rate and the    │
│ required samples given through programs │
└──────────────────────────────────────┘
    │
┌──────────────────────────────────────┐
│ Retreive the data from array and store │
│ in files for further processing       │
└──────────────────────────────────────┘
    │
┌───────┐
│ End   │
└───────┘
```
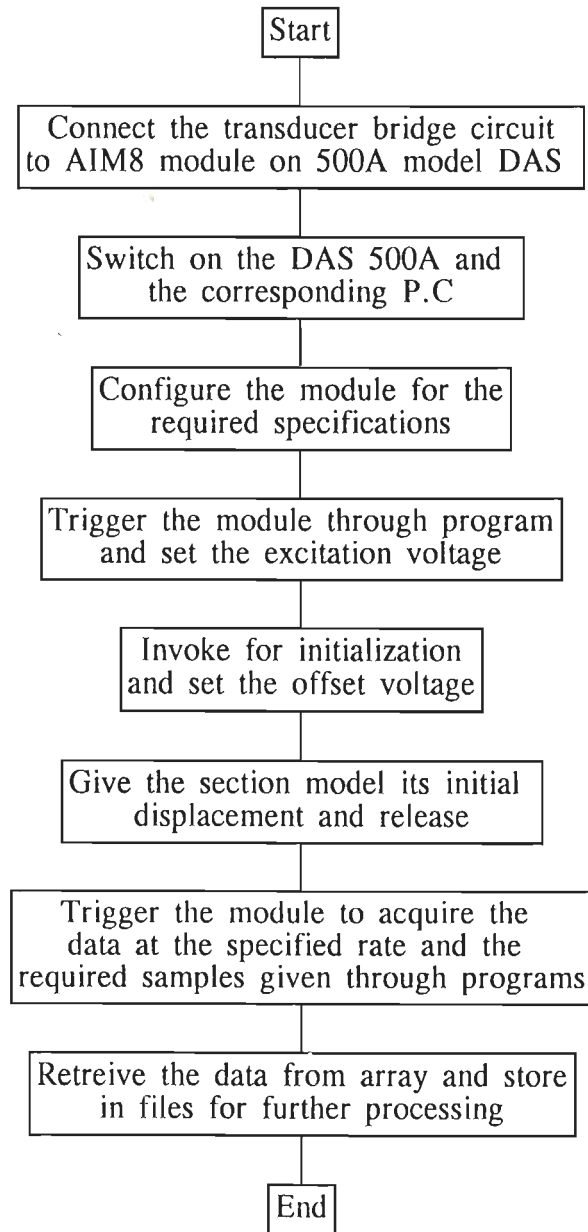
Fig.A.3 Schematic diagram of the steps involved in the
Data acquisition